Research Journal of Chemistry and Environment

Vol. 17 (9)
September 2013

Journal is indexed by Chemical Abstracts, SCIE and SCOPUS having Impact Factor 0.636

GOD IS

Govt. of India Regn. No.: 68381/98 Print ISSN No. 0972-0626; E-ISSN No.: 2278 – 4527

RESEARCH JOURNAL OF CHEMISTRY AND ENVIRONMENT

An International Research Journal of Chemical Sciences and Environmental Sciences

Res. J. Chem. Environ., Volume **17**, No. **(9)**, Pages 1-99, September **(2013), SCI Impact Factor 0.636**

Editor- in- Chief (Hon.)
Dr. SHANKAR LAL GARGH
M. Sc., Ph.D., M.B.A., LL.B., FICCE, FISBT, A. Inst. Pet.
Phone: +91-731-4004000 Mobile: 094250-56228

Correspondence Address:
Research Journal of Chemistry and Environment
Sector AG/80, Scheme No. 54, **Indore** 452 010 (M.P.) **INDIA**
Phones: 2552837, 4004000 Fax: 0731-2552837

Website<**www.shankargargh.net**>
<**www.chemenviron.net**>

E-mail: **info@shankargargh.net**

CONTENTS

❖ EDITORIAL BOARD: P II ❖ INSTRUCTIONS TO AUTHORS: P III ❖ MEMBERSHIP FORM: P VI

Instructions to Authors

For uploading the manuscript online for all our monthly journals published by us, please go to our website www.shankargargh.net

Please click the menu "Instructions to Authors". Please see that manuscript submitted by you is as per our standard format and as per Instructions to Authors. Authors are requested to check the latest issue of any of our journals for format.

Then select the journal where you wish to submit your paper for example "Research Journal of Chemistry and Environment" and then go to menu "paper submission". Follow the instructions and you can upload your paper online. Please submit manuscripts, tables, figures, references all together in one shot. It is a must to agree to terms and conditions of declaration given there.

Then go to menu "paper received" and you will find your paper there. Please see that all entries are correct otherwise submit again. In case you find any problem in uploading, please send your paper by email as attachment at papershankargargh@gmail.com . Write name of the journal in the subject when you send manuscript by email. If you send paper by email, then please attach the declaration as well.

Please see that you submit processing fees or membership subscription (fellow or life or annual) along with membership form within 10 days otherwise it will not be possible for us to process your manuscript. Your manuscript will be sent for blind review to two experts anywhere in the world and their decision will be final and binding. Please note that membership subscription or processing fees will not be returned by us whether your manuscript is accepted or rejected by the experts. Decision of experts will be informed within a month of receipt of membership subscription or processing fees. If your manuscript is accepted, it will be published soon in coming issues. If your manuscript is rejected, you will be permitted to submit to another journal. Every subscriber must receive receipt of payment and membership number. If one does not receive within 30 days, then you should inform us immediately.

Instruction for preparing the manuscript:

All our journals publish research papers, case studies and short communications containing original research work of good standard and review papers of contemporary relevance from all over the world. Following types of contributions are considered for publication:

RESEARCH PAPERS (Full Length - Maximum of 12 pages-A/4 size)
CASE STUDIES
SHORT COMMUNICATIONS
REVIEW PAPERS including Mini Reviews

We also publish informative articles of high standard and information about latest products in Industry, Recent Research, Information about Awards/Prizes, Scholarships, News and Views, Seminars, Conferences, Appointments etc.

1. Papers are accepted only in English (Except for journal "International Research Journal of Languages" where one can submit paper in any recognized language). English spelling and punctuation is preferred. All the matter and information should be submitted online by uploading at the menu "Paper Submission". If one finds difficulty in uploading, then one can send manuscript as attachment on email papershankargargh@gmail.com Manuscript format

should be in MS word only. Charts, Tables and Diagrams should be in MS Excel or MS Word and images in JPG format using maximum possible 72dpi resolution. All the matter should be typed in Times New Roman Font size - 11 point with single spacing.

2. Full length Research Papers (Maximum of 12 pages in A/4 size) should be divided as follows: Title, Authors names (family names first in bold followed by initials) with institutional address and corresponding author email (One author should be identified as the Corresponding Author), Abstract in Italics, Keywords, Introduction, Material and Methods, Results and Discussion, (Tables and Figures must be in separate sheet), Acknowledgement and References. Pages should be properly numbered. Mathematical data should be strictly provided. References should be in alphabetical order.

3. References must be in separate sheet alphabetically and typed in the following order:
Family name first and then initials followed by title of paper, name of journal in abbreviated form in Italics (name of book in normal), volume no. in Bold, page no. in normal and publication year in Bold in bracket e.g.

1. Patel R.M., Patel D.M., Shah K.P. and Patel D.A., Synthesis of Polyketones and their Antimicrobial Study, *Res. J. Chem. Environ.*, **3 (2),** 47 **(1999)**

2. Rao C.N.R., Chemical Applications of IR Spectroscopy, Academic Press, London, 250 **(1963)**

4. References must be serially numbered and should be arranged alphabetically by family name (surname) first. References must be quoted compulsorily in the text as numerals at the end of the sentence e.g. .....solution.[1]

5. Authors and co-authors must be members of Journal. If authors are not members, they should pay processing fees.

6. After receipt of research paper and membership subscription of all the authors or processing fees, your paper will be sent to two experts. Both experts should approve the paper and their decision regarding acceptance will be final and binding. The editorial board reserves the right to condense or make changes in the paper.

7. Manuscripts should be strictly in accordance with prescribed FORMAT of the journal. They will not be returned in any case whether accepted or rejected. Manuscripts and all other correspondence should be addressed to Editor. Acceptance communication will be sent to authors in one month time. Rejected manuscripts can be sent by authors to other journals only after our prior permission. Please note that your membership subscription or processing fees will not be refunded in any case whether your paper is rejected or accepted.

8. **Declaration to be given by authors:** The facts and views in the manuscript are ours and we are totally responsible for authenticity, validity and originality etc. I / We undertake and agree that the manuscripts submitted to your journal have not been published elsewhere and have not been simultaneously submitted to other journals. I / We also declare that manuscripts are our original work and we have not copied from any where else. There is no plagiarism in our manuscripts. Our manuscripts whether accepted or rejected will be property of the publisher of the journal and all the copyrights will be with the publisher of the journal.

9. Please correspond by email and always mention title of manuscript, name of the journal, date of submission of manuscript and payment details of membership or processing fees. Please write the name of the journal in subject.

Instructions for Manuscript-format

a) Page Layout: A4 (21cm × 28 cm) leaving 2 cm margin on all sides of the text. All the text should be single spaced and the pages should be numbered consecutively. Alignment should be Left.

b) Use MS word (2003-2007) for text and TIFF, JPEG or Paint for figures.

c) The first page should contain:

Title-bold, 18 point size
Name/s of author/s-bold, 10 point size (Surname or Family name first in bold)
Affiliation/s-address of all the author/s followed by email of corresponding author in 8.5 point size
Abstract in italics up to 200 words in 12 point size
Keywords- at least 5 keywords in 11 point size

d) Main Text-The paper should be divided into the following sections:

Introduction, Material and Methods, Results and Discussion, Conclusion, Acknowledgement and References. Tables and Figures of good resolution (72 dpi) should be numbered consecutively and given alphabetically by surname or family name in the order of their appearance in the text. References should be alphabetical in order.

e) References-References should be cited in the text as superscript [1, 2] on persons name or at the end of the sentence.

Names of journals in abbreviated form should be in italics and volume number should be in bold.
Reference to papers e.g. Okuyama K. and Lenggoro I. W., *Chem.Eng. Sci.,* **58**, 537 **(2003)**
Reference to books e.g. Durbin R., Eddy S.R., Krogh A. and Mitchison G., Biological Sequence Analysis: Probabilistic Models of Proteins and Nucleic Acids. Cambridge University Press **(1999)**

f) Please check the latest issue of the journal for format and prepare the manuscript accordingly.

Acceptance

As soon as one submits the paper online, it will appear in heading "Papers Received". When we receive the paper along with "Declaration of Authors" and either membership subscription or processing fees, we will send your paper to two experts for comments any where in the world. After acceptance by both the experts, we will try our best to inform you regarding acceptance within one month. If it is accepted, we will send you acceptance letter and your paper will be published at earliest in coming issues. If your paper is rejected, you can submit to other journal with our prior permission. Please note that your membership subscription or processing fees will not be refunded in any case whether your paper is rejected or accepted.

******

✂

GOD IS

Govt. of India Regn. No.: 68381/98 Print ISSN No. 0972-0626, E-ISSN No.: 2278 - 4527

Phone & Fax: +91- 731- 2552837 **E-Mail :** info@shankargargh.net

Website : www.chemenviron.net ; www.shankargargh.net

***17th Year of Publication*, SCI Impact Factor 0.636 ;**

Journal is indexed by Chemical Abstracts, SCIE, SCOPUS

RESEARCH JOURNAL OF CHEMISTRY AND ENVIRONMENT

Sector AG/80, Scheme No. 54, Vijay Nagar, A.B.Road, Indore 452010 (M.P.) INDIA

MEMBERSHIP FORM

Dear Editor,

I / We wish to be an Annual Member/ Life Member/ Fellow Member of **"Research Journal of Chemistry and Environment"** and agree to abide by your rules and regulations.

1. Name in Full : _____Male☐ Female☐
   (In Block Letters)
2. Nationality : _____3. Date of Birth_____
4. Correspondence Address :_____
   _____
5. Institutional/Business Address :_____
   _____
6. Mobile_____ E-Mail_____
7. Academic Qualifications : _____
8. Profession and Experience : _____
9. Present Position/Post : _____
10. Chemistry Interest : _____
11. How you came to know of Journal : _____

Membership Fees	Fellow	Life	Annual
Individual	Rs. 20,000/-, US $ 2000	Rs. 15,000/-, US $ 1500	Rs. 3000/-, US $ 300
Institutional	Rs. 30,000/-, US $ 3000	Rs. 20,000/-, US $ 2000	Rs. 4000/-, US $ 400

(Processing fees for three authors: Rs. 2000/-, US $ 200.)

Fellow Members can use the title **"FICCE"**, (Fellow, International Congress of Chemistry and Environment) and **Associate Members (Life)** can use the title **"AICCE"** (Associate, International Congress of Chemistry and Environment) after their names, after approval by the editors.

Rs./$ _____remitted by Bank Draft No./Cheque No./Cash/M.O. Receipt No._____Date_____Banker's Name _____.

[For Cheques, please add Rs. 125/-(US $ 25) extra towards collection charges. Drafts/ Cheques should be in name of "**Research Journal of Chemistry and Environment**"]

Place : _____
Date : _____

(Signature of the applicant)

From the Editor's Desk

The Development Tendency of Minerals Processing Technology: A Synthesis of Multiple Disciplines

Yao Jin
Our guest editor from College of Resources and Civil Engineering, Northeastern University, Liaoning, Shenyang 110819, CHINA
yaojin_82@126.com

"Population, Development and Environment" is an international common issue in 21th century. On one hand, the growth of population and need for resources are increasing every day but the amount of resources are decreasing. On the other hand, people are paying more and more attention on the environment problems. The scientific utilization of resources is placed on an important location. Minerals processing engineering has been developed into a mature system with many new technologies. But along with change of usable resources and the development of technologies, the minerals processing engineering will face on many challenges. The sustainable development of human society requires the processing of minerals to have high efficiency, low energy cost and non pollution which lead to the in-depth exploration on the problems and development orientation of minerals processing technology.

Minerals processing is a technology that extracts useful materials from mineral resources such as ores, secondary resources, industrial and life waste etc. by physical or chemical methods of separation, enrichment or purification. The traditional minerals processing technology is facing serious challenges because the composition of mineral resources to be processed is becoming more and more complex and the processing for secondary resources, industrial waste and marine resources is becoming important objective in minerals processing. Directly separating or processing mineral materials and chemicals from various resources is the trend of the development of minerals processing which can make the process high in efficiency, low in energy cost and pollution.

Facing the technical problems and newly discovered resources, scientists in the minerals processing and relative disciplines are marching in new exploration. The combination of minerals processing and adjacent disciplines e.g. physics, chemistry, biology, mathematics, computation, mining engineering, materials engineering, has greatly promoted the development of minerals processing technology.

The enrichment, separation and comprehensive utilization of minerals are traditional minerals processing methods, mainly focus on processing the refractory ores, treating the "three wastes" in mining and metallurgy, recycling secondary resources, developing new technology, process and equipment and researching the fundamental theory in the procedure. The traditional minerals processing research field includes floatation chemistry, molecular designing of flotation reagents and minerals processing in composite physical fields etc. On the direction of those traditional disciplines, new technologies such as potential regulation flotation technology in processing sulfide ores, cold-bound pellet direct reduction technology and dry beneficiation for coal have been developed which will boost the improvement in minerals processing technology and economic benefit.

Minerals extraction has become a new discipline based on minerals processing, metallurgy, bioengineering and electrochemistry etc. It mainly aims at developing and utilizing of complex mineral resources and marine resources. One of the typical extraction technologies is the leaching-extracting-electrode position technology for copper, which uses sulfuric acid solution, even with bacteria enzyme, to dissolve element Cu in ores, then extracts the Cu contained solution and uses electrode position to obtain high grade copper. This method has replaced the traditional beneficiation and metallurgy process which was high in economy and ecology cost.

Minerals material engineering is based on minerals processing engineering and chemical engineering, researching on methods directly producing various materials from minerals without smelting process such as materials by modified ultrafine minerals powder which are used as padding and catalyst in petroleum and chemical industry, used as electronic paste, magnetic recording materials and light wave adsorption materials in electronic industry.

Computer technology and minerals economy in minerals processing are important discipline direction in minerals processing engineering, which research on computer simulating and optimization designing for the whole process of minerals processing, building the expert system for mines and plants, managing the manufacture and operation.

Minerals processing technology can also be applied in the enrichment and separation for non-mineral resources to broaden the domain. The principle of minerals processing technology is to separate or enrich materials depending on the differences in the physical and chemical properties of objects which can be extended to other scientific fields, such as using high grade magnetic separation technology for the separation of red blood cells in medicine, the ions

separation in biology and the separation of nuclear radioactive solid raw material etc. using flotation method to recycle cellulose from pulp waste liquid or separate the printing ink and carbon black from waste paper or separating mycobacterium tuberculosis and *escherichia coli* in medical microbiology.

People's need on better environment and sufficient resources requires fast development of minerals processing technology. At the mean time, a sustainable development of human society relies on the technological development of resource utilization.

*****

Fire dynamics simulation of multiple ethanol pool fires

Bahman Abdolhamidzadeh[1], Vahid Bab[2], Davood Rashtchian[2] and Genserik Reniers[3*]
1. Department of Chemical Engineering, Faculty of Engineering, University of Malaya, 50603, Kuala Lumpur, MALAYSIA
2. Center for Process Design, Safety and Loss Prevention (CPSL), Department of Chemical and Petroleum Engineering, Sharif University of Technology, Tehran, IRAN
3. Antwerp Research Group on Safety and Security (ARGoSS), University of Antwerp and Hogeschool-Universiteit Brussel/KULeuven, Prinsstraat, 13, 2000 Antwerpen, BELGIUM
*genserik.reniers@ua.ac.be

Abstract
In this study, a well-known Computational Fluid Dynamics software, so-called Fire Dynamics Simulator (FDS), has been used to simulate multiple ethanol pool fire scenarios. Influences and reciprocal impacts in terms of dynamics and growth of the pool fires have been investigated. Heat release rates temperature and flame shapes have been monitored as the main outputs of the simulations. Based on the simulation results, it can be concluded that the amounts of mass burning rate, the radiation energy and the pool fire flame height were significantly higher in multiple pool fires, when compared with the theoretical values obtained by the mere summation of single pool fires. Furthermore, the effects of different grid sizes on the accuracy of the pool fire simulations have also been investigated and are discussed.

Keywords: Pool fire, multiple pool fire, modeling, CFD software, FDS software.

Introduction
Fire is one of the most destructive and costly causes of damage in the chemical industry. According to an analysis based on a survey of 6099 cases, fire (as a phenomenon) is the most frequent accident in the process industries (41.5%) and among the different types of fire, so-called pool fires are the most likely ones(53%)[20]. Pool fires have usually more localized effects comparing to other process accidents such as explosions or toxic releases. However, in densely organized process plants the thermal effects of a pool fire may lead to devastating cascading effects. Many major accidents occurred where a pool fire was the initiating event of a series of events leading to a major accident. Some examples are Nigata, Japan (1964); Beaumont, USA (1970); Las Piedras, Venezuela (1984) and Thessalonika, Greece (1986).[1]

Moreover, in a comprehensive past accidents survey carried out by the authors, it was revealed that among the different types of fire, pool fires have been the initiator of a domino chain in 80% of the cases[2]. In those accidents multiple pool fires usually occur. Hence, neglecting the possibility (and the heightened risk) of multiple pool fires in Quantitative Risk Assessments may lead to risk underestimations. However, the complex nature of the pool fire phenomenon and difficulties to adequately model pool fires, even single ones, hamper multiple pool fire simulations.

Author for Correspondence

A pool fire can be defined as the turbulent diffusion flame which burns above a horizontal vaporizing fuel pool where the fuel vapor has negligible initial momentum[19] and may result from different scenarios. The pool could for example result from the overfilling of a storage tank or the rupture of a pipe or vessel. The source of fuel may be instantaneous or a continuous release. An insight into the pool fire mechanism is indeed required to make an effective analysis of this phenomenon. The difficulties in understanding the fire dynamics originate from the complex interactions between fluid motion, combustion, radiation and multiphase flow, which all take place in a turbulent buoyancy-driven environment. Fire growth is also strongly affected by various external conditions such as wind speed, direction and the presence of any obstacles such as pipe racks, other equipment or even other fires.

Pool fires have been experimentally investigated in several studies such as e.g. Weckman and Sobiesiak[27], Hamins et al[9], Cetegen and Ahmed[4], Malasekera et al[14], Cetegen[5] and Mandin and Most[15]. Numerous investigations have also been conducted using Computational Fluid Dynamics (CFD) techniques[8,22,23,26], however the vast majority of them for single pool fires. Although extensive research has been performed about modeling of different aspects of pool fires, interaction between pool fires in multiple fires is a somewhat neglected study domain. Nonetheless, the merging of flames in multiple fires is believed to make a fire more destructive and out-of-control, causing difficulties in firefighting and possibly leading to fire whirls. Despite the dangerous nature of multiple fires, at present, few researchers have considered multiple fires in experimental modeling.[1,10-12,25]

Moreover, these limited number of studies which have been carried out in multiple fire areas, seem scattered. Some of these studies have been performed for multiple jet fires[21] and the fuel phase and type vary a lot in different researches. Multiple solid fires were also investigated.[10]

Thus, on the one hand, many different arrangements, sizes and setups have been used in past studies. On the other hand, researches about multiple pool fires have been performed a long time ago while computational resources were not available as they have become available in our present time[3,21]. Almost all of these experiments have been done with small fires (comparing to actual industrial fires) and normally a scale-up process is required after using the

derived correlations, many uncertainties arise during scale-up processes making accurate simulations very difficult.

Over the last years, with huge advancements in computer processing power, the modeling of fires has been shifted from the engineering application of correlation-based methods such as Zone methods towards filtered discrete solution equations by the CFD techniques. The Fire Dynamics Simulator (FDS), developed by the National Institute of Standards and Technology, is receiving increasingly wide applications within the fire society. FDS is a CFD model of a fire-driven fluid flow. The model solves numerically a form of the Navier-Stokes equations appropriate for a low-speed, thermally-driven flow with an emphasis on smoke and heat transport from fires. The partial derivatives of the conservation equations of mass, momentum and energy are approximated as finite differences and the solution is updated in time on a three-dimensional, rectilinear grid. Thermal radiation is computed using a finite volume technique on the same grid as the flow solver. Lagrangian particles are used to simulate smoke movement, sprinkler discharge and fuel sprays[17]. Recently, FDS has been used for consequence modeling of different accidents.[18,22,28].

In this paper, FDS is employed to simulate multiple pool fires originating from industrial-scale storage tanks filled with ethanol. Ethanol has been chosen as a substance because this component was involved in some of the past domino accidents. Moreover, an industrial case was present in Southern Iran with such storage tanks. The objective of this study is to compare the thermal characteristics of multiple pool fires with one single pool fire. These characteristics were the mass burning rate, temperature profiles, the radiation energy and the flame height. Fire dynamics and flame shape were also investigated in multiple pool fire scenarios.

Furthermore, mesh sizes in simulations possibly significantly influence the accuracy of CFD predicted results of fire scenarios. Therefore, the study also included an investigation into the appropriate mesh size to be used for simulating the characteristics of multiple pool fires.

FDS Simulations

Setting up the model –Computational domain and case description: The first step in performing a simulation in FDS is to generate an input file with all required information to describe the scenario(s) under consideration. The key inputs needed for the pool fire simulations are the physical size of the overall domain, the grid dimensions, the additional geometrical features and the inlet and boundary conditions. Finally, there are a number of parameters that customize the output files to capture the desired quantities.

The fire is basically modeled as the ejection of pyrolyzed fuel from a liquid surface that burns when mixed with oxygen. The heat of vaporization for the fuel is specified and thus its burning rate is dependent on the heat feedback from the fire or any other heat source.

In this research, a rectangular computational domain has been considered with dimensions of 80m(W)× 80m(D)× 60m (H) in a Cartesian coordinate system. The curved surface of pools was represented by a stepwise grid approximation. The FDS program has built-in ability to prevent the formation of vortices at sharp corners and smoothes the jagged steps that make up the obstruction[17]. Except for the floor, all other boundaries have been considered open in this study.

The storage tanks that were simulated in this study have been selected by reference to an Iranian industrial plant (as already mentioned). All storage tanks have the same dimension, that is 20m diameter and 5m height and the distance between the centers of two adjacent tanks was assumed to be 30m. Figure 1 shows the layout used in the study.

Table 1
Summary of mesh sizes / grid resolutions for FDS simulations

Mesh		$R^*(\Delta x / D^*)$	Number of cells in each axis			
No.	Mesh Type		X	Y	Z	Total Number of cells in domain
1	SM	1/4	20	20	15	6000
2	SM	1/8	40	40	30	48000
3	MM	1/13	60	60	22	79200
4	MM	1/14	64	64	24	98304
5	SM	1/17	80	80	60	384000
6	MM	1/19	96	96	36	331776
7	MM	1/21	104	104	39	421824
8	MM	1/23	112	112	42	489216
9	MM	1/25	128	128	48	786432

SM: Single size mesh, MM: Multiple size mesh; D^*: characteristic diameter (m); ΔX: mesh size (m) ; Domain (X,Y,Z): 80×80×60 m

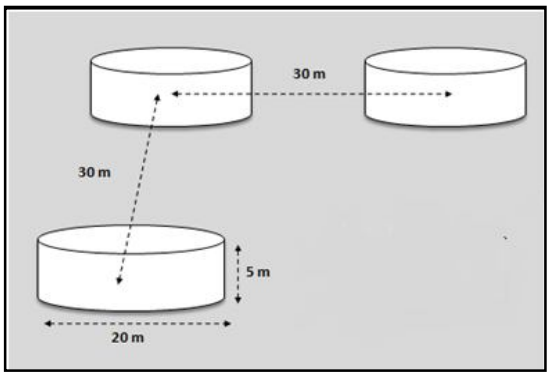

Figure 1: Layout of the ethanol tanks in our study

Numerical grid: The number of meshes used in a simulation is one of the most important numerical parameters in CFD modeling dictating its numerical accuracy. In order to investigate the influence of the size and resolution of the numerical grid, several simulations for each case have been carried out with different numbers of meshes. Cubic cells with equal sizes in all coordinates were used in a single size meshing, but meshes with different sizes have been used in multi size meshing of the domain. This technique adds more flexibility to the grid generation process and makes it possible to have a higher resolution in the areas where needed. The mesh sizes and resolutions for these numerical grids are listed in table 1.

In table 1, R^*, the normalized mesh size of a numerical grid is defined as the ratio of mesh size to the characteristic diameter of pool fire which in case of a symmetric circular pool is the pool diameter (D*). R^* is considered as the mesh resolution indicator in simulations.

$$R^* = \frac{\Delta X}{D^*} \qquad (1)$$

where Δx is the length of a cell for a given grid.

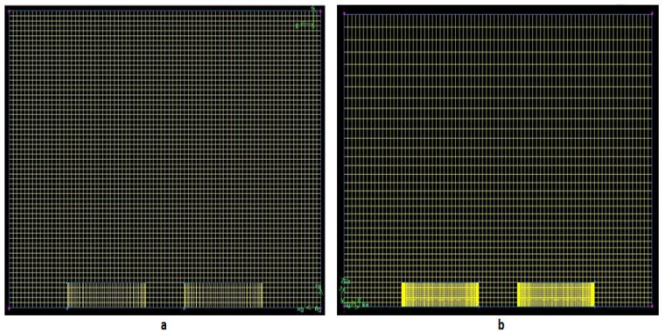

Figure 2: The meshed domain for (a) a SM Mesh Type and (b) a MM Mesh Type.

As it can be seen from figures 2a and 2b, in a SM Mesh type, all the coordinates are equally divided while in a MM Mesh type, the mesh sizes are smaller around the fire and large in other parts of the domain.

Mesh size sensitivity analysis

The selection of the mesh size for any CFD simulation significantly influences the simulation results. Smaller meshes may provide better numerical solutions but also lead to a higher computation time.

The required resolution (R^*) suggested for a single pool fire in most of the past studies is between 1/5 and 1/1[6,17]. Other studies suggest a resolution of 1/20 to successfully predict the pool fire flame height[13]. But all these suggestions have been made for single fire simulation. In this study different cases have been studied in order to find the optimum resolution value. Because although using finer mesh sizes, or in other words smaller values for resolution, may theoretically lead to more accurate simulation, it increases the simulation time excessively.

Figure 3 is presented here as an example of the above mentioned studies. Figure 3 shows the predicted distributions of radiative heat fluxes along time for the CFD simulations with different mesh sizes. These radiative heats are emitted from multiple pool fires.

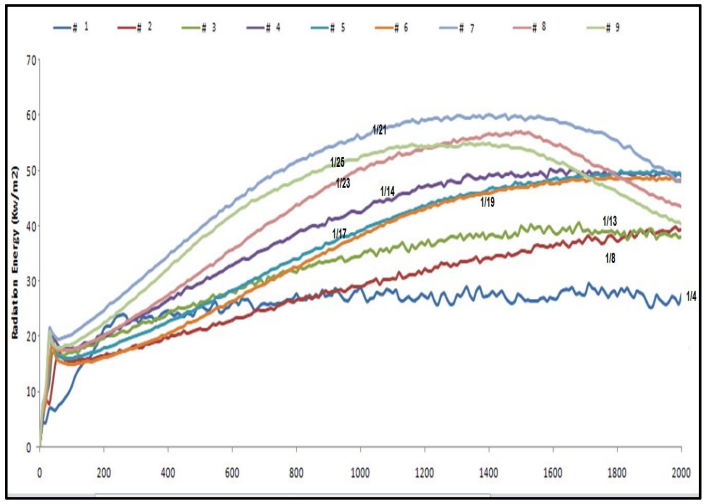

Figure 3: Radiation energy from a single pool fire for different mesh size (Different line colors show different mesh sizes with reference to table 1, relevant R^* is shown for each line)

The predicted radiative heat fluxes increase by decreasing mesh size (i.e. lower R^* values) and for R^*values less than 1/14, the predicted results are very close to each other. The comparison results thus indicate that a mesh size with R^* = 1/14 is optimal, taking accuracy and computation time both into account, to predict the distributions of radiative heat fluxes. Selecting R^* = 1/14 was also supported by simulation results from other cases.

The comparison between the prediction results of Mesh system numbers 5 (Single Mesh Type) and 6 (Multiple Mesh Type) from table 1 in figure 3 shows consistency between single and multiple meshes, while for larger

meshes (with less 'optimal' R^* values) this consistency cannot be seen. This reveals that the use of multiple meshes (of course with properly selected R^*) for numerical modeling of pool fires gives the required result's accuracy along with lower computation time as the number of meshes can be lower in multiple mesh modeling. The domain for numerical analysis should be divided into different mesh regions. Meshes should be small in the area where a fire takes place and also near the fire. But they can be larger in other parts of the domain such as the boundaries.

Results and Discussion

Multiple pool fires occur when adjacent fuel tanks or adjacent fuel spills simultaneously catch fire. The fire characteristics and dynamics of these multiple pool fires may vary from single pool fires. The flow of air between multiple fires may also be different. The radiation or mass burning rates for 3 separate pool fires (all with the same diameter) that are very close to each other may not be equal to three times the radiation or the mass burning rate of a single pool fire (with a diameter of 3 times that of the single pool fires). This study therefore investigates the possible differences of a single pool fire and a multiple pool fire. As it was mentioned before, three neighboring ethanol tanks have been selected for simulation and analysis. Different scenarios have been modeled by FDS software in order to determine the differences between single and multiple pool fire behavior.

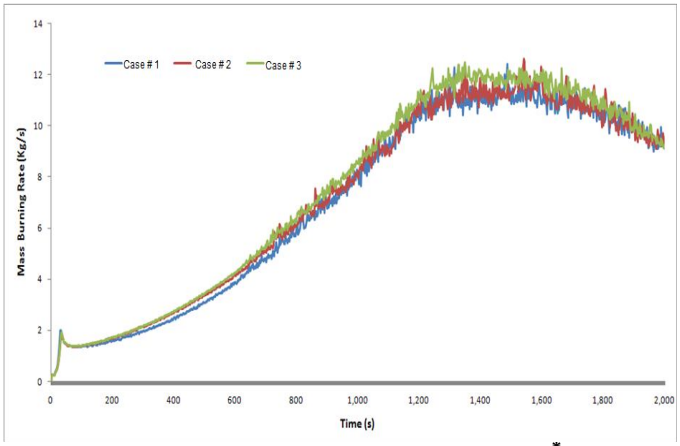

Figure 4: Mass burning rates of a pool fire(R^* = 1/14) for case #1, case #2 and case #3

Mass burning rate: Figure 4 shows the plotted average mass burning rates of an ethanol pool fire in three different cases. From figure 4, the mass burning rate for case #3 (3 ethanol tanks on fire) is the highest comparing to case #1 (single pool fire) and case #2 (2 ethanol tanks on fire). The mass burning rate of case #2, when there are two pool fires, is also higher than the case of a single pool fire (case #1).

It seems that radiation energy received from adjacent fires by the pool surface increases the flame temperature leading to increases in mass burning rate. So, this additional radiation energy is the major cause of the observed increase in mass burning rate in case of multiple pool fires. From these observations, it can be concluded that in addition to the fuel type and the pool diameter, neighboring pool fires have an effect on the mass burning rate and the flame behavior of each pool fire.

Temperature profile: The temperature profile is one of the most important characteristics of a pool fire; it has a significant effect on the amount of radiation energy emitted from the pool fire to the surrounding objects. Different scenarios have been modeled in this study and results have been observed over time. The predicted temperature distributions at a typical time (t=1200s) are shown in figure 5 for single and multiple pool fires.

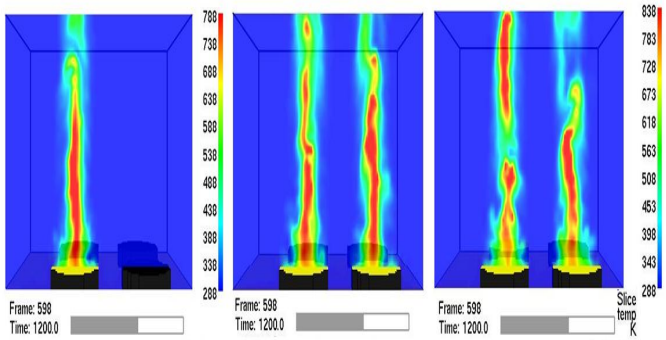

Figure 5: Temperature distribution at 1200 seconds after ignition in case #1, case #2 and case #3

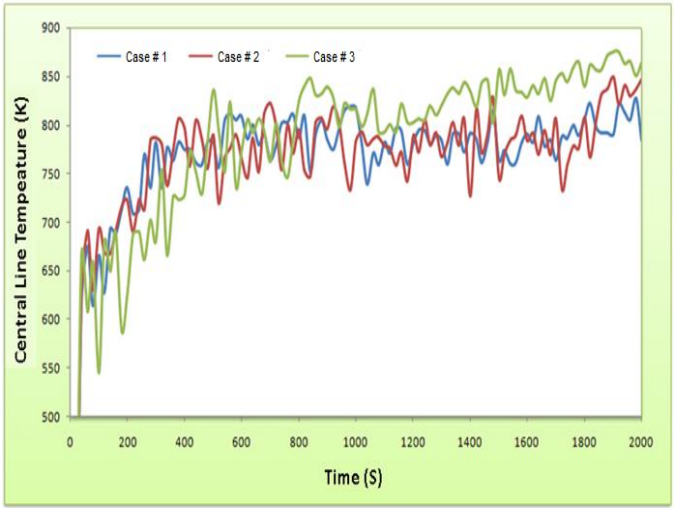

Figure 6: Centre line average temperature values in tanks in (R* = 1/14) case #1, case #2 and case #3

Figure 5 indicates that for a single ethanol tank pool fire, the maximum temperature line is located just on the geometrical center line of the pool, but in multiple fires these lines are shifted towards a hypothetical point in the center of the pools. Also the magnitude of the average temperature is increased locally. The center line average temperature values for tanks are shown in figure 6.

Figure 6 demonstrates that the temperature value in a multiple pool fire is higher than in a single pool fire. The maximum temperature for a multiple pool fire in case #3 and case #2 is approximately 50°C higher than for a single pool fire. This phenomenon is due to hot gas forced recycling through space among the fires and also due to an increased mass burning rate that occurs in case of multiple pool fires.

Flame shape: Flame dynamics is a key factor in fire propagation and also affects the fire destructive power. The flame height, one of the most important fire characteristics, even may lead to a change in suppression strategy and the flame tilt determines how fire will propagate.

Three snap shots of the simulated fire in case #1, case #2 and case #3 are shown in figure 7.

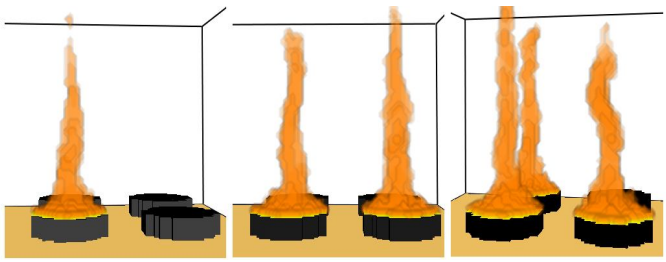

Figure 7: Flame shape snap shots at t=1000 s after ignition for case #1, case #2 and case #3

The snapshots from figure 7 were taken at 1000s to ensure that the flames were fully shaped and initial transition phases passed. It is obvious that multiple pool fires have higher flame lengths compared with single pool fires and also their flames are tilted towards each other. When pool fires are close to each other, oxygen deficiency occurs in the fire area and more in particular in the area between the fires. Because of the oxygen deficiency, the shape of flames changes. The flames seek to reach oxygen and therefore they become longer and narrower. Also in case of multiple pool fires, there is a pressure difference in the area between the pool fires and the outer side, while in a single pool fire the, pressure is equal in the surrounding area (in a single pool fire without a strong wind, the flame shape is usually symmetric). Hence, oxygen deficiency means air entrainment reduction in pool fires and it makes a pressure difference between open and close boundaries of pool fires.

This pressure difference causes fire flames slopes to the inner side (close boundary) and it avoids flame growth in the outer sides (open boundary). Hence, flames in multiple pool fires have to be narrow and tilted to provide oxygen. So these pool fires, in contrast with single pool fires, have long, narrow and tilted flames. From a practical point of view, if multiple pool fires merge, the conditions are much harder to control for firefighters. Some equipment and lines may become engulfed and fire fighters have much more difficulties cooling them, compared with controlling single pool fires.

Radiation energy: Radiative heat transfer due to its special characteristics (such as being independent of the transfer medium) is more effective and destructive than other mechanisms of heat transfer (conduction and convection) in industrial accidents. That is why radiation intensity of fires has been always one of the key parameters in consequence modeling and risk assessment. In the present study, the radiation energy received at a hypothetical point located in the center of the tank area with 5 m height has been measured by a radiometer. Figure 8 shows the amount of radiation energy received at that point for the different cases.

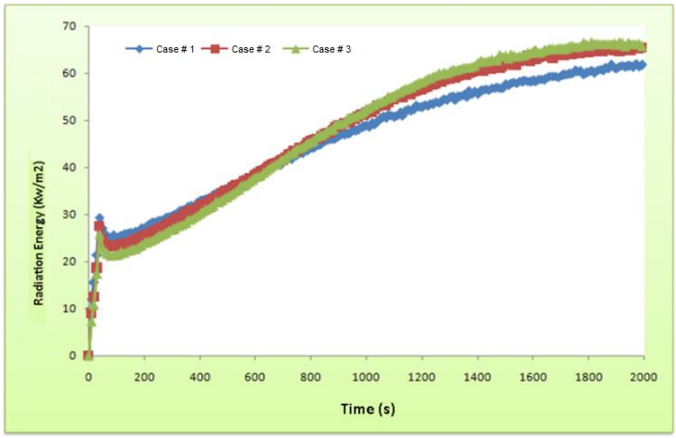

Figure 8: Comparison of the radiative heat flux distributions between predicted results (R^* = 1/14) for case #1, case #2 and case #3

Figure 8 shows that the radiation energy level received on the target (i.e. the geometrical center of the tank area with 5m height, as mentioned before), is higher for a multiple pool fire than for a single pool fire. The radiation energy originating from a pool fire depends on several parameters such as the fuel emissive power, the fraction of radiated heat that may reach to a specified target (called the 'view factor') and the atmospheric transmissivity to thermal radiation. The mass burning rate is increased in multiple pool fires up to 10% (as it was already mentioned). Flame temperature is also increased. Hence, besides the increase in mass burning rate and flame temperature values, the view factors (which depend on the target position), the flame height and -diameter, the velocity and the path of wind, are increased for multiple pool fires due to an increase in the flame height and a relative decrease in pool fire diameter.

Conclusion

Pool fires occur frequently in different industrial plants handling hazardous materials and their consequences should be considered in any QRA study. But pool fire modeling is inherently complex and this complexity increases when several pool fires at once are involved. The characteristics and dynamics of these multiple fires are investigated and are found to be quite different from single pool fires.

Several case studies on ethanol storage tanks have been studied with FDS software. The application of CFD software is advantageous as there are no proper correlation-based methods available at present to simulate the behavior of multiple pool fires. Results of these studies have revealed that some of the characteristics of pool fires, such as flame temperature and height, mass burning rate and radiation energy, increase substantially in case of multiple pool fires. The authors have clarified the reasons behind these behaviors based on fire dynamics. Due to the increasing of these parameters and due to the possibility of fires merging into one fire (which is a phenomenon which has been observed during the simulations), impacts of multiple pool fires seem possibly worse than the mere adding up of single pool fires' consequences. In brief, considering multiple pool fire scenarios and their consequences in risk assessments increase their accuracy and merely considering single pool fire scenarios may lead to risk underestimations.

In addition to comparing the characteristics of single and multiple pool fires, mesh size effects in CFD simulations of pool fires have been investigated in this paper. Based on the sensitivity analysis which has been carried out, the minimum required mesh resolution to obtain appropriate results in multiple pool fire modeling should be less than 7 percent of the characteristic pool fire diameter. Similar conclusion shave also been obtained for the predicted distribution of radiative heat fluxes. The predicted radiative heat flux values increase with decreasing mesh sizes and their distributions show little variation for a normalized mesh size (R^*) of a numerical grid lower than 1/14. In order to obtain accurate predictions in reasonable computation times, the optimum recommended mesh resolution was thus determined to be 1/14 for multiple pool fire scenarios.

References

1. Abdolhamidzadeh B. and Rashtchian D., Simultaneous pool fires modeling using the combination of semi-empirical and CFD tools, 18th International Congress of Chemical and Process Engineering, 24-28 August, Czech Republic **(2008)**

2. Abdolhamidzadeh B., Abbasi T., Rashtchian D. and Abbasi S.A., Domino effect in process industry accidents - An inventory of past events and identification of some patterns, *Journal of Loss Prevention in the Process Industries*, **24,** 575-593 **(2011)**

3. Baldwin R., Flame merging in multiple fires, *Combustion and Flame*, **12(4)**, 318–324 **(1968)**

4. Cetegen B. M. and Ahmed T., Experiments on the periodic instability of buoyant plumes and pool fires, *Combustion and Flame*, **93,** 157-184 **(1993)**

5. Cetegen B. M., Behavior of naturally oscillating and periodically forced axi-symmetric buoyant plumes of helium and helium-air mixtures, *Physics of Fluids*, **9(12)**, 3742-3753 **(1997)**

6. Dreisbach J. and McGrattan K., Verification and Validation of Selected Fire Models for Nuclear Power Plant Applications, Volume 7: Fire Dynamics Simulator (FDS), NUREG-1824 Final Report, U.S. Nuclear Regulatory Commission, Office of Nuclear Regulatory Research **(2007)**

7. Ferng Y.M. and Lin C.H., Investigation of appropriate mesh size and solid angle number for CFD simulating the characteristics of pool fires with experiments assessment, *Nuclear Engineering and Design*, **240(4),** 816-822 **(2010)**

8. Forney G.P., User's Guide for Smokeview Version 5 - A Tool for Visualizing Fire Dynamics Simulation Data. NIST Special Publication, National Institute of Standards and Technology, Gaithersburg, Maryland **(2007)**

9. Hamins A., Yang T.C. and Kashiwagi T., An experimental investigationof the pulsation frequency of flames, Proceedings of the Combustion Institute, **24,** 1695–1702 **(1992)**

10. Kamikawa D., Weng W.G., Kagiya K., Fukuda Y., Mase R. and Hasemi Y., Experimental study of merged flames from multi fire sources in propane and wood crib burners, *Combustion and Flame*, **142,** 17–23 **(2005)**

11. Liu N., Liu Q., Deng Z., Kohyu S. and Zhu J., Burn-out time data analysis on interaction effects among multiple fires in fire arrays, Proceedings of the Combustion Institute, **31,** 2589–2597 **(2007)**

12. Liu N., Liu O., Lozano J.S., Shu L., Zhang L., Zhu J., Deng Z. and Satoh K., Global burning rate of square fire arrays: Experimental correlation and interpretation, Proceedings of the Combustion Institute, **32(2)**, 2519-2526 **(2009)**

13. Ma T.G. and Quintiere J.G., Numerical simulation of axi-symmetric fire plumes: accuracy and limitations, *Fire Safety Journal*, **38,** 467-492 **(2003)**

14. Malalasekera W.M.G., Versteeg H.K. and Gilchrist K., A review of research and an experimental study on the pulsation of buoyant diffusion flames and pool fires, *Fire and Materials*, **20,** 261–271 **(1996)**

15. Mandin O. and Most J.M., Characterization of the puffing phenomenon on a pool fire, Proceedings of the sixth international symposium on fire safety science, 1137–1148 **(1999)**

16. McGrattan K.B., Rehm R.G. and Baum H.R., Fire-Driven Flows in Enclosures, *Journal of Computational Physics*, **110(2),** 285–291 **(1994)**

17. McGrattan K., Fire Dynamics Simulator (Version 4), Technical Reference Guide, NIST Special Publication 1018, National Institute of Standards and Technology, Gaithersburg, Maryland **(2004)**

18. Mouilleau Y. and Champassith A., CFD simulations of atmospheric gas dispersion using the Fire Dynamics Simulator (FDS), *Journal of Loss Prevention in the Process Industries*, **22,** 316–323 **(2009)**

19. Mudan K. S. and Croce P. A., Fire Hazard Calculations for Large Open Hydrocarbon Fires, SFPE Hand book on Fire Protection Engineering, 2nd ed., National Fire Protection Association, 2-45 -2-87 **(1988)**

20. Planas-Cuchi E., Montiel H. and Casal J., A survey of the origin, type and consequences of fire accidents in process plants and in the transportation of hazardous materials, *Trans. I Chem E*, Part B, **75,** 3–8 **(1997)**

21. Putnam A.A. and Speich C.F., A model study of the interaction of multiple turbulent diffusion flames, Symposium (International) on Combustion, **9(1)**, 867–877 **(1963)**

22. Ryder N.L., Sutula J. A., Schemel C. F., Hamer A. J. and Van Brunt V., Consequence modeling using the fire dynamics simulator, *Journal of Hazardous Materials*, **115(1-3),** 149-154 **(2004)**

23. Sinai Y. L., Exploratory CFD modeling of pool fire instabilities without cross-wind, *Fire Safety Journal*, **35(1),** 51-61 **(2000)**

24. Smagorinsky J., General Circulation Experiments with the Primitive Equations, The Basic Experiment, *Monthly Weather Review*, **91(3),** 99–164 **(1963)**

25. Sugawa S. and Oka Y., Fire Safety Science, Proceedings of the 7th International Symposium, 891–903 **(2002)**

26. Wang H.Y. and Joulain P., Modeling on the Interaction of the Turbulent Diffusion Flames between a Vertical Burning Wall and a Pool Fire, Fire Safety Science–Proceedings of the 5th International Symposium, 475-486 **(1997)**

27. Weckman E.J. and Sobiesiak A., The oscillatory behavior of medium scale pool fires, Proceedings of the Combustion Institute, **22,** 1299–1310 **(1988)**

28. Xin Y., Filatyev S.A., Biswas K., Gore J.P., Rehm R.G. and Baum H.R., Fire dynamics simulations of a one-meter diameter methane fire, *Combustionand Flame*, **153,** 499–509 **(2008).**

(Received 30th January 2013, accepted 20th June 2013)

Solubilising Water involved in Amoxicillin Extract using Mixed AOT/TWEEN 85 Reverse Micelles

Siti Hamidah Mohd-Setapar*, Chuo Sing Chuong and Siti Norazimah Mohamad-Aziz
Centre of Lipids Engineering and Applied Research (CLEAR), Faculty of Chemical Engineering, Universiti Teknologi Malaysia, 81310 UTM Skudai, Johor, MALAYSIA
*sitihamidah@cheme.utm.my

Abstract

Solubilisation of water in mixed reverse micellar systems formed with anionic surfactant sodium bis-2-ethylhexyl sulfosuccinate (AOT) and nonionic surfactants TWEEN 85 in iso-octane was investigated. The interfacial association of reverse micelle for amoxicillin solubilisation also was studied. It was found that a maximum solubilisation capacity of water occurred for a mixed AOT/TWEEN 85 reverse micelles in the presence of ethylene oxide (EO) chain length of the non-ionic surfactant. The solubilisation capacity of water was determined by two main factors including stability of the reverse micelle interfacial film and reverse micelle size. The amoxicillin molecules also were found to be interfacial active molecule at every tested pH and tested concentration of mixed AOT/TWEEN 85. The estimated values of reverse micellar size (Rm) using empirical and geometrical models show that the R_m is higher after the extraction when compared to R_m before extraction process.

Keyword: Solubilisation water, AOT, TWEEN 85, mixed reverse micelle, reverse micellar size.

Introduction

Solubilisation of water in reverse micellar has received interest since it gives significant influence in pharmaceutical, oil recovery, cosmetics and enzymatic catalysis applications [1]. Previous studies reported that water content (W_o) strongly influenced the solubilisation of bio-molecule and their characteristics of reverse micelle mixtures[2]. Mohd-Setapar et al.[3] stated that the water content analysis is important for understanding the properties of reverse micelles, mainly their size. The solubilisation capacity of water in reverse micelles depends on many factors such as the hydrocarbon group of the surfactant, nature of the polar group and addition of co-surfactant[1]. The addition of co-surfactant frequently gives rise to boost performance over the individual components for a wide variety of applications[4]. Therefore, it is expected that enhanced solubilisation of water in reverse micelles can also be achieved with surfactant mixtures.

Material and Methods

Materials: Amoxicillin trihydrate was obtained from Bio-WORLD, USA and was used as received. Sodium bis-2-ethylhexyl sulfosuccinate (AOT), Polyoxyethylene sorbitan tri-oleate (TWEEN 85) and iso-octane (HPLC grade) were purchased from Sigma, U.S. and were used as received. All other chemicals used for the experiments and analyses were of analytical grade.

Methods: Forward extraction was carried out by slowly injecting amoxicillin solution into 5 mL of AOT/ TWEEN/ iso-octane solution and by stirring the solution for 15 minutes with 350 rpm to obtain a clear solution. The solution was left for 24 hours for phase separation. Back extraction of amoxicillin from reverse micelles was carried out by contacting 5 mL of clear reverse micellar solution from the forward extraction with 5 ml of new fresh aqueous solution of known pH and salt concentration. Then the solution was stirred at 350 rpm for 15 minutes for the separation of the phases. The organic phase was analyzed for water and amoxicillin content. All the experiments were carried out at 20±2 ^{o}C in duplicate.

Amoxicillin and Water Content: The amoxicillin content was determined by measuring the absorbance at 285.5 nm. The sample analysis was performed against respective blank solutions. The amoxicillin concentration readings were taken in duplicate and an average value is used for the mass balance. Water content in the organic phase after forward extraction was measured by water determination balance FD620 and the equation was expressed as:

$$\text{Water content} = \frac{[\text{Water}]}{[\text{AOT}] + [\text{TWEEN 85}]} \quad (1)$$

Estimation of Reverse Micelle Size: The estimation of the reverse micellar radius was obtained by using W_o value and the empirical and geometrical models are reported in the table 1.

Result and Discussion

Phase Volume Changes in Reverse Micelle: Volume ratio between organic phases to aqueous phase after extraction is a critical parameter in the solubilisation of bio-molecule by using reverse micelle[5]. Figure 1 shows the volume ratio of aqueous to organic phase (V_a/V_o) as a function of the concentration of AOT/TWEEN 85, AOT and TWEEN 85 for both forward and backward extractions respectively. By increasing the AOT/TWEEN 85 concentration from 10 g/L to 80 g/L, the volume ratio aqueous phase to organic phase V_a/V_o decreased simultaneously from 0.9608 to 0.6367.

In theory, the increase of surfactant concentration more

than the critical micelle concentration would exhibit the formation of micelle number and the adsorption of bio-molecules and water molecule on the surfactant tails will also be high [6], therefore enhancing the mass transfer from the interfaces between aqueous and organic into the water pool of reverse micelles. Meanwhile, for the extraction using AOT only, the volume ratio of aqueous to organic phase was slightly lower compared with AOT/TWEEN 85. The presence of non-ionic TWEEN 85 surfactant alters the interface of organic phase in such a way that the interface becomes more flexible to incorporate more water and to facilitate droplet fusion and hence the percolation process.

It may be due to the presence of the head group of nonionic TWEEN 85 surfactant at the interface shields and the head group repulsion of AOT molecules and makes the interface more flexible [7]. Primary investigations on backward transfer of amoxicillin showed that the volume ratio of aqueous for these three systems did not affect much with the change of the surfactant concentration from 10 g/L to 80 g/L. For mixed AOT/TWEEN 85 reverse micelle, by increasing the surfactant concentration, the volume transfer from organic phase into aqueous phase was increased slowly from volume ratio V_a/V_o, 1 to 1.1346.

Table 1
Empirical and geometrical model

Empirical Models	
Hebbar et al[14]	For empty micelle (before extraction) $R_m = 0.138\ W_o$
	For filled micelle (after extraction) $R_m = 0.136\ W_o$
Kinugasa et al[10]	$R_m = 0.145\ W_o + 0.57$
Motlekar and Bhagwat[15]	$R_m = 0.15\ W_o$
Gaikar and Kulkarni[12]	$R_m = 0.164\ W_o$
Bru et al[11]	$R_m = 0.175\ W_o$
Geometrical Models	
Jolivalt et al [13]	$R_m =$ ———

Interfacial Association of Reverse Micelle: Figure 2 show that amoxicillin was an interfacial active molecule at every tested pH AOT /TWEEN 85 concentration 50 g/L, 80 g/L and 100 g/L. The measurement of surface activity depends on the slope of the graph. For the extraction condition of 80 g/L with pH 3.5 and 80 g/L with pH 7.5, the deviation of the data plot was farther from the 45° line which indicates that the surface activity was the highest, while the least surface activity was determined at extraction condition of pH 7.5 and 100 g/L.

Furthermore, the solubilisation behaviour of the amoxicillin can also be shown by the plot of molecule transfer t_a versus the fractional water transfer t_w to the organic phase as demonstrated in figure 3. The same trend was found since the data distribution at all tested surfactant concentration and pH was deviated far from the 45° line, indicating that the amoxicillin molecules were interfacially active with the presence of AOT and TWEEN 85 surfactant.

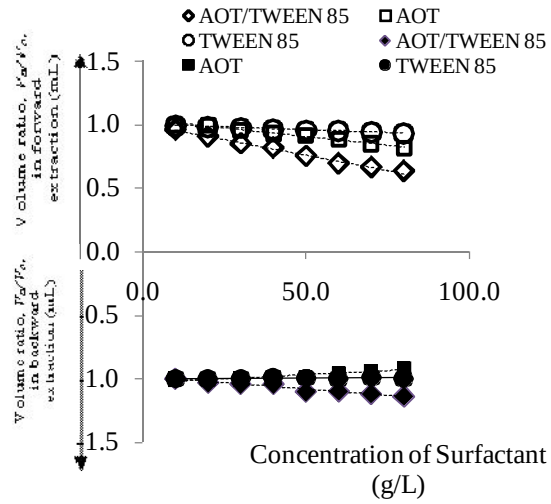

Figure 1: Effects of volume ratio of the phases, V_a/V_o at varied concentrations

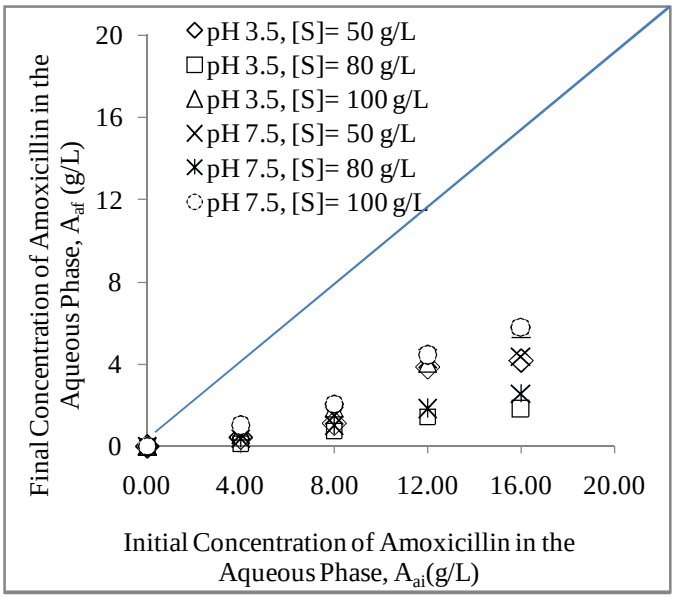

Figure 2: Final amoxicillin concentrations in the aqueous phase against the initial amoxicillin concentration before forward extraction

Moreover, through this graph, it was shown that the interfacial association is strongly dependent on both AOT/TWEEN 85 concentration and pH of fresh aqueous phase, since the deviation of data plotted for pH 3.5 and 80 g/L was further from the 45° line than the data plotted with pH 7.5 and 100 g/L. It indicates that at this extraction condition, the solubilisation of amoxicillin molecules from an aqueous into an organic phase was more favourable and the activities of amoxicillin molecule at interfaces were the highest among others.

Water Content Determination: Previous studies reported

that W_o strongly influenced the solubilisation of bio-molecule and their characteristics of reverse micelle mixtures [2, 7]. Figure 4 shows the change of water content in reverse micellar phase with mixed AOT/TWEEN 85 concentration. The W_o after extraction process (filled with amoxicillin) sharply increased from mixed surfactant concentration 5 g/L until 80 g/L and the decrease in water content from 33.87 to 9.62 was observed as the concentration was further increased from 90 to 100 g/L respectively. The increase of W_0 seemed to reflect the formations of new reverse micelles with the same size kept increasing in organic phase.

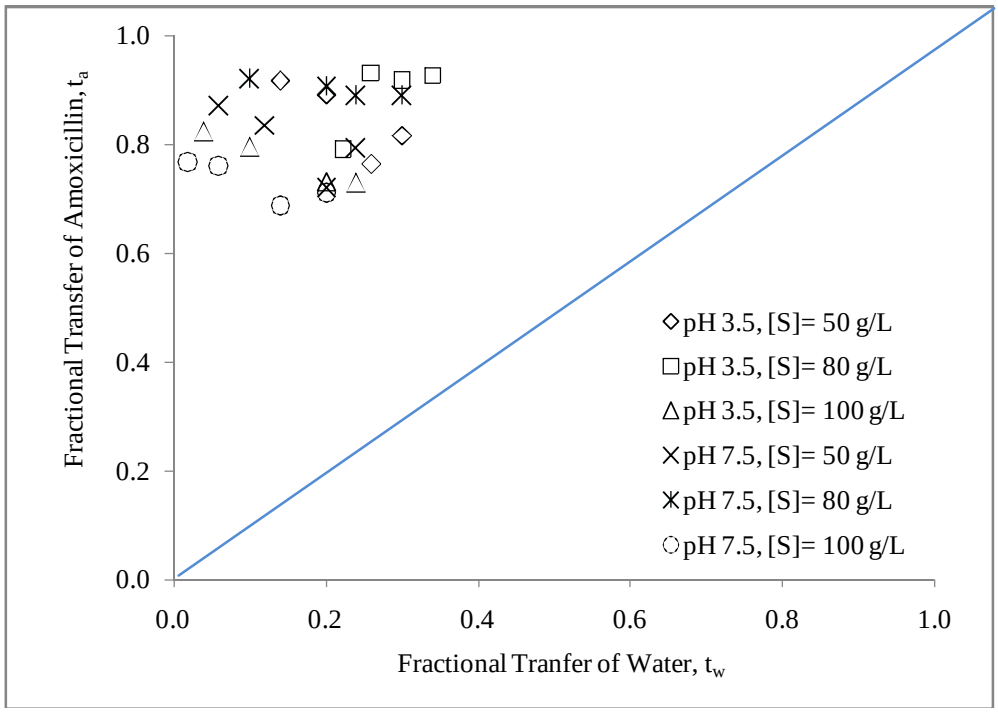

Figure 3: Amoxicillin transfer t_a versus the fractional water transfer, t_w at various surfactant concentration and aqueous pH

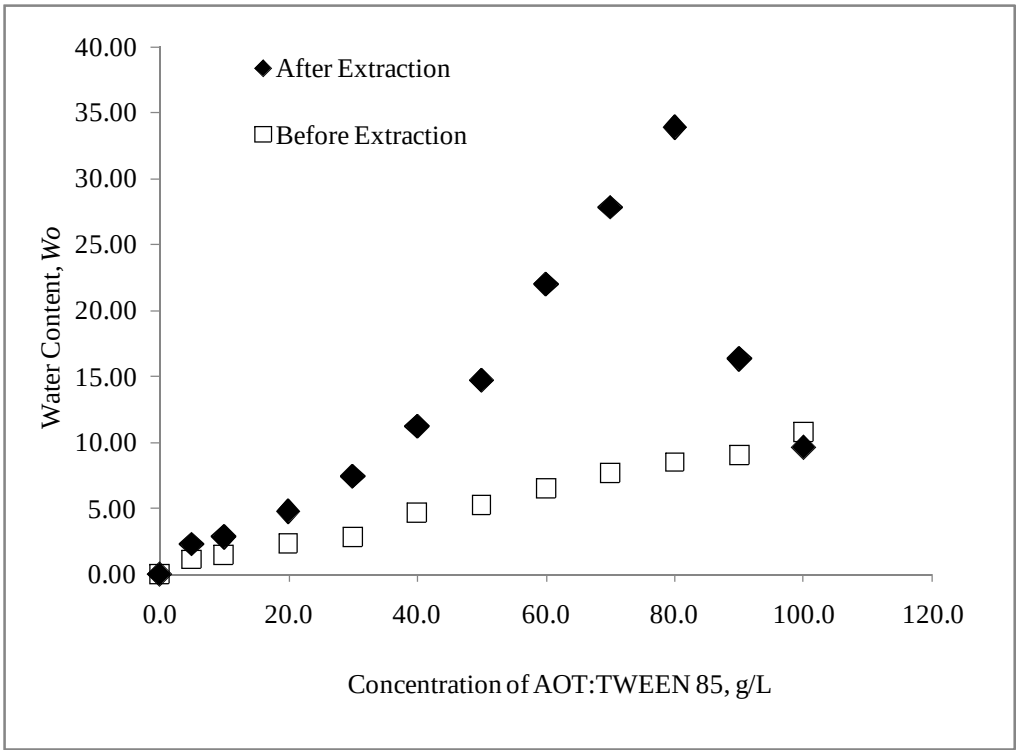

Figure 4: Effect of mixed AOT/TWEEN 85 concentration on water content in reverse micellar phase

For water content before extraction, the values of W_o were increased and directly proportional to the AOT/TWEEN 85 concentration from 0 to 100 g/L. This increase would contain the water uptake by the exchange of the counter ion of mixed AOT/TWEEN 85. In addition, the value of W_o after extraction process was higher than the W_o before the extraction process. A similar trend also had been observed by Ichikawa et al[8] since it was reported that the amount of solubilised water containing protein was found to be more than in protein free system due to the presence of extracted protein in the reversed micelles. The addition of co-surfactant frequently offer rise to boost performance over the individual components for a wide variety of applications[4, 9].

Estimation Size of Reverse Micelles: Reverse micellar radius (R_m) is one of influential parameter that determines the selectivity in solubilisation and water content and has been sparingly reported by previous researches in forward extraction[1]. It was observed that the entire models proposed resulted in bigger size of R_m for reverse micelle after extraction (AF) compared to R_m for reverse micelle before extraction (BF), except for the concentration of AOT/TWEEN 85, 100 g/L (Table 2-7), since the amoxicillin molecules were solubilised and located in the empty reverse micelle core after the extraction had been carried out. The model proposed by Kinugasa et al[10] and Bru et al[11] gave relatively highest values of R_m before extraction, 0.91 nm-2.14 nm and 0.41 nm-1.89 nm and after extraction, 1.26 nm-1.97 nm and 0.84 nm-1.68 nm respectively. This was due to the higher multiplication W_o factor and constant value of the model.

The results showed that the change of mixed AOT/TWEEN 85 concentration not only changed the number of reverse micelle, but seemed to increase the reverse micelle size before extraction and after extraction, except for the concentration of 100 g/L which was different from the reports by previous studies for single surfactant.[12] The presence of non-ionic surfactant in the organic chain increases its EO chain length of the surfactant, hence raising the radius of the micelle droplets.[1]

The results of reverse micellar radius estimation illustrated a convincing verification of the above statement, indicating that the radius of a micelle droplet, R_m increased obviously as the non-ionic TWEEN 85 surfactants were added into the reverse micellar phase containing AOT/water/iso-octane. Therefore it could be concluded that the presence of TWEEN 85 in AOT/water/iso-octane modified the reverse micellar size. With more addition of non-ionic surfactant, the longer the EO chains would be, the droplet of micellar radius would be bigger.

The results for empirical model proposed by Bru et al[13] were found to be closer with the values of geometrical model reported by Jolivalt et al[13] and both model resulted in relatively bigger size R_m compared to other models for the condition after extraction.

Table 2
Estimation of reverse micellar size using empirical model[14]

AOT/TWEEN 85, g/L	Water Content, W_o		Reverse Micellar Size, R_m (nm)	
	Before Extraction	After Extraction	Before Extraction	After Extraction
20.0	2.32	4.78	0.32	0.66
40.0	4.68	11.23	0.65	1.55
60.0	6.53	21.99	0.90	3.03
80.0	8.49	33.87	1.17	4.67
100.0	10.82	9.62	1.49	1.32

Table 3
Estimation of reverse micellar size using empirical model[10]

AOT/TWEEN 85, g/L	Water Content, W_o		Reverse Micellar Size, R_m (nm)	
	Before Extraction	After Extraction	Before Extraction	After Extraction
20.0	2.32	4.78	0.91	1.26
40.0	4.68	11.23	1.25	2.19
60.0	6.53	21.99	1.52	3.76
80.0	8.49	33.87	1.80	5.48
100.0	10.82	9.62	2.14	1.97

Table 4
Estimation of reverse micellar size Using empirical model[15]

AOT/TWEEN 85, g/L	Water Content, W_o		Reverse Micellar Size, R_m (nm)	
	BE	AE	BE	AE
20.0	2.32	4.78	0.35	0.72
40.0	4.68	11.23	0.70	1.69
60.0	6.53	21.99	0.98	3.29
80.0	8.49	33.87	1.27	5.08
100.0	10.82	9.62	1.62	1.44

Table 5
Estimation of reverse micellar size using empirical model[12]

AOT/TWEEN 85, g/L	Water Content, W_o		Reverse Micellar Size, R_m (nm)	
	BE	AE	BE	AE
20.0	2.32	4.78	0.38	0.78
40.0	4.68	11.23	0.77	1.84
60.0	6.53	21.99	1.07	3.61
80.0	8.49	33.87	1.39	5.56
100.0	10.82	9.62	1.77	1.58

Table 6
Estimation of reverse micellar size using empirical model[11]

AOT/TWEEN 85, g/L	Water Content, W_o		Reverse Micellar Size, R_m (nm)	
	BE	AE	BE	AE
20.0	2.32	4.78	0.41	0.84
40.0	4.68	11.23	0.82	1.97
60.0	6.53	21.99	1.14	3.85
80.0	8.49	33.87	1.49	5.93
100.0	10.82	9.62	1.89	1.68

Table 7
Estimation of reverse micellar size using geometrical model[13]

AOT/TWEEN 85, g/L	Water Content, W_o		Reverse Micellar Size, R_m (nm)	
	BE	AE	BE	AE
20.0	2.32	4.78	0.41	0.84
40.0	4.68	11.23	0.83	1.98
60.0	6.53	21.99	1.15	3.88
80.0	8.49	33.87	1.49	5.97
100.0	10.82	9.62	1.91	1.69

In order to derive the empirical relationship for mixed AOT/TWEEN 85 reverse micelle a plot of R_m at different values W_o is shown in figure 5. Models from previous studies focused more on the single surfactant only,[10,14-16] therefore it is important to develop the empirical model of mixed reverse micelle radius in order to understand the relationship between W_o in the organic phase and R_m for mixed reverse micellar. The correlation between R_m and W_o for condition before extraction and after extraction is given below:

$R_m = 0.176\ W_o - 5 \times 10^{-6}$, after extraction (1)
$R_m = 0.173\ W_o - 0.004$, before extraction (2)

Both equations obtained were observed to be similar to the model proposed by Bru et al[11] ($R_m = 0.175\ W_o$). In order to validate the empirical equation developed from previous model, a parity plot of predicted values versus estimated value was constructed as shown in figure 6. The predicted and estimated values for R_m showed an excellent fit with $R^2 = 1$ and $R^2 = 0.998$ for both conditions for before extraction and after extraction.

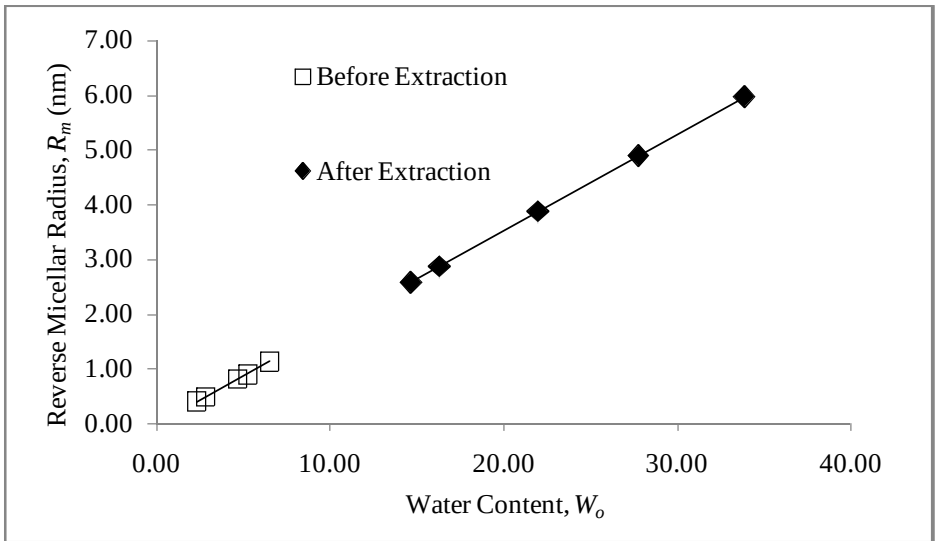

Figure 5: Variation of reverse micellar size with different water content

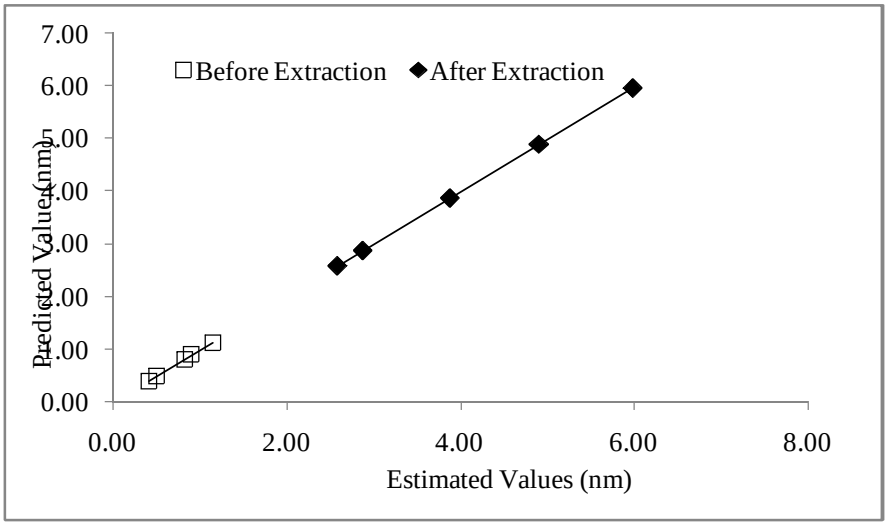

Figure 6: Parity plot for estimation of reverse micelle radius

Conclusion

The solubilisation of water by using mixed AOT/TWEEN 85 reverse micelles was investigated. Mixed reverse micelle was able to solubilise a high amount of water compared with single surfactant alone. Amoxicillin also was found to be interfacially active at every tested pH and mixed AOT/TWEEN 85 surfactant concentration. All the models predicted a bigger size of the filled reverse micelles as compared to that of the unfilled ones. The empirical model obtained showed a good correlation ($R^2 = 1$ and $R^2 = 0.998$) for both conditions for before extraction and after extraction between the estimated and the predicted values.

Acknowledgement

The authors are grateful to Ministry of Science, Technology and Innovation (MOSTI) grants no. R.J130000.7944.4S020 and Universiti Teknologi Malaysia for financial support.

References

1. Liu D., Ma J., Cheng H. and Zhao Z., *Colloids and Surfaces A: Physicochemical and Engineering Aspects*, **143**, 59-68 **(1998)**

2. Tonova K. and Lazarova Z., *Biotechnology Advances*, **26**, 516–532 **(2008)**

3. Mohd-Setapar S. H., Wakeman R. J. and Tarleton E. S., *Chemical Engineering Research and Design*, **87**, 883-842 **(2009)**

4. Hemavathi A. B., Umesh Hebbar H. and Raghavarao K. S. M. S., *Separation and Purification Technology*, **71**, 263–268 **(2010)**

5. Mohd-Setapar S. H.**,** Mohamad-Aziz S. N., Harun N. H. and Hussin H., *Advanced Materials Research*, **545,** 240-244 **(2012a)**

6. Mohd-Setapar S. H., Mohamad-Aziz S. N. and Joannes C., *Jurnal Teknologi*, **58**, 7-11 **(2012b)**

7. Mitra R. K. and Paul B. K., *Colloids and Surfaces A: Physicochem. Eng. Aspects*, **252**, 243-259 **(2005)**

8. Ichikawa S., Imai M. and Shimazu M., *Biotechnol. Bioeng.*, **355**, 843 **(1992)**

9. Goto M., Ishikawa Y., Ono T., Nakashio F. and T. A. Hatton, *Biotechnol. Prog.*, **14**, 729-734 **(1998)**

10. Kinugasa T., Kondo A., Mouri E., Ichikawa S., Nakagawa S., Nishii Y., Watanabe K. and Takeuchi H., *Sep. Purif. Technol.*, **31**, 251 **(2003)**

11. Bru R., Sanchez-Ferrer A. and Garcia-Carmona F. A., *Biochem. J.*, **259**, 355 **(1989)**

12. Gaikaiwari R. P., Wagh S. A. and Kulkarni B. D., *Bioresource Technology*, **108**, 224-230 **(2012)**

13. Jolivalt C., Minier M. and Renon H., *Biotechnol. Prog.*, **9,** 456 **(1993)**

14. Hebbar H. U., Hemavathi A. B., Sumana B. and Raghavarao K. S. M. S., *Separation Science and Technology*, **46**, 1656-1664 **(2011)**

15. Motlekar N. A. and Bhagwat S. S., *J. Chem. Technol. Biotechnol.*, **76**, 643 **(2001)**

16. Gaikar V. G. and Kulkarni M. S., *J. Chem. Technol. Biotechnol.*, **76**, 729 **(2001).**

(Received 12th April 2013, accepted 22nd June 2013)

Development and Validation of Analytical Method for Zidovudine, Lamivudine and Nevirapine by HPLC

Arun R.[1] and Anton Smith A.[2]*
1. Karpagam University, Pollachi Main Road, Eachanari Post, Coimbatore, Tamil Nadu, INDIA
2. Department of Pharmacy, Annamalai University, Annamalai Nagar, Tamil Nadu, INDIA
*auantonsmith@yahoo.co.in

Abstract

This paper describes the development and validation of a HPLC method (216nm) for the quantitation of Zidovudine, Lamivudine and Nevirapine in pure form for pharmaceutical formulations. The method showed to be linear (r^2 > 0.999), precise (R.S.D. < 0.80%), accurate (recovery of 100.95% for Zidovudine, 100.73 % for Lamivudine and 99.94% for Nevirapine), specific and robust. Three batches of Zidovudine, Lamivudine, Nevirapine tablets were assayed by the validated method. The Zidovudine contents in the tablets samples varied from 99.82 to 101.43%, The Lamivudine content in the tablets samples varied from 99.28 to 101.24% while Nevirapine content varied from 100.56 to 101.35%.

The developed method showed to be a simple and suitable technique to quantify the antiretroviral and might be employed for quality control analysis, as well as in other matrices, such as plasma. The ZID, LAM, NEV tablets analyzed by the validated method showed adequate quality and drug contents in concordance with the labeled amount.

Keywords: Zidovudine, Lamivudine, Nevirapine, Antiretro viral, HPLC-UV.

Introduction

Human Immunodeficiency Virus (HIV) has been one of the most devastating diseases affecting a large pediatric and adult population of the world. Due to the development thereafter of various antiretrovirals, it led to the significant decrease in the morbidity and mortality rates of the HIV infected population. The standard antiretroviral (ARV) therapy in treatment of these HIV-infections entails the use of combination drug therapy, usually a triple combination such as two-nucleoside or nucleotide reverse transcriptase inhibitors (NRTIs) as a backbone and a non-nucleoside reverse transcriptase inhibitor (NNRTI) [7].

Out of existing various ARV drugs currently recommended by World Health Organization for HIV infection in pediatric population in resource limited countries, the combination of zidovudine (ZID)/lamivudine(LAM) (NRTI backbone) and nevirapine(NEV) (NNRTI) is considered as one of the preferred ARV treatment[20,21].

Chemically LAM is (4-amino-1-[(2R,5S)-2-(hydroxymethyl)- 1, 3-oxathio-lan-5-yl]1, 2dihydro pyrimi dine- 2-one) (3TC) and ZID is (1-[(2R,4S,5S)-4-azido-5-(hydroxymethyl) oxolan-2-yl]-5-methyl- 1,2,3,4-tetrahydropyrimidine-2,4-dione) (Figure 1).

Both the nucleoside analogues were possessing potent inhibitory activities against HIV reverse transcriptase. They are phosphorylated by kinases into the triphosphates, they are in pharmacologically active form. Chain termination is carried out by the active metabolite which is incorporated into HIV DNA acting as a competitive inhibitor of reverse transcriptase. NEV is chemically 11-cyclopropoyl-5, 11-dihydro- 4-methyl-6H-dipyrido [3, 2-b: 2', 3'-e][1,4] diazepin-6-one (Figure 1). It is a non-competitive inhibitor DNA and RNA dependent polymerase that binds to a distant site from the reverse transcriptase enzymes active site HIV-1 RNA to induce a conformational change at the active site and disrupt catalytic activity of the virus to transcribe viral RNA into DNA[3].

Numerous analytical methods such as high performance liquid chromatography (HPLC) with UV detection[15, 18], mass spectrometry detection[11] and radioimmunoassay[13,17] have been reported for either ZID/LAM. Some authors have described the analysis of ZID/LAM/NEV in plasma based on HPLC[5, 6, 19], stability indicating[4]. Some authors have described the analysis of ZID/LAM/NEV in plasma and fixed dose combinations based on HPLC, HPTLC[1,2,4-6,8-10,12,14,16,19]. Even though, there some methods reported regarding the quantitation of ZID, LAM and NEV in pure form and pharmaceutical formulations, the run time of those methods is more than 10 min, which raises cost of the mobile phase.

Hence, the aim of this study was to develop and validate a HPLC method, using UV detection to quantify ZID, LAM, and NEV in pure form for pharmaceutical formulations. Molar absorptivity of ZID, LAM and NEV in the UV region was found to be at 216nm. The validated method was applied to the analysis of tablets containing ZID, LAM and NEV (300+150+200 mg).

Material and Methods

Reagents and Materials: ZID, LAM, NEV reference standards were purchased from Cipla Laboratories, Mumbai. Tablets for analysis were obtained from local pharmacies. Ultra-pure water was obtained from a Millipore system (Bedford, MA, USA). Methanol (HPLC grade) was obtained from E. Merck **(**India**)** Ltd. All other chemicals used in the analysis were AR grade.

Instrumental and analytical conditions: The HPLC analyses were carried out on Waters 2695 separation module (Waters Corporation, USA) equipped with auto sampler and Waters 2998 PDA detector, Kromasil C8 (150 × 4.6mm, 5µm) column. UV spectra scanning from 190 to 400 nm were online recorded for peak identification and the detection was performed at 216 nm. The injection volume of sample was 10 µl. An isocratic mobile phase containing methanol and buffer (32:68), at the pH 2.6 was carried out with the flow rate of 1ml/min. The separation of ZID, LAM and NEV was evaluated in different proportions of this mobile phase and for each condition, retention factor (k) and resolution (R) were calculated.

Preparation of buffer (pH 2.6): Accurately weighed 0.70 g of potassium dihydrogen phosphate and 1.0 g of Octane sulphonic acid salt were dissolved in 1000 ml of water. 1 ml of triethylamine was added and the pH of the solution was adjusted to 2.6 with orthophosphoric acid. Further the solution was filtered through 0.45 µm membrane filter.

Preparation of standard solution: Approximately 300.0 mg of ZID, 150.0 mg of LAM, 200 mg of NEV reference standards were accurately weighed and transferred to a 50 ml volumetric flask, 20 ml of methanol was added to ensure the complete solubilisation and the volume was adjusted with the mobile phase. Further dilutions were made to get the final concentration of 0.15 mg/ml of ZID, 0.075 mg/ml of LAM and 0.1mg/ml of NEV.

Analysis of fixed dose combination tablets: Three different batches of tablets were analyzed using the validated method. ZID, LAM, NEV standard was added to the samples, with the aim of increasing the peak area of ZID, LAM, NEV in the chromatograms and thereby improving the detection of this compound. For the analysis, six replicates of each batch were assayed. The tablets were weighed and finely powdered. Equivalent to about 300.0 mg of ZID, 150.0 mg of LAM and 200.0 mg of NEV of the powder were accurately weighed and transferred to a 500 ml volumetric flask followed by the addition of 250 ml of methanol. The solution was sonicated for 30 minutes and diluted with mobile phase to volume. Further dilutions were made to get the final concentration equivalent to 0.15 mg/ml of ZID, 0.075 mg/ml of LAM and 0.1mg/ml of NEV.

Validation

Linearity: Standard solutions containing 0.15 mg/ml of ZID, 0.75 mg/ml of LAM and 0.1mg of NEV were prepared in triplicate. Aliquots of the above solutions were diluted in mobile phase to six different concentrations, corresponding to 80, 100, 120, 140, 160 and 180 mg/ml of ZID, LAM and NEV. Calibration curves for concentration versus peak area were plotted for ZID, LAM and NEV obtained data subjected to regression analysis using the least squares method with a weighting factor of 1/*x*.

Precision: The intra-day precision was evaluated by analyzing six sample solutions (n = 6), at the final concentration of analyses (150 µg/ml) of ZID, (75 µg/ml) of LAM and (100 µg/ml) of NEV. Similarly the inter-day precision was evaluated in three consecutive days (n=18). The ZID, LAM, NEV concentrations were determined and the relative standard deviations (R.S.D) were calculated.

Accuracy: ZID, LAM, NEV reference standards were accurately weighed and added to a mixture of the tablets excipients, at three different concentration levels (80, 100 and 120 % of ZID, LAM and NEV). At each level, samples were prepared in triplicate and the recovery percentage was determined.

Specificity: Spectral purities of ZID, LAM, NEV chromatographic peaks were evaluated using the UV spectra recorded by a UV detector. In addition, a solution containing a mixture of the tablets excipients was prepared using the sample preparation procedure and injected on to the chromatograph, to evaluate possible interfering peaks.

Robustness: Six sample solutions were prepared and analyzed under the established conditions and by variation of the following analytical parameters: flow rate of the mobile phase (0.9 and 1.1 ml/min), methanol and buffer as mobile phase (33.4:66.6, 32:68, 30.6:69.4), mobile phase pH (2.4, 2.8) and column temperature (25 and 35^{o}C). The ZID, LAM, NEV contents were determined for each condition and the obtained data were submitted for statistical analysis (ANOVA test)

Detection and quantitation limits: Limit of detection LOD (signal-to- noise ratio of 3) and limit of quantification LOQ (signal-to- noise ratio of 10) were measured based on the signal-to-noise ratio. Determination of the signal-to-noise is performed by comparing measured signals samples with known low concentration of analyte with those of blank samples establishing the minimum concentration at which the analyte can be reliably detected and quantified.

Results and Discussion

The chromatographic parameters were initially evaluated using a Kromasil C8 (150 × 4.6mm, 5µm) column and a mobile phase composed of methanol and buffer (32:68). Using this column, different proportions of mobile phase solvents were evaluated to obtain a good peak (Table 1). Under these conditions the retention factors obtained for ZID, LAM, and NEV were 3.13, 4.15 and 7.75 and a short run rime (10 min), and so, this condition was adopted in subsequent analysis (Fig. 2). After the evaluation of the ZID, LAM, NEV UV spectrum in the range of 190-400 nm, the wavelength of 216 nm was selected for detection due to the adequate molar absorptivity of ZID, LAM, NEV in this region and the higher selectivity of this wavelength regarding possible interfering compounds or solvents in the sample.

Validation

Linearity: A linear correlation was found between the peak areas and the concentrations of ZID, LAM and NEV in the assayed range. The regression analysis data were presented in table 2. The regression coefficients (r^2) obtained was higher than 0.999 for both compounds (Fig. 3) which attest the linearity of the method.

Precision: Mean contents of ZID, LAM, NEV in the intra-day precision analysis (n = 6) were 150 µg/ml (R.S.D = 0.66%), 75 µg/ml (R.S.D = 0.68%) and 100 µg/ml (R.S.D = 0.32%) respectively. For the inter-day precision (n=18) the mean contents obtained were 150 µg/ml (R.S.D = 0.60%), 75 µg/ml (R.S.D = 0.62%) and 100 µg/ml (R.S.D = 0.37%) for ZID, LAM, NEV respectively. R.S.D values lower than 2.0% assure the precision of the method.

Accuracy: It was investigated by means of addition of ZID, LAM, NEV reference standards to a mixture of the tablets excipients. ZID mean recovery (n =9) was 100.50% (R.S.D. = 0.33 %), LAM mean recovery was 100.68% (R.S.D = 0.67%) and NEV mean recovery (n =9) was 100.17% (R.S.D. = 0.50 %) demonstrating the accuracy of the method.

Specificity: Peak purities higher than 99.0% were obtained for ZID, LAM and NEV in the chromatograms of sample solutions, proven that other compounds did not co-elute with the main peaks. The chromatogram obtained with the excipients in the capsule showed no interfering peaks in the same retention time of ZID, LAM and NEV.

Robustness: Statistical analysis showed no significant difference between results obtained employing the analytical conditions established for the method and those obtained in the experiments in which variations of some parameters were introduced. Thus, the method showed to be robust for changes in mobile phase flow rate 0.9 and 1.1 ml/min, methanol: buffer proportion (33.4:66.6, 32:68, 30.6:69.4), mobile phase pH (2.4 and 2.8) and column temperature (25 and 35^{o}C).

Detection and quantitation limits: According to the determined signal-to-noise ratio, ZID, LAM, NEV presented limits of detection of 0.32-0.2 µg/ml and limits of quantitation of 0.47-0.3µg/ml respectively where the compounds proportion was found in the sample solutions injected onto the chromatograph. However, the objective of the method is the quantitation of ZID, LAM, NEV, so that the values obtained for ZID, LAM, NEV should be considered as the limit of method sensitivity.

Analysis of fixed dose combination tablets: Samples of fixed dose combination tablets containing 300 mg of ZID, 150 mg of LAM and 200 mg of NEV were analyzed using the validated method. The results obtained were presented in table 3. All the analyzed batches presented ZID, LAM and NEV contents very close to the labeled amount. The ZID content in the tablets samples varied from 99.82 to 101.43%. The LAM content in the tablets samples varied from 99.28 to 101.24% while NEV content varied from 100.56 to 101.35%.

The development of simple and reliable method is essential to assure the identification and quantitative determination of antiretroviral drugs since the problem of counterfeit or substandard antiretroviral is well established all over the world. The quality control of the antiretroviral pharmaceutical preparations marketed nowadays may help to assure the treatment efficacy and avoid the development of resistance to antiretroviral drugs.

Conclusion

This study was the report of development and validation of ZID, LAM, and NEV in pure form for pharmaceutical formulations. The developed method showed to be a simple and suitable technique to quantify the antiretroviral and might be employed for quality control analysis as well as in other matrices, such as plasma. The ZID, LAM, NEV tablets analyzed by the validated method showed adequate quality and drug contents in concordance with the labeled amount.

References

1. Anand babu K. and Jayakar B., Analytical method development and validation for simultaneous estimation of lamivudine, zidovudine and nevirapine tablets by RP-HPLC, *Int. J Pharma .Res. Deve.,* **3(7),** 9-14 **(2011)**

2. Anantha Kumar D., Naveen Babu M.V., Seshagiri Rao J.V.L.N. and Jayathirtha Rao V., Simultaneous determination of lamivudine, zidovudine and nevirapine in tablet dosage forms by RP-HPLC method, *Rasayan J. Chem.,* **3(1),** 94-99 **(2010)**

3. Brunton L.L., Chabner B.A. and Knollmann B.C., Goodman and Gilman's The Pharmacological Basis of Therapeutics, 12th ed., Macmillan Publishing Co., New York **(2011)**

4. Dunge A., Sharda N., Singh B. and Singh S., Validated specific HPLC method for determination of zidovudine during stability studies, *J Pharm. Biomed. Anal.,* **37,** 1109-1114 **(2005)**

5. Fan B. and Stewart J.T., Determination of zidovudine/ lamivudine/ nevirapine in human plasma using ion-pair HPLC, *J Pharm. Biomed. Anal.,* **28(5),** 903-908 **(2001)**

6. Geetha Ramachandran A.K., Hemanthkumar V., Kumaraswami and Soumya Swaminathan, A simple and rapid liquid chromatography method for simultaneous Determination of zidovudine and nevirapine in plasma, *J. Chromatogr.* B, **843,** 339–344 **(2006)**

7. Guidelines for the use of Antiretroviral agents in Pediatric HIV infection, developed by working group on antiretroviral therapy and medical management of HIV infected children convened by the National resource center at the Francois Xavier bagnoud center, UMDJ, the health resources and services administration (HSRA) and the National Institutes of health **(2009)**

Table 1
Optimized chromatographic parameters for ZID, LAM, NEV using a Kromasil C8 (150 × 4.6mm, 5µm) column

Mobile phase composition Methanol:Buffer	Zidovudine Retention factor (K)	Lamivudine Retention factor (K)	Nevirapine Retention factor (K)	Resolution (R)
33.4:66.6	2.01	3.04	6.00	10.79
32:68	2.14	3.16	6.76	10.81
30.6:69.4	2.13	3.17	6.80	10.82

Table 2
Analytical parameter of the proposed method

Regression parameters	Zidovudine	Lamivudine	Nevirapine
Correlation coefficient (r^2)	0.999	0.999	0.999
Slope ± standard error	57063±0.04	38757± 0.096	112694±0.01
Intercept ± standard error (%)	-5.69 ±0.28	1.55±0.01	1.83±0.023
Concentration range(µg/ml) [a]	80-180	80-180	80-180
Number of points	6	6	6
Intra-day precision (RSD)	0.66%	0.68%	0.32%
Inter-day precision (RSD) [b]	0.60%	0.62%	0.37%
Accuracy (RSD)	0.33%	0.67%	0.50%
LOD µg/ml	0.32	0.2	0.28
LOQ µg/ml	1.065	0.666	0.932

Table 3
Contents of ZID, LAM and NEV in the fixed dose combination tablets (n=6)

Sample tablet Batch	Content (%) + S.D		
	Zidovudine	Lamivudine	Nevirapine
A	99.82±0.62	99.28 ±0.66	101.34 ±0.31
B	100.15±0.54	100.41±0.52	101.10±0.24
C	100.75±0.42	100.12 ±0.58	101.35±0.22

S.D.=Standard Deviation

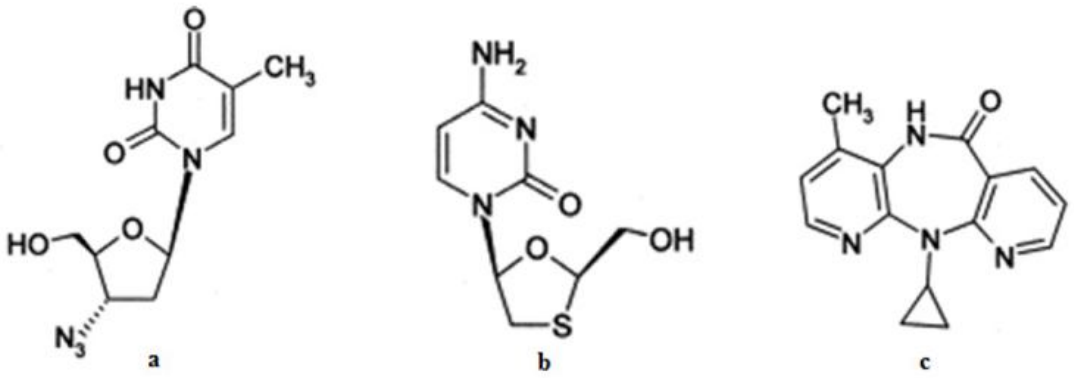

Fig. 1: Chemical structure of (a) Lamivudine (b) Zidovudine and (c) Nevirapine

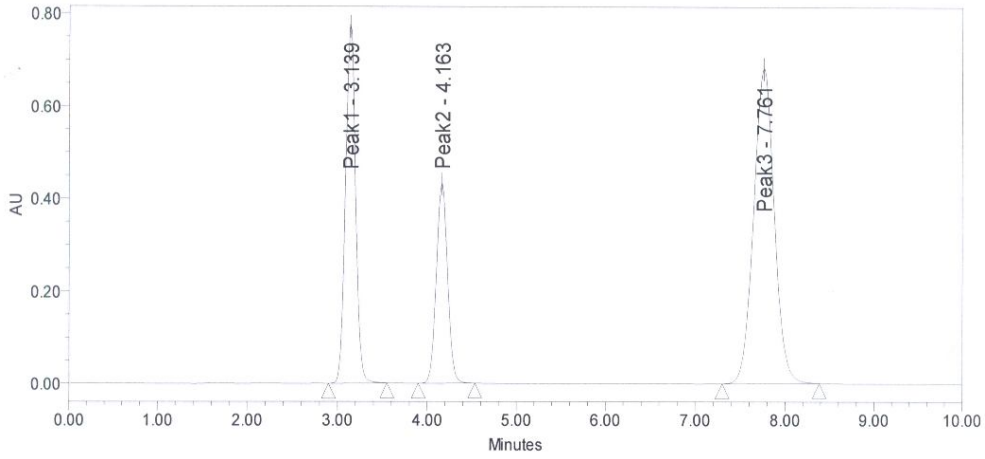

Fig. 2: Chromatogram of Zidovudine, Lamivudine and Nevirapine

8. Savic Ivan M., Nikolic Vesna D., Savic Ivana M., Nikolic Ljubisa B. and Stankovic Mihajlo Z., Development and validation of HPLC method for the determination of amygdalin in the plant extract of plum kernel, *Res. J. Chem. Environ.*, **16(4),** 80-86 **(2012)**

9. Joshi A. and Christianah Adeyeye M., Reversed Phase LC-UV Method Development and Validation for Simultaneous determination of three antiretroviral lamivudine, zidovudine, nevirapine and possible degradants in a Fixed Dose Pharmaceutical Product, *J. Pharma. Techno. Drug Res.*, **1,** 1-4 **(2012)**

10.Kapoor N., Khandavilli S. and Panchagnula R., Simultaneous determination of lamivudine, stavudine and nevirapine in antiretroviral fixed dose combinations by high performance liquid chromatography, *Analytica Chimica Acta,* **570 (1)**, 41-45 **(2006)**

11.Kenny K.B., Wring S.A., Carr R.M. and Wells G.N., Simultaneous determination of zidovudine and lamivudine in human serum using HPLC with tandem mass spectrometry, *J. Pharm. Biomed. Anal.*, **22**, 967–983 **(2000)**

12. Lavra Z.M.M., Neto P.J.R., Da Silva R.M.F. and De Medeiros F.P.M., Development and validation of an analytical method for simultaneous determination of fixed dose combination tablets of lamivudine, zidovudine and nevirapine by high performance liquid chromatography, *Quim. Nova.*, **31,** 969-74 **(2008)**

13 Mei J.V., Harry Hannon W. and Dobbs T.L., Radioimmunoassay for monitoring zidovudine in dried blood spot specimens, *Clin. Chem.*, **44,** 281-286 **(1998)**

14. Nandi U., Das A., Roy B., Choudhury H., Gorain B. and Pal T.K., Development and validation of an HPLC-UV method for simultaneous determination of zidovudine, lamivudine, and nevirapine in human plasma and its application to pharmacokinetic study in human volunteers, *Drug Test Anal*., doi: 10.1002/dta.419 **(2012)**

15. Sarkar M., Khandavilli S. and Panchagulla R., Development and validation of RP-HPLC and ultraviolet spectrophotometric methods of analysis for the quantitative estimation of antiretroviral drugs in pharmaceutical dosage forms, *J Chromatogr.* B, **830,** 349–354 **(2006)**

16. Solomon G., Hymete A., Mohamed A.M.I. and Bekhit A.A., HPTLC densitometric method development and validation for simultaneous determination of lamivudine, nevirapine and zidovudine in fixed dose combinations, *Thai. J. Pharm. Sci.*, **35**, 77-88 **(2010)**

17. Tadepalli S.M., Puckett L. and Jeal S., Differential assay of zidovudine and its glucuronide metabolite in serum and urine with a radioimmunoassay kit, *Clin. Chem.*, **36,** 897–900 **(1990)**

18. Venkatesh P., Lydia Smiley and Mahesh D., Simultaneous estimation of Zidovudine and Lamivudine tablets by RP-HPLC method, *Int. J. Chem.Tech. Res.*, **3,** 376-380 **(2011)**

19. Verweij-van Wissen C.P.W.G.M., Aarnoutse R.E. and Burger D.M., Simultaneous determination of the HIV nucleoside analogue reverse transcriptase inhibitors lamivudine, didanosine, stavudine, zidovudine and abacavir in human plasma by reversed phase high Performance liquid chromatography, *J. Chromatogr.* B, **816,** 121–129 **(2005)**

20. World Health Organization, Pediatric guideline on Antiretroviral therapy of HIV infection in infants and children in resource limited settings: towards universal access **(2006)**

21. World Health Organization, Towards universal access: scaling up priority HIV/AIDS interventions in the health sector: Progress Report **(2009).**

(Received 11th February 2013, accepted 18th April 2013)

Volumetric Properties, Viscosities and Refractive Indices of Aqueous Solutions of 2-Amino-2-methyl-1-propanol (AMP)

Murshid Ghulam,* Shariff Azmi Mohd, Bustam Muhammad Azmi and Ahmad Faizan
Department of Chemical Engineering, Universiti Teknologi PETRONAS, 31750 - Tronoh, Perak, MALAYSIA
*ghulam.murshid@petronas.com.my

Abstract

The physical properties such as density (ρ), viscosity (η) and refractive index (n_D) of aqueous solutions of 2-amino-2-methyl-1-propanol (AMP) were measured for the whole range of composition. The measurements were made over the temperature range of 303.15 K to 333.15 K. Excess molar volumes (V^E), viscosity deviations ($\Delta\eta$) and refractive index deviations (Δn_D) were calculated from the experimental results of density, viscosity, refractive index and correlated by using Redlich Kister equation. Partial molar volumes at infinite dilution were determined using apparent molar volumes. Excess molar volumes, viscosity deviations and refractive index deviations results show good interaction between water and AMP molecules.

Keywords: Sterically hindered amine, Excess molar volume, Viscosity deviation, Refractive index deviation, Redlich Kister equation.

Introduction

The acid gases such as carbon dioxide (CO_2) and hydrogen sulphide (H_2S) are removed from sour natural gas through amine based absorption process. The most frequently used amines around the globe are mono-ethanolamine (MEA), di-ethanolamine (DEA) and *N*-methyldiethanolamine (MDEA)[1]. There is a new emerging class of amines to overcome the limitations of primary, secondary and tertiary amines (Low CO_2 intake, high heat of regeneration) which is known as sterically hindered amine (SHA). Sterically hindered amines such as 2-Amino-2methyl-1-propanol (AMP) and 2-Amino-2-hydroxymethyl-1,3-propanediol (AHPD) contain bulkier substituent identified as most promising solvents due to lower stability of carbamate, higher CO_2 loading capacity and higher reactivity for CO_2.[7,8]

The knowledge of physical properties of solvents is important for process design, simulation, rate modeling and smooth operation of the acid gas removal system [9-11]. Literature review on physical properties of binary solutions of AMP shows that most of the work is published on ternary or quaternary systems with other amines[4-6,9-14]. However, the literature available on binary solutions of AMP is scarce and limited to certain concentrations and temperatures[2,17-18]. Therefore densities, excess molar volumes, viscosities, viscosity deviations, refractive index and refractive index deviations are important to understand the intermolecular interactions and in designing of acid gas removal system. All the properties were measured for whole range of AMP composition and over the wide range of temperature from 298.15 K to 333.15 K. All the measured properties were correlated using Redlich Kister type of equation.

Material and Methods

Materials: AMP with purity of 95 % was purchased from Merck, Malaysia and it was used without further purification. All the aqueous solutions were prepared with the water of Milipore quality and concentrations of all solutions were reported gravimetrically (Mettler Toledo AS120S) with a measuring accuracy of ±0.0001 g. All the concentrations were also verified by titration with 0.5 M HCl using methyl orange indicator and the concentrations were accurate within ± 0.1 %.

Apparatus and Procedure: A digital vibrating glass U-tube densitometer (DMA 5000, Anton Paar) with the measuring accuracy of ± 1.0 x 10^{-5} g·cm^{-3} was used to measure the density of binary solutions of AMP. The details of the measuring methods and calibration procedures can be found in our previous work.[11] All the densities were measured at a temperature range of (298.15 to 333.15) K with a temperature controlled accuracy of ± 0.01 K (PT 100). The experimental uncertainty of measured density at corresponding temperature was estimated to be as 3.0 x 10^{-5} g·cm^{-3} and ± 0.02 K.

Kinematic viscosities were measured by using calibrated Ubbelohde viscometers of various sizes. The viscometers containing aqueous solutions were kept in the water bath for at least 15 minutes before any measurements were made in order to attain the desired temperature[11]. The efflux time was measured using a manual stop watch with an accuracy of ± 0.01 s. The kinematic viscosities were reproducible within ± 1 %. Refractive indices of aqueous solutions were measured using digital refractometer (Atago, RX-5000 alpha) covering the range of temperature from 303.15 K to 333.15 K with a measuring accuracy of 4.0 x10^{-5}. The reported values are the averages of three measurements and the measured experimental uncertainty at a given temperature was found to be 5.0 x 10^{-5} and 0.05 K respectively.

Results and Discussion

The experimentally measured densities of aqueous

solutions of AMP for whole range of composition are presented in table 1 and illustrated in fig. 1. Densities of pure AMP were compared with literature[2,4,17] and good agreement was found between the values of this work and literature with % average absolute deviations (%AAD) of 0.06, 0.1 and 0.24 (%) respectively as shown in table 2. It can be observed from fig. 1 that there is a decrease in density values while increasing AMP concentration into water. This is also in agreement with literature. The measured densities were used to calculate excess molar volume V^E as

$$V^E / cm^{-3} \cdot mol^{-1} = V_m - (x_1 V_1 + x_2 V_2) \quad (2)$$

$$V_m = (x_1 M_1 + x_2 M_2) / \rho \quad (3)$$

where V_m is the molar volume, x_1, x_2, V_1, V_2 *and* M_1, M_2 are mole fractions, molar volume and molecular weight of pure component water and AMP respectively. The values of excess molar volumes are presented in table 2 and illustrated in fig. 3. It can be observed from fig. 3 that excess molar volume shows negative deviations from the ideality at all temperatures studied in this work which is a common property of all miscible solvents with a minimum value 40 mol %. This indicates that there is a volume contraction. This volume contraction could be due to the formation of hydrogen bonds of –OH group with water molecules[19,20]. Excess molar volumes (V^E) also show sharp change in water rich region. Excess molar volume (V^E) values become less negative with increasing temperature. This could be due to the decrease in self association and cross association interaction of h-bonds. The excess molar volumes were correlated by using the following Redlich Kister equation:[21]

$$V^E / cm^3 \cdot mol^{-1} = x_1 x_2 \sum_{i=0}^{n} a_i (x_1 - x_2)^i \quad (4)$$

Parameters of the above equation are presented in table 3 along with the standard deviations. The standard deviations (SD) were calculated as:

$$SD = \left[\sum_{i}^{n} (Z_{exptl} - Z_{calcd})^2 / n \right]^{1/2} \quad (5)$$

where *SD* represents standard deviations, Z_{exptl} represents measured excess molar volume, Z_{calcd} represents calculated excess molar volumes and *n* represents the total number of data points. Partial molar volumes of AMP in water at infinite dilution (x_2 = 0) were calculated using the following equation as suggested by Hawrylak et al.[20]

$$\bar{V}_2^{\,o} = V_2 + \sum_{i=0}^{n} A_i \quad (6)$$

The partial molar volumes of AMP in water at infinite dilution ($\bar{V}_2^{\,o}$) increase with increasing temperature as shown in table 4. All excess molar volume values of AMP at infinite dilution in water were found to be lower than that of molar volume of pure AMP as shown in table 4. This could be due to the fitting of AMP molecules into open or empty spaces in water[22].

Viscosity values of aqueous solutions of AMP are presented in table 5 as a function of mole fraction and temperature. Measurements were made over the temperature range of 303.15 K to 333.15 K and compared with literature[4,17] as presented in table 2 with % AAD of 4.21 and 2.95 (%) respectively. Figure 4 shows S-shape curve for viscosity values with maximum value in AMP rich region. A sharp increase in viscosity values can be observed with addition of AMP after 40 mol % and it decreases with increasing temperature. S-shape curve of viscosity values shows that there is a formation of stable complexes with water molecules[23]. The measured viscosity values were used to calculate the viscosity deviation ($\Delta\eta$) by the following equation;

$$\Delta\eta = \eta - \eta_1 x_1 - \eta_2 x_2 \quad (7)$$

where η is the viscosity of mixtures, η_1, η_2, x_1, x_2 are viscosity and mole fraction of pure component water and AMP respectively.

The $\Delta\eta$ values are presented in table 6. Viscosity deviations of aqueous AMP are negative with a minimum of 20 mol % and maximum of 40 mol % as shown in fig. 5. It becomes positive after 40 mol % with a maximum of 70 mol % for all temperatures and mole fractions. This is a normal behavior for all types of amines. The calculated values of $\Delta\eta$ were fit to Redlich Kister relation as follows:

$$\Delta\eta / mPa \cdot s = x_1 x_2 \sum_{i=0}^{n} a_i (x_1 - x_2)^i \quad (8)$$

where x_1 and x_2 are the mole fractions of pure components water and AMP. Parameters of the above equation are presented in table 7 along with the standard deviations (SD).

The experimentally measured values of refractive index (n_D) are presented in table 8 as a function of temperature and mole fractions. The measurements were made for entire range of concentration and at temperature range of 303.15 K to 333.15 K. Refractive index values increase while increasing AMP concentration in water. However, it decreases with increasing temperature as shown in fig. 6. The measure n_D values were used to calculate the deviation of refractive index (Δn_D) by the following equation and presented in table 9:

$$\Delta n_D = n_D - n_{D_1} x_1 - n_{D_2} x_2 \quad (9)$$

where n_D is the refractive index of mixtures, n_{D1}, n_{D2}, x_1, x_2 is refractive indices and mole fraction of pure component

water and AMP respectively. The Δn_D values were fitted to the Redlich Kister equation:

$$\Delta n_D = x_1 x_2 \sum_{i=0}^{n} a_i (x_1 - x_2)^i \quad (10)$$

where x_1 and x_2 are the mole fractions of pure components water and AMP. Parameters of the above equation are presented in table 10 along with standard deviations (SD).

It can be observed from figure 7 that all values of Δn_D exhibit positive deviations. Since the values of V^E are negative and all Δn_D values are positive, it shows good molecular interaction between AMP and water molecules[24].

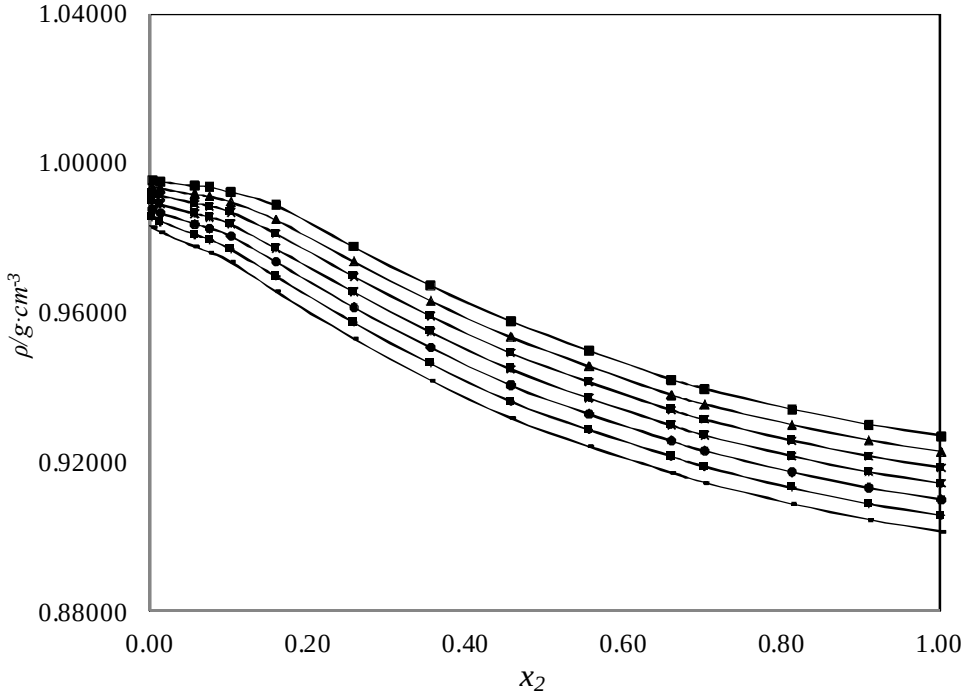

Figure 1: Densities of water (1) + AMP (2) at various temperatures: □, 303.15 K; Δ, 308.15K; ×, 313.15 K; * 318.15 K; ○, 323.15 K; +, 328.15 K, -, 333.15 K

Table 1
Density of mixtures of Water (1) + AMP (2) at various Temperatures

	ρ/ g·cm^{-3}						
x_2	**303.15**	**308.15**	**313.15**	**318.15**	**323.15**	**328.15**	**333.15**
0.0000	0.99571	0.99409	0.99228	0.99028	0.98806	0.98576	0.98327
0.0105	0.99528	0.99349	0.99149	0.98932	0.98694	0.98450	0.98187
0.0539	0.99422	0.99190	0.98939	0.98675	0.98394	0.98102	0.97797
0.0728	0.99390	0.99137	0.98863	0.98577	0.98277	0.97968	0.97645
0.1000	0.99246	0.98990	0.98707	0.98403	0.98076	0.97716	0.97394
0.1571	0.98901	0.98522	0.98139	0.97751	0.97390	0.96990	0.96606
0.2559	0.97798	0.97398	0.96994	0.96586	0.96168	0.95756	0.95335
0.3532	0.96749	0.96346	0.95939	0.95521	0.95100	0.94664	0.94225
0.4546	0.95797	0.95376	0.94950	0.94520	0.94089	0.93652	0.93212
0.5537	0.95010	0.94592	0.94170	0.93748	0.93322	0.92893	0.92454
0.6580	0.94234	0.93826	0.93426	0.93024	0.92603	0.92190	0.91754
0.7001	0.93981	0.93570	0.93168	0.92751	0.92334	0.91910	0.91484
0.8108	0.93429	0.93021	0.92608	0.92191	0.91770	0.91345	0.90916
0.9082	0.93018	0.92605	0.92188	0.91769	0.91346	0.90919	0.90490
1.0000	0.92712	0.92298	0.91880	0.91459	0.91035	0.90606	0.90175

Table 2
Comparison of the viscosity and density values of pure AMP with literature

	Ref. 4	**Ref. 17**	**This work**		**Ref. 4**	**Ref. 17**	**Ref. 2**	**This work**
T/K	***η*/mPa.s**				***ρ*/g·cm^{-3}**			
313.15			43.7		0.9179	0.91965		0.9188
323.15	24.21	24.21	23.05		0.9096	0.91124	0.9062	0.9103
333.15	13.99	13.99	14.5		0.9011	0.90287	0.897	0.9018

Table 3
Excess molar volume of mixtures of Water (1) + AMP (2) at various Temperatures

	V^E/cm^{-3} ·mol^{-1}						
x_2	**303.15**	**308.15**	**313.15**	**318.15**	**323.15**	**328.15**	**333.15**
0.0000	0.0000	0.0000	0.0000	0.0000	0.0000	0.0000	0.0000
0.0105	-0.0615	-0.0612	-0.0605	-0.0600	-0.0595	-0.0593	-0.0590
0.0539	-0.3241	-0.3237	-0.3229	-0.3226	-0.3225	-0.3216	-0.3213
0.0728	-0.4399	-0.4390	-0.4369	-0.4354	-0.4345	-0.4332	-0.4321
0.1000	-0.5799	-0.5840	-0.5850	-0.5841	-0.5811	-0.5714	-0.5751
0.1571	-0.8422	-0.8212	-0.8025	-0.7856	-0.7807	-0.7657	-0.7590
0.2559	-1.0357	-1.0157	-0.9979	-0.9818	-0.9654	-0.9537	-0.9415
0.3532	-1.0760	-1.0604	-1.0472	-1.0321	-1.0190	-1.0011	-0.9849
0.4546	-1.0195	-0.9994	-0.9804	-0.9623	-0.9469	-0.9310	-0.9163
0.5537	-0.9005	-0.8852	-0.8714	-0.8607	-0.8509	-0.8422	-0.8299
0.6580	-0.6719	-0.6663	-0.6711	-0.6777	-0.6737	-0.6793	-0.6705
0.7001	-0.5869	-0.5804	-0.5853	-0.5814	-0.5814	-0.5802	-0.5795
0.8108	-0.3738	-0.3733	-0.3731	-0.3725	-0.3718	-0.3715	-0.3707
0.9082	-0.1706	-0.1683	-0.1668	-0.1668	-0.1665	-0.1657	-0.1670
1.0000	0.0000	0.0000	0.0000	0.0000	0.0000	0.0000	0.0000

Table 4
Redlich-Kister Equation Fitting Parameters of Excess Molar Volumes with Standard Deviations

T/K	**A_o**	**A_1**	**A_2**	**A_3**	**A_4**	**A_5**	**SD**
303.15	-3.8499	2.612	-0.9102	2.1274	0.2793	-3.0867	0.0115
308.15	-3.7858	2.5728	-0.9171	1.6956	0.2321	-2.3538	0.0102
313.15	-3.7325	2.4529	-1.0446	1.551	0.4157	-1.8682	0.0083
318.15	-3.6857	2.323	-1.0536	1.6261	0.3943	-1.7281	0.0085
323.15	-3.6367	2.2224	-1.1122	1.7488	0.4087	-1.7066	0.0087
328.15	-3.5925	2.0841	-1.1635	1.9004	0.4938	-1.6853	0.0082
333.15	-3.5355	2.006	-1.2443	1.9993	0.4777	-1.6812	0.0083

Table 5
Partial Molar Volume of AMP in Water at Infinite Dilution

T/K	$\overline{V}_2^o$	V_2	ΔV
303.15	93.32	96.14	-2.82
308.15	93.59	96.14	-2.55
313.15	93.92	96.14	-2.22
318.15	94.02	96.14	-2.12
323.15	94.07	96.14	-2.07
328.15	94.18	96.14	-1.96
333.15	94.17	96.14	-1.97

Table 6
Viscosities of mixtures of Water (1) + AMP (2) at various Temperatures

	η/mPa·s						
x_2	**303.15**	**308.15**	**313.15**	**318.15**	**323.15**	**328.15**	**333.15**
0.0000	0.80	0.72	0.66	0.60	0.55	0.50	0.47
0.0105	0.88	0.79	0.72	0.65	0.52	0.56	0.51
0.0539	1.80	1.59	1.39	1.23	1.00	1.07	1.13
0.0728	2.48	2.10	1.80	1.56	1.29	1.30	1.34
0.1000	3.54	2.74	2.29	1.96	1.70	1.61	1.57
0.1571	6.33	4.28	3.11	2.86	2.58	2.35	2.27
0.2559	13.30	7.93	5.49	5.09	4.51	4.07	3.56
0.3532	23.78	16.16	12.24	9.26	7.50	6.18	5.17
0.4546	41.28	27.92	20.29	15.33	10.88	8.77	7.14
0.5537	56.60	38.93	28.36	20.90	14.59	11.16	8.84
0.6580	71.44	49.28	35.14	25.89	18.35	13.62	10.80
0.7001	76.44	53.22	37.30	27.62	19.80	14.56	11.49
0.8108	85.30	57.86	41.82	31.42	22.59	16.70	13.25
0.9082	88.75	60.00	43.00	32.18	22.98	17.90	14.31
1.0000	89.00	60.80	43.70	32.20	23.05	18.01	14.50

Table 7
Viscosity deviation of mixtures of Water (1) + AMP (2) at various Temperatures

	$\Delta\eta$/mPa·s						
x_2	**303.15**	**308.15**	**313.15**	**318.15**	**323.15**	**328.15**	**333.15**
0.0000	0.0000	0.0000	0.0000	0.0000	0.0000	0.0000	0.0000
0.0105	-0.8442	-0.5613	-0.3926	-0.2823	-0.2666	-0.1241	-0.1075
0.0539	-3.7476	-2.3627	-1.5892	-1.0728	-0.7624	-0.3735	-0.0960
0.0728	-4.7403	-2.9988	-1.9938	-1.3408	-0.8982	-0.4749	-0.1515
0.1000	-6.0805	-3.9894	-2.6750	-1.8007	-1.1005	-0.6414	-0.3033
0.1571	-8.3240	-5.8792	-4.3121	-2.7047	-1.5050	-0.9010	-0.4043
0.2559	-10.0660	-8.1618	-6.1820	-3.5951	-1.7968	-0.9100	-0.4997
0.3532	-8.1678	-5.7774	-3.6197	-2.4996	-0.9959	-0.5037	-0.2547
0.4546	0.3828	-0.1140	0.0629	0.3638	0.0991	0.3095	0.2916
0.5537	6.9668	4.9463	3.8707	2.8045	1.5827	0.9655	0.5988
0.6580	12.6065	9.0297	6.1614	4.4984	2.9959	1.5991	1.0988
0.7001	13.8907	10.4360	6.5063	4.8958	3.4970	1.8007	1.1971
0.8108	12.9854	10.5972	6.2632	5.1988	3.7970	2.0029	1.4045
0.9082	7.8432	5.4147	3.5506	2.8805	1.9953	1.4972	1.0978
1.0000	0.0000	0.0000	0.0000	0.0000	0.0000	0.0000	0.0000

Table 8
Redlich-Kister Equation Fitting Parameters of Viscosity Deviations with Standard Deviations

T/K	A_o	A_1	A_2	A_3	A_4	A_5	SD
303.15	12.3889	159.7283	-16.1341	-143.5570	27.6259	82.5555	0.3917
308.15	7.5922	112.6963	2.9571	-43.6219	3.8562	-31.5203	0.3653
313.15	7.3179	78.2283	-29.9727	-50.3597	43.0566	3.8123	0.2500
318.15	5.3214	52.8104	-6.6005	-24.3290	15.8255	-3.5839	0.1905
323.15	2.8487	29.0078	16.3651	8.0303	-18.1526	-25.2507	0.0827
328.15	2.3838	14.8822	-0.5175	2.2423	7.5730	-1.8619	0.0284
333.15	1.6808	9.0993	0.5680	3.1241	6.9844	-2.8555	0.0458

Table 9
Refractive index of mixtures of Water (1) + AMP (2) at various Temperatures

	n_D						
x_2	**303.15**	**308.15**	**313.15**	**318.15**	**323.15**	**328.15**	**333.15**
0.0000	1.33221	1.33147	1.33065	1.32983	1.32804	1.32812	1.32721
0.0105	1.34107	1.34014	1.33920	1.33830	1.33639	1.33600	1.33560
0.0539	1.36497	1.36370	1.36240	1.36109	1.35900	1.35853	1.35707
0.0728	1.37345	1.37165	1.36990	1.36866	1.36620	1.36580	1.36420
0.1000	1.38379	1.38202	1.38026	1.37843	1.37580	1.37483	1.37305
0.1571	1.40010	1.39855	1.39701	1.39565	1.39329	1.39236	1.39060
0.2559	1.41805	1.41599	1.41385	1.41175	1.40900	1.40760	1.40540
0.3532	1.42753	1.42566	1.42385	1.42198	1.41970	1.41819	1.41614
0.4546	1.43409	1.43201	1.43004	1.42792	1.42540	1.42380	1.42181
0.5537	1.43837	1.43621	1.43401	1.43196	1.42970	1.42808	1.42589
0.6580	1.44162	1.43962	1.43761	1.43563	1.43366	1.43220	1.43010
0.7001	1.44286	1.44078	1.43870	1.43685	1.43460	1.43297	1.43100
0.8108	1.44500	1.44304	1.44100	1.43915	1.43730	1.43515	1.43300
0.9082	1.44691	1.44496	1.44300	1.44101	1.43900	1.43705	1.43510
1.0000	1.44875	1.44662	1.44448	1.44249	1.44056	1.43858	1.43661

Table 10
Refractive index Deviation of mixtures of Water (1) + AMP (2) at various Temperatures

	Δn_D						
x_2	**303.15**	**308.15**	**313.15**	**318.15**	**323.15**	**328.15**	**333.15**
0.0000	0.0000	0.0000	0.0000	0.0000	0.0000	0.0000	0.0000
0.0105	0.0076	0.0075	0.0074	0.0073	0.0072	0.0067	0.0072
0.0539	0.0265	0.0260	0.0256	0.0252	0.0249	0.0245	0.0240
0.0728	0.0328	0.0318	0.0310	0.0306	0.0300	0.0296	0.0290
0.1000	0.0399	0.0390	0.0382	0.0373	0.0365	0.0357	0.0349
0.1571	0.0496	0.0490	0.0485	0.0481	0.0476	0.0469	0.0462
0.2559	0.0560	0.0551	0.0541	0.0531	0.0522	0.0512	0.0502
0.3532	0.0542	0.0535	0.0530	0.0524	0.0519	0.0511	0.0503
0.4546	0.0489	0.0482	0.0476	0.0469	0.0462	0.0455	0.0449
0.5537	0.0416	0.0410	0.0403	0.0398	0.0394	0.0388	0.0381
0.6580	0.0327	0.0324	0.0321	0.0317	0.0316	0.0314	0.0309
0.7001	0.0291	0.0287	0.0284	0.0281	0.0278	0.0275	0.0272
0.8108	0.0183	0.0182	0.0181	0.0180	0.0180	0.0175	0.0171
0.9082	0.0089	0.0089	0.0090	0.0089	0.0088	0.0086	0.0085
1.0000	0.0000	0.0000	0.0000	0.0000	0.0000	0.0000	0.0000

Table 11
Redlich-Kister Equation Fitting Parameters of Refractive Index Deviations with Standard Deviations

T/K	A_o	A_1	A_2	A_3	A_4	A_5	SD
303.15	0.1833	-0.1499	0.1009	-0.0436	0.0694	-0.0838	0.0004
308.15	0.1807	-0.1473	0.1025	-0.0453	0.0624	-0.0734	0.0004
313.15	0.1783	-0.1457	0.1037	-0.0412	0.0575	-0.0704	0.0005
318.15	0.1758	-0.1433	0.1040	-0.0389	0.0537	-0.0711	0.0005
323.15	0.1738	-0.1404	0.1054	-0.0365	0.0470	-0.0728	0.0006
328.15	0.1713	-0.1340	0.1016	-0.0566	0.0465	-0.0503	0.0006
333.15	0.1689	-0.1325	0.0970	-0.0492	0.0488	-0.0565	0.0008

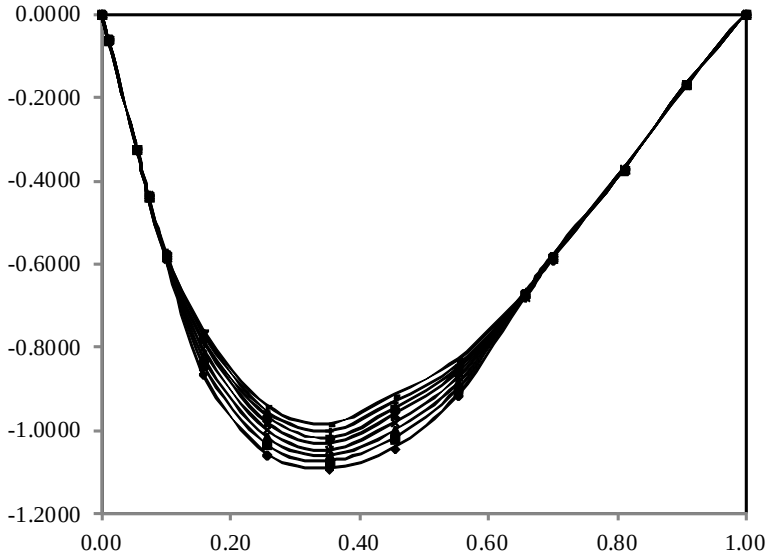

Figure 2: Excess molar volume (VE) of water (1) + AMP (2) at various temperatures: Δ, 303.15 K; *, 308.15 K; +, 313.15 K; -, 318.15 K; □, 323.15 K; ×, 328.15 K; ○, 333.15 K. The solid lines were calculated by using Redlich Kister equation

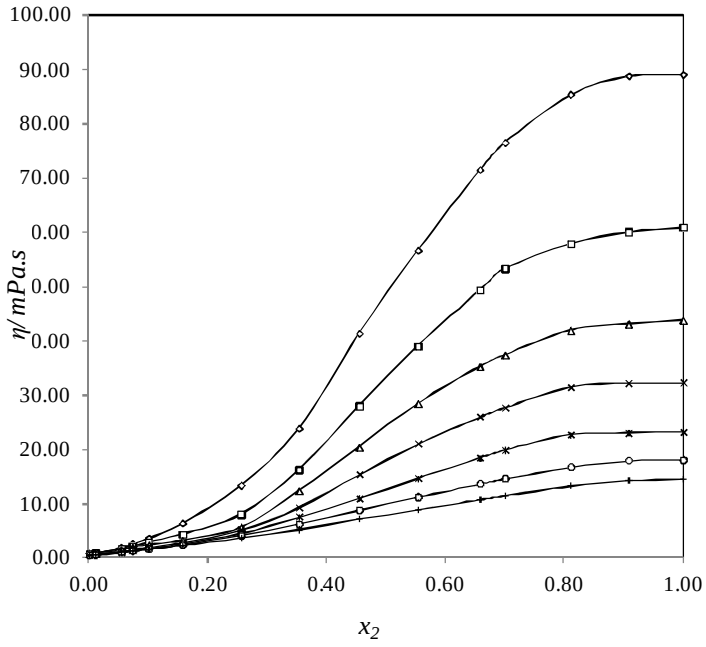

Figure 3: Viscosities (η) of of water (1) + AMP (2) at various temperatures: ◊, 303.15 K; □, 308.15 K; Δ, 313.15 K; ×, 318.15 K; *, 323.15 K; ○, 328.15 K; +, 333.15 K.

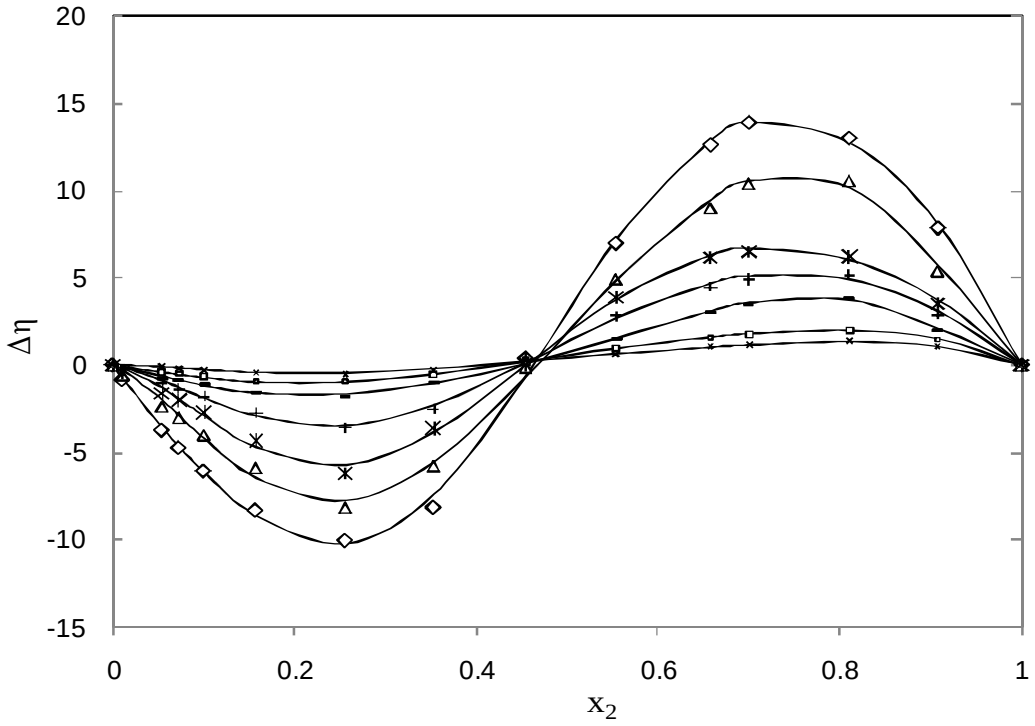

Figure 4: Viscosity deviation Δη of water (1) + AMP (2) at various temperatures: ◊, 303.15 K; Δ, 308.15 K; *, 313.15 K; +, 318.15 K;-, 323.15 K; □, 328.15 K; ×, 333.15 K. The solid curves were calculated by Redlich Kister equation

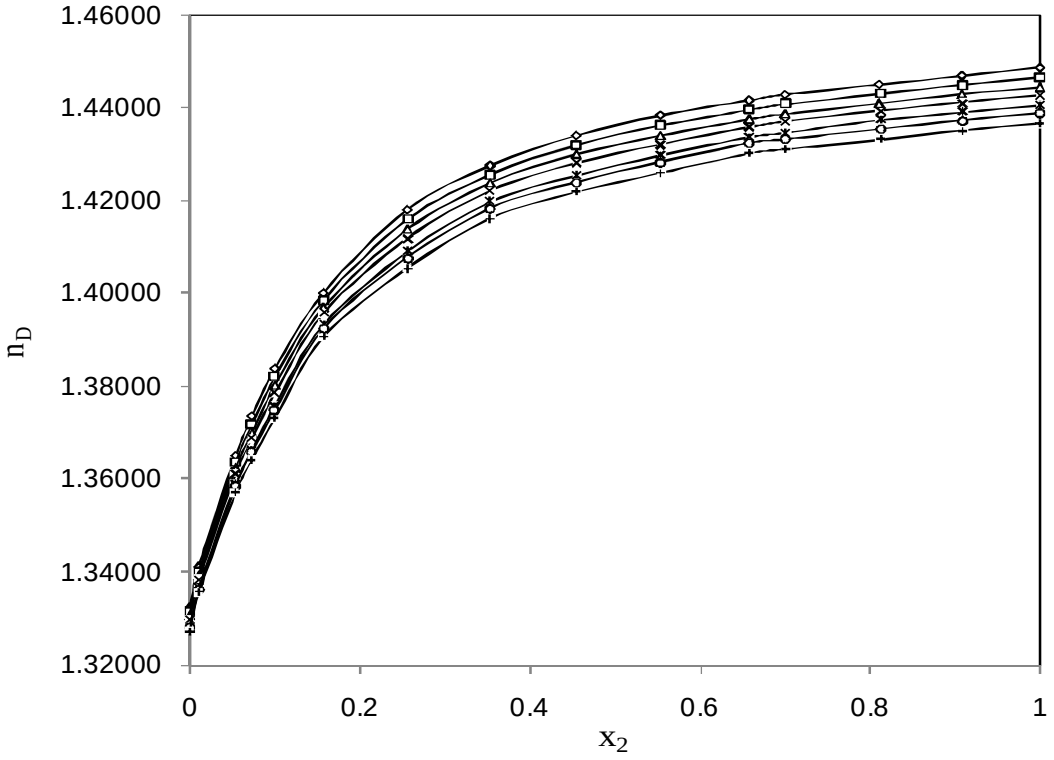

Figure 5: Refractive index deviation (nD) of Water (1) + AMP (2) + Water (2) at various temperatures: ◊, 303.15 K; □, 308.15 K; Δ, 313.15 K; ×, 318.15 K; *, 323.15 K; ○, 328.15 K; +, 333.15 K.

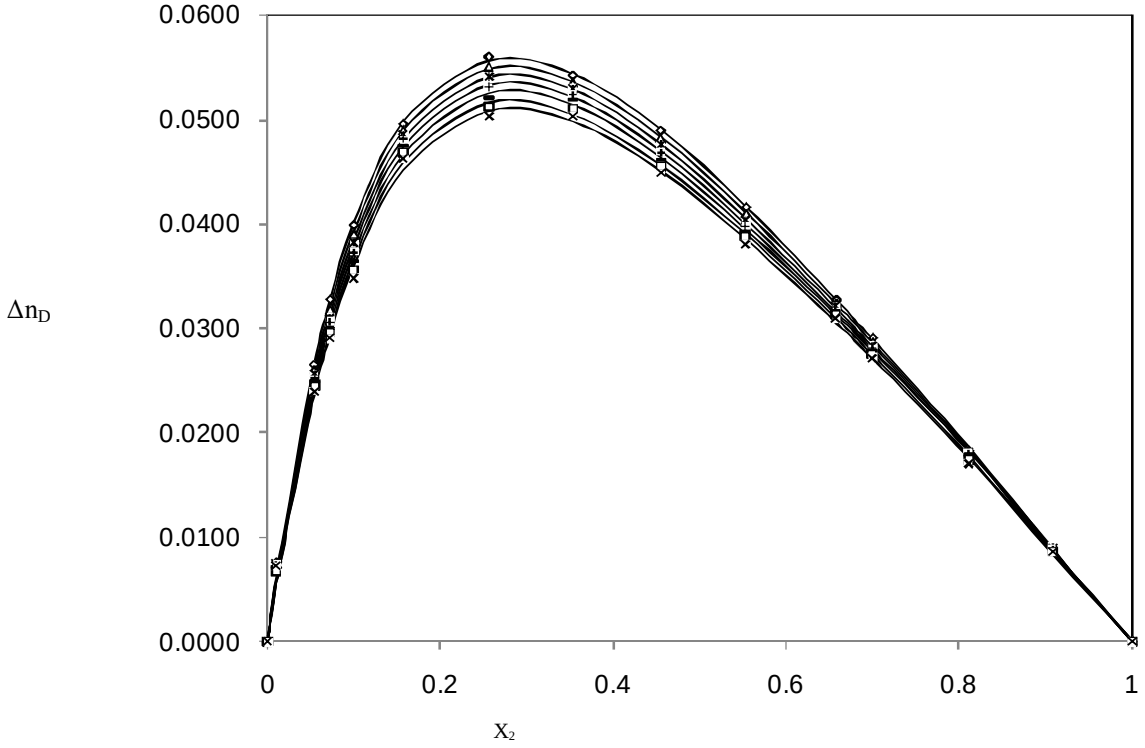

Figure 6: Refractive index deviation (ΔnD) of Water (1) + AMP (2) + Water (2) at various temperatures: ◊, 303.15 K; Δ, 308.15 K; *, 313.15 K; +, 318.15 K; -, 323.15 K; □, 328.15 K; ×, 333.15 K. The solid curves were calculated by using Redlich Kister equation

Conclusion

Physical properties like density, viscosity and refractive index of aqueous solutions of AMP were measured for the whole range of compositions and temperature. The measurements were made over the temperature range of 303.15 K to 333.15 K. The derived properties such as excess molar volumes (V^E), molar volumes at infinite dilution ($\overline{V}_2^o$), viscosity deviations ($\Delta\eta$) and refractive index deviations (Δn_D) were also determined from the density, viscosity and refractive index values. The results show that there is a good interaction between AMP and water molecules. All the properties were correlated using Redlich Kister equation.

References

1. Kohl A. and Riesenfekd F., Gas purification, third ed., Gulf Publishing Company, Texas **(1979)**

2. Xu S., Otto F.D. and Mather A.E., Solubilities of Carbon Dioxide in Water + Monoethanolamine + 2-Amino-2-methyl-1-propanol, *J. Chem. Eng. Data*, **36**, 71-75 **(1991)**

3. Li M.H. and Chang B.C., Solubilities of Carbon Dioxide in Water + Monoethanolamine + 2-Amino-2-methyl-1-propanol, *J. Chem. Eng. Data*, **39**, 448-452 **(1994)**

4. Li M.H. and Lie Y.C., Densities and Viscosities of Solutions of Monoethanolamine + N-methyldiethanolamine + Water and Monoethanolamine + 2-Amino-2-methyl-1-propanol + Water, *J. Chem. Eng. Data*, **39**, 444-447 **(1994)**

5. Yoon S.J., Densities, Viscosities and Surface Tensions of Aqueous 2-Amino-2-ethyl-1,3-propanediol Solutions, *J. Chem. Eng. Data*, **47**, 30-32 **(2001)**

6. Samanta A. and Bandyopadhyay S.S., Density and Viscosity of Aqueous Solutions of Piperazine and (2-Amino-2-methyl-1-propanol + Piperazine) from 298 to 333 K, *J. Chem. Eng. Data*, **51**, 467-470 **(2006)**

7. Park J.Y., Yoon S.J. and Lee H., Effect of Steric Hindrance on Carbon Dioxide Absorption into New Amine Solutions: Thermodynamic and Spectroscopic Verification through Solubility and NMR Analysis, *Environ. Sci. Technol*., **37,** 47-52 1670-1675 **(2003)**

8. Desale Bhatu S., Hasan Mehdi and Patil Hari A., Excess Molar Volumes and Deviations in Viscosity of Binary Mixtures of Propyl Acetate with Butan-1-ol, *Res. J. Chem. Environ.*, **10(4), (2006)**

9. Braun N.O., Persson U.A. and Karlsson H.T., Densities and Viscosities of Mono(ethylene glycol) + 2-Amino-2-methyl-1-propanol + Water, *J. Chem. Eng. Data*, **46,** 805-808 **(2001)**

10. Paul S. and Mandal B., Density and Viscosity of Aqueous Solutions of (N-Methyldiethanolamine + Piperazine) and (2-Amino-2-methyl-1-propanol + Piperazine) from (288 to 333) K, *J. Chem. Eng. Data*, **51**, 1808-1810 **(2006)**

11. Murshid G. Shariff A., Lau K. and Bustam M., Physical Properties of Aqueous Solutions of Piperazine and (2-Amino-2-methyl-1-propanol + Piperazine) from (298.15 to 333.15) K, *J.*

Chem. Eng. Data, **56,** 2660-2663 **(2011)**

12. Paul S. and Mandal B., Density and Viscosity of Aqueous Solutions of (2-Piperidineethanol + Piperazine) from (288 to 333) K and Surface Tension of Aqueous Solutions of (N-Methyldiethanolamine + Piperazine), (2-Amino-2-methyl-1-propanol + Piperazine) and (2-Piperidineethanol + Piperazine) from (293 to 323) K, *J. Chem. Eng. Data*, **51**, 2242-2245 **(2006)**

13. Mandal B., Kundu M. and Bandyopadhyay S.S., Density and Viscosity of Aqueous Solutions of (N-Methyldiethanolamine + Monoethanolamine), (N-Methyldiethanolamine + Diethanolamine), (2-Amino-2-methyl-1-propanol + Monoethanolamine) and (2-Amino-2-methyl-1-propanol + Diethanolamine), *J. Chem. Eng. Data*, **48**, 703-707 **(2003)**

14. Rebolledo-Libreros M.E. and Trejo A., Density and Viscosity of Aqueous Blends of Three Alkanolamines: N-Methyldiethanolamine, Diethanolamine and 2-Amino-2-methyl-1-propanol in the Range of (303 to 343) K, *J. Chem. Eng. Data*, **51**, 702-707 **(2006)**

15. Alvarez E., Cancela A., Maceiras R., Navaza J.M. and Taboas R., Surface Tension of Aqueous Binary Mixtures of 1-Amino-2-Propanol and 3-Amino-1-Propanol and Aqueous Ternary Mixtures of These Amines with Diethanolamine, Triethanolamine and 2-Amino-2-methyl-1-propanol from (298.15 to 323.15) K, *J. Chem. Eng. Data*, **48**, 32-35 **(2003)**

16. Vazquez G., Alvarez E., Navaza J.M., Rendo R. and Romero E., Surface Tension of Binary Mixtures of Water + Monoethanolamine and Water + 2-Amino-2-methyl-1-propanol and Tertiary Mixtures of These Amines with Water from 25 °C to 50 °C, *J. Chem. Eng. Data*, **42**, 57-59 **(1997)**

17. Chan C., Maham Y., Mather A.E. and Mathonat C., Densities and volumetric properties of the aqueous solutions of 2-amino-2-methyl-1-propanol, n-butyldiethanolamine and n-propylethanolamine at temperatures from 298.15 to 353.15 K, *Fluid Phase Equilib.*, **198**, 239-250 **(2002)**

18. Henni A., Hromek J.J., Tontiwachuthikul P. and Chakma A., Volumetric Properties and Viscosities for Aqueous AMP Solutions from 25 °C to 70 °C, *J. Chem. Eng. Data*, **48**, 551-556 **(2003)**

19. Zuniga-Moreno A., Galicia-Luna L.A., Bernal-Garcia J.M. and Iglesias-Silva G.A., Densities and Derived Thermodynamic Properties of 2-Amino-2-methyl-1-propanol + Water Mixtures at Temperatures from (313 to 363) K and Pressures up to 24 MPa, *J. Chem. Eng. Data*, **53**, 100-107 **(2008)**

20. Pal A. and Singh Y.P., Excess Molar Volumes and Viscosities for Glycol Ether−Water Solutions at the Temperature 308.15 K: Ethylene Glycol Monomethyl, Diethylene Glycol Monomethyl and Triethylene Glycol Monomethyl Ethers, *J. Chem. Eng. Data*, **41**, 425-427 **(1996)**

21. Hawrylak B., Burke S.E. and Palepu R., Partial Molar and Excess Volumes and Adiabatic Compressibilities of Binary Mixtures of Ethanolamines with water, *J. Solution Chem.*, **29**, 575-594 **(2000)**

22. Muhammad A., Mutalib M.I., Murugesan T. and Shafeeq A., Density and Excess Properties of Aqueous N-Methyldiethanolamine Solutions from (298.15 to 338.15) K, *J. Chem. Eng. Data*, **53**, 2217-2221 **(2008)**

23. Fort R.J. and Moore W.R., Viscosities of binary liquid mixtures, *Trans Faraday Soc*., **62**, 1112-1119 **(1966)**

24. Bhatia S.C., Rani R. and Bhatia R., Viscosities, densities, speeds of sound and refractive indices of binary mixtures of o-xylene, m-xylene, p-xylene, ethylbenzene and mesitylene with 1-decanol at 298.15 and 308.15 K, *J. Mol. Liq.*, **159**, 132-141 **(2011).**

(Received 14th April 2013, accepted 04th June 2013)

Bioremoval of Trichloroethylene/Toluene Mixture by *Burkholderia vietnamiensis* G4 from Water

Dong S.,[1] Li J.[1,2] and Shim H.[1]*
1. Department of Civil and Environmental Engineering, Faculty of Science and Technology, University of Macau, Macau SAR, CHINA
2. College of Natural Resources and Environment, South China Agricultural University, CHINA
* hjshim@umac.mo

Abstract

Environmental contamination by mixed organics has become the most important environmental issues. As mixed wastes, petroleum/gasoline compounds and such chlorinated compounds as trichloroethylene (TCE) are among the most frequently found subsurface contaminants. Especially, TCE is considered among the most frequently found groundwater contaminant around the world. This study is investigating the bioremoval of these compounds when present in mixture and better removing these mixtures from the contaminated water, using combined physical and biological methods. The effects of different concentrations of TCE (0.5, 1 and 1.5 mg/L), toluene (50, 100 and 150 mg/L) as growth substrate, inoculum (Burkholderia vietnamiensis G4; optical density, 1 and 3), activated carbon (1 and 3%, w/v) and dissolved oxygen (with or without additional oxygen source, hydrogen peroxide) on the aerobic removal of TCE/toluene mixture were investigated and the conditions were further optimized.

The overall optimal condition for the bioremoval of TCE/toluene mixture was found at toluene 150 mg/L, TCE 1.5 mg/L with 3% powdered activated carbon, without hydrogen peroxide with initial optical density 1 in mineral medium. Results obtained would provide a better understanding of interactions among contaminants even before the application of any remediation technology and would enhance the applicability of the combined remediation technology to the mixed waste contaminated environmental sites.

Keywords: *Burkholderia vietnamiensis* G4, Bioremoval kinetics, Trichloroethylene, Environmental conditions, Toluene.

Introduction

In recent decades, contaminations of volatile organic waste are widespread in the environment along with the rapid industrialization and urbanization[1]. Petroleum/gasoline compounds and chlorinated aliphatic hydrocarbons (CAHs) are among the most frequently found subsurface contaminants, due to the increasing usage and the accidental spillage of these organic compounds. In many petroleum products, BTEX (benzene, toluene, ethylbenzene and three isomers of xylene) are major aromatic components and often found in groundwater as results of leaks in underground storage tanks and pipelines, improper waste disposal practices and inadvertent spills[2]. Trichloroethylene (TCE), as a representative CAH, is widely used in various industrial processes. It is among the most prevalent hazardous organic compounds present in the environment and has been considered as a suspected carcinogen hazardous to humans[3,4].

Among all the currently existing remediation technologies, biological treatment is regarded as the most economical and environmentally sound approach. However, no microorganism has been isolated, which can utilize TCE as a sole carbon or energy source[5]. Under aerobic conditions, TCE can be mineralized through co-metabolism, reaction catalyzed by existing microbial enzymes yielding no carbon or energy benefits to the transforming microorganisms[6], to carbon dioxide, water and chloride, without harmful byproducts. If such organics as toluene are provided as the primary source of carbon, organisms that grow on toluene are able to co-metabolize TCE[7].

There are a number of factors affecting the biodegradation efficiency including bioavailability, quality and quantity of contaminants, oxygen etc. These factors are essential for formulating successful bioremediation strategies[8]. For TCE, *Burkholderia vietnamiensis* G4 has been known capable of stably and continuously degrading toluene and TCE simultaneously in a single-reactor system without biomass retention under aerobic condition[9]. Under aerobic conditions, oxygen is one of the key factors which affects the biological metabolism of organisms[10,11].

The main objective of this study was to investigate the bioremoval kinetics of toluene/TCE mixture using *B. vietnamiensis* G4. Effects of different parameters, including concentrations of TCE and toluene as a growth substrate, inoculum size and concentrations of dissolved oxygen and powdered activated carbon, with or without hydrogen peroxide as an additional oxygen source, on the aerobic bioremoval of TCE/toluene mixture were evaluated and the conditions were further optimized.

Material and Methods

Chemicals: Toluene (purity, 99%) and trichloroethylene (purity, 99%) were purchased from the International Laboratory (USA) and Da Mao Chemical Manufacturer in Tianjin, China, respectively. All other chemicals and

reagents used were of the highest purities and were sterilized before use.

Microbial Culture: *Burkholderia vietnamiensis* G4 (ATCC 53617) was obtained from the American Type Culture Collection (ATCC). *B. vietnamiensis* G4 possesses toluene monooyxgenase known to co-metabolize TCE while utilizing toluene as a growth substrate. The stock culture was stored in 15% glycerol at -60°C and the subcultures were enriched from the stock culture and used in this study.

Culture Medium: Three different culture media were used: nutrient broth which contained (per liter of water) 3.0 g/L beef extract and 5.0 g/L peptone, defined mineral salts medium [MSM; Bushnell-Hass (BH) medium] which contained (per liter of water) 1.0 g KH_2PO_4, 1.0 g K_2HPO_4, 1.0 g NH_4NO_3, 0.2 g $MgSO_4.7H_2O$, 0.05 g $FeCl_3$ and 0.02 g $CaCl_2.2H_2O$ and chloride free mineral medium (MCl) which contained (per liter of water) 0.024 g $Ca(NO_3)_2.4H_2O$, 0.246 g $MgSO_4.7H_2O$, 7.0 g Na_2PO_4, 3.0 g KH_2PO_4 and 2.52g $(NH_4)_2PO_4$. The pH of the medium was adjusted to 7.0±0.2 by adding HNO_3 or NaOH solution and measured by using a pH meter (pH S-25). All the instruments and media were autoclaved before use at 121°C and at 1 atm for 20 min (LDZX-50KBS).

Culture Condition: Cells were first added into the nutrient broth (NB) and incubated for 12 hours at 28°C to achieve the log phase growth. The microorganism was grown in this medium which contained abundant easily degradable carbon sources to ensure a better adaptation to the new environment/conditions used in this study. Then the cultures were centrifuged (5430R, Eppendorf) at 4,500 rpm for ten min and the cell pellet was washed/rinsed twice using specific medium, depending on the experimental setup to obtain a designed optical density. Optical density (OD) was measured using a spectrophotometer (UV mini 1240, Shimadzu). After centrifuging, the harvested culture was transferred into serum bottles (WHEATON) and used for the experiments. Serum bottles were sealed with stoppers [90% teflon / 10% silicone discs (OHIO VALLEY)] and aluminum crimp (OHIO VALLEY) using a crimper (OHIO VALLEY), before inverted and placed on an orbital shaker (JINGDA, HZQ-C) at 150 rpm and at 28°C.

Experimental Design: Effects of different concentrations of TCE (0.5, 1 and 1.5 mg/L) were investigated for co-metabolism and adsorption, with different concentrations of toluene (50, 100 and 150 mg/L) as growth substrate under different amounts of inoculum size (initial OD 1 and 3), powdered activated carbon (PAC; 1 and 3%, w/v) and dissolved oxygen (with or without hydrogen peroxide addition). The selection of ranges within which each factor varied was based on both literature review and preliminary experimentation.

Two different culture media (MCl and MSM) were compared for the effect on TCE mineralization. The effect of hydrogen peroxide (H_2O_2) as an additional oxygen source on toluene/TCE biodegradation was studied by aseptically injecting H_2O_2 stock solution (30%) to give a final concentration of 100 mg/L. Parallel experiments without H_2O_2 were also carried out at the same time for comparison. The effect of activated carbon, considering its adsorption properties towards toluene/TCE degradation, was studied by adding 1 and 3% (w/v) PAC for comparison.

All the experiments were performed under aerobic conditions. After the serum bottles were sealed with stoppers and aluminum crimps, they were inverted to minimize the volatilization of these compounds, then incubated on the shaker at 150 rpm at 28°C. Bottles containing certain medium with these compounds but without microorganisms served as controls.

Analytical Methods: The concentrations of toluene and TCE were measured using a gas chromatograph (Agilent, 6890N, Agilent Technologies Co. Ltd., China) equipped with a flame ionization detector (FID) and a capillary column (HP-5; 30 m length × 0.53 μm I.D. with a stationary-phase film thickness of 0.88 μm). One microliter of liquid samples was injected by the autosampler injector (7638 Series, Agilent Technologies Co. Ltd., China) equipped with a tapered microsyringe (5181-1267, Hamilton Company, USA). Nitrogen was used as carrier gas at a flow rate of 20 mL/min. The flow rates of hydrogen gas and synthetic air were 40 and 400 mL/min respectively. The inlet and detector temperatures were 260 and 280°C respectively. The column temperature was programmed as initial temperature, 40°C (hold for 2 min), then incrementally increased at 12°C/min to 300°C, then hold for 10 min.

Results and Discussion

The effects of substrate concentration on specific growth rate (μ; h^{-1}) and substrate degradation rate (D, $mgL^{-1}h^{-1}$) were studied. D was determined from the initial or maximum slope of the concentration curve while μ was estimated from the slope of the semi-logarithmic plot of OD versus time. Based on previous study[2], considering 1 OD represented 500 mg/L biomass (dry wt), specific (per unit amount of biomass) degradation rate was also estimated.

Tables 1 and 2 show the effects of different concentrations of TCE (0.5, 1 and 1.5 mg/L), toluene (50, 100 and 150 mg/L) as growth substrate, inoculum size (*Burkholderia vietnamiensis* G4; OD 1 and 3), activated carbon (1 and 3%, w/v) and dissolved oxygen (with or without peroxide) on the aerobic removal of TCE/toluene mixture. For batch tests using cells with initial OD 3, it was much clear to estimate kinetic parameters, compared to cells with initial OD 1. In addition, among all the conditions tested, in case of microorganisms with initial OD 3, regardless of the presence of additional oxygen source peroxide, the result

clearly showed the substrate inhibition kinetics, showing the toluene/TCE degradation rate increased with increasing substrate concentration and then decreased after reaching a maximum.

On the other hand, *B. vietnamiensis* G4 showed the Monod kinetics, regardless of the amount/percentage of PAC used, with the growth rate increased in proportion to the increase in substrate concentration, while at above some moderately high levels of substrate, the growth rate did not increase as markedly with increasing substrate concentrations.

In general, the batch tests in mineral salts medium (MSM) showed a better bioremoval performance under the same condition compared to the ones in chloride free mineral medium (MCl). For the effect of additional oxygen source, the result did not show a significant difference in specific growth rate and degradation rate may be due to only one hydrogen peroxide concentration tested. Further studies with different peroxide concentrations will be needed for the exact effect on bioremoval. In case of PAC, on the other hand, results showed almost no effect on specific growth rate while the presence of PAC protected microorganisms to better adapt to the substrates, shown by the half saturation (substrate affinity) constant.

For the TCE/toluene mixture, the lowest degradation rate of toluene (5.70 mg/L/h) was shown at TCE 1 mg/L, toluene 50 mg/L, with hydrogen peroxide and without PAC in MSM with initial OD 3 and the highest degradation rate (35.72 mg/L/h) at TCE 1.5 mg/L, toluene 150 mg/L, with 3% PAC and without hydrogen peroxide in MSM with initial OD 1.

Even though most conditions with higher OD of 3 were shown with a better performance in terms of specific growth rate and degradation rate, the optimal condition especially in terms of specific (per unit amount of biomass) degradation rate of substrate did not occur at initial OD 3. Tables 3 and 4 show the specific degradation rates at initial OD 1 and 3 respectively. As shown, the initial OD of 1 (less inoculum size) provided higher specific degradation rate. This further implies that increasing inoculum size would not necessarily be an efficient way of better degradation under the experimental setup tested in this study, thus the optimal inoculum size should also be considered as an important factor in real application on site.

Table 1
Bioremoval of toluene/TCE mixture with initial optical density 1

Medium	TCE (mg/L)	Toluene (mg/L)	For substrate		With H_2O_2		With 1% PAC		With 3% PAC	
			μ (h^{-1})	D ($mgL^{-1}h^{-1}$)	μ (h^{-1})	D ($mgL^{-1}h^{-1}$)	μ (h^{-1})	D ($mgL^{-1}h^{-1}$)	μ (h^{-1})	D ($mgL^{-1}h^{-1}$)
MCl	0.5	50	0.04	8.47	0.04	9.62	0.07	12.83	0.09	16.02
		100	0.04	12.53	0.06	14.95	0.08	26.40	0.12	27.62
		150	0.04	14.77	0.06	14.57	0.10	24.33	0.10	34.50
	1.0	50	0.05	6.72	0.05	6.31	0.09	10.34	0.10	15.18
		100	0.05	16.51	0.06	15.38	0.11	30.33	0.13	29.91
		150	0.05	16.84	0.06	16.08	0.10	33.11	0.11	35.10
	1.5	50	0.04	7.87	0.04	8.00	0.10	16.38	0.11	15.63
		100	0.06	18.45	0.06	15.15	0.11	30.93	0.13	30.39
		150	0.06	19.04	0.06	17.67	0.10	35.18	0.12	34.86
MSM	0.5	50	0.03	7.67	0.03	8.88	0.07	11.19	0.07	15.39
		100	0.03	13.07	0.03	13.58	0.10	25.81	0.08	29.00
		150	0.04	19.62	0.04	18.72	0.12	25.85	0.10	25.85
	1.0	50	0.04	6.74	0.04	6.52	0.09	11.61	0.09	15.33
		100	0.05	17.15	0.04	16.77	0.11	29.49	0.10	30.75
		150	0.04	16.72	0.04	16.75	0.12	29.69	0.12	29.69
	1.5	50	0.03	7.25	0.03	7.34	0.09	13.56	0.09	16.27
		100	0.04	18.25	0.04	15.75	0.12	29.81	0.09	29.81
		150	0.04	18.34	0.05	16.89	0.13	35.71	0.12	35.72

Table 2
Bioremoval of toluene/TCE mixture with initial optical density 3

Medium	TCE (mg/L)	Toluene (mg/L)	For substrate		With H_2O_2		With 1% PAC		With 3% PAC	
			μ (h^{-1})	D ($mgL^{-1}h^{-1}$)	μ (h^{-1})	D ($mgL^{-1}h^{-1}$)	μ (h^{-1})	D ($mgL^{-1}h^{-1}$)	μ (h^{-1})	D ($mgL^{-1}h^{-1}$)
MCl	0.5	50	0.35	13.18	0.29	10.34	0.09	12.11	0.09	17.12
		100	0.42	17.15	0.36	17.46	0.12	27.50	0.10	29.10
		150	0.26	14.26	0.18	15.84	0.11	27.13	0.12	34.42
	1.0	50	0.42	12.61	0.28	7.00	0.09	11.14	0.11	16.61
		100	0.43	20.24	0.29	17.63	0.12	23.50	0.12	27.55
		150	0.27	20.02	0.20	13.92	0.13	29.31	0.14	28.71
	1.5	50	0.35	8.63	0.20	9.40	0.12	11.63	0.11	18.40
		100	0.42	19.82	0.29	20.23	0.13	21.53	0.12	30.92
		150	0.29	20.57	0.22	19.98	0.14	32.61	0.15	30.23
MSM	0.5	50	0.32	13.07	0.25	10.42	0.09	11.81	0.09	16.83
		100	0.33	21.51	0.32	20.29	0.10	24.29	0.11	30.95
		150	0.12	18.43	0.17	15.44	0.12	23.25	0.12	34.33
	1.0	50	0.33	12.91	0.33	5.70	0.10	10.82	0.10	16.40
		100	0.36	20.55	0.34	17.28	0.11	23.11	0.12	29.53
		150	0.33	19.47	0.21	13.62	0.14	29.45	0.15	32.09
	1.5	50	0.26	8.24	0.25	9.20	0.11	11.11	0.12	18.67
		100	0.37	19.54	0.34	19.85	0.11	23.50	0.12	32.01
		150	0.25	19.18	0.20	17.35	0.15	33.30	0.17	32.88

Table 3
Specific degradation rates at initial optical density 1

Medium	TCE (mg/L)	Toluene (mg/L)	For substrate	With H_2O_2	With 1% PAC	With 3% PAC
			D (dry wt h^{-1})	D (dry wt h^{-1})	D (dry wt h^{-1})	D (dry wt h^{-1})
MCl	0.5	50	0.017	0.019	0.026	0.032
		100	0.025	0.030	0.053	0.055
		150	0.030	0.029	0.049	0.069
	1.0	50	0.013	0.013	0.021	0.030
		100	0.033	0.031	0.061	0.060
		150	0.034	0.032	0.066	0.070
	1.5	50	0.016	0.016	0.033	0.031
		100	0.037	0.030	0.062	0.061
		150	0.038	0.035	0.070	0.070
MSM	0.5	50	0.015	0.018	0.022	0.031
		100	0.026	0.027	0.052	0.058
		150	0.039	0.037	0.052	0.052
	1.0	50	0.013	0.013	0.023	0.031
		100	0.034	0.034	0.059	0.062
		150	0.033	0.033	0.059	0.059
	1.5	50	0.014	0.015	0.027	0.033
		100	0.037	0.032	0.060	0.060
		150	0.037	0.034	0.071	0.071

Table 4
Specific degradation rates at initial optical density 3

Medium	TCE (mg/L)	Toluene (mg/L)	For substrate	With H_2O_2	With 1% PAC	With 3% PAC
			D (dry wt h^{-1})	D (dry wt h^{-1})	D (dry wt h^{-1})	D (dry wt h^{-1})
MCl	0.5	50	0.009	0.007	0.008	0.011
		100	0.011	0.012	0.018	0.019
		150	0.010	0.011	0.018	0.023
	1.0	50	0.008	0.005	0.007	0.011
		100	0.013	0.012	0.016	0.018
		150	0.013	0.009	0.020	0.019
	1.5	50	0.006	0.006	0.008	0.012
		100	0.013	0.013	0.014	0.021
		150	0.014	0.013	0.022	0.020
MSM	0.5	50	0.009	0.007	0.008	0.011
		100	0.014	0.014	0.016	0.021
		150	0.012	0.010	0.016	0.023
	1.0	50	0.009	0.004	0.007	0.011
		100	0.014	0.012	0.015	0.020
		150	0.013	0.009	0.020	0.021
	1.5	50	0.005	0.006	0.007	0.012
		100	0.013	0.013	0.016	0.021
		150	0.013	0.012	0.022	0.022

Conclusion

A complete and simultaneous degradation of toluene/TCE mixture was achieved under different conditions. In terms of the degradation rates for both toluene and TCE, the optimal condition for mixture degradation occurred at 150 mg/L toluene, 1.5 mg/L TCE with 3% PAC and without hydrogen peroxide in mineral medium with initial optical density 1. The presence of PAC was helpful on the mixture degradation, further implying the combined (biological and physical) treatment method for contamination applicable for more effective degradation.

The experimental results from this study, including kinetic parameters (especially, specific degradation rate) estimated under different conditions, would be helpful to better understand the behavior of microorganisms selected under different conditions, even though further studies with more variables/degrees are still warranted. Better understanding of bioremoval kinetics towards contaminants mixtures would provide more efficient way of bioremediation.

Acknowledgement

This study was supported by a research grant from the University of Macau Research Committee.

References

1. Jo M.S., Rene E.R., Kim S.H. and Park H.S., Removal of BTEX compounds by industrial sludge microbes in batch systems, statistical analysis of main and interaction effects, *World Journal of Microbiology and Biotechnology*, **24,** 73-78 **(2008)**

2. Shim H. and Yang S.T., Biodegradation of benzene, toluene, ethylbenzene and *o*-xylene by a coculture of *Pseudomonas putida* and *Pseudomonas fluorescens* immobilized in a fibrous-bed bioreactor, *Journal of Biotechnology*, **67,** 99-112 **(1999)**

3. Shim H., Ma W., Lin A. and Chan K., Bio-removal of mixture of benzene, toluene, ethylbenzene and xylenes/total petroleum hydrocarbons/trichloroethylene from contaminated water, *Journal of Environmental Sciences*, **21,** 758-763 **(2009)**

4. ATSDR (Agency for Toxic Substances and Disease Registry), Toxicology Profile for Trichloroethylene, Atlanta, Georgia, USA **(1997)**

5. Wu W.M., Shi J. and Hickey R.F., Long-term performance of co-metabolic degradation of trichloroethylene in a fluidized bed reactor fed with benzene, toluene and xylene, *Journal of Chemical Technology and Biotechnology*, **83,** 513-523 **(2008)**

6. Horvath R.S., Microbial co-metabolism and the

degradation of organic compounds in nature, *Bacteriological Reviews*, **36**, 146-155 **(1972)**

7. Bodkhe S.Y., A Generalized Mathematical Model for the Anaerobic Biodegradation Process, *Res. J. Chem. Environ.*, **10(4),** 13-17 **(2006)**

8. Trupti K.V. and Dave B.P., Effect of crude oil concentrations, temperature and pH on growth and degradation of crude oil by marine bacteria, *Indian Journal of Marine Sciences*, **36,** 76-85 **(2007)**

9. Landa A.S., Sipkema E.M., Weijma J., Beenackers A.A.C.M., Dolfing J. and Janssen D.B., Cometabolic Degradation of Trichloroethylene by *Pseudomonas cepacia* G4 in a chemostat with toluene as the primary substrate, *Applied and Environmental Microbiology*, **60,** 3368-3374 **(1994)**

10. Atlas R.M., Microbial Degradation of Petroleum-Hydrocarbons–an Environmental Perspective, *Microbiological Reviews*, **45**, 180-209 **(1981)**

11. Cerniglia C.E., Biodegradation of polycyclic aromatic hydrocarbons, *Biodegradation*, **3,** 351-368 **(1992).**

(Received 20th March 2013, accepted 12th June 2013)

The Effect of Magnetic Field on Total Dissolved Solid of Water

Golestani Alizadeh H.* and Nikmanesh E.
Department of Chemical Engineering, Islamic Azad University, Quchan Branch, Quchan, IRAN
*golestani40@yahoo.com

Abstract

This paper presents the results of the effect of permanent magnetic field at various intensities and pH, on Total Dissolved Solid in samples of water containing different concentrations of calcium carbonate and magnesium carbonate. The magnets were fixed on vessels in a batch system to magnetize the water in Intensities of 5000 (G), 3500 (G), 2700 (G) and water samples stirred in various RPMs and durations.

The results indicate for both of $CaCO_3$ and $MgCO_3$ an increase in magnetic field intensity in a constant concentration of $CaCO_3$ and $MgCO_3$ caused, in turn, by an increase in TDS and this effect is higher for $MgCO_3$ than $CaCO_3$. So it can be concluded that magnetized water has an anti-scale effect; because of increasing the solubility of $CaCO_3$ and $MgCO_3$ which are most important agents in sedimentation.

Keywords: Magnetic field, total dissolved solid, $CaCO_3$, $MgCO_3$, water treatment.

Introduction

Total dissolved solids (TDS) is the term used to describe the inorganic salts and small amounts of organic matter present in the form of solution in water. The principal constituents are usually calcium, magnesium, sodium and potassium cations and carbonate, hydrogen carbonate, chloride, sulfate and nitrate anions [1]. TDS can be naturally present in water as a result of mining, oil and gas drilling or some industrial and municipal water treatment[2]. In other words total Dissolved Solids (TDS) is defined as the portion of solids that passes through a filter of 2.0 microns nominal pore size [3].

The existence of magnetic field effects (i.e. an increase in the dissolving rate of salts in the magnetized water) in such experiments was repeatedly reported. The effect of magnetic field on water can be classified in upstream and downstream effects as follows:[4,5]

Upstream effects

- Mechanism of MF action
- Effect of water chemistry and its impurities
- Effect of hydrodynamic parameters (geometrical factors of the treating system, velocity)
- Effect of MF arrangement
- Nucleation process (effect of impurity, frequency and growth of nuclei).

Downstream effects

- Changes in the properties of treated water (conductivity, pH, surface tension, solubility)
- Zeta potential of the produced calcium carbonate particles
- Morphology of precipitated calcium carbonate (size, shape)
- Newly produced entities (free radicals, reactive agents) Suppression of the rate of scale formation.

The change in the properties of water under the effect of magnetic field is just a typical case. Since 1950s, it has been shown that water can be magnetized when exposed in a magnetic field, although the effect is very small[6,7]. But by now, there is still no systemic study on the mechanisms and features of magnetization of water[8]. For example, the magnetic field (MF) would be able to disturb the double ionic layer surrounding the colloidal particles and their zeta potentials[9-11]. He and Liu[12] investigated the nonlinear magnetization dynamics in a ferromagnetic nanowire with spin current and Licinio et al[13] investigated the nonlinear dielectric response of Ferro fluids under action of magnetic field. Besides, Ozeki et al[14] investigated the absorption of water on the solid surface under the effect of magnetic field.

Also, the unique properties of water make it perhaps the most important substance. Water structure, under the effect of weak varying magnetic fields was investigated by the methods of absorption and luminescent spectroscopy[15] in which the changes in water structure are due to the clusters present in water that control the optical heterogeneity of the medium.

Material and Methods

Magnetic field: Permanent magnets were the product of Kimia Sanat Sharif Company in Iran. These magnets were fixed on vessels in batch system to magnetize the water. Intensities of magnetic field were 5000 (G), 3500 (G), 2700 (G) and 0.0 (G).The detailed structure of the magnetic devices is shown in fig.1. The water can be stirred in various RPMs and durations.

Sample Preparation: In order to avoid any side effects by foreign ions and other solids, distilled water was used for preparing the sample by dissolving 100 to 300 (mg/l) reagent of $CaCO_3$ or $MgCO_3$ in deionized water. The pH changed with 0.1 N HCl and 1 N NaOH that was prepared in Islamic Azad University laboratory, Qouchan, Iran.

TDS and pH Measurement: Total Dissolved Solid contains calcium carbonate or magnesium carbonate measured by TDS meter Model 4510 and pH measured by meter Model GP 353.

Results and Discussion

The effect of magnetic field on TDS in various concentrations of $CaCO_3$ and pH : To compare the effect of magnetic field on TDS, the experiments were conducted at different magnetic intensities, with the magnets being fixed on vessels in a batch system. Samples were collected from three different concentrations of $CaCO_3$. All the experiments have been repeated three times. The results are shown in fig. 2 for 100(mg/lit), fig. 3 for 200(mg/lit) and fig. 4 for 300(mg/lit) concentration of $CaCO_3$ at different pH respectively.

These figures indicate that the magnetic field in different intensities has been affected by TDS and solubility of $CaCO_3$ below and above initial pH. The results also show an increase in magnetic intensities caused by an increase in TDS in water containing Ca^{2+}, CO_3^{2-} and ions produced by adding acid and alkalinity. The solubility of $CaCO_3$ depends on the pH as shown in the following equation:

$$Ca^{+2} + H_2O + CO_2 \longrightarrow CaCO_3 + 2H^+$$

The equilibrium can be shifted to the right side to convert $CaCO_3$ to soluble $Ca(HCO_3)_2$ by adding an acid (i.e. lowering the pH). Moreover, by adding a base (NaOH) there is little change in $CaCO_3$ solubility as pH increases. Magnetic treatment of water clearly demonstrates that only its physical properties are modified by the effect of magnetic field, while the chemical composition and other properties remain unchanged[16].

Also figures 2-4 show an increase in the magnetic field intensities caused by an increase in TDS. For instance, in fig. 2 where pH=1.87, concentration of $CaCO_3$ is 100(mg/lit) and magnetic field with 5000, 3500, 2700 and 0 guess, the TDS is about 1045,980, 960 and 910 ppm respectively[11]. The same trends are present for other concentrations of $CaCO_3$ as shown in fig. 3 and fig. 4. Also indicated in these figures is the effect of a magnetic field on total dissolved solid that was less significant in the higher pH range and magnetic field with maximum intensity having a greater effect on total dissolved solid. This effect is referred to as Magneto chemistry (study of the magnetic properties of materials) i.e. when water that has nonpolar molecules such as H_2 and O_2 is exposed to a magnetic field, these molecules become polarized by MF and are called induced dipoles[17.]

Therefore, as these non-polar molecules become polarized, restoring forces (If the system is perturbed away from the equilibrium, the restoring force will tend to bring the system back into equilibrium) come into play on the displaced charges, pulling them together much as if they were connected by a spring. These restoring forces vary in magnitude from one type of molecule to another with proportionate differences in the displacement produced by a given field. Polar molecules are oriented at random when no magnetic field is present[17-19].

The effect of the magnetic field on TDS in various concentrations of $MgCO_3$ and pH : Since solubility of Magnesium carbonate in distilled water is low, acid (HCl) and base (NaOH) are used to increase solubility. Thus, the investigation of the effect of magnetic fields with different intensities on solubility of $MgCO_3$ in water started at different pH and concentrations of $MgCO_3$ (100-300 mg/l). The experimental results are shown in figures 5-7.

According to the figures 5-7, it can be found that the total Dissolved Solid increases with an increase in the magnetic field intensity. This is because under the effect of the magnetic field, the charges separate until the restoring force is equal and opposing the force exerted on the charges by the field, therefore water molecules in these conditions will be different from ordinary, then smaller molecules of water will be formed and the number of water molecules per unit volume will be increased and consequently the water solubility and TDS get increased.

Fig. 5 presents the typical variations of the TDS versus pH for different magnetic field intensities. In the present example, at pH=1.88, 100(mg/lit) concentration of $MgCO_3$ and magnetic field intensities of 5000, 3500, 2700 and 0 guess, the TDS is about 1360, 1220, 1190 and 1110 ppm respectively. In the magnetically treated water there are at maximum, four hydrogen bridge connections containing protons that spin to the same direction. These are called clusters. Water that is completely organized consists of clusters. The magnetic fields on water are to change the dimensions of those clusters which affect the physical properties of water[15].

Conclusion

The results of this experimental study show that the magnetic field has been affected by TDS and solubility of $CaCO_3$ for low and high initial pH. Furthermore, the results indicate for both of $CaCO_3$ and $MgCO_3$ that an increase in the magnetic field intensity in a constant concentration of $CaCO_3$ and $MgCO_3$ causes an increase in TDS and this effect is higher for $MgCO_3$ than $CaCO_3$. Application of magnetic field makes alignment of water clusters and water molecules (including cation and anion). This effect may be increased by increasing the magnetic field strength. So, it can be concluded that magnetic treatment of water has an anti-scale effect for MF and can increase the solubility of $CaCO_3$ and $MgCO_3$ which are most important agents in sedimentation.

Acknowledgement

This work has been supported by the Azad University Quechan Branch.

Fig.1: The detailed structure of the magnetic devices

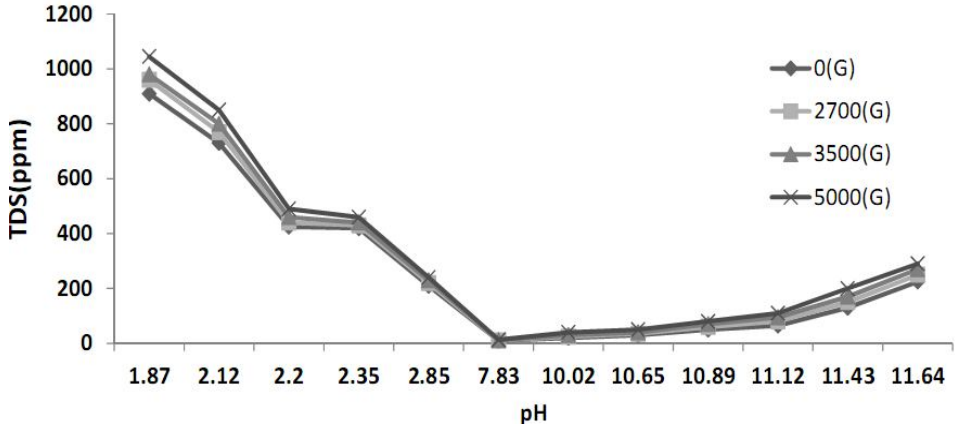

Fig.2: The effect of magnetic field on TDS at 100(mg/l) of $CaCO_3$

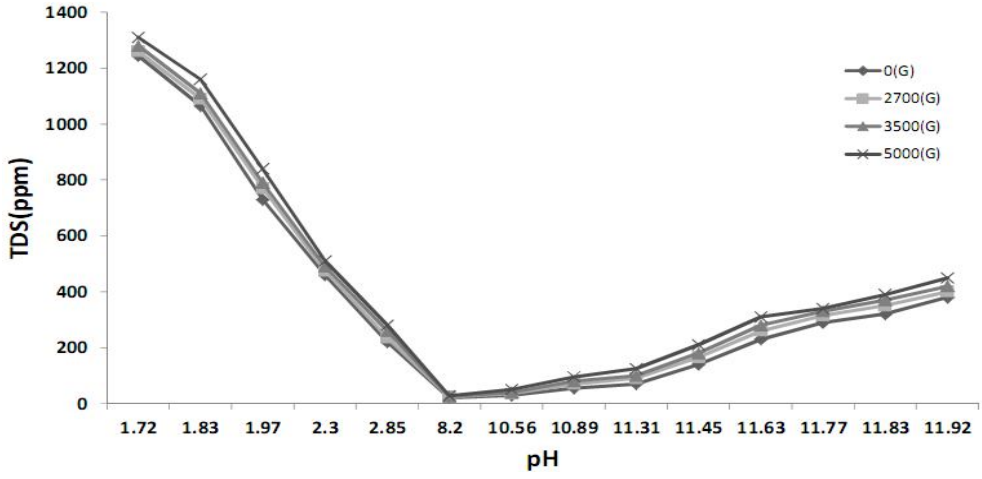

Fig.3: The effect of magnetic field on TDS at 200(mg/l) of $CaCO_3$

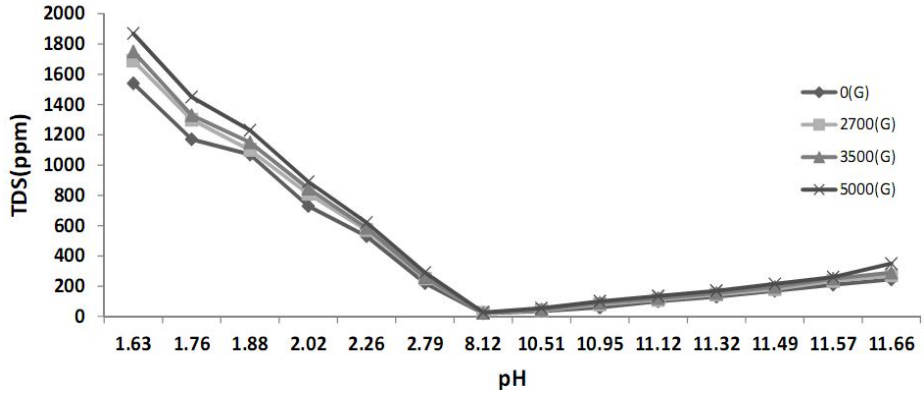

Fig.4: The effect of magnetic field on TDS at 300(mg/l) of $CaCO_3$

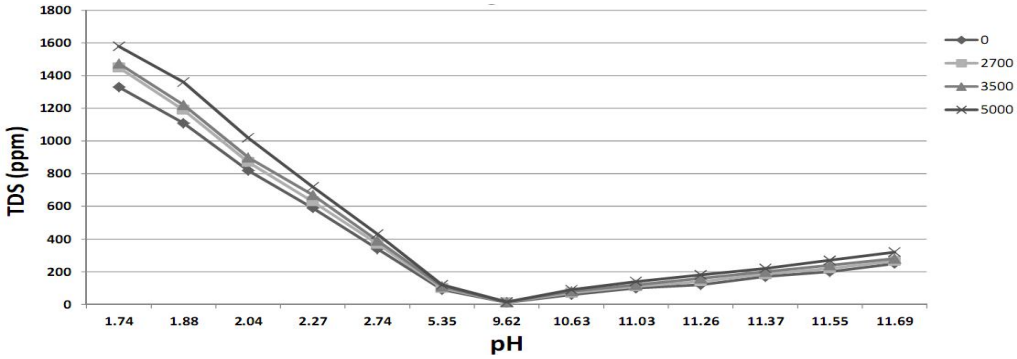

Fig.5: The effect of magnetic field on TDS at 100(mg/lit) of $MgCO_3$

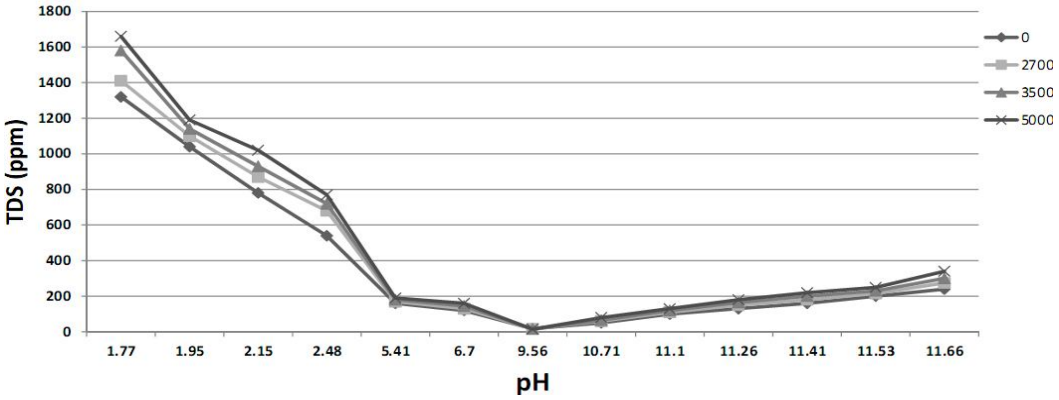

Fig.6: The effect of magnetic field on TDS at 200(mg/lit) of $MgCO_3$

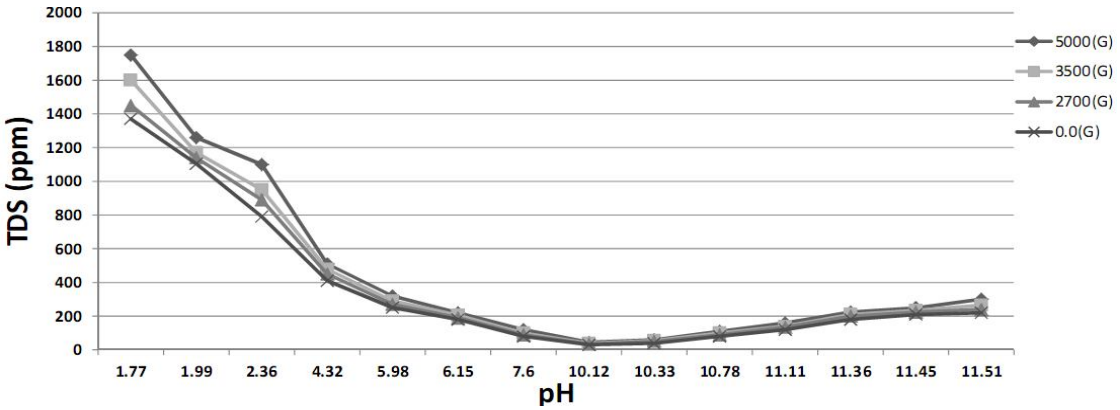

Fig.7: The effect of magnetic field on TDS at 300(mg/lit) of $MgCO_3$

References

1. Fawell J.K., Lund U. and Mintz B., Guidelines for drinking-water quality, 2nd ed., Health criteria and other supporting information, World Health Organization, Geneva **(1996)**

2. P.A. Dep. Permitting Strategy for High Total Dissolved Solids (TDS) Wastewater Discharges, April 11, 2009.www.depweb.state.pa.us/watersupply/cwp/view.asp?a=1260&Q=545730 & water supply Nav=|30160|, Accessed 9/3/09 **(2009)**

3. Dowdell C., Fach B. and Steinbock B., Total Dissolved Solids, DEP SOPNU-047-4.15, 05/25/2011 **(2011)**

4. Sharma Meena, Gupta Deepika, Jain Anamika and Killedar Rekha, Effect of Magnetic Field on Thermodynamic Functions uring Membrane Transport, *Res. J. Chem. Environ.*, **6(4)**, 47-50 **(2002)**

5. Amiri M.C. and Ali A. Dadkhah, On reduction in the surface tension of water due to magnetic treatment, *Colloids and Surfaces A: Physicochem. Eng. Aspects*, **278**, 252–255 **(2006)**

6. Bour P., A cluster model of liquid water and its IR spectroscopic response, *Chem Phys Lett.*, **365,** 82-88 **(2002)**

7. Ohata R., Tomita N. and Ikada Y., Effect of a static magnetic field on iontransport in a cellulose membrane, *J. Coll Interf Sci.*, **270(2),** 413-416 **(2004)**

8. Deng Bo and Pang Xiao Feng, Variations of optic properties of water under action ofstatic magnetic field, *Chinese Science Bulletin*, December, **52(23)**, 3179-3182 **(2007)**

9. Gamayunov N.I., Coagulation of suspension after magnetictreatment, *J. Appl. Chem.*, **56**, 975–982 **(1983)**

10. Higashitani K. and Oshitani J., Magnetic effects on thickness of adsorbed layer in aqueous solutions evaluated directly by atomic force microscope, *J. Colloid Interf. Sci.*, **204**, 363–368 **(1998)**

11. Parsons S., Judd S.J., Stephenson T., Udol S. and Wang B.L., Magnetically augmented water treatment, *Trans. Inst. Chem. Eng.*, **75(B)**, 98–104 **(1997)**

12. He P.B. and Liu W.M., Nonlinear magnetization dynamics in a ferromagnetic nanowire with spin current, *Phys Rev* B, **72,** 064410 **(2005)**

13. Licinio P., Teixera A.V. and Figueiredo J. M. A., Non-linear dielectric response of ferrofluids under magnetic field, *J Mag Mat.*, **289,** 181-183 **(2005)**

14. Ozeki S. et al, Water-solid interactions understeady magnetic fields: Magnetic-field-induced adsorption and desorption of water, *J. Phys. Chem.*, **100,** 4205-4212 **(1996)**

15. Baranov A. N., Kiselev V. F., Rozanov V. V. and Soletskii A. M., Aviakosm, *Ekolog. Med.*, **29(6)**, 45 **(1995)**

16. Singh M. and Singh K. P., *J. Anat. Soc. India*, **51(1)**, 47 **(2002)**

17. Jack Quinn C., Craig Molden T. and Charles H. Sanderson, Magnetic treatment of water prevents mineral build-up, Project Engineer—Superior Manufacturing Div., Magnatech Corp., Fort Wayne, Ind. July 47-53 **(1997)**

18. Rubin A. J., To Determine if Magnetic Water Treatment is effective in Preventing Scale, Ohio State University **(1973)**

19. Reimers R. S., DeKernion P. S. and Leftwich D. B., Sonics and Electrostatics: An Innovative Approach to Water and Waste Treatment, Proceedings of Water Reuse Symposium, AWWA Research Evaluation, Denver, Colorado, March, **2**, 1390-1416 **(1979).**

(Received 27th January 2013, accepted 12th April 2013)

Removal of Chromium (VI) Ions from Wastewaters by Low Cost Adsorbent

Rawal Nekram[1*] and Jarouliya Urmila [2]
1. Civil Engineering Department, Motilal Nehru National Institute of Technology, Allahabad-211004, INDIA
2. Centre for Biotechnology, University of Allahabad-211002, INDIA
* nek_friend@rediffmail.com

Abstract

The presence of heavy metal ions such as chromium in industrial wastewaters and municipal wastewaters is a potential hazard to aquatic, animal and human life. Chromium compounds are widely used in a number of industries such as leather, textile, chemical printing, dye-ink manufacturing, electroplating industries etc. From all these processes, Hexavalent Chromium (CrVI) can escape into the environment through the effluents. Chromium (VI) is 100 to 1000 times more toxic than other chromium compounds.

In this study, capability of low cost natural chitosan and its derivatives (cross-linked chitosan) to remove chromium (VI) metal ions is evaluated and also optimum adsorption capacity is determined. This study indicated that adsorption kinetics as well as removal capacity are highly favourable for using cross-linked chitosan than pure chitosan as an adsorbent. The concentration of contaminated water is lowered to the limits of acceptable level by adsorption process using pure chitosan and their derivatives as an adsorbent. The adsorption obeyed the Langmuir and Freundlich adsorption isotherms.

Keywords: Chitosan, crosslinked chitosan, adsorption, chromium (VI).

Introduction

The hexavalent form of chromium is highly toxic and is known to be both carcinogenic and mutagenic to living organisms. It is difficult to remove toxic metal ions in trace quantity such as chromium (VI) from aqueous solution. Adsorption is one of the good alternative and available methods for such situations. Numbers of low cost adsorbent materials have been evaluated for their capability of removing toxic metal ions, chitosan is one of the natural low cost adsorbent. Chitosan is a modified carbohydrate polymer derived from chitin which occurs principally in the organisms of the phylum, arthropoda and outer skeleton of insect, crab and lobsters. These materials are currently available in large quantities as waste product and by-products of fish industry.

The primary unit in the chitin polymer is 2-deoxy-2 (acetylamino) glucose[9]. These units are combined by 1-4 glucoside linkage, formally a long chain linear polymer.[13] This polymer is capable of adsorbing a number of metal ions with or without cross-linkage from the aqueous solution at neutral pH[15]. The ability of chitosan to recover metal ions from water / wastewaters has been widely studied for the last 30 years. The comparisons of uptake potentials for various chitosans are presented in table 1. Since the sorption depends heavily on experimental conditions such as pH, metal concentrations, ligand concentration, competing ions and particle size, aim of this present work is to investigate the adsorption efficiency of chromium (VI) by using a biopolymer chitosan material and cross-linked material as an adsorbent.

Material and Methods

Purified chitosan raw materials: Chitosan polymer was washed with deionised distilled water. After each wash, the chitosan was filtered and dried and then washed again for a total of 6 times for 24 h. After each washing, the chitosan samples were analyzed using a spectrophotometer. The result showed that the washed chitosan was pure enough to be used. The washed chitosan was then dried and is used for further adsorption studies.[1]

Cross-linked chitosan: The cross-linked chitosan is prepared by different methods; one of them is described by Masri et al[11]. In this method, 9.0g of mesh chitosan was added to a mixture of 4.5ml of 25% aqueous glutaraldehyde and 36ml distilled water. The mixture was kept at 20 ^{o}C and stirred occasionally for 1 h. The solid material was collected by filtration washed with water and methanol and air-dried and used for treatment[7]. The chromium (VI) solution in water using A.R. grade potassium dichromate ($K_2Cr_2O_7$) was prepared as per standard methods prescribed by Manivasakam[10] and the same was used in all the experiments.

Batch adsorption experiments were performed at room temperature in a rotary shaker. The solid adsorbent was separated by filtration and the amount of chromium (VI) remaining in the solution was determined in atomic adsorption spectrophotometer model (2380). Dynamic experiments were preformed to investigate adsorption kinetics. Adsorption equilibrium isothermal studies were performed on chitosan and cross-linked chitosan.

Results and Discussion

Sorption kinetic study was conducted using 300 ml sampling bottles containing 100 ml of three sorbate concentration, 7.5 mg/L, 10.0 mg/L and 12.5 mg/L at normal pH. A dose of 5.0 g/L of chitosan and cross-linked chitosan was added to the each set of reaction mixtures.

Table 1
The adsorption capacities of chitosan[2]

Material	Cd	Cr(III)	Cr(VI)	Hg	Pb
Chitin[11]				100	
Chitosan[7,11,12]	6.4,558	92	27.3	1123,815	796
Chitosan (from lobster shell)[14]	430				
Chitosan powder[16]	420				
Chitosan beads[16]	518				
N-Acylates chitosan beads[6]	216				
N-Acylates Cross – linkedchitosan beads[6]	136				

The same was agitated in a vertical rotary shaker at 38 rpm for 6 hours. Samples from sampling bottles were taken out at 60, 120, 180,240 and 300 minutes interval of time. Samples were filtered and then analyzed for residual chromium (VI) concentration. From figure 1, it is seen that residual chromium (VI) concentration decreases with respect to time. It indicates that the rate of adsorption increases initially and then decreases gradually. From fig.1, it is clearly seen that cross-linked chitosan shows good adsorption as compared to chitosan. All the experiments were conducted with cross-linked chitosan.

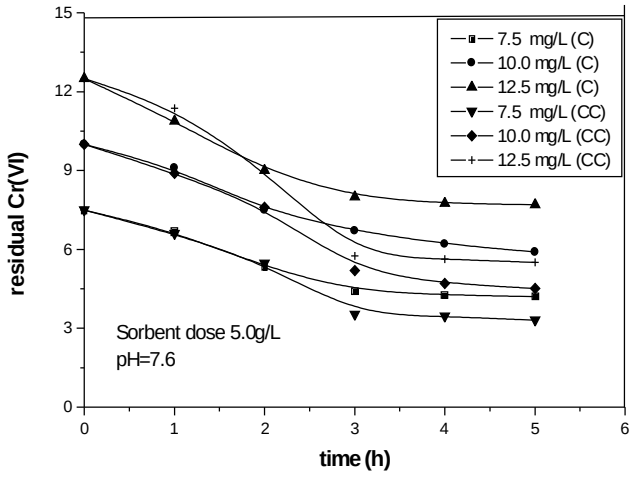

Fig. 1: Plot of Adsorption kinetics of chromium (VI) on chitosan (C) and cross-linked chitosan (CC) at different initial chromium (VI) concentration

Cross-linked chitosan can be considered a microporous material. When an amorphous polymer is below its glass transition, the thermal movements of the chain segments are restricted. Because of the relatively bulky chitosan chains, pores are large enough to let small molecules and ions through.

The distinction between film and pore diffusion controlled process can be made by performing the interruption test. This test has been suggested by Helfferich[5] and Zogerski et al[18]. The reaction mixture is containing 100ml of 7.5mg/L concentration of Cr(VI) solution and 5.0g/L adsorbent of cross-linked chitosan. Two numbers of identical bottles were used in the study. The reaction mixture was agitated in a rotary shaker. Separating adsorbent from adsorbate for 30 min at predetermined intervals of time interrupted the adsorption and an aliquot was withdrawn for chromium (VI) analysis. The adsorbent was remixed in respective bottles after the interruption period and the mixtures were again agitated.

Thus, the interruption test is a simple test for determining the large concentration gradient existing within the pores of the adsorbent. Results of interruption test conducted for cross-linked chitosan for adsorption of chromium from contaminated water are presented in figure 2. The result of conditions test (i.e. without interruption) is also plotted in figure to facilitate comparison.

There are essentially three consecutive steps involved in the adsorption of adsorbate from solutions by porous adsorbents suggested by Helfferich:[5]

(1) Transport of chromium through a surface film to the exterior surface of the exterior surface of the adsorbent i.e. film diffusion.
(2) Diffusion of the chromium within the pores of the adsorbent i.e. pore diffusion or intraparticle transport.
(3) Adsorption of the chromium on the interior surfaces bounding the pore and capillary spaces of the adsorbent[17].

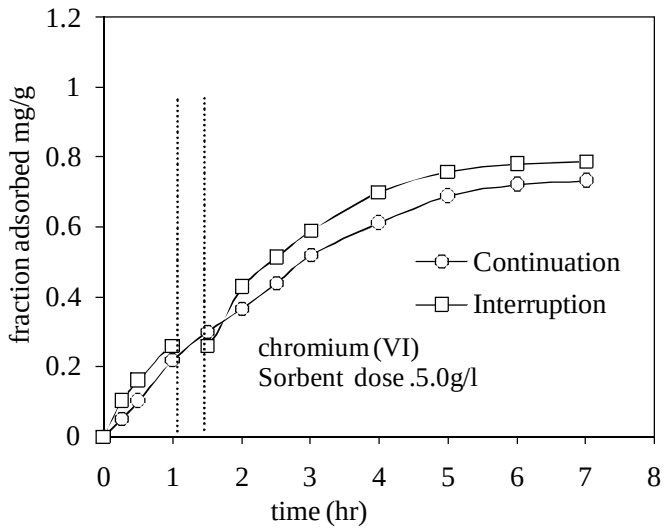

Fig. 2: Interruption test for adsorption of chromium (VI) on cross-linked chitosan

It is generally agreed that the adsorption process itself is rapid and hence step (c) does not represent the rate limiting step in the uptake of chromium. The remaining two steps (a) and (b) are supposed to be rate governing steps. Performing interruption test can make the distinction between film diffusion and intraparticle pore diffusion controlled process. Examination of figure (2) indicates that the results obtained for continuous and interrupted test are almost similar. No influence of interruption on adsorption of chromium indicates non-redistributes of solute molecules within the interior and hence external transport (film diffusion) is rate limiting. If adsorption is enhanced upon interruption, it could have been interrupted that intra particle transport (pore diffusion) is rate limiting. The effective rate of adsorption evidently will be controlled mainly by the step exerting greatest resistance to mass transfer i.e. the slowest step. Thus depending on operating conditions, either 'Film diffusion' or /pore diffusion may be slower of the two steps and hence rate controlling.

The Langmuir and Freundlich isotherms are the mathematical expressions most frequently used to describe the adsorption kinetic of an adsorbent surface. Langmuir[8] developed a quantitative model that has been widely applied to describe experimental adsorption capacity data. The Langmuir adsorption isotherm is expressed as:

$$\frac{X}{M} = \frac{Q_0 b C_e}{(1 + bC_e)} \tag{1}$$

The above equation can be rearranged to the following linear form:

$$\frac{1}{X/M} = \frac{1}{Q_0 b} \cdot \frac{1}{C_e} + \frac{1}{Q_0} \tag{2}$$

$$\frac{C_e}{X/M} = \frac{1}{Qob} + \frac{C_e}{Qo} \tag{3}$$

Any of these two equations may be used to evaluate Langmuir constants Q_0 and b from experimental data using graphic or least square analysis. The ability of these equations to predict accurately the true least square values of Q_0 and b is not the same. For the same experimental isotherm data, both equations calculate different values of Q_0 and b. These solutions are only the estimates of the least square best fit values of Q_0 and b. The equation giving the maximum value of coefficient of correlation for the particular set of data is to be used to determine Q_0 and b.

The Freundlich[4] isotherm can be expressed mathematically in the form given below:

$$\frac{X}{M} = K_F C_e^{\frac{1}{n}} \tag{4}$$

Estimation of these constants are possible by simple transformation of equation in logarithmic form as:

$$\log \frac{X}{M} = \log K_F + \frac{1}{n} \log C_e \tag{5}$$

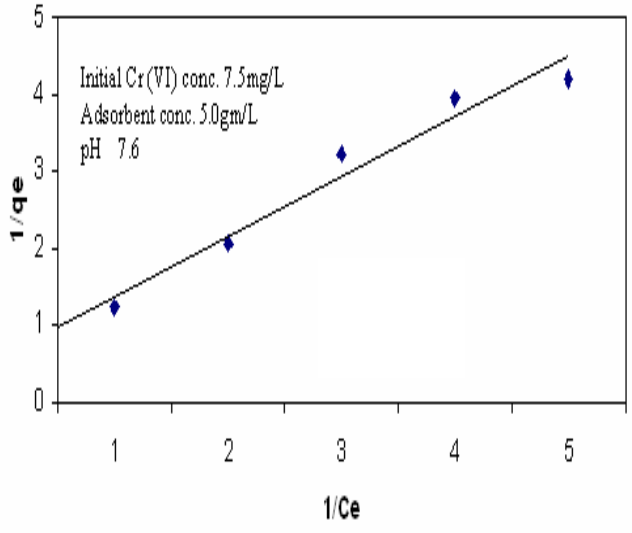

Fig. 3: Langmuir Plot of 1/Ce and 1/qe

The Freundlich equation generally agrees quite well with the Langmuir equation and experimental data over moderate ranges of concentration. However, it does not express X /M as a linear form at very low concentrations. As a result, Freundlich Isotherm predicts infinite surface coverage at infinite concentration, a condition that does not occur. Therefore its application is limited to intermediate surface coverage.

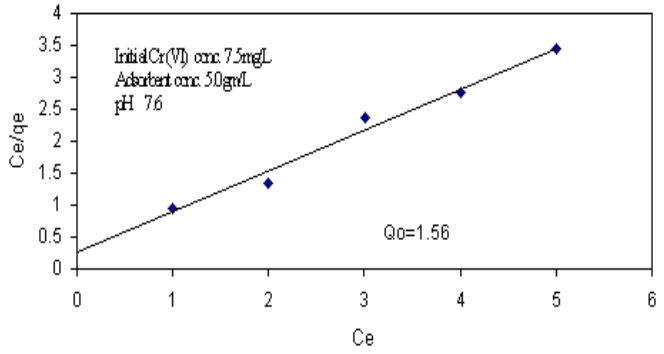

Fig. 4: Langmuir Isotherm for Cr (VI) Adsorption

Langmuir isotherms using both linearised forms of equations I and II were plotted using least square method as shown in figs. 3 and 4. The Cr (VI) adsorption capacity (Q_0) of adsorbent to form a monolayer deposit is shown. The best regression equation to evaluate Q_0 and b is eq. (III) which contains only one reciprocal quantity. It can be seen that Q_0 values i.e. Cr (VI) adsorption capacity of cross-linked chitosan vary from 1.56 to 1.7 mg/g using two liberalized form from same experimental data.

The Freundlich constants K_F and 1/n have been evaluated from the curve using intercept and slope of the regression line respectively. Freundlich equation can be expressed as:

$$X/M = 1.26\ C_e^{-0.138}$$

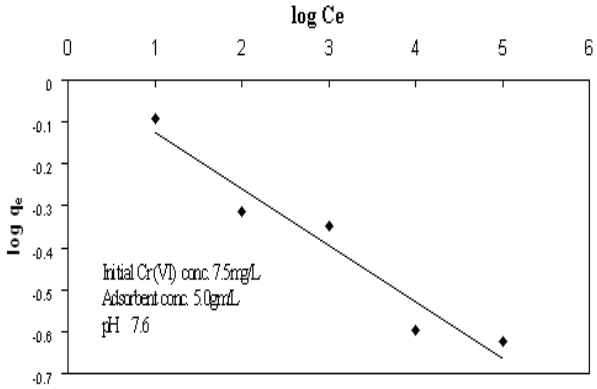

Fig.5: Freundlich Plot of log q_e Vs log Ce

The value of K_F which is a measure of adsorption capacity of adsorbent cross-linked chitosan, is comparatively less than those obtained from Langmuir equation (I) for the same experimental conditions. This indicates that the experimental data can be described better by Langmuir equation for this adsorbent. The isotherm data can be used to calculate the ultimate adsorption capacities by substituting the initial concentration in equation (I, II and III), a situation that corresponds to total exhaustion of adsorbent bed. For an initial concentration of 7.5 mg/L, the ultimate adsorption capacity for adsorbent is 1.56 mg/g according to the Langmuir isotherm. This information on ultimately adsorption capacities may be extended to get an idea about the competitive adsorption of other ions present in water.

Conclusion

Chitosan and their derivatives as biopolymer may be used as a viable adsorbent for the removal of chromium (VI) metal ions from water and wastewaters especially industrial wastewaters. The adsorption kinetic studies were conducted on chitosan and cross-linked chitosan.

1. It was observed that cross-linked chitosan is good for removal of chromium from wastewaters than chitosan.

2. It was observed that rate-limiting step for cross-linked chitosan in water was film diffusion.

3. The adsorption equilibrium data were found to fit Langmuir equation. Adsorption capacities were evaluated from both equations and these values are 1.56 and 1.70 mg/g.

References

1. Selvi V. and Jeyanthi G.P., Chromium (VI) Uptake by Nitrated and Sulphonated Coconut Shell Carbon, *Res. J. Chem. Environ.*, **8(1),** 20-23 **(2004)**

2. Bailey S.E., Olin, T.J., Bricka R.M. and Adrian D.D., A review of potentially low costs sorbents for heavy metals, *Water Research*, **33 (11**), 2469-2479 **(1999)**

3. Elson C. M., Davies D. H. and Hayes E. R., Removal of arsenic from contaminated drinking water by a chitosan/chitin mixture, *Water Research*, **14 (9**), 1307-1311 **(1980)**

4. Freundlich H., Capillary and colloid chemistry, Methuen and Co., London **(1926)**

5. Helfferich F., Ion Exchange, McGraw-Hill Book Company, New York **(1962)**

6. Hsien T.Y. and Rorrer G.L., Effect of acylation and crosslinking on the material properties and cadmium ion adsorption capacity of porous chitosan beads, *Sep Science Technology*, **30 (12),** 2455-1575 **(1995)**

7. Jha I.N., Iyengar L. and Rao AVSP., Removal of cadmium using chitosan, *Journal Environmental Engineering (ASCE)*, **114**, 962-974 **(1988)**

8. Langmuir I., The constitution and fundamental properties of solid and liquid II, *Journal of American Chemical Society*, **39**, 1848-1906 **(1918)**

9. Madhavan P., Science lecture series, Central institute of fisheries technology, Kochi **(1992)**

10. Manivasakam N., Physico-Chemical Examination of water Sewage and Industrial Effluents, Pragati Prakashan, Meerut **(1996)**

11. Masri M.A. and Randall V.G., Proceedings of First International conference on Chitin/Chitosan, Massachusetts Institute of technology, MA, 277-291 **(1978)**

12. Mckay G., Bino M.J. and Altameni A.R., The Adsorption of various pollutants from aqueous solution onto Activated carbon, *Water Research*, **19**, 491-495 **(1985)**

13. Milot C., Mcbrien J., Allen S. and Goibal E., Influence of Physicochemical and Structural Characteristics of Chitosan Flakes on Molybdate sorption, *Journal of applied polymer science*, **68**, 571-579 **(1998)**

14. Peniche-Covas C. et al, The adsorption of mercuric ions by chitosan, *Journal of Applied Polymer Science*, **46(7),** 1147-1150 **(1992)**

15. Rawal N., Vaishya R.C. and Dutta P.K., Removal of Heavy Metal Ions from Industrial Effluent Using Chitosan and their Derivatives-A Review, In proceedings of National Seminar on Polymer: A Smart Material Opportunities and Needs in Polymer Science & Future Technologies held in M.N.N.I.T., Allahabad **(2002)**

16. Rorrer G.L., Hsien T.Y. and Way J.D., Synthesis of porousmagnetic chitosan beads for removal of cadmium ions from waste water, *Industrial and Engineering Chemistry Research*, **32 (9)**, 2170-2178 **(1993)**

17. Weber W.J. and Morris J.C., Kinetics of adsorbent on Carbon from Solution, *Journal Environmental Engineering (ASCE)*, **87(7),** 31-59 **(1963)**

18. Zogorski J.S., Faust S.D. and Hass J.H., The kinetics of dsorption of Phenols by Granular Activated Carbon, *Journal of Colloid and Interface Science*, **55**, 329-341 **(1976)**.

(Received 20th April 2013, accepted 25th June 2013)

Synthesis of Some-2-thioxo-3-substituted-2,3-dihydro-1H-quinazolin-4-one Derivatives as Potential Antibacterial and Antifungal agents

Al-ALshaikh Monirah *, Al-Shammary Danah and El-Baih Fatima
Medical Studies and Sciences Section, Chemistry Department College of Science, King Saud University, Riyadh, SAUDI ARABIA
*mshaikh@ksu.edu.sa

Abstract

A series of 2-thioxoquinazolinone derivatives 2a-d have been synthesized via condensation of the anthranilic acid derivatives with aryl isothiocyanate in the presence of absolute ethanol using ultrasound irradiation method. The substituted-4-oxoquinazolin-2-yl-thioethylacetate derivatives 3a-d were prepared by S-alkylation of quinazolin-2-thione derivatives 2a-d with ethyl chloro acetate followed by hydrazine hydrate offered the hydrazide derivatives 4a-d. The structures of the synthesized compounds were mainly confirmed on the basis of spectroscopic methods. The synthesized compounds 2a-d, 3a-d, 4a and 4c,d were screened for antibacterial and antifungal activities.

Keywords: Ultrasound irradiation, potential anti microbial, 3-substituted-2-thioxoquinazolinone.

Introduction

Synthesis of quinazolinone heterocycles is an attractive field for synthetic chemists due to their diverse range of pharmacological activities.[1,2] New derivatives of 2-thioxo-3-subtituted-2,3-dihydro-1*H*-quinazolin-4-one were synthesized and evaluated as anti-inflammatory which exhibited significant anti-inflammatory activity compared to that of standard drug diclofenac sodium[3]. One of the most frequently encountered heterocycle in medicinal chemistry is quinazolin-4(3*H*)-one and its derivatives are reported to possess variety of biological applications as anti-HIV[4], antitumor[5-7], anti histamic,[8] antimicrobial[9-11], antibacterial[12-14] and antidepressant[15,16]. Moreover, quinazolinone skeleton is very common in several naturally occurring alkaloids displayed in a wide range of biological activities as antimalarial agent.[17]

Material and Methods

All melting points (^{o}C, uncorrected) were determined using an electrothermal's IA 9000 series digital capillary melting point apparatus. IR spectra were obtained as KBr discs on a 1000 Perkin Elmer FT-IR spectrophotometer. ^{1}H and ^{13}C-NMR spectra were recorded on JEOL spectrometer ECP-300, 400 and 600 MHz in DMSO-d_6 as solvent and TMS as internal standard. Chemical shifts are given in ppm and coupling constants (*J*) are given in Hz. Ultrasound experiment was carried in a J.P. Selecta with frequency of 50/60 Hz and a nominal power of 770 W. Methods A and B refer to classical heating and ultrasound (US) respectively.

General procedure for the synthesis of 2a-d-Method A: Compounds 2a-d were prepared according to the literature procedures[9] by minor modification. An equimolar mixture of anthranilic acid derivatives (0.05 mol) and aryl isothiocyanate derivatives (0.05 mol) in absolute ethanol (50 ml) was refluxed for 6 h. The solvent was then evaporated under reduced pressure. The precipitated solid mass was filtered, washed with water, dried and re-crystallized from aq. ethanol.

Method B: An equimolar mixture of anthranilic acid derivatives (0.002 mol) and aryl isothiocyanate derivatives (0.002 mol) in absolute ethanol (3 ml) was irradiated in water bath of an ultrasonic cleaner at 80^{o}C for 30-60 min. The precipitate thus obtained was filtered, washed with ethanol (95%). The solid product was pure and did not need re-crystallization.

3-(4-Methoxyphenyl)-2-thioxo-2,3-dihydroquinazolin-4 (*1H*)-one (2a): White cubes, m.p. 281^{o}C; yield 68A, 75B%; IR (KBr, γ_{max}, cm^{-1}): 3232 (NH), 1662 (C=O), 1199 (C=S); ^{1}H-NMR (DMSO-d_6): δ, ppm = 3.79 (3H, s, OCH_3), 6.99 (2H, d, ^{3}J = 8.8, H-3',5', AA' part of AA'XX' system), 7.16 (2H, d, ^{3}J = 8.8, H-2',6', XX' part of AA'XX' system), 7.78 (1H, td, ^{3}J = 8.3, ^{4}J = 1.5, H-7), 7.79-7.30 (2H, m, H-6,8), 7.93 (1H, d, ^{3}J = 8.3, H-5), 13.01 (1H, br.s, NH); ^{13}C-NMR: 55.8 (OCH_3), 114.5, 114.6 (2C), 116.2, 116.7, 124.9, 128.1, 130.5 (2C), 132.5, 136.1, 140.1, 159.3, 177.0.

7-Chloro-3-phenyl-2-thioxo-2,3-dihydroquinazolin-4 (*1H*) -one (2b): White fine needles, m.p. 283^{o}C; yield 49A, 66B%; IR (KBr, γ_{max}, cm^{-1}): 3241 (NH), 1660 (C=O), 1192 (C=S); ^{1}H-NMR (DMSO-d_6): δ, ppm = 7.26 (2H, dd, ^{3}J = 7.7, ^{4}J = 1.4, H-2',6'), 7.34-7.47 (5H, m, H-5,8,3',4',5'), 7.92 (1H, dd, ^{3}J = 8.4, ^{4}J = 1.5, H-6), 13.10 (1H, br.s, NH); ^{13}C-NMR: 114.4, 114.6, 123.8, 127.6, 128.3 (2C), 128.4 (2C), 129.0, 138.5, 139.3, 139.9, 158.6, 175.9

6-Bromo-3-(4-methylphenyl)-2-thioxo-2,3-dihydroquinazolin-4(*1H*)-one (2c): White cubes, m.p. >300^{o}C; yield 17A, 60B%; IR (KBr, γ_{max}, cm^{-1}): 3233 (NH), 1662 (C=O), 1207 (C=S); ^{1}H-NMR (DMSO-d_6): δ, ppm = 2.37 (3H, s, CH_3), 7.13 (2H, d, ^{3}J = 8.02, H-3',5', AA' part of AA'XX' system), 7.27 (2H, d, ^{3}J = 8.02, H-2',6', XX' part of AA'XX' system), 7.38 (1H, d, ^{3}J = 8.8, H-8), 7.95 (1H, d, ^{3}J = 8.8, H-7), 7.99 (1H, d, ^{4}J = 1.8, H-5), 13.10 (1H, br.s, NH); ^{13}C-NMR: 21.3 (CH_3), 115.4, 117.5, 117.6, 128.1 (2C), 128.8, 129.0 (2C), 136.0, 137.1, 137.7, 138.2, 158.3, 175.7.

6-Iodo-3-phenyl-2-thioxo-2,3-dihydroquinazolin-4(*1H*)-one (2d): Yellowish cubes, m.p. >300°C; yield 50A, 68B%; IR (KBr, γ_{max}, cm^{-1}): 3232 (NH), 1661 (C=O), 1200 (C=S); ^{1}H-NMR (DMSO-d_6): δ, ppm = 7.23-7.27 (3H, m, H-8,2',6'), 7.41 (1H, t, ^3J = 7.32, H-4'), 7.47 (2H, t, ^3J = 7.32, H-3',5'), 8.08 (1H, dd, ^3J = 8.8, ^4J = 2.2, H-7), 8.18 (1H, d, ^4J = 2.2, H-5), 13.11 (1H, br.s, NH); ^{13}C-NMR: 88.3, 118.5, 118.8, 128.8, 129.4 (2C), 129.5 (2C), 135.8, 139.6, 139.7, 144.2, 159.1, 176.6.

General procedure for the synthesis of 3a-d: A mixture of 2a-d (0.001 mol) and sodium hydroxide (0.04 g) in absilute ethanol (3 ml) was stirred vigorously, then ethyl chloroacetate (0.2 ml) was added drop wise during 15-60 min with stirring. The solid product was filtered and washed with ethanol. The solid product was pure and did not need re-crystallization.

Ethyl{[3-(4-methoxylphenyl)-4-oxo-3,4-dihydroquinazolin-2-yl]thio}acetate (3a): White powder, m.p. 197°C; yield 74%; IR (KBr, γ_{max}, cm^{-1}): 1687, 1735 (2C=O); ^{1}H-NMR (DMSO-d_6): δ, ppm = 1.22 (3H, t, ^3J = 7.3, $\underline{CH_3}$–CH_2–), 3.83 (3H, s, OCH_3), 3.93 (2H, s, CH_2–), 4.11 (2H, q, ^3J = 6.9, CH_3–$\underline{CH_2}$–O), 7.09 (2H, d, ^3J = 8.8, H-3',5', AA' part of AA'XX' system), 7.35 (2H, d, ^3J = 8.8, H-2',6', XX' part of AA'XX' system), 7.43-7.48 (2H, m, H-6,8), 7.81 (1H, td, ^3J = 8.3, ^4J = 1.5, H-7), 8.04 (1H, d, ^3J = 8.3, H-5); ^{13}C-NMR: 13.7 ($\underline{CH_3}$–CH_2–), 35.0 (CH_2–CO–C), 55.1 (OCH_3), 60.6 (CH_3–$\underline{CH_2}$–O), 114.3 (2C), 118.9, 125.4, 125.6, 126.7, 127.5, 130.1 (2C), 134.5, 146.5, 156.7, 159.7 (C=O lactam), 160.3 (C-2), 167.9 (C=O ester).

Ethyl [(7-chloro-4-oxo-3-phenyl-3,4-dihydroquinazolin-2-yl)thio]acetate (3b): White fine needles, m.p. 130°C; yield 51%; IR (KBr, γ_{max}, cm^{-1}): 1695, 1741 (2C=O); ^{1}H-NMR (DMSO-d_6): δ, ppm = 1.19 (3H, t, ^3J = 6.9, $\underline{CH_3}$–CH_2–), 3.97 (2H, s, CH_2–), 4.12 (2H, q, ^3J = 6.9, CH_3–$\underline{CH_2}$–O), 7.44-7.51 (4H, m, H-8,2',4',6'), 7.56-7.58 (3H, m, H-5,3',5'), 8.08 (1H, d, ^3J = 9.2, H-6); ^{13}C-NMR: 13.7 ($\underline{CH_3}$–CH_2–), 34.9 (CH_2–CO–C), 60.7 (CH_3–$\underline{CH_2}$–O), 117.9, 124.4, 125.4, 125.8, 128.3, 128.8 (2C), 129.2 (2C), 129.7, 134.9, 138.7, 147.4, 158.1 (C=O lactam), 159.1 (C-2), 167.7 (C=O ester).

Ethyl{[6-bromo-3-(4-methylphenyl)-4-oxo-3,4-dihydroquinazolin-2-yl]thio}acetate (3c): White powder, m.p. 148°C; yield 94%; IR (KBr, γ_{max}, cm^{-1}): 1688, 1738 (2C=O); ^{1}H-NMR (DMSO-d_6): δ, ppm = 1.18 (3H, t, ^3J = 7.3, $\underline{CH_3}$–CH_2–), 2.47 (3H, s, CH_3), 3.94 (2H, s, CH_2–), 4.11 (2H, q, ^3J = 7.3, CH_3–$\underline{CH_2}$–O), 7.31 (2H, d, ^3J = 7.7, H-3',5', AA' part of AA'XX' system), 7.37 (2H, d, ^3J = 7.7, H-2',6', XX' part of AA'XX' system), 7.42 (1H, d, ^3J = 8.6, H-8), 7.95 (1H, d, ^3J = 8.6, H-7), 8.11 (1H, d, ^4J =1.8, H-5); ^{13}C-NMR: 13.7 ($\underline{CH_3}$–CH_2–), 20.4 (CH_3), 34.0 (CH_2–CO–C), 60.6 (CH_3–$\underline{CH_2}$–O), 117.7, 120.7, 127.8, 128.1, 128.4 (2C), 129.7 (2C), 132.3, 137.3, 139.5, 145.1, 157.4 (C=O lactam), 159.1 (C-2), 167.8 (C=O ester).

Ethyl [(6-iodo-4-oxo-3-phenyl-3,4-dihydroquinazolin-2-yl)thio]acetate (3d): White powder, m.p. 140°C; yield 68%; IR (KBr, γ_{max}, cm^{-1}): 1690, 1732 (2C=O); ^{1}H-NMR (DMSO-d_6): δ, ppm = 1.21 (3H, t, ^3J = 7.3, $\underline{CH_3}$–CH_2–), 3.95 (2H, s, CH_2–), 4.13 (2H, q, ^3J = 7.3, CH_3–$\underline{CH_2}$–O), 7.29 (1H, d, ^3J = 8.4, H-8), 7.48 (2H, t, ^3J = 8.8, H-3',5'), 7.59-7.60 (3H, m, H-2',4',6'), 8.12 (1H, dd, ^3J = 8.4, ^4J = 1.4, H-7), 8.3 (1H, d, ^4J = 1.4, H-5); ^{13}C-NMR: 14.7 ($\underline{CH_3}$–CH_2–), 35.0 (CH_2–CO–C), 61.6 (CH_3–$\underline{CH_2}$–O), 91.2, 121.9, 128.6, 129.8 (2C), 130.2 (2C), 130.7, 135.3, 136.0, 143.9, 146.8, 158.4 (C=O lactam), 159.9 (C-2), 168.8 (C=O ester).

General procedure for the synthesis of 4a-d: Hydrazine hydrate (0.2 ml) was added to a solution of each of 3a-d (0.0008 mol) in absolute ethanol (3 ml). The mixture was stirred at room temperature for 14-45 min. The precipitated solid mass was filtered and dried. The solid obtained was pure and did not need re-crystallization.

2-{[3-(4-methoxyphenyl)-4-oxo-3,4-dihydroquinazolin-2-yl]thio}acetohydrazide (4a): White fine needles, m.p. 210°C; yield 56%; IR (KBr, γ_{max}, cm^{-1}): 3446 (NH), 3337, 3308 (NH_2), 1689 (C=O lactam), 1649 (C=O hydrazide); ^{1}H-NMR (DMSO-d_6): δ, ppm = 3.83 (2H, s, CH_2–), 3.85 (3H, s, OCH_3), 4.28 (2H, br.s, NH_2),7.12 (2H, d, ^3J = 9.2, H-3',5', AA' part of AA'XX' system), 7.38 (2H, d, ^3J = 9.2, H-2',6', XX' part of AA'XX' system), 7.48 (1H, t, ^3J = 7.9, H-6), 7.61 (1H, d, ^3J = 7.9, H-8), 7.84 (1H, t, ^3J = 7.9, H-7), 8.08 (1H, d, ^3J = 7.9, H-5), 9.31 (1H, br.s, NH); ^{13}C-NMR: 35.0 (CH_2–CO–C), 56.0 (OCH_3), 115.2 (2C), 120.1, 126.5, 126.6, 127.1, 128.7, 131.2 (2C), 135.4, 147.7, 158.0, 160.7 (C=O lactam), 161.4 (2C), 166.7 (C=O hydrazide).

2-[(7-Chloro-4-oxo-3-phenyl-3,4-dihydroquinazolin-2-yl)thio]acetohydrazide (4b): White fine needles, m.p. 180°C; yield 59%; IR (KBr, γ_{max}, cm^{-1}): 3336 (NH), 3273, 3077 (NH_2), 1689 (C=O lactam), 1641 (C=O hydrazide); ^{1}H-NMR (DMSO-d_6): δ, ppm = 3.79 (2H, s, CH_2–), 4.28 (2H, br.s, NH_2), 7.47-7.57 (6H, m, H-6,2',3',4',5',6'), 7.70 (1H, d, ^4J = 1.8, H-8), 8.05 (1H, d, ^3J = 8.8, H-5), 9.31 (1H, br.s, NH); ^{13}C-NMR: 35.1 (CH_2–CO–C), 117.9, 124.8, 125.7, 128.2, 128.8 (2C), 129.1 (2C), 129.6, 134.7, 138.9, 147.9, 158.4 (C=O lactam), 159.6 (C-2), 165.7 (C=O hydrazide).

2-{[6-Bromo-3-(4-methylphenyl)-4-oxo-3,4-dihydroquinazolin-2-yl]thio}acetohydrazide (4c): White powder, m.p. 219°C; yield 96%; IR (KBr, γ_{max}, cm^{-1}): 3551 (NH), 3476, 3413 (NH_2), 1699 (C=O lactam), 1637 (C=O hydrazide); ^{1}H-NMR (DMSO-d_6): δ, ppm = 2.42 (3H, s, CH_3), 3.82 (2H, s, CH_2–), 4.28 (2H, br.s, NH_2), 7.33 (2H, d, ^3J = 8.1, H-3',5', AA' part of AA'XX' system), 7.38 (2H, d, ^3J = 8.1, H-2',6', XX' part of AA'XX' system), 7.57 (1H, d, ^3J = 8.8, H-8), 8.13 (1H, d, ^4J = 2.2, H-5), 8.24 (1H, dd, ^3J = 8.8, ^4J = 2.2, H-7), 9.31 (1H, br.s, NH); ^{13}C-NMR: 21.4 (CH_3), 35.1 (CH_2–CO–C), 118.5, 121.8, 128.8, 129.1

(2C), 129.6 (2C), 130.4, 138.2, 140.4, 146.7, 158.6 (C=O lactam), 160.2 (C-2),166.6 (C=O hydrazide).

2-[(6-Iodo-4-oxo-3-phenyl-3,4-dihydroquinazolin-2-yl) thio] acetohydrazide (4d): White powder, m.p. 220°C; yield 66%; IR (KBr, γ_{max}, cm^{-1}): 3429 (NH), 3314, 3202 (NH_2), 1693 (C=O lactam), 1661 (C=O hydrazide); ^{1}H-NMR (DMSO-d_6): δ, ppm = 3.83 (2H, s, CH_2–), 4.28 (2H, br.s, NH_2), 7.41-7.48 (5H, m, H-2',3',4',5',6'), 7.57 (1H, d, ^3J = 8.8, H-8), 8.13 (1H, dd, ^3J = 8.8, ^4J = 1.5, H-7), 8.33 (1H, d, ^4J = 1.5, H-5), 9.32 (1H, br.s, NH); ^{13}C-NMR: 35.0 (CH_2–CO–C), 90.9, 122.0, 128.9, 129.9 (2C), 130.1 (2C), 130.7, 135.2, 136.1, 143.7, 147.0, 158.3 (C=O lactam), 159.9 (C-2), 166.6 (C=O hydrazide).

Results and Discussion

The strategy to synthesize the target compounds 2a-d, 3a-d and 4a-d is shown in scheme 1. The synthesis of 2-thioxo-3-subtituted-2, 3-dihydro-1*H*-quinazolin-4-ones 2a-d was carried out in a moderate to good yield using conventional method. Furthermore, we have applied ultrasound irradiation method in order to prepare previous thioxoquinazolinone derivatives. In comparison with traditional methodology, the ultrasound irradiation has a number of advantages such as reducing the reaction time, simplicity, reducing pollution, high purity and improving the overall yields. The reaction conditions and yields of both methods are shown in table 1. The structures of 2a-d were assigned on the basis of spectroscopic analysis. Thus IR spectra of 2a-d showed three characteristic bands 3232-3241, 1660-1662 and 1192-1207 cm^{-1}, due to absorption of NH, C=O and C=S groups respectively. The protons and carbons in the NMR spectra of 2a-d were seen at their expected chemical shifts and integral values (c.f.exp).

Substituted-4-oxoquinazolin-2-yl-thioethylacetate derivatives 3a-d were obtained by the treatment of the corresponding 2a-d derivatives with ethylcholoroacetate in the presence of alcoholic sodium hydroxide by stirring at room temperature. This reaction gave us the ethyl ester derivatives in 51-94% yields. IR, ^{1}H-NMR and ^{13}C-NMR spectral data of 3a-d were in complete consistent with their structures. Thus, the IR spectra of 3a-d displayed two bands at 1732-1741 cm^{-1} and at 1688-1695 cm^{-1} attributed for 2 C=O stretching of ester and lactam groups respectively. ^{1}H-NMR spectrum of 3d exhibited a triplet with J = 7.3 Hz at δ 1.21ppm for (CH_3-CH_2), singlet at 3.95 ppm for (CH_2-), quartet with J = 7.3 Hz at δ 4.13 for (CH_3-CH_2O). The ^{13}C-NMR indicated the presence of two C=O signals. Acetohydrazide derivatives 4a-d were prepared by hydrazinolysis of the ethylester 3a-d with hydrazine hydrate via nueclophilic nitrogen attack of the hydrazine moiety to the carbonyl group of ester group through tetrahedral mechanism.

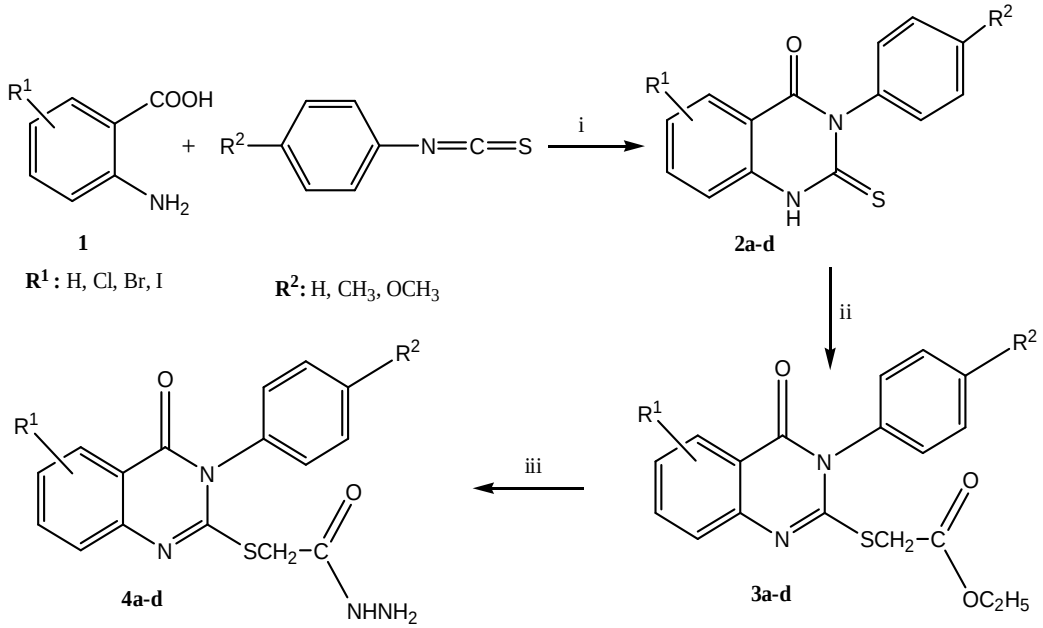

	R^1	R^2
a	H	OCH_3
b	Cl	H
c	Br	CH_3
d	I	H

i) A: absolute EtOH, reflux, 6 h; B: U.S, 30-60 min.
ii) Ethyl chloroacetate, absolute EtOH/ NaOH (0.04%), stirring, r.t, 15-60 min.
iii) $NH_2NH_2.H_2O$, absolute Et OH, stirring, r.t., 15-45 min.

Scheme 1
Synthetic pathway for compounds 2a-d, 3a-d and 4a-d

Table 1
Yields and reaction conditions used for the synthesis of 2a-d

Compound No.	US (80°C)		Classical method	
	t (min)	Yield (%)	t (h)	Yield (%)
2a	60	75	6	68
2b	30	66	6	49
2c	60	60	6	17
2d	60	68	6	50

Table 2
Antimicrobial activity of the tested compounds at 100 mg/ml concentration

Compound No.	*EC*	*K P*	*P V*	*PA*	*B S*	*S A*	*S P*	*CA*	*S C*	*F M*	*A F*
2a	08	00	00	00	00	00	00	00	00	00	00
2b	07	00	00	09	08	08	07	00	00	09	08
2c	10	11	09	09	08	00	00	08	09	00	00
2d	09	07	07	07	00	00	00	00	00	00	00
3a	00	00	07	07	09	07	07	00	08	00	00
3b	08	07	00	00	09	10	08	00	00	00	00
3c	00	00	00	00	08	00	00	00	00	00	00
3d	08	00	07	00	07	00	00	07	07	00	00
4a	00	00	08	07	09	08	00	00	00	08	00
4c	00	00	00	00	00	00	00	00	00	00	00
4d	08	00	00	07	07	07	07	00	00	00	00
Gentamicin	20	19	19	17	NT	NT	NT	NT	NT	NT	NT
Ampicillin	NT	NT	NT	NT	32	27	24	NT	NT	NT	NT
Amphotericin B	NT	NT	NT	NT	NT	NT	NT	25	28	24	19

NT = not tested

The structures of the synthesized compounds were confirmed by spectroscopic analysis. Thus IR spectra of 4a-d exhibited characteristic bands at 3336-3551 and 3077-3413 due to the absorption of symmetric and asymmetric bands of NH/NH_2, two significant bands at 1686-1699 cm^{-1} and at 1637-1661 cm^{-1} attributed for 2C=O stretching of lactam and hydrazide groups respectively. ^{1}H-NMR spectrum of 4c showed a singlet at δ 2.42 ppm for the protons of the methyl group, singlet at δ 3.82 ppm for (CH_2-), two broad singlets at δ 4.28 ppm and δ 9.31 ppm for NH_2 and NH protons respectively. The spectrum of the aromatic protons appeared as a pair of doublets at δ 7.33 ppm (H-$\hat{3}$,$\hat{5}$) and δ 7.38 ppm (H-$\hat{2}$,$\hat{6}$) with J = 8.1. The ^{13}C-NMR spectral data was in good agreement with its structure (c.f.exp).

Antimicrobial Testing

Preliminary experiments were carried out to determine microbial activities of titled compounds in vitro using the following organisms : (i) Gram – negative bacteria including *Escherichia coli* (*EC*), *Klebsiella pneumonia (KP*), *Porteus vulgaris* (*PV*), *Pseudomonas aeruginosa* (*PA*).(ii) Gram-positive bacteria including *Bacillus subtilis* (*BS*), *Staphylococcus aureus* (*SA*), *Streptococcus pneumonia* (*SP*) and (iii)Unicellular and filamentous fungi including *Candida albicans* (*CA*), *Saccharomyces cirivisae* (*SC*), *Fusarium moniliforme* (*FM*) and *Aspergillus fumigatus* (*AF*), respectively by well diffusion method according to National Committee for Clinical Laboratory Standards.[18] Petri plates containing 20 ml of nutrient for bacteria or malt extract for fungi agar medium were seeded with 1-3 days grown cultures of microbial inoculums (standardized inoculums 1-2 × 10^7 cfu/ml 0.5 McFarland Standard). Wells (6 mm in diameter) were divided into agar and 50 µl of compound was tested in a concentration of 100 mg/ml and incubated at 37°C (bacterial strains) and at 25°C (fungal strains) for 24-48h. The antimicrobial activities were determined based on measurement of the diameter of the inhibition zone formed around the well using gentamicin, ampicillin and amphotericin B as the positive controls.

Antimicrobial Screening

Table 2 shows the antimicrobial activities of the compounds (2a – 2d), (3a – 3d) and (4a, 4c, 4d) on the three selective microbial groups in comparison to the standard antibiotic inhibition zones. Compound 2a gave a moderate 40% inhibitory activity to *EC*, but compound 2b has a wider effect on these microbial groups (*EC*, *PA*, *BS*, *SA*, *SP*, *FM* and *AF*) ranging from 30 – 42 %. Also compound 2c emphasized a moderate to good activity on gram – negative bacteria and unicellular fungi (*EC*, *KP*, *PV*, *PA*, *CA* and *SC*). Both compounds 2c and 2b have shown a good inhibitory effect on some of these microbial groups (30 – 57%), while compound 2d showed a moderate activity only on gram – negative bacteria (36 – 45%) (*EC*, *KP*, *PV* and *PA*).

Compound 3a has a slight to moderate inhibition against some of these pathogens specially gram – negative and some of the gram positive and unicellular fungi ranging from 26 – 41 % (*PV, PA, BS, SA, SP* and *SC*), but compound 3b has a more moderate effect (28 – 40%) against both gram – negative and gram – positive bacteria (*EC* and *KP*) and (*BS, SA* and *SP*) respectively, while compound 3c showed slight activity 25% on (*BS*) only, compound 3d has also a slight to moderate activity (21 – 40%) on these microbial groups (*EC, PV, BS, CA* and *SC*), both compounds 4a and 4d have a similar inhibitory activities (21 – 41%) on some of these organisms (*PV, PA, BS, SA, SP* and *FM*). Moreover, compound 4c did not have any inhibitory effect toward these organisms.

In conclusion, compounds 2b, 2c, 3a, 3b, 3d and 4d have a promising inhibitory effect that requires further study and exploration.

Conclusion

Synthesis of some 2-thioxo-3-substituted-2,3-dihydro-*1H*-quinazolin-4-one derivatives has been described using ultrasound irradiation method as eco-friendly energy source. Structures of the prepared compounds were elucidated on the basis of various spectroscopic methods.

Acknowledgement

This research project was supported by a grant from the "Research Center of the Center for Female Scientific and Medical

References

1. Hattori K., Kido Y., Yamamoto H., Ishida J., Iwashita A. and Mihara K., *Bioorg., Med. Chem. Lett.*, **17**, 5577-5581 **(2007)**

2. Ye C., You J., Li X., You R., Weng Y., Li J. and Wang Y., *Pestic. Biochem. Phys.*, **97**, 194-198 **(2010)**

3. Aiydu R., Velayuthem R. and Sabarimuthu D., *Japan. J. Pharm. Sci.*, **131(7),** 1079-108 **(2011)**

4. Al-Omran F., Elassar A. and El-Kair A., *Tetrahedron*, **57**, 10163-10170 **(2001)**

5. Al-Rashood S.T., Aboldahb I.A., Nagi M.N., Abouzeid L.A., Abdelaziz A.A., Abdelhamide S.G., Yousef K.M., Al-Obaid A.M. and El-Subbagh H.I., *Bioorg. Med. Chem.*, **14**, 8608-8621 **(2006)**

6. Al-Obaid A.M., Abdelhamide S.G., El-Kashef H.A., Abdelaziz A. M., El-Azab A.S., Al-Khamees H.A. and El-Subbagh H.I., *Eur. J. Med. Chem.*, **44**, 2379-2391 **(2009)**

7. El-Azab A.S., Al-Omar M.A., Abdelaziz A.A., Abdelaziz N.I., El-Sayed M.A., Aleisa A.M., Sayedahmed M.M. and Abdelhamide S.G., *Eur. J. Med. Chem.*, **45**, 4188-4198 **(2010)**

8. Fazal Mohamed M.I., Krishnamoorthy G. and Venkatraman B.R., Synthesis, Antibacterial and Antifungal Activities of Mannich Bases of 8-hydroxyquinoline Derivatives, *Res. J. Chem. Environ.,* **10(4),** 93-96 **(2006)**

9. Pandey S.K., Singh A. and Nizamuddin A., *Eur. J. Med. Chem.*, **44**, 1188-1197 **(2009)**

10. Suresha G.P., Suhas R., Kapfo W. and Gowda D.C., *Eur. J. Med. Chem.*, **46**, 2530-2540 **(2011)**

11. Prasad K.S., Kumar L.S., Chandan S., Jayalakshmi B. and Revanasiddappa H.D., *Spectrochimica Acta,* Part A**, 81**, 276-282 **(2011)**

12. Mallikarjuna B.P., Sastry B.S., Kumar G.V., Rajendraprasad Y., Chandrashekar S.M. and Sathisha K., *Eur. J. Med. Chem.*, **44**, 4739-4746 **(2009)**

13. Mohamed M.S., Kamel M.M., Kassem E.M., Abotaleb N., El-moez S.I. and Ahmed M.F., *Eur. J. Med. Chem.*, **45**, 3311-3319 **(2010)**

14. Kumar K., Sharma P., Kumari P. and Kalal B.L., *Bioorg. Med. Chem.*, **21**, 4353-4357 **(2011)**

15. Na Y.H., Hong S.H., Lee J.H., Park W.K., Baek D.J., Koh H.Y., Cho Y.S., Choo H. and Pae A.N., *Bioorg. Med. Chem.*, **16**, 2570-2578 **(2008)**

16. Kelekci N.G., Koyunoğlu S., Yabanöglu S., Yelekci K., Özgen Ö., Ucar G., Erol K., Kendi E. and Yesilada A., *Bioorg. Med. Chem.*, **17**, 675-689 **(2009)**

17. Zhu S., Wang J., Chandrashekar G., Smith E., Liu X. and Zhang Y., *Eur. J. Med. Chem.*, **45**, 3864-3869 **(2010)**

18. National Committee for Clinical Laboratory Standards, Reference Method for Broth Dilution Antifungal Susceptibility Testing of Conidium-Forming Filamentous Fungi: Proposed Standard M38-A.NCCLS, Wayne, PA, USA **(2002).**

(Received 04th March 2013, accepted 12th June 2013)

Removal of Pb(II) from aqueous solution using natural rice husk

Ong Siew-Teng[1*], Foo Yee-Cheong[2] and Hung Yung-Tse[3]
1. Department of Chemical Science, Faculty of Science, Universiti Tunku Abdul Rahman, Jalan Universiti, Bandar Barat, 31900 Kampar, Perak, MALAYSIA
2. Department of Science, Faculty of Engineering and Science, Universiti Tunku Abdul Rahman, Jalan Genting Kelang, Setapak 53300 Kuala Lumpur, MALAYSIA
3. Department of Civil and Environmental Engineering, Cleveland State University, Cleveland, Ohio USA
*ongst@utar.edu.my

Abstract
The potential of natural rice husk (NRH) to adsorb Pb(II) from aqueous solution was being investigated under various experimental conditions. The parameters studied were pH, initial concentration of metal solutions, contact time, sorption isotherm, agitation rate and sorbent dosage. Results from batch study showed that the sorption process was pH dependent and the efficient pH range for maximum uptake was 5.0 to 7.0. From the contact time study, the uptake of Pb(II) was very rapid and equilibrium was attained in less than 30 minutes.

By fitting the experimental data into pseudo- first and pseudo-second kinetic model equations, the sorption process was better explained by the latter. An increase in percentage uptake of Pb(II) can be observed with increasing contact time, agitation rate and sorbent dosage. The sorption process conformed to the Langmuir isotherm with the maximum sorption capacities of 12.08 mg/g.

Keywords: Sorption, Pb(II), Rice husks, Batch study, Sorption isotherm, Kinetic study.

Introduction

Wastewater from electroplating, mining operation, tanneries, smelting and battery manufacturing industries are usually contaminated with a variety of heavy metal ions that have to be removed before their discharge into waterways. Unlike organic pollutants, the majority of which are susceptible to biological degradation, heavy metal ions do not degrade into harmless end products. The excessive release of heavy metals into the environment due to industrialization and urbanization has therefore posed a great problem worldwide due to their toxicity to the ecosystem and health.

Heavy metals may be defined as the elements having atomic weights between 63.5 and 200.6 and have a minimum specific gravity of 5[1]. Heavy metals become toxic when they are not metabolized by the body and accumulate in the soft tissues. The routes in which heavy metals may enter the human body are through food, water, air or absorption through the skin. Amongst all, industrial exposure accounts for the most common route of exposure for adults and as for children, it is through ingestion.

Lead (Pb) is one of the few common metals that have a widespread usage in the industries. The major uses of lead and its compounds are storage battery, pigment, plumbing, cable covering and ammunition. As a result, this leads to a significance level of lead wastes in the environment. The removal of lead wastes has been of great concern because lead is categorized as one of the top 20 hazardous substances under U.S. Environmental Protection Agency.

According to Malaysia Environmental Quality (Sewage and Industrial Effluent) Regulation 1979, the limit of lead content in effluent to be discharged is required to be not more than 0.1 mg/L. Strict regulation has been imposed because lead is toxic in all forms and it has also been reported that the exposure to lead increases the risk of kidney failure, disruption of central nervous system, brain damage and even death in cases of extremely high exposure[2].

A number of technologies have been developed over the years to remove toxic metal ions from wastewater. Some of the most commonly treatment methods include chemical precipitation, ion exchange, electrode-position and membrane process. However, there are still some problems associated with these conventional treatment methods. For example, the generation of sludge from chemical precipitation creates another environmental problem[3]. Besides, this method is not really applicable if the targeted metal ion is highly soluble and does not precipitate out from the solution at any pH. Ion exchange and membrane process are generally effective but have rather high maintenance and operation costs and subject to fouling.

In view of the limitations and problems associated with the treatment processes mentioned above, studies have been intensified on the search of developing a more economical approach to remove heavy metal from aqueous solution. In this regard, adsorption appears to be a practicable method, in particular, if the sorbent is of naturally occurring, locally available and inexpensive material. A number of investigations have shown the potential of using low cost materials as alternative sorbent for the removal of heavy metals and these include tea leaves, wheat, chitosan and fly ash[4-7].

In our continuing effort to search for the low cost sorbent for heavy metal removal, the potential of rice husk to remove lead from aqueous solution was being explored. Rice hull was selected as the sorbent in this study because it is generated as a waste during the first stage of rice milling, when rough rice or paddy rice is husked (husk is separated from the rest of the grain). The amount of husk produced would depend on the types of grains, but generally, 100 kg of paddy rice will generate 20 kg of husk. Hence, the utilization of this waste material will not only reduce the environment burden but could also be beneficial to the economy.

Material and Methods

Preparation of reagents: All the chemicals used in this experiment were of A.R. grade. The synthetic heavy metal solution was prepared from A.R. grade $Pb(NO_3)_2$.

Preparation of sorbent: The rice husk was collected from a local rice mill. It was washed thoroughly with water and then sun dried. The dried rice husk was ground to size of 1 mm using a grinder and labeled as natural rice husk (NRH).

Batch experiments: All the batch experiments were carried out in duplicate and the results given are the means with a relative standard deviation (RSD) of less than 5 %. Control experiments were performed without sorbent to ascertain that the sorption was by the sorbent and not the wall of the container. All the sorption experiments were performed by agitating 0.10 g of NRH in 20 mL of Pb(II) solution in a centrifuge tube. The mixtures were agitated at 150 rpm on an orbital shaker for 4 hours at room temperature (25 $\pm$ 2 ^{o}C) unless otherwise stated. The sorbent-sorbate mixture was then centrifuged at 3.0×10^3 rpm for phase separation. The final concentrations of the metal ions were analyzed by ICP-AES to obtain the amount of Pb(II) sorbed by NRH.

The effect of pH on Pb(II) sorption was studied by equilibrating the sorption mixture at different pH values. This was achieved by the addition of HCl or NaOH solution. The study pH range was 2-7 and the initial Pb(II) concentration was 50 mg/L. Contact time experiments were performed using Pb(II) concentrations ranging from 25 to 100 mg/L. The samples were withdrawn and analyzed for their Pb(II) concentrations at predetermined intervals. The effect of agitation rate was investigated by varying the agitation rates from 50 to 250 rpm using Pb(II) solution of 50 mg/L. Sorption isotherms were obtained by varying Pb(II) concentrations from 20 to 150 mg/L. The effect of sorbent dosage was studied by varying the amount of NRH from 0.05 to 0.60 g with 50 mg/L Pb(II) solutions.

Results and Discussion

Effect of pH: In most of the sorption process of heavy metal ions, pH is known to be having an influential effect on the uptake of the metal ions. Therefore, the sorption behavior of Pb(II) was examined under different pH values. From figure 1, it can be seen that the uptake of Pb(II) by NRH increased in the pH range of 2 to 4 and thereafter remained relatively constant. The lower uptake at pH below 3 was associated with the presence of excess hydronium ions. When NRH was surrounded by hydronium ions, this inhibits Pb(II) from reaching the binding sites and subsequently leads to a lower uptake. Besides, under acidic condition, the protonation of carboxylic groups might occur, hence incapable to bind Pb(II) ions[8]. It was obvious that Pb(II) was effectively sorbed in the pH range of 5.0-7.0. With increasing pH values, sorption became favorable because negative sorption sites were made available by more COO^- functional groups on the NRH for binding with Pb(II). Since the difference in the percentage uptake of Pb(II) at the natural pH (pH 6) and pH 7.0 was minimal, thus for all the subsequent experiments, it was carried out at the natural pH of the Pb(II) solution. A similar trend was reported in the study on removal of lead from aqueous solution using low cost abundantly available adsorbents[9].

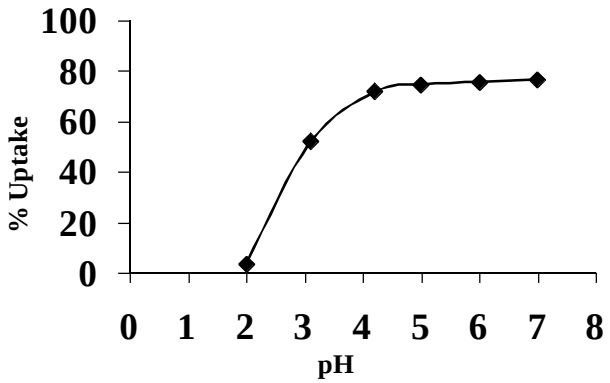

Figure 1: Effect of pH on the sorption of Pb(II) by NRH

Effect of Contact Time and Initial Concentrations: The sorption rate of Pb(II) by NRH is shown in figure 2. Regardless of the initial concentrations, the uptake of Pb(II) was very rapid and equilibrium was attained in less than 30 minutes. Based on the results obtained, it is suggested that the sorption process might involve more than one mechanism. The fast and rapid uptake at the beginning might be due to the fast ion exchange whereas the slower portion is closely related to chemisorption[10]. As for the effect of varying concentrations, the trend obtained followed a typical and normal course of sorption process whereby the least concentrated showed the highest uptake. The uptake of Pb(II) is highly dependent on the availability of the binding sites. When all the available binding sites have been occupied by the sorbates, the percentage uptake would remain almost constant. Any additional time would no longer influence the sorption process.

Sorption Kinetic: The kinetics study of a sorption process is important because it provides information such as the time needed to attain equilibrium, reaction pathways and mechanisms of sorption reaction. In order to explore the kinetics involved in Pb(II) sorption, the experimental data were fitted into the following equations[11,12]:

$$\log (q_e - q_t) = \log q_e - k_1 t/2.303 \text{ (pseudo-first order)} \quad (1)$$

$$t/q_t = 1/h + t/q_e \text{ (pseudo-second order)} \quad (2)$$

where q_e = the amount of Pb(II) sorbed at equilibrium (mg/g), q_t = the amount of Pb(II) sorbed at time t (mg/g), k_1= the rate constant of pseudo-first order sorption (1/min), h ($k_2 q_e^2$) = the initial sorption rate (mg/g min) and k_2= the rate constant of pseudo-second order kinetics (g/mg min). The experimental result indicated that the sorption process of Pb(II) by NRH does not fit well into pseudo-first order kinetic equation. The non applicability of pseudo-first order equation of Lagergren in biosorption processes has also been previously reported in the some of the studies involving durian peel, rice husk, sugarcane bagasse and fly ash[13-16]. Linear plots of t/q_t versus t with high correlation coefficients (Figure 3) indicate that the sorption process of Pb(II) is more appropriately described by the pseudo-second order model which was based on the assumption that the rate limiting step may be chemical sorption or chemisorption involving valency forces through sharing or exchange of electron between sorbent and sorbate [17].

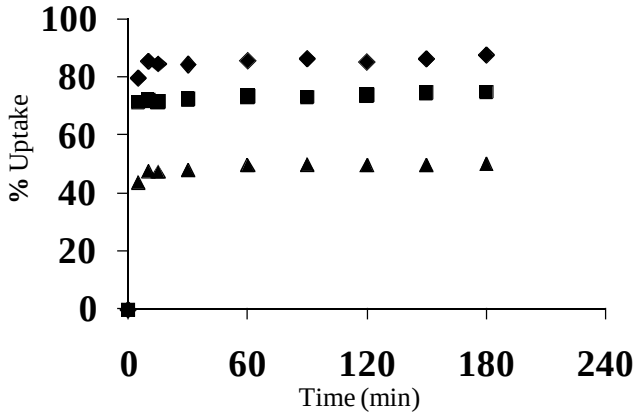

Figure 2: Effect of initial concentrations and contact time on the sorption of Pb(II) by NRH. ♦, ■, ▲ – 50, 100 and 200 mg/L of Pb(II)

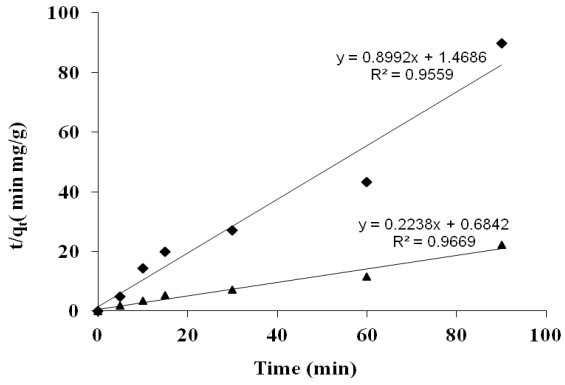

Figure 3: Pseudo-second order sorption kinetics of Pb(II) on NRH. ♦,▲ – 25 and 50 mg/L of Pb(II)

Sorption Iostherm: The relationship between the amount of sorbates sorbed and the remaining sorbates in solution is described by an isotherm. Equilibrium isotherms are commonly used to determine the capacity of the sorbent for the sorbates. In this study, the two most common isotherm models, namely Langmuir and Freundlich isotherms are being used to identify which one could provide reasonable fittings for the sorption data of Pb(II) onto NRH. The Langmuir model assumes that sorption cannot proceed beyond monolayer coverage and it is having constant sorption energy. As for Freundlich model, it can be used for non ideal sorption that involves heterogenous sorption. The linearized equation for Langmuir model is expressed by the following:

$$\frac{C_e}{N_e} = \frac{1}{Q_o K_L} + \frac{C_e}{Q_o} \quad (3)$$

whereas the linear form of Freundlich isotherm model can be represented as:

$$\log N_e = \frac{\log C_e}{n} + \log K_f \quad (4)$$

where C_e = the equilibrium liquid phase Pb(II) concentration (mg/L), N_e = the amount of Pb(II) sorbed at equilibrium (mg/g), Q_o = the maximum sorption capacity (mg/g), K_L = the sorption equilibrium constant (L/mg), n = Freundlich constant for intensity and K_f = Freundlich constant for sorption capacity. Based on the correlation coefficient values from figures 4-5, the sorption data of Pb(II) onto NRH appeared to conform more closely to the Langmuir model.

Effect of Agitation Rate: The effect of the agitation of the sorbent/sorbate system in Pb(II) sorption was monitored at low, medium and high speed of agitation speeds (Figure 6). The uptake of Pb(II) was found to be agitation dependent from 50 to 150 rpm but thereafter the effect was minimal. The uptake increased from 66.57% to 73.08% as the agitation rate increased from 50 rpm to 250 rpm. This is because agitation facilitates a proper contact between the metal ions in solution and the biomass binding sites and thereby promotes effective transfer of sorbate ions to the sorbent sites. The minimal effect of agitation speed on the sorption rate and capacity beyond 150 rpm indicates that the external mass transfer was not limiting in a well agitated system.

Effect of Sorbent Dosage: The effect of sorbent dosage on the uptake of Pb(II) by NRH is shown in table 1. It followed the usual pattern of increasing uptake as the sorbent dosage increased. The uptake increased from 48.49% to 93.29% when the sorbent dosage increased from 0.05 g to 0.3 g. This is corresponding to the increase of binding sites for sorption. Saturation occurred at around 0.30 g to 0.50 g of sorbent dosage for Pb(II) whereby

further increase in sorbent dosage had little effect on the sorption. This suggests that with certain amount of sorbent dosage, maximum sorption was achieved; hence the amount of ions bound to the sorbent and the amount of free ions remained constant even with further addition of the dose of sorbent.

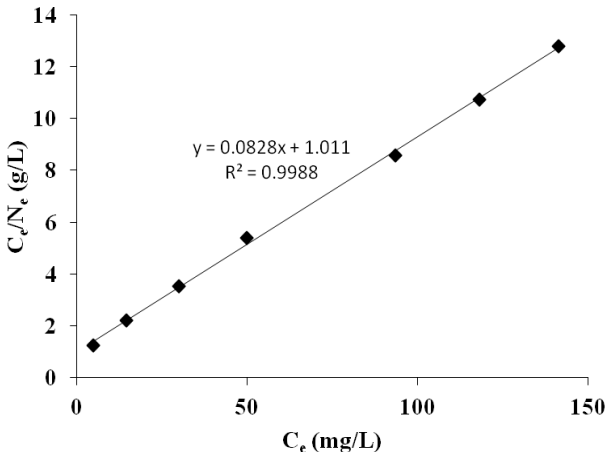

Figure 4: Langmuir isotherm for the sorption of Pb(II) by NRH

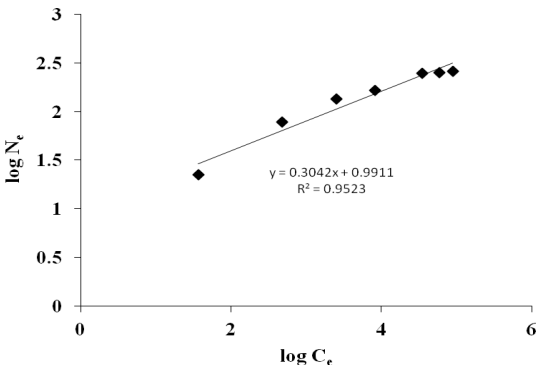

Figure 5: Freundlich isotherm for the sorption of Pb(II) by NRH

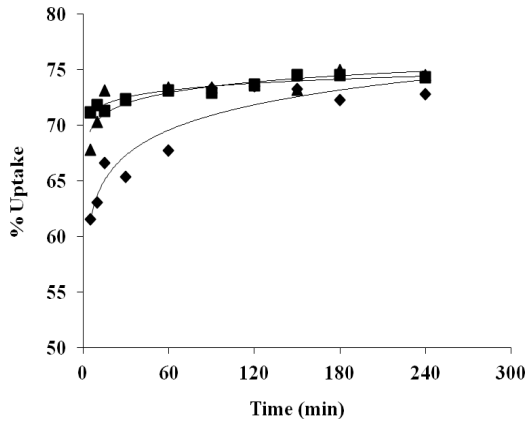

Figure 6: Effect of agitation rate on Pb(II) uptake by NRH. ♦,▲, ■ – 50, 150 and 250 rpm

Table 1
Effect of sorbent dosage on the sorption of Pb(II) by NRH

Dosage (g)	Uptake (%)
0	0
0.05	48.49
0.10	74.41
0.20	89.91
0.30	93.29
0.40	95.07
0.50	95.31
0.60	95.24

Conclusion

This study shows that NRH can serve as an attractive, yet economical sorbent for Pb(II) removal from aqueous solution. The results obtained indicated that sorption efficiency of NRH was considerably affected by pH, initial Pb(II) concentrations, contact time, agitation rate and sorbent dosage. The optimal pH range for maximum uptake was 5.0 to 7.0 and based on the contact time study, it can be concluded that the uptake of Pb(II) was very rapid and equilibrium was achieved in less than 30 minutes. The equilibrium data conform to Langmuir isotherm with maximum sorption capacity of 12.08 mg/g. Analysis of the kinetics data implied that pseudo-second order kinetics model provided a better correlation of the experimental results than pseudo-first order kinetic.

Acknowledgement

The authors are grateful to the support of the International Foundation for Science, Stockholm, Sweden and the Organisation for the Prohibition of Chemical Weapons, The Hague, The Netherlands via grant no. W/4386-1 and Universiti Tunku Abdul Rahman (UTAR).

References

1. Srivastava N.K. and Majumder C.B., Novel biofiltration methods for the treatment of heavy metals from industrial wastewater, *J. Hazard. Mater.*, **151**, 1-8 **(2008)**

2. Jones D.J., Primary prevention and health outcomes: Treatment of residential lead-based paint hazards and the prevalence of childhood lead poisoning, *J. Urban Economics*, **71**, 151-164 **(2012)**

3. Barakat M.A., New trends in removing heavy metals from industrial wastewater, *Arabian J. Chem.*, **4**, 361-377 **(2011)**

4. Huang G.L., Zhang H.Y., Jeffrey X.S. and Tim A.G.L., Adsorption of chromium (VI) from aqueous solutions using cross-linked magnetic chitosan beads, *Industrial & Eng. Chem. Res.*, **48**, 2646–2651 **(2009)**

5. Hossain M.A., Kumita M., Michigami Y. and More S., Optimization of parameters for Cr (VI) adsorption on used black tea leaves, *Adsorption*, **11**, 561-568 **(2005)**

6. Hsu T.C., Yu C.C. and Yeh C.M., Adsorption of Cu^{2+} from water using raw and modified coal fly ashes, *Fuel*, **87**, 1355-1359 **(2008)**

7. Farooq U., Khan M.A., Atharc M. and Kozinskia J.A., Effect of modification of environmentally friendly biosorbent wheat (Triticum aestivum) on the biosorptive removal of cadmium(II) ions from aqueous solution, *Chem. Eng. J.*, **171**, 400-410 **(2011)**

8. Abdel-Ghani N.T., Hefny M. and El-Chaghaby G.A.F., Removal of lead from aqueous solution using low-cost abundantly available adsorbents, *Int. J. Environ. Sci. Technol*., **4**, 67-74 **(2007)**

9. Ong S.T., Keng P.S. and Lee C.K., Determination of the role of different surface functional groups on EDA modified rice hull in the sorption of dyes, *Asian. J. Chem.*, **24,** 2665-2667 **(2012)**

10. Low K.S., Lee C.K. and Tai C.H., Biosorption of copper by water hyacinth roots, *J. Environ. Sci. Health*, **A29**, 171-188 **(1994)**

11. Rahman I. A., Sing Y. Y., Bari M. F. and Saad B., Adsorption of Paraquat by Treated and Untreated Rice Husks Studied by Flow Injection-Analysis, *Res. J. Chem. Environ.*, **9(1)**, 17-22, **(2005)**

12. Ho Y. S. and McKay G., Pseudo second order model for sorption process, *Proc. Biochem.*, **34**, 451-465 **(1999)**

13. Ong S.T., Khoo E.C., Hii S.L. and Ha S.T., Utilization of sugarcane bagasse for removal of basic dyes from aqueous environment in single and binary systems, *Desalination and Water Treatment J.*, **20,** 86-95 **(2010)**

14. Ong S.T., Tan S.Y., Khoo E.C., Lee S.L. and Ha S.T., Equilibrium studies for Basic blue 3 adsorption onto durian peel (Durio zibethinus Murray), *Desalination and Water Treatment J*., **45,** 161-169 **(2012)**

15. Ho Y. S. and McKay G., Comparative sorption kinetic studies of dye and aromatic compounds onto fly ash, *J. Environ. Sci. Health*, **A34**, 1179-1204 **(1999)**

16. Wong K. K., Lee C. K., Low K. S. and Haron M. J., Removal of Cu and Pb from electroplating wastewater using tartaric acid modified rice husk, *Pr. Biochem.*, **39**, 437-445 **(2003)**

17. Ho Y. S. and McKay G., The kinetics of sorption of divalent metals ions onto sphagnum moss peat, *Wat. Res.*, **34**, 735-742 **(2000).**

(Received 02nd March 2013, accepted 27th June 2013)

Influence of Soil Components on Phosphorus availability in some soils of Egypt

Wahba M. M.
Soils and Water Use Department, National Research Centre, Cairo, EGYPT
moniermorad@yahoo.com

Abstract

Structure of calcite mineral is very important to study the supplying power of phosphorus in the soil. In addition, calculating the bonding energy and the Phosphorus Recovery Index (PRI) may assess the phosphorous deficiency in the soil. These parameters can be used as indicators for the supplying power of phosphorus and its dynamics in the soil-plant system rather than the classical determination of available phosphorus. Soil components, namely, clay, calcium carbonate (calcite mineral) and iron oxides contents were investigated as they are among the main factors affecting phosphorus availability in the soil. Therefore a structure of calcite mineral is proposed in the current study to understand the mechanism of phosphorus adsorption and desorption process. Three soil types, namely alluvial (Typic Haplotorrerts), calcareous (Typic Haplocalcids) and sandy (Typic Torripsamments) represented by two soil profiles for each were used. These soils represent the main soil types most prevailing in Egypt.

The isotherm equations of Freundlich and Langmuir were applied to determine the bonding energy and the adsorbed phosphorus quantities as well as PRI values were calculated for the soils under investigation. The results showed that the highest values of phosphorus adsorption and bonding energy were found in the calcareous soil which is followed by alluvial and sandy soils respectively. On the other hand, the desorption of phosphorus from soils decreases significantly in the following order; sandy> alluvial> calcareous soils. In contrast, the PRI value is highest in sandy soils followed by alluvial and calcareous soils, respectively. According to the calculated PRI values, it is found that calcareous soil has the extreme phosphorus deficiency.

Keywords: Adsorption, structure, bonding energy, calcium carbonate, PRI.

Introduction

Phosphorus availability in the soil depends considerably on its concentration in the soil solution. The concentration of P in the soil solution is very low and can differ widely depending on the soil properties. The low availability of phosphorus to growing plants in arid and semiarid regions is a general problem. In addition, the efficiency of phosphate fertilizers was found to be low and was generally attributed to phosphate retention phenomenon by soil components. This reaction is generally affected by many soil factors such as pH, clay minerals, reactive surface containing some components as iron and aluminum oxides, calcium carbonate etc. and surface area of calcium carbonate particles, through its effect on soil reaction (pH) , its reactive surface and as a source of the common ion , exerts a dominant effect on the nature and properties of phosphate in calcareous soils. In this respect, Riffaldi et al[8], Wahba[12] and Zhang et al[13] found a positive correlation between adsorbed P and calcium carbonate content.

For the Mediterranean area, Carreira and LaJtha[2] stated that dolomitic soils gave support to the idea that crystalline Fe - oxides appear to be the most important P - sorbing component and that carbonate may also be a significant contributing factor to P - sorption especially in younger soils. For the alluvial soils, the great problem is the attached phosphorus by soil colloids. McDowell and Sharpley[4] and Zhang et al[13] declared that the sorption / desorption of phosphorus by colloids in solution was great and more P was sorbed by colloids attributed to the surface charge characteristics and their relations to mineralogy of each soil. On the other hand, the type of clay mineral plays an important role whereas the maximum adsorption capacity of montmorillonite was greater than that of kaolinite but decreased the bonding energy[9,12]. In sandy soils the problem of phosphorus is its escape from the soil since the bonding energy of sand particles to the phosphorus is very weak.

As respect to describe phosphorus adsorption by Freundlich and Langmiuir, models, Tsadilas et al[10], Richard and Leo[7] and Riffaldi et al[8] applied these models and concluded that these models were satisfactory to describe P - adsorption . The determination of available soil phosphate is complicated as phosphates of different types are present in the soil. The most important soil phosphates are the Ca-phosphates, Fe- and Al-phosphates and organic phosphates. The aim of this paper is trying to design of calcite mineral structure to understand the adsorption mechanism of phosphate with it and to evaluate for phosphorus deficiency in different soils own pedogenic genesis.

Material and Methods

Six soil profiles were selected to represent the most dominant soils in Egypt i.e. alluvial soils "Typic Haplotorrerts" taken from El-Menofia governorate represented by profiles no. 1 and 2, calcareous soils "Typic

Haplocalcids" taken from El - Hammam North western coast and represented by profiles no. 3 and 4 and sandy soils Typic Torripsamments taken from Sinai and represented by profiles no. 5 and 6. The studied soils are classified according to USDA[11]. The collected soil samples were air-dried and passed through a 2mm sieve and analyzed for some physical and chemical properties according to Black et al.[1] Iron oxides were extracted by Na-dithionite citrate bicarbonate as recommended by Mehra and Jackson.[5]

P-Adsorption / Desorption studies: The P-adsorption data were obtained by shaking equilibrating 2g soil samples for 24 hours at room temperature with 40 ml of solutions of KH_2PO_4 having concentrations of 2, 5,10, 20 and 30 µg P/ml. After centrifuging at 10.000 rpm for 15 min, the supernatants were taken for phosphorus analyses according to Murphy and Riley[6]. The amount of P adsorbed was calculated by subtracting the amount of P in the supernatant solution from the amount of P – added.

In the desorption study, the supernatant carried over from the adsorption was removed by drying the soil samples at 25^0 C, simulate the wetting and drying process that takes place under natural conditions. Then 40 ml 0.01M $CaCl_2$ was added to the sample which was equilibrated for 24 hr at room temperature as in the adsorption study. The fixation of P was recovered by the extracting considered to be desorbed. Phosphorus was determined as before. The data obtained were plotted according to the linear forms of both the Freundlich and Langmuir equations as described below:

Freundlich Equation:

$$\mathbf{X = K\ C^n}$$

where X = The amount of P sorbed per weight of soil (µg P / g soil); C = P-concentration in the equilibrium solution (µg P / L); K and n = Constants characteristic of the system.

Langmuir Equation:

$$C/X = 1/KQ + C/Q$$

where K = Sorption constant related to bonding energy and Q =The maximum amount of P sorbed.

Results and Discussion

General soil characteristics: Profiles description showed in table 1. Data in table 2 show profiles no. (1,2) El-Manofia governorate (alluvial). These soils are characterized by high clay content in all layers. The clay content ranged from 64.7 to 71.9%. The main factor of P-adsorption process in this soil is considered clay content. Meanwhile profiles no. (3 and 4) El-Hammam are markedly high in calcium carbonate content which ranged from 20.14 to 28.31% and it is considered the main factor in these soils. In Sinai profiles no. (5,6) are characterized by high sand content (94.3%). All these differences attributed to soil genesis and soil formation processes which play important role in adsorption and desorption process. Another factor is very important to these studies i.e. the content of CDB extractable (Fe) in soils. It is noteworthy that the content of CDB extractable Fe in calcareous soils was the highest (4123ppm), whereas the alluvial soils contain (3520 ppm). These differences are attributed to circumstance formation soils.

Maximum phosphorus adsorption and its equilibrium in solution are important parameters for optimum growth. Table 2 shows phosphate sorption parameters, the values for the P-sorption parameters derived from the Frendulich and Langmuir equations are given. The values of the correlation coefficients in table 2 indicate conforming to both Frendulich and Langmuir equations, these results are in agreement with Zhang et al[13] and Riffaldi et al.[8]

It is noteworthy that the highest values of maximum amount of P-sorbed (Q) and bonding energy (K) were 450.35 and 2.76 respectively in calcareous soil. This result can be attributed to the high calcium carbonate content and iron oxides content in this soil. In this respect, alluvial soil followed the calcareous soil, whereas the (Q) and (K) values were recorded to 332.43 and 0.95 respectively which can be due to the high clay content in this soil. On the other hand the lowest values of (Q) and (K) were obtained in the sandy soil 175.43 and 0.43 respectively, the result can be due to that sandy soils have less amounts in calcium carbonate, iron oxides and clay content as compared to other soils under study. These soils components are considered the main factors to determine the P-adsorption process. The values of (K,n) constants of Freundlich equation confirm the same result.

Riffaldi et al[8] assured on importance of calcium carbonate in adsorbed phosphate and Wahba[12] stated that pure calcium carbonate adsorbed quantities of phosphate more than some clay minerals. From these results, the important role of calcium carbonate in P-adsorption process in the soil can be ascertained. Therefore, the structure of calcite mineral is easy to understand the mechanism phosphorus adsorption process and this designing agrees with Kuo and Lotse[3]. In calcium carbonate structure each Ca^{2+} ion is coordinated by six oxygen atoms of six CO_3^{2-} groups and each oxygen atom is bound to two Ca^{2+} ions–in a water suspension of $CaCO_3$ crystallites , oxygen atoms of water molecules , bicarbonate ions and hydroxyl ions may fill the vacant coordinate positions of exposed surface Ca^{2+} ions (Fig.1). Phosphate ions may replace adsorbed water molecules, bicarbonate ions and hydroxyl ions. The relative adsorption strength of the phosphate ions and other anions present in the system will depend upon the solubility of the compound formed with surface Ca^{2+} ions according to the Fajans–Paneth rule.

Since the solubility constants of $CaHPO_4$, $Ca(OH)_2$ and $Ca(HCO_3)_2$ are $10^{-6.66}$, $10^{-5.43}$ and $10^{-1.20}$ respectively

phosphate ions will be more strongly adsorbed than bicarbonate and hydroxyl ions. Therefore, the $CaCO_3$ crystal and its surface are reasonably well understood. In Egyptian alkaline soils which contain high amounts of soluble and exchangeable Ca^{2+} ions and free calcium carbonate frequently also, phosphate is reported to react with both the ionic and the carbonate form of Ca^{2+}. The reactions can be illustrated as follows:

$$3Ca^{2+} + 2\ PO_4^{3-} \rightarrow Ca_3(PO_4)_2 \text{ insoluble}\downarrow$$
$$3\ CaCO_3 + 2\ PO_4^{3-} \rightarrow Ca_3(PO_4)_2 \text{ insoluble}\downarrow + CO_2\uparrow$$

The tri calcium phosphate formed is insoluble and precipitates out of the solution. Other forms of insoluble Ca– phosphate can also be formed by this type of reaction between calcium and phosphate e.g. out of Ca–fluorapatite $\{Ca_5(PO_4)_3F\}$, Ca – chlorapatite $\{Ca_5(PO_4)_3Cl\}$ and ca – hydroxyl apatite $\{Ca_3(PO_4)_3(OH)\}$ of three types of apatite minerals, Ca– fluorapatite is reported as the most common mineral whereas the other two are rare. A complete isomorphous series of minerals are present between these three apatite minerals because F,Cl and OH can substitute for each other. Carbonate $(CO_3)^{2-}$ and OH groups can also substitute for PO_4, giving the carbonate–apatite series with $CaCO_3$ and Ca–hydroxylapatite making up the end members.

Partial substitution of PO_4 group and SiO_4 or groups is also possible. On the other hand we can explain the mechanism adsorption process by calcite as the rhombohedral unit cell consists of two $CaCO_3$ units and has a=b=0.636 nm, C=0.303 nm and d=46^0.

Table 1
Some chemical and physical analyses of the studied soils

Location	Soil classification	Profile No.	sample No.	Depth Cm	Particle size distribution %			Texture	$CaCO_3$ %	Fe_2O_3 ppm
					Sand	Silt	Clay			
El-Menofia (Alluvial)	Typic Haplotorrets	1	1	0-25	17.1	18.2	64.7	Clay	1.52	3289
			2	25-70	12.7		71.9	Clay	2.14	3520
			3	70-130	5.5	15.4	69.2	Clay	1.83	3327
		2	4	0-30	15.3	25.3	67.3	Clay	1.32	3433
			5	30-60	4.5		70.9	Clay	2.33	3511
			6	60-140	4.9	17.4	68.7	Clay	1.75	3295
						24.6				
						26.4				
El-Hammam (Calcareous)	Typic Haplocalcids	3	7	0-30	69.8	19.3	10.9	S.L	22.42	3972
			8	30-60	61.3		15.5	S.C.L	28.31	4105
			9	60-120	66.7	23.2	25.5	S.C.L	20.14	3723
		4	10	0-25	69.7	7.8	9.9	S.L	23.24	3832
			11	25-60	60.2		17.5	S.C.L	27.52	4123
			12	60-130	63.7	20.4	27.8	S.C.L	21.23	3755
						22.3				
						8.5				
Sinai (Sandy)	Typic Torripsamments	5	13	0-10	93.6	2.3	4.1	Sand	0.45	2058
			14	10-40	90.4	5.1	4.5	Sand	0.51	2153
			15	40-100	94.3	1.95	3.75	Sand	0.62	2248
		6	16	0-40	92.3		4.1	Sand	0.35	2134
			17	40-100	93.5	3.62.3	4.2	Sand	0.73	2253

Table 2
Some phosphate adsorption parameters of the studied soil

Type soil	Location	Profile No.	Sample No.	Depth cm	Freundlich			Langmuir		
					K	n	r^2	Q	K	r^2
Alluvial	El-Menofia	1	1	0-25	115.87	0.29	0.990	270.40	0.67	0.924
			2	25-70	144.91	0.27	0.999	317.08	0.99	0.940
			3	70-130	117.90	0.31	0.977	278.81	0.73	0.878
		2	4	0-30	110.43	0.26	0.976	275.62	0.72	0.943
			5	30-60	154.35	0.28	0.989	332.43	0.95	0.933
			6	60-140	123.21	0.33	0.997	290.22	0.84	0.905
Calcareous	El-Hammam	3	7	0-30	206.34	0.35	0.998	407.97	1.97	0.980
			8	30-60	237.89	0.33	0.983	443.27	2.33	0.965
			9	60-120	198.29	0.39	0.971	400.46	1.82	0.941
		4	10	0-25	215.32	0.39	0.997	415.43	1.83	0.956
			11	25-60	244.53	0.37	0.989	450.35	2.76	0.973
			12	60-130	201.23	0.38	0.988	401.26	1.94	0.952
Sandy	Sinai	5	13	0-10	56.14	0.32	0.968	163.51	0.37	0.883
			14	10-40	57.42	0.32	0.978	166.34	0.38	0.905
			15	40-100	59.99	0.33	0.995	174.21	0.39	0.937
		6	16	0-40	60.32	0.24	0.987	170.53	0.43	0.905
			17	40-100	63.44	0.23	0.997	175.43	0.37	0.924

In simple terms, the lattice consists of planes of Ca^{2+} ions 0.303 nm apart with the ions in any plane regularly placed in equilateral triangles of side length 0.496 nm. Between each plane there is a single layer of CO_3^{2-} with the oxygen coordinating to the Ca^{2+} above and below. The result is to give a rhombohedral crystal face with alternate Ca^{2+} and CO_3^{2-} ions on the surface.

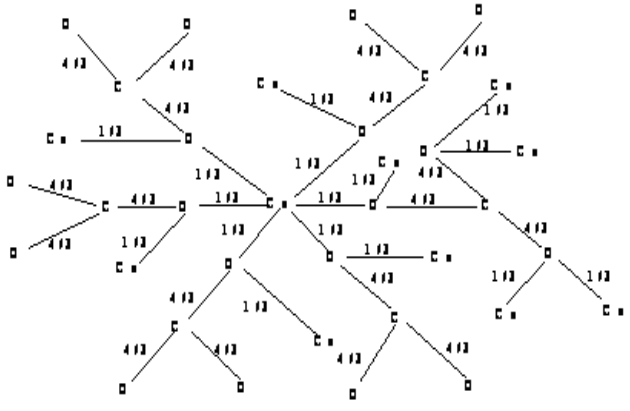

Fig.1: Proposed structure of calcium carbonate

There are two mechanisms which will give rise to such a charge. First, because the $CaCO_3$ is sparingly soluble, either Ca^{2+} or CO_3^{2-} might preferentially leave the surface plane and result in a net charge of opposite sign. This charge would tend to retain the "escaping" ions in diffuse layer.

Such a mechanism would explain any subsequent incorporation into the lattice of "foreign" anions for example SO_4^{2-}. Secondly, the surface, since it is solvated; might adsorb potential determining ions such as H^+ or OH^- and so acquire charge.

On the other hand after studying the structure of calcium carbonate and the mechanism of adsorption it is revealed that to study adsorption / desorption process is not enough to give indication about the quantity of phosphorus adsorbed but it is necessary to calculate the bonding energy and Phosphorus Recovery Index PRI. The percentage of (PRI) gives the ratio recovery of phosphorus from P – adsorbed

$$PRI = \frac{\text{P - dsorption (ug P / g soil)}}{\text{P - adsorption (ug P / g soil)}} \times 100$$

So, the value of (PRI) is to estimate phosphorus deficient in the soil and according to the PRI values, the deficiency degree of phosphorus in soils can be classified as in table 3. If the PRI value is less than the half adsorption value, add phosphorus fertilizer to the soil in order to repair phosphorus deficient in the soil. If the PRI value is equal or more than half adsorption value, it is adequate for successful growth of most crops with no problem in the phosphorus program. Therefore this equation is very important to estimate deficiency of phosphorus in the soils.

With regard to the data recorded in table 3, they reveal that in alluvial soils average value of PRI is less than the half average value of phosphorus adsorption this is indicator to deficiency of phosphorus in these soils and these soils are classified according to PRI values to moderate deficiency degree of phosphorus. In calcareous soils, the deficiency of phosphorus is clear whereas the average value of PRI in all profiles is lower than the half average value of phosphorus adsorption so the difference between them is very much and is more than the values of alluvial soils.

Consequently, the deficient of phosphorus in this soil is huge so these soils are classified to extreme deficiency degree of phosphorus. These results are in agreement with Richard and Leo[7] and Riffaldi et al[8]. On the other hand, some layers in sandy soils have average value of PRI more than the average value phosphorus adsorption and other layers in this soil were having average value of phosphorus adsorption, so these soils can be classified to weak deficiency degree of phosphorus. It is noteworthy that the highest value of average PRI is recorded in sandy soils followed by alluvial and calcareous soils respectively. So the value of PRI depends on soil components and type of soils. Whereas the calcareous soil is rich in calcium carbonate and iron oxides content, alluvial soil is rich in clay and iron oxides content. In contrast sandy soil is poor in calcium carbonate and iron oxides content. These results confirmed on existing deficiency of phosphorus in calcareous soils followed by alluvial and sandy soils respectively.

Table 3
Adsorption / desorption and value PRI of phosphorus of the studied soils

Profile No.	Sample No.	Depth cm	P-conc. ug/ml	*P.ads ug/g	*P.des ug/g	Average PRI % *	Classification class	P-deficiency degree
1	1	0-25	2 5 10 20 30	39.82 88.80 153.79 213.60 268.29	5.67 13.37 40.48 95.17 130.81	37.35	Typic Haplotorrets	moderate
Average				152.86	57.10			
1	2	25-70	2 5 10 20 30	39.61 94.73 169.88 260.25 317.76	3.78 11.75 36.77 89.72 122.11	29.94	Typic Haplotorrets	moderate
Average				176.45	52.83			
1	3	70-130	2 5 10 20 30	39.82 88.80 153.79 213.61 290.29	4.01 12.23 38.14 91.23 127.11	34.68	Typic Haplotorrets	moderate
Average				157.26	54.54			
2	4	0-30	2 5 10 20 30	37.40 84.91 147.45 202.54 257.32	4.52 11.45 37.35 91.43 127.25	37.28	Typic Haplotorrets	moderate
Average				145.92	54.40			
2	5	30-60	2 5 10 20 30	37.24 90.35 160.57 253.47 310.34	5.52 10.23 33.25 84.16 118.75	29.22	Typic Haplotorrets	moderate
Average				170.39	49.78			

2	6	60-140	2 5 10 20 30	36.34 83.25 148.47 207.85 285.75	3.03 10.32 35.21 85.46 121.35	33.53	Typic Haplotorrets	moderate
Average				152.33	51.07			
3	7	0-30	2 5 10 20 30	39.55 97.67 140.87 341.34 400.56	2.72 8.45 24.92 78.35 99.27	20.95	Typic Haplocalcids	extreme
Average				204.00	42.74			
3	8	30-60	2 5 10 20 30	39.68 97.56 193.90 341.17 455.57	1.99 7.32 20.31 70.75 97.42	17.54	Typic Haplocalcids	extreme
Average				225.58	39.56			
3	9	60-120	2 5 10 20 30	39.55 80.69 140.94 300.73 410.53	3.01 9.72 27.21 81.73 116.45	24.48	Typic Haplocalcids	extreme
Average				194.49	47.62			
4	10	0-25	2 5 10 20 30	37.54 94.34 138.27 335.38 397.47	1.95 7.32 21.39 74.78 95.65	20.05	Typic Haplocalcids	extreme
Average				200.60	40.22			
4	11	25-60	2 5 10 20 30	38.25 93.45 187.47 328.56 446.78	1.22 5.68 18.77 67.45 94.32	17.13	Typic Haplocalcids	extreme
Average				218.90	37.49			
4	12	60-130	2 5 10 20 30	37.95 77.45 137.55 294.74 404.52	2.85 8.74 25.23 78.72 113.57	24.06	Typic Haplocalcids	extreme
Average				190.44	45.82			
5	13	0-10	2 5 10 20 30	35.44 69.65 75.62 140.76 150.28	7.28 22.14 50.43 101.56 122.72	64.47	Typic Torripsamments	weak
Average				94.35	60.83			

5	14	10-40	2 5 10 20 30	35.54 69.56 80.88 145.95 152.23	7.02 18.23 47.12 97.53 120.13	59.90	Typic Torripsamments	weak
Average				96.84	58.01			
5	15	40-100	2 5 10 20 30	35.54 69.68 100.68 145.54 162.34	6.89 17.11 44.23 94.33 117.35	54.47	Typic Torripsam ments	weak
Average				102.76	55.98			
5	15	40-100	2 5 10 20 30	35.54 69.68 100.68 145.54 162.34	6.89 17.11 44.23 94.33 117.35	54.47	Typic Torripsam ments	weak
Average				102.76	55.98			
6	16	0-40	2 5 10 20 30	33.24 65.78 74.50 137.32 144.34	6.56 21.43 49.23 98.24 114.29	63.65	Typic Torripsamme nts	weak
Average				91.04	57.95			
6	17	40-100	2 5 10 20 30	34.88 65.78 98.43 140.77 158.73	5.87 15.21 41.25 92.31 113.24	53.73	Typic Torripsamme nts	weak
Average				99.72	53.58			

*P.ads. Phosphorus adsorbed (µg P/g soil); *P.des. Phosphorus desorbed (µg P/g soil).

$$\text{*Average PRI \%} = \frac{\text{average P-desorption}}{\text{average P-adsorption}} \times 100$$

Conclusion

Both the Freundlich and Langmuir equations were tested for their ability to describe phosphorus adsorption. Freundlich isotherm consistently gave a closer fit to the P-adsorption data more than Langmuir isotherm. The highest values of phosphorus adsorption and its bonding energy were obtained in calcareous soils followed by alluvial and sandy soils respectively. In contrast, phosphorous desorption was in descending order as follows: sandy soils > alluvial soils > calcareous soils. Therefore a schematic model proposed of crystal calcium carbonate was very important to understand mechanism adsorption process. In the light of the current study it could be said that calcium carbonate, iron oxides and clay content in a soil play an important role in phosphorous adsorption/ desorption process as well as values of Phosphorus Recovery Index. So the value of PRI depends on soil components and type of soils.

References

1. Black C.A., Evans D.D., White J.I., Ensminger L.E. and Clark F.E., Methods of Soil Analysis, Amer. Soc. Agronomy Inc. Publisher, Medison, Wisconsin, U.S .A. **(1982)**

2. Carreira J.A. and LaJtha K., Factors affecting phosphate sorption along Mediterranean, dolomitic soil and vegetation chronosequence, *European J . Soil Sci.,* **48,** 139 **(1997)**

3. Kuo S. and Lotse E.G., Kinetics of phosphate adsorption by calcium carbonate and Ca-kaolinite, *Soil Sci. Amer.Proc.,* **36,** 725 **(1972)**

4. McDowell R. W. and Sharpley A. N., Soil phosphorus fractions in solution influence of fertilizer and manure filtration and method of determination, *Chemo sphere*, **45,** 737 **(2001)**

5. Mehra O. P. and Jackson M. L., Iron oxide removal from soils and clays by dithionite – citrate system buffered with sodium bicarbonate, *Clays Clay Mineral,* **7,** 317 **(1960)**

6. Murphy J. and Riley J. P., A modified single solution method for the determination of phosphate in natural waters, *Anal. Chem. Acta*, **27,** 31 **(1962)**

7. Richard Mc. and Leo C., Influence of soil constituents on soil phosphorus sorption and desorption, *Commun. Soil Sci. and Plant Anal*, **32,** 2531 **(2001)**

8. Riffaldi R., Saviozzi A., Levi – Minzi R. and Wahba M. M., Phosphate sorption by some Egyptian and Italian calcareous soils, *Agrochimica*, **14,** 147 **(2001)**

9. Hong Peng, Effects of Resuspension on the transfer and Transformation of Nitrogen and Phosphorus species at Sediments-Water Interface in Simulative Lake System, *Res. J. Chem. Environ.*, **15(4)**, 14-17 **(2011)**

10. Tsadilas C. D., Samaras V. and Dimoyiannis D., Phosphate sorption by red Mediterranean soils from Greece, *Commun. Soil Sci. and Plant Anal*, **27,** 2279 **(1996)**

11. USDA, Soil Taxonomy, Natural Resources Conservation Service, Washington D. C. 20402 **(1999)**

12. Wahba M. M., Characteristics of calcareous Soils and Phosphate Adsorption, Ph. D. Thesis, Fac. Agric., Pisa Univ., Italy **(1999)**

13. Zhang M. J., Wilson M. J., He Zhenli L. and Duthie D. M., Phosphate adsorption and surface charge characteristics and their relation to mineralogy of some soils from southern china, *Pedosphere*, **8,** 297 **(1998).**

(Received 10th February 2013, accepted 15th June 2013)

Feasibility of Acetone-Butanol-Ethanol Production from the Fermentation of Oil Palm Trunk Juice

Norhazimah A.H.,* Asmadiyana M. and Faizal Che Ku M.
Biofuel Research Group, Faculty of Chemical and Natural Resources Engineering,
Universiti Malaysia Pahang, 26300 Gambang, Kuantan, Pahang, MALAYSIA
*aimc.azim@gmail.com

Abstract

Oil palm trunk (OPT) juice has the potential to be used for acetone-butanol-ethanol (ABE) production. In this study, fermentation of OPT juice was carried out to produce ABE without the addition of nutrient. In general, C. acetobutylicum showed better ABE yield compared to C. beijerinckii even though both strains were capable to convert sugar in OPT juice to ABE. The result showed maximum acetone, butanol and ethanol concentration of 12.25, 4.56 and 4.28 g/l, respectively using C. acetobutylicum. These results showed that OPT juice has a great potential for ABE production.

Keywords: ABE, *Clostridium acetobutylicum*, *Clostridium beijerinckii*, oil palm trunk juice and sap.

Introduction

The research on the production of ABE through fermentation process using agricultural waste-based substrates has been increased since decades. The economics of ABE fermentation are greatly affected by the raw materials where agricultural waste could be a good option for reducing the cost[1]. Selection of an inexpensive raw material has an important impact on process economic[2]. Oil palm is one of the important commodity crops for lipid-based industry. Currently, palm oil is the world largest source of edible oil, providing 43.1 million tons or 27% of the world's total production of edible oil and fat[3]. Oil palm produces higher yields per hectare than any other oilseed crops when properly cultivated[4]. Even though oil palm trees can live longer than 30 years, they only have 25 to 30 years of economic fruit production.

Oil palm trunk (OPT) is an agricultural waste abundantly available in the Southeast Asian countries due to replantation of oil palm trees. OPT can be squeezed to obtain liquid juice that contains fermentable sugar. Beside fermentable sugar, OPT juice also contains a lot of amino acids, minerals and vitamins[5]. Several attempts have been made by researchers to produce biofuel such as bioethanol from OPT juice[5,6]. In search of viable alternatives for biofuels, OPT juice is used as an alternative raw material for ABE production. In this research, considering the amount of sugar available in OPT juice, the production of ABE via fermentation of OPT juice using *C. acetobutylicum* and *C. beijerinckii* without the addition of nutrient and pretreatment was attempted.

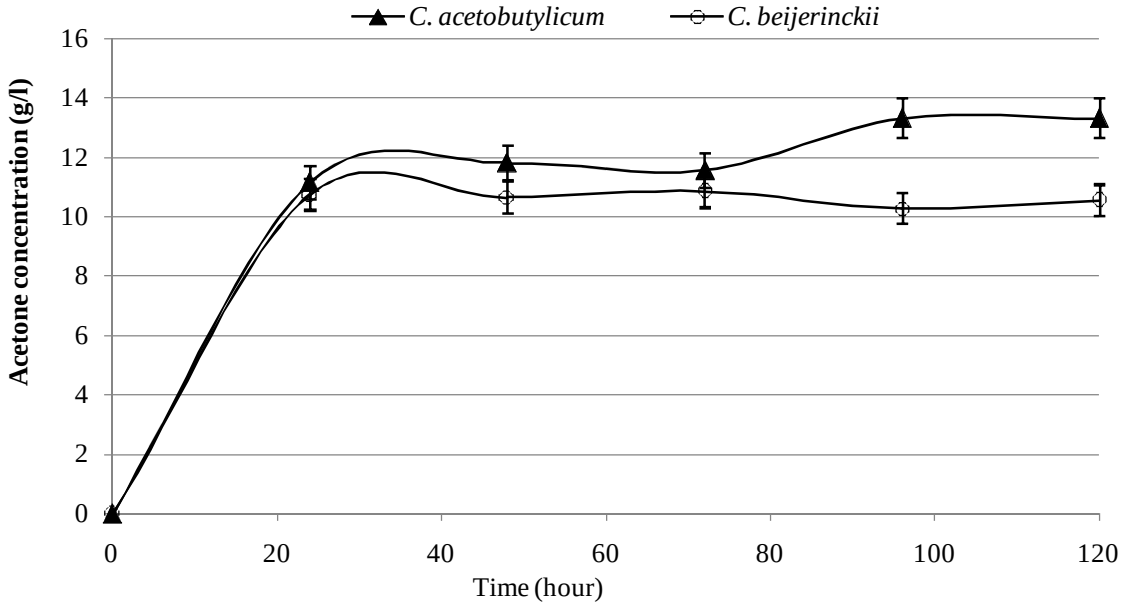

Fig. 1: Production of acetone from oil palm trunk juice

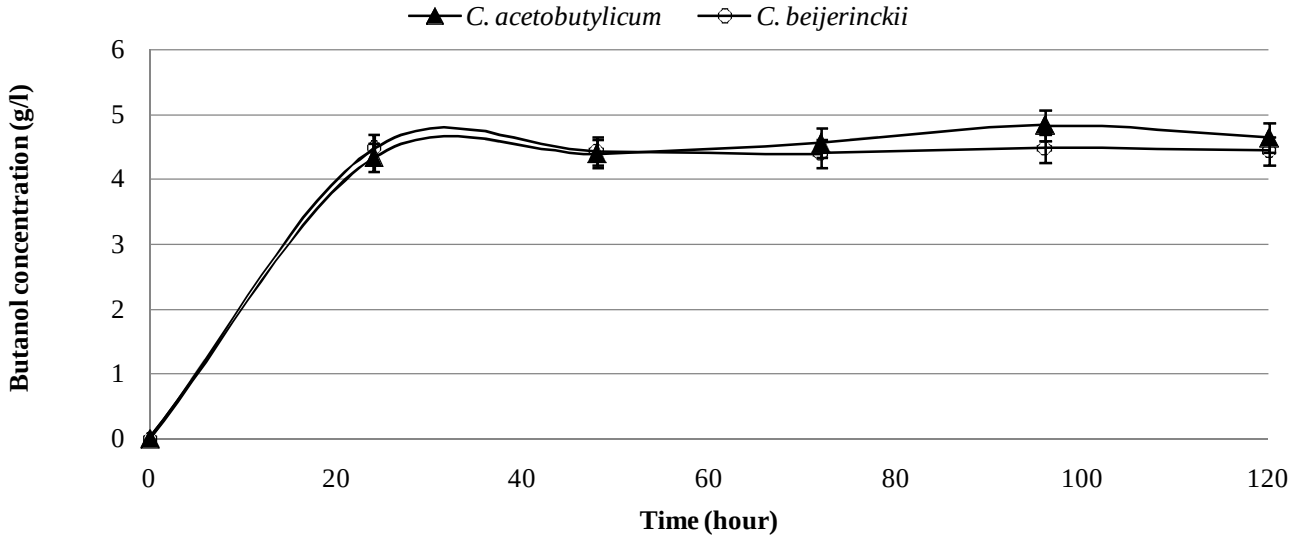

Fig. 2: Production of butanol from oil palm trunk juice

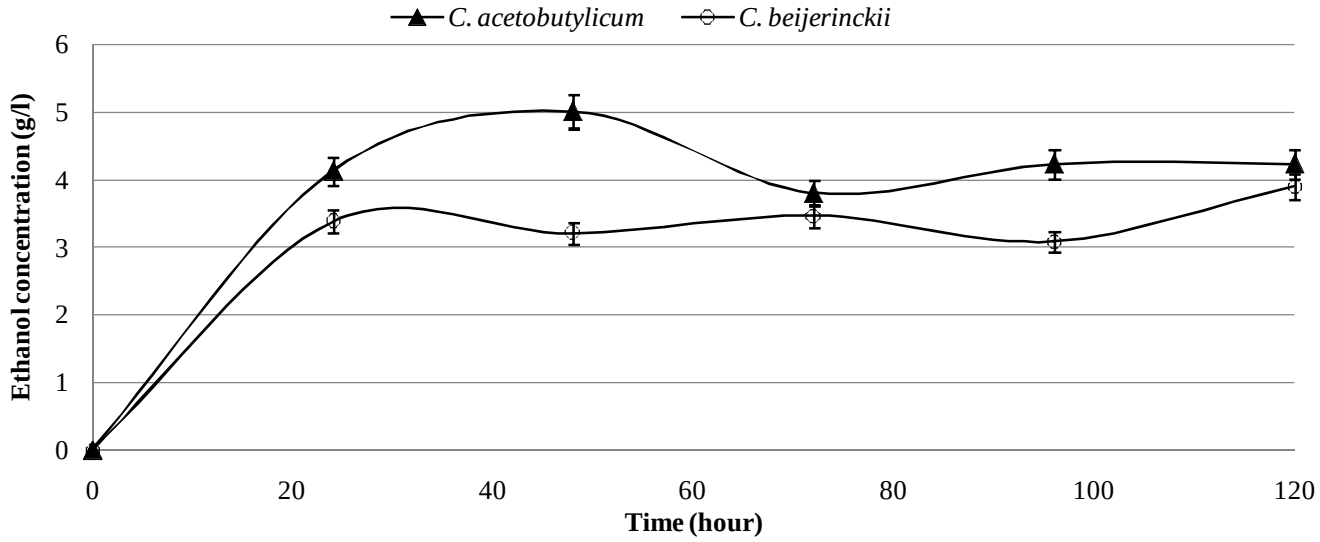

Fig. 3: Production of ethanol from oil palm trunk juice

Material and Methods

Raw Material and Inoculum Preparation: OPT was obtained from Oil Palm Plantation in Pahang, Malaysia. The OPT juice (sap) was obtained by pressing the trunk using a press machine. The total sugar content in OPT juice used in this study is shown in table 1. *Clostridium acetobutylicum* JCM 1419 (ATCC 824) and *Clostridium beijerinckii* JCM 1390 (ATCC 25752) were purchased from the Japan Collection of Microorganism (JCM). The inoculums were grown for 48 h at 37 °C in Reinforced Clostridial Medium (RCM).

ABE Fermentation: The fermentation of OPT juice was performed in 250 ml shake flask with 100 ml working volume. It was done in anaerobic condition at 37 °C for 120 h. The preparation of anaerobic medium was completed by degassing the medium with oxygen-free nitrogen gas at 500 ml/min for 10 min.

Analytical Methods: At 24 h intervals, samples were removed from fermentation flask and analyzed for ABE and sugar content. Total ABE was determined by a gas chromatography with the HP-INNOwax column. Initially, the sample was held at 80 °C for 4 min and then the temperature was increased at the rate of 20 °C per min until 180 °C and held for 2 min. Nitrogen was used as the carrier gas while isobutanol was used as the internal standard. Total sugar was determined by HPLC-RID with Agilent Carbohydrate Analysis Column. The ABE yield was determined by dividing solvent produced by the total sugar utilized (g/g). The productivity was calculated as the total solvent divided by fermentation time (g/l.h).

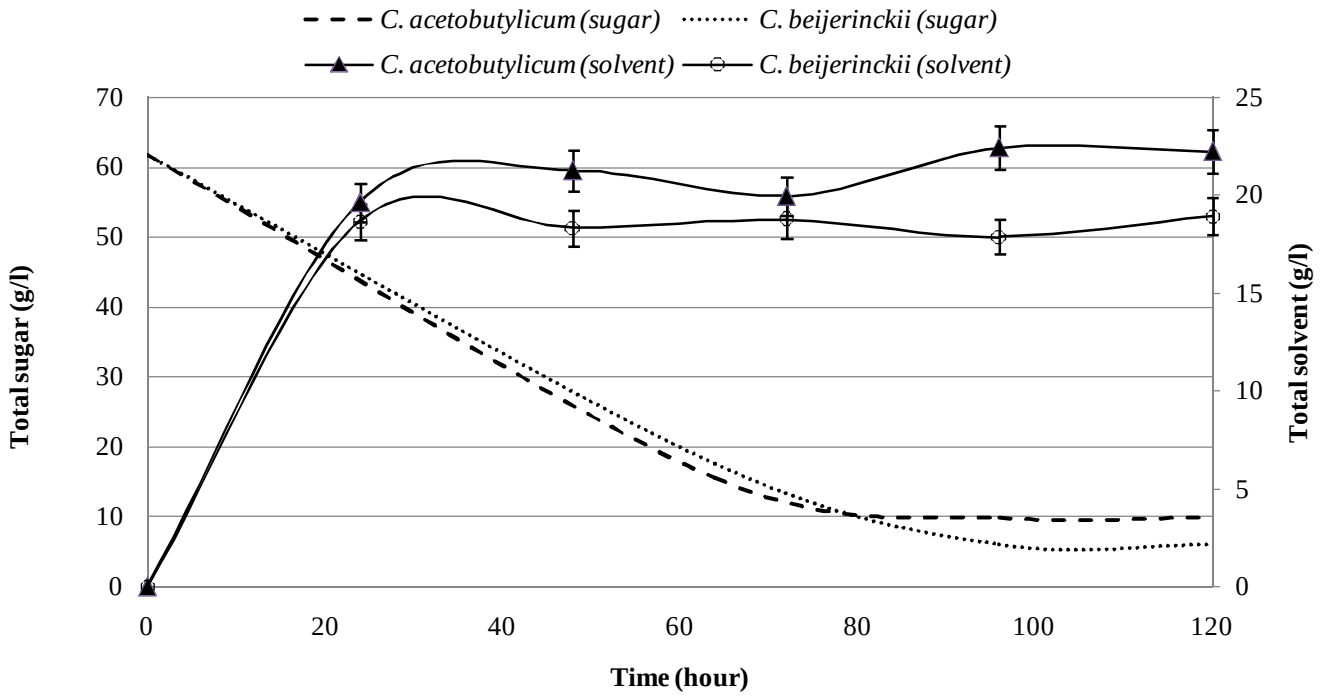

Fig. 4: Total ABE production and total sugar consumption in oil palm trunk juice

Results and Discussion

Feasibility of ABE production from OPT juice: The production of ABE is shown in figure 1, 2 and 3. At the end of the fermentation process, *C. acetobutylicum* and *C. beijerinckii* produced 12.25 g/l and 10.63 g/l of acetone respectively. The final butanol and ethanol concentration obtained in this study ranged from 4.45-4.56 g/l and 3.41-4.28 g/l respectively. In general, *C. acetobutylicum* showed better ABE yield compared to *C. beijerinckii*. *C. acetobutylicum* always produced higher acetone and ethanol concentration than *C. beijerinckii* at each time point. For butanol production, *C. acetobutylicum* produced higher ethanol concentration only after third day of fermentation.

Table 1
Sugar content in OPT juice

Type of Sugar	Concentration (g/l)
Sucrose	13.94
Glucose	42.97
Galactose	3.37
Fructose	4.03

After 120 h of fermentation, the concentration of acetone was still higher than butanol and ethanol and this did not follow the usual ratio ABE i.e. 3:6:1. This can be explained by the observation in Rajan et al[7] where the butanol concentration was detected less than the acetone concentration within the first 9 days of fermentation. After ninth day, the butanol concentration increased, exceeding the acetone concentration. The usual ratio might be observed if the fermentation was carried out for more than 10 days to complete the solventogenesis phases for ABE fermentation.

Table 2
Analysis of fermentation broth at the end of fermentation

	C. acetobutylicum	***C. beijerinckii***
Total ABE (g/l)	22.21	18.92
Percentage sugar utilization (%)	83.99	90.17
Final acetone concentration (g/l)	12.25	10.63
Final butanol concentration (g/l)	4.56	4.45
Final ethanol concentration (g/l)	4.28	3.41
Total ABE yield (g/g)	0.38	0.34
Acetone yield (g/g)	0.21	0.19
Butanol yield (g/g)	0.08	0.08
Ethanol yield (g/g)	0.07	0.06
Volumetric ABE productivity (g/l.h)	0.19	0.16

The time course of total ABE production from the OPT juice by both strains is shown in figure 4. The highest total ABE production in this study was 22.40 g/l by using *C. acetobutylicum* in 96 h of fermentation. This included 13.33 g/l acetone, 4.84 g/l butanol and 4.23 g/l ethanol. This ABE yield corresponded to 0.38 g/g from the total

sugar utilized. The comparative performance of these two strains is summarized in table 2. The total sugar utilization profile was nearly similar for both strains where more than 80% of the sugar was used during the fermentation process.

The volumetric ABE productivity of *C. acetobutylicum* was 18.75% higher than *C. beijerinckii*. From the overall observation, it can be concluded that OPT juice can be used as a substrate for ABE production. These results reveal the possibility of ABE production using *C. acetobutylicum* and *C. beijerinckii* without the addition of nutrient supplementation and costly pretreatment. Both strains were capable to convert sugar in OPT juice to ABE. However, the butanol concentration obtained was still lower than acetone production and this needed some further process enhancement.

Conclusion

The production of ABE from the fermentation of OPT juice using *C. acetobutylicum* and *C. beijerinckii* showed that ABE can be produced without nutrient supplementation. This present study demonstrated that OPT juice can be used as an inexpensive raw material for ABE production. The study also indicated that both strains can be used to produce ABE from OPT juice. The optimization study for a larger scale of ABE production from OPT juice has been carried out currently and it will be compared with other agricultural waste.

Acknowledgement

The authors wish to thank the Ministry of Education (Malaysia) and Universiti Malaysia Pahang for GRS100316.

References

1. Wang L. and Chen H., Acetone-butanol-ethanol fermentation and isoflavone extraction using kudzu roots, *Biotechnol. Bioprocess Eng.*, **16,** 739-745 **(2011)**

2. Shuler M.L. and Kargi F., Bioprocess Engineering Basic Concepts, 2nd ed.,Prentice Hall International Series **(2000)**

3. Chiew Y.L., Iwata T. and Shimada S., System analysis for effective use of palm oil waste as energy resources, *Biomass Bioenerg.*, **35(7),** 2925-2935 **(2011)**

4. Henderson J. and Osborne D., The oil palm in all our lives: how this came about, *Endeavour*, **24**, 63-68 **(2000)**

5. Kosugi A., Tanaka R., Magara K., Murata Y., Arai T., Sulaiman O., Hashim R., Hamid Z.A.A., Yahya M.K.A.Y., Yusof M.N.M., Ibrahim W.A. and Mori Y., Ethanol and lactic acid production using sap squeezed from oil palm trunks felled for replanting, *J. Biosci. Bioeng.*, **110(3),** 322-325 **(2010)**

6. Norhazimah A.H. and Faizal C.K.M., Production of bio-ethanol from oil palm trunks sap waste as new substrate by baker's yeast *Saccharomyces cerevisiae*, *Res. J. Chem. Environ.*, **15 (2)**, 205-208 **(2011)**

7. Ranjan A., Khanna S. and Moholkar V.S., Feasibility of rice straw as alternate substrate for biobutanol production, *Appl. Energ.*, **103**, 32-38 **(2013).**

(Received 10th March 2013, accepted 22nd June 2013)

Potential of using bio-coagulants indigenous to Malaysia for surface water clarification

Khodapanah N., Ahamad I.S.[*] and Idris A.
Department of Chemical and Environmental Engineering, Faculty of Engineering, Universiti Putra Malaysia in Selangor, MALAYSIA
[*]salwani@upm.edu.my

Abstract

Water treatment processes in developing countries typically include coagulation and flocculation and often use alum as the coagulant. Coagulation is a critical step in drinking water treatment because of removing the colloidal particles as well as pathogens that are often attached to the particles. However, the cost of the imported chemicals in hard currency has caused to consider the natural coagulants as a promising alternative. In the present study, turbidity removal of Moringa oleifera, Jatropha curcas, chitosan, dragon fruit foliage and alum were compared using surface turbid water. The efficacy of four bio-coagulants has been tested based on some critical parameters including dosages of coagulant, pH of turbid water and change in pH value of finished water. All studied coagulants obviously possessed positive coagulation abilities.

The turbidity achieved using M. oleifera and chitosan at pH 6.4 of surface water was less than the required standard of 5 NTU, while M. oleifera recorded turbidity value (3.5 NTU) with removal efficiency of 98.5%. The best performance for J. curcas and D. F. foliage was obtained at pH 4 of turbid water with turbidity removals of 98.1% and 78% making the final turbidity dropped to 4.5 and 51.7 NTU respectively. Optimum dosage for chitosan is much less than studied coagulants. The overall optimum dose for tests between pH 4 and 9 varied between 0.2 and 4 mg/L. Final pH of finished water at its original pH of 6.4 was 6.7, 6.4, 6.5 and 6.5 for treated water by M. oleifera, J. curcas, chitosan and D. F. foliage, respectively while, the pH of water treated by alum decreased from 6.4 to 5.1. Therefore M. oleifera could be considered as a suitable alternative for the replacement of alum as coagulant in surface water treatment, since M. oleifera is a natural product with less side effects as compared to alum as a chemical agent.

Keywords: Natural coagulants, Surface water, Water treatment, *Jatropha curcas*, Dragon fruit foliage, *Moringa oleifera*, Chitosan.

Introduction

Access to safe drinking water is one of major global concern of humankind over the last decades. In developing countries, the cost of imported chemicals, such as aluminum salts and poly aluminum chloride, for conventional water purification is exorbitantly expensive. Disposal difficulties of the high volume sludge because of its aluminum content, residual aluminum concentration in the treated water, reaction of aluminum with alkalinity present in the water leading to the big drop in the pH of water and its low coagulating efficiency in cold water are the main problems which water treatment plants face with[2,7]. Additionally, recent studies have pointed out possible negative effect on consumers' health associated with using aluminum-based coagulants[3,6]. McLachlan[8] reported that extensive intake of alum may cause Alzheimer's disease.

Thus, in recent years, there has been an important challenge to develop sustainable technologies to treat turbid water with a better alternative for conventional coagulants, preferably from natural and locally grown or harvested.

Aqueous extracts of several dry seeds have been recommended for their performance in water treatment applications in developing communities[1,7,10,12]. Natural polyelectrolytes, which can be derived from plants and animal life such as Vegetable tannins and cactus mucilage[9,14,16] and chitosan[2] are alternatives to synthetic polymers or alum. A large number of bio materials in which coagulating properties have been observed, are available long time ago, but applying them in cheaper way and sustainable is still a serious challenge.

Present study is aimed to test the natural source materials that are indigenous and abundantly available in Southeast Asia region, particularly Malaysia, as renewable sources of natural coagulants. Four natural materials, which have properties similar to those previously described for natural coagulants, were chosen to examine the quality of the surface water treated by them and to compare them with that of the water treated with alum. Two seed plants, *Moringa oleifera* and *Jatropha curcas*, one animal-based polymer, chitosan, one plant mucilage, dragon fruit (*Hylocereus costaricensis*) foliage, have been selected to examine their applicability in surface water treatment.

Material and Methods

Experimental Procedures: Coagulation activity of each natural coagulant was carried out using Jar test (VELP Scientifica, Italy). Sedimentation jar tests were employed to determine the coagulation properties of the coagulant solutions used in this research. Six glass beakers (600 ml) were filled with 500 ml of surface water. A rapid mixing

period of 4 min at 100 rpm was then followed by a slow mixing period of 25 min at 40 rpm to allow coagulation to occur. Various doses of each natural coagulant were added into the beakers during rapid mixing as recommended by Katayon et al[6]. The solution was then kept to stand for 30 min to allow the coagulated particles to settle to the bottom. After a settling time of 30 min, the samples were collected from about 1 cm below the surface[1,6]. All experiments were run at room temperature (25±1 °C) and pH of surface water was adjusted exactly before each run using sodium hydroxide (0.1 and 1M) and hydrochloric acid (0.1 and 1M).

In this study, the effect of initial pH value of turbid water and the dosage of coagulant solution for each studied natural coagulant on the coagulation process was investigated. The performance of each coagulant was evaluated by measuring the finished water turbidity, the pH of the treated water samples and the required dosage to produce maximal turbidity removal. The turbidity reduction/removal (%) is given by the difference between initial and residual turbidity of surface water over the initial turbidity, multiplied by 100.

Turbid water samples: The raw water for experiments was collected in 2010 from a river from Selangor, Malaysia (Sungai Langat). The samples were stored at around 4 °C. Before each experiment, the required volume of surface water was put outside the cooling room to bring it to room temperature. Table 1 shows the average physical and chemical characteristics of Sungai Langat water being used in the experiments.

Table 1
Raw water characteristics from Sungai Langat in February 2010

Parameter	Surface water
pH	6.3-6.4
Turbidity	235-240 NTU
Temperature	25-26 °C
Conductivity	51-53 µs/cm
Resistivity	1.9-1.93 kΩ.cm
TDS	33-35 mg/L
Salinity	0.03 ppt
COD	165 mg/L
TSS	65 mg/L

Preparation of various coagulant powders and solutions: In order to prevent any aging effects, such as change in pH and coagulation activity due to microbial decomposition during storage, a fresh solution was prepared for each experiment other than chitosan stock solution. The stock suspension of coagulants was 1%, 1g of coagulant powder dissolved into 100ml of media.

***Moringa oleifera* and *Jatropha curcas*:** For preparation of coagulant powder, good qualities of seeds (*Moringa oleifera* from Seri Serdang, Malaysia and *Jatropha curcas* from Universiti Putra Malaysia farm, Malaysia) were identified from those which were not rotten and dried once opened. The seeds were dried in the oven for 24 h at 50 ^{o}C[6]. The hulls and wings were manually removed from the kernels. The kernels were crushed and ground to the medium fine powder with a mortar and pestle and 1.0 g of the kernel powder was mixed with 40 ml of the distilled water. The mixture was blended using domestic blender for 2 min at high speed to extract the active ingredient of the kernel. The suspension was then made up to 100 ml and filtered through a muslin cloth to give a stock solution 1%[6].

Chitosan: Chitosan is virtually insoluble in water under normal conditions. It can dissolve in carboxylic acid solutions as well as inorganic acids such as hydrochloric acid[4]. Chitosan stock solution was prepared as follows: 1g of chitosan (R and M Chemicals, DD 70-97%) was dissolved in 2.5mL of 2M HCl and 47.5mL of distilled water by stirring overnight at room temperature or mildly heated until completely dissolved. After that, 50mL of distilled water were added to make 1% stock solution[13]. This solution was kept at a closed container inside refrigerator to prevent any deterioration.

Dragon fruit foliage: A batch (~3 kg) of fresh cactus (*Hylocereus costaricensis*) foliages was obtained from Universiti Putra Malaysia farm, Malaysia. Before drying, the fresh cactus foliages were washed and cleaned to remove thorns and cut into small pieces (~1×1 cm) with kitchen knife. These pieces were washed twice with distilled water and dried at 80-100 ^{o}C, then ground into a medium fine powder with domestic food blender and sieved to a particle size of 0.45 mm to 1.25 mm[5]. To extract coagulation agent of dried foliage in distilled water, 1.0 g of the powder was mixed with 40 ml of the distilled water. The mixture was blended using domestic blender for 2 min at high speed. The suspension was made up to 100 ml to give a stock solution of 1%.

Results and Discussion

Effect of coagulant dosage on turbidity removal across various pH values of turbid water: To assess and compare performance of studied natural coagulants, turbidity reduction was tested across a range of pH value from 4 to 9 while the initial pH value of surface water was 6.35-6.4. The results to treat Sungai Langat surface water with *M. oleifera*, *J. curcas*, chitosan and D. F. foliage solutions are presented in figs. 1 (A, B, C and D) respect-tively. Turbidity profiles between pH value 4 and 9 with *M. oleifera* solution (Fig. 1A) were found to be similar in appearance. As the dose level increases, an optimum point is reached corresponding to maximum reduction in

turbidity. After this optimum, the turbidity generally remains constant as the *M. oleifera* dose becomes higher.

Additionally, there is a relationship between pH and coagulation process with *M. oleifera* solution. It was observed that as the pH increased towards pH 9, the coagulation efficiency decreased and therefore the residual turbidity increased. At pH values 4, 5 and 6.4, residual turbidities dropped to less than 5 NTU.

Final turbidity of 5 NTU or lower is equal to about 98 % or higher reduction in turbidity with initial turbidity of 235 NTU of turbid water [(5 NTU is WHO (2011)[15] guideline value for drinking water)]. The percentages of turbidity removal at pH values 7, 8 and 9 were 97, 95 and 93 % at optimum dose respectively. Generally speaking, *M. oleifera* solution showed better performance at pH values 4, 5 and 6.4 which was original pH of surface water.

Fig. 1B shows that the best circumstance in which *J. curcas* coagulant solution appears to work well as a coagulant agent, is under highly acidic media. The percentage of turbidity removal for pH 4 is about 98.1% at optimum dose whereas, at pH 5 to 9, there is a significant reduction in the coagulant performance. Removal percentage at pH 9 was higher with *J. curcas* coagulant solution (82.5 %) than at pH 5(73%). *J. curcas* efficiency dropped to 65-70 % removal at neutral pH values 6-8. It seems that *J. curcas* operates well as a coagulant agent under highly acidic and highly alkaline circumstances[1].

The coagulation efficiency of chitosan coagulant over pH range of 4-9 was depicted in fig. 1C. A small amount of chitosan is enough to achieve to a peak in terms of turbidity reduction at acidic conditions. After this point, further increase in chitosan concentration at lower pH values of surface water sharply reduced efficiency of coagulation. In other words, coagulation is less effective at extreme dosage values presenting the U-shaped trend.

It is noted that particularly at lower pH overdosing showed the worst effect on turbidity reduction. It may be ascribed to the mechanism of the coagulation process by chitosan; adsorption and bridging that is sensitive to overdosing[2,9]. However, residual turbidities were 5 NTU or less than 5 NTU only at pH values of 4, 5 and 6.4 and at other studied pH, finished water turbidities did not decline to WHO (2011) guideline value.[15] In optimum dose, percentages of turbidity removal were 98.5, 98, 98, 97, 94.5 and 92 at pH 4, 5, 6.4, 7, 8 and 9 of surface water respectively.

Fig. 1D shows reduction in turbidity as a function of D. F. foliage concentration over pH 4-9. D. F. foliage solution was strongly efficient coagulant at acidic condition of surface water and increase in coagulant dosage did not have very drastic effect on coagulating process particularly at acidic pH. The coagulation activity of D. F. foliage is greatest at pH value 4 with 78% efficiency in turbidity removal and at pH value 9 was lowest with 40.5 % removal at optimum dosage.

Practically, compared to other studied bio coagulants in present work, the worst percentage reduction results were obtained with surface water treated with D. F. foliage. It was noted that over all studied pH values and coagulant dosages, finished water turbidity did not drop within WHO (2011) guideline value[15] with D. F. foliage coagulant solution.

Optimum dose for coagulation: It was established during the turbidity tests that a dose of each coagulant produced optimum coagulation across the pH range. These results were tabulated in table 2 to illustrate the effect of pH on minimal dosage associated to maximum coagulation process. It is obvious from table 2 that there is a positive strong correlation between *M. oleifera* dosage and initial pH value of sample water. For example, initial pH values from 4 to 9 would require *M. oleifera* doses from 40 to 200 mg/L. The overall observation is that the optimum dose increases linearly as initial pH increases.

As mentioned, *J. curcas* extract exposed good potential as natural coagulant at pH 4 and to a great extent at pH 9. The smallest amount of *J. curcas* in which the biggest coagulation efficiency occurred was 100 mg/L at pH 4 and 9 of water. Although a minimum amount 20 mg/L was necessary to give 65% to 70% reduction in turbidity at pH values 5-8, turbidity values did not sufficiently reduce to fall within the WHO (2011) guideline value[15] even with increasing coagulant dosage.

The overall optimum dose for tests between pH 4 and 9 varied between 0.5 and 4 by chitosan coagulant solution. Results show that optimum chitosan dosage was smaller at lower pH. It seems that the increase in number of protonated amine groups on chitosan at acidic pH leaded to a substantial drop in optimum dosage[2].On the other hand, the optimal dose of *D. F.* foliage was constant regardless of initial pH value of water that was 10 mg/L.

Comparison of turbidity removal of natural coagulants with Alum: To assess and compare performance of studied natural coagulants, percentages of turbidity removal were plotted versus a range of pH value from 4 to 9 at optimum dosage of each coagulant in every pH value (Fig. 2). The dose of each coagulant was according to data presented in table 2.

M. oleifera and chitosan reduced the turbidity of surface water in its original pH 6.4 lower than the WHO (2011) guideline value[15] of 5 NTU. From fig. 2 both coagulants *M. oleifera* and chitosan showed a high efficiency of turbidity removal at pH 4, 5 and 6.4. The trend also shows the decrease in turbidity removal for both coagulants as the pH of real water increases from 7 to 9.

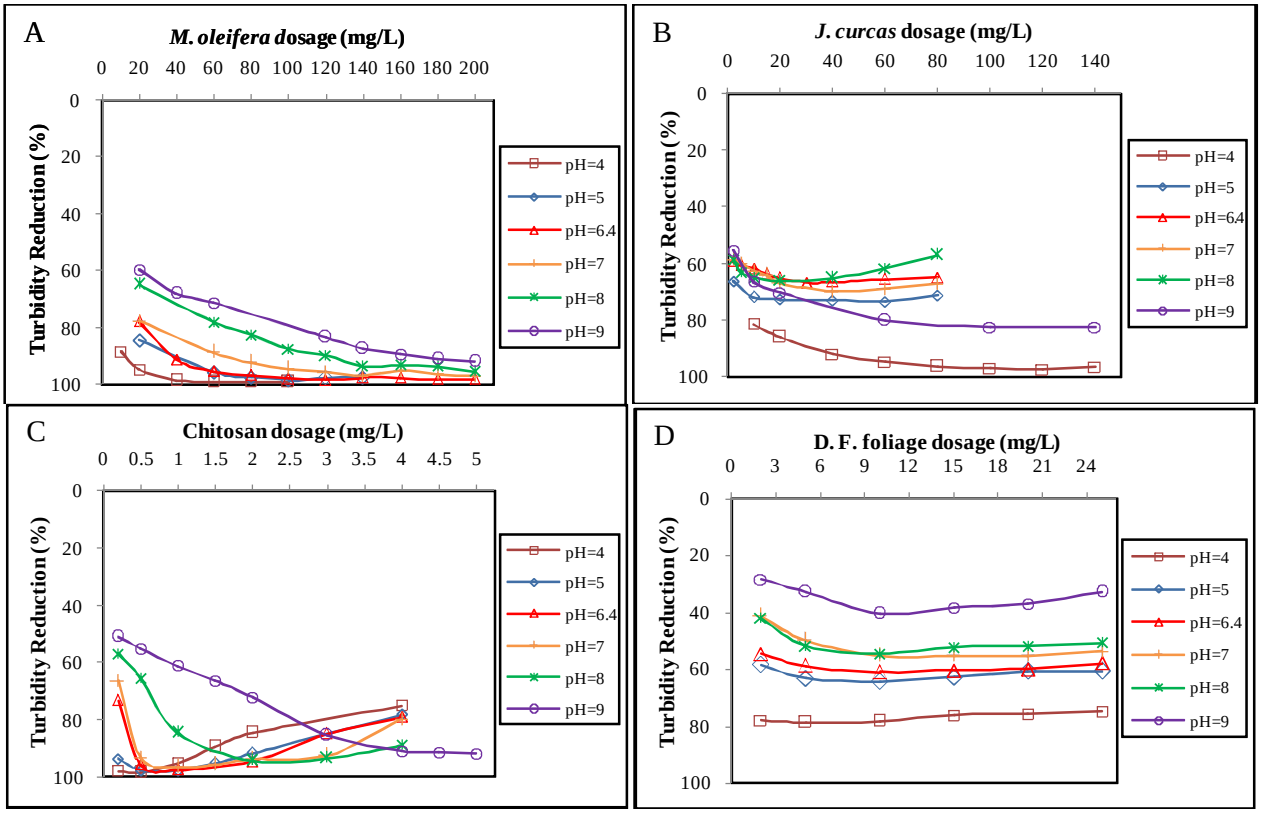

Fig. 1: Variation in turbidity reduction in Sungai Langat water dosed with (A) *M. oleifera*, (B) *J. curcas*, (C) chitosan and (D) D. F. foliage solutions at various pH values of water.

Table 2
Optimum bio coagulant dosages for turbidity reduction in surface water based on initial pH value of water.

	Optimum dosage (mg/L)			
pH	***M. oleifera***	***J. curcas***	**chitosan**	**D. F. foliage**
4	40	100	0.5	10
5	100	20	0.5	10
6	120	20	1	10
7	140	20	1	10
8	140	20	2	10
9	200	100	4	10

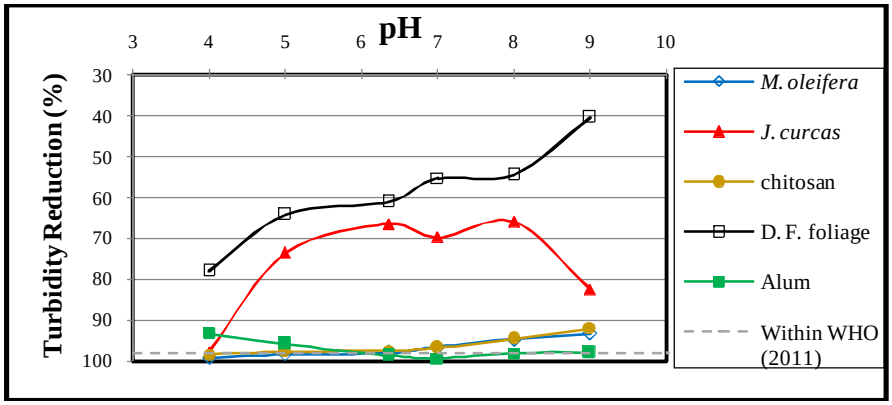

Fig. 2: Coagulation performance of 4 bio coagulants (*M. oleifera, J. curcas,* chitosan and D. F. folige) at various pH values of Sungai Langat water. Performances are represented by turbidity reduction at optimum dosage of each coagulant (Alum dosage: 20 mg/L).

Using *M. oleifera* as coagulant caused the turbidity removal of surface water with pH 4 over 99% and decreases to 93.3% when applied to water with pH 9. The same pattern is shown when using chitosan as coagulant. At pH 4, the turbidity removal is 98.5% and decreases to 92% at pH 9.

A conclusion that can be made from fig. 2 is that *J. curcas* coagulant is good for both acidic and alkaline water but only at pH 4 of surface water could reduce turbidity values sufficiently to fall within the WHO (2011) guideline value[15]. From fig. 2, the turbidity reduction decreased inconsistently from pH 4 to 8 and then again raised to pH 9. At pH 4, the turbidity removal is the highest and at pH 8, the turbidity removal is the lowest which gives 66%.

D. F. foliage coagulant showed a decrease in turbidity removal as the pH value of real water increased from 4 to 9. Turbidity reduction by this coagulant at pH range tested, did not reach WHO (2011) guideline value.[15] For pH 4, the turbidity removal was 78% and the performance declines to as lower as 40.5% when water at pH 9 is tested.

The pH of treated Sungai Langat water at optimum dosage for each coagulant was also documented throughout the testing stages (Fig. 3). The dashed line on the graph signifies that no change in pH occurred. The area above the dashed line is for the increase in pH while the area below the line represents the drop in pH.

The WHO[15] recommends that the pH of the drinking water should be between 6.5 and 8.5. It is noted that the pH of water treated by alum decreased from 6.4 to 5.1 meaning that chemicals need to be added to raise the pH of water to the required guideline value. From fig. 3, *M. oleifera* coagulant raised the pH when the initial pH is 4 to 7 but as the initial pH adjusted to 9, a slight drop in pH was observed. This trend is in agreement with *M. oleifera* results of Nkurunziza et al[11].

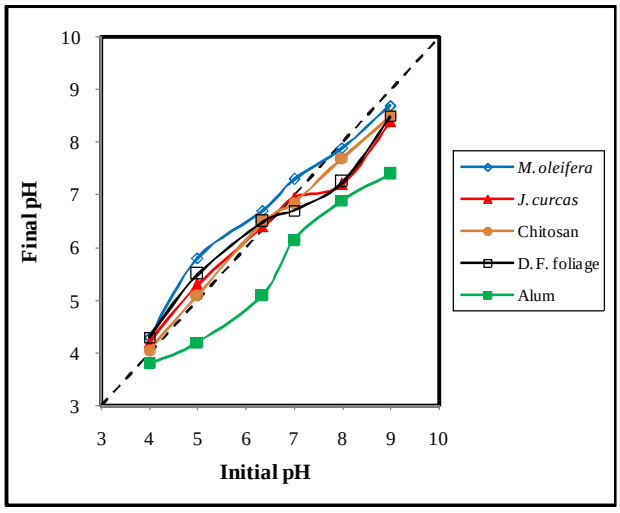

Fig. 3: Change in pH of Sungai Langat water samples for varying applied coagulants.

Chitosan coagulant solution is acidic due to preparing procedure[7], hence there was a very small pH drop observed in the treated water at alkaline pH. However, required dosage to have maximum turbidity removal was so low to have significant effect on pH value of treated water.

Both *J. curcas* and D. F. foliage, showed the same effect on final pH of treated water. Under acidic condition, pH values 4 and 5, final pH of treated water increased and at neutral pH values 6 and 7 of surface water, final pH did not alter. On the other hand, the pH of treated water started to drop at alkaline condition.

Final pH of treated water at its original pH of 6.4 was 6.7, 6.4, 6.5 and 6.5 for treated water by *M. oleifera*, *J. curcas*, chitosan and D. F. foliage respectively. With the addition of the natural extracts, all samples were within the WHO[15] range and further chemical addition is not necessary in order to correct the pH value of finished water in contrast to alum.

Conclusion

The purpose of this work was to investigate the ability of some natural coagulants, abundantly available in Malaysia– extracts of *M. oleifera* and *J. curcas* seeds as well as D. F. foliage and chitosan solution for turbid water clarification. The coagulants investigated, obviously possess positive coagulation abilities. Two of these coagulants, *M. oleifera* and chitosan, gave a high removal of the initial turbidity for surface water, in particular at pH values 4, 5 and 6.4. Meanwhile, there is a strong relationship between pH and coagulation activity for tow coagulants *J. curcas* and D. F. foliage. Results showed that the most appropriate pH for both investigated extracts to perform coagulation was pH 4, while in pH range from 6 to 8 extracts showed very low coagulation activities.

All four natural coagulants raised the pH value of treated turbid water at acidic pH values 4 and 5 and decreased at alkaline pH values 8 and 9. About neutral pH value 7, in addition, final pH values of treated water have been less than 7 for chitosan and D. F. foliage. The maximum effect of coagulant on final pH value related to *M. oleifera* seeds at pH values less than 7, compared to others. Generally, pH value of finished water at its initial pH 6.4 remained within WHO (2011) guideline value[15] and further investigation on the final pH of the treated samples with investigated natural coagulants revealed that not much alteration was recorded compared with the initial pH. Unlike natural coagulants, the pH of water treated by alum decreased from 6.4 to 5.1, this procedure, hence incurred cost, is not necessary when using natural coagulants.

Acknowledgement

This research was partially supported by a grant from PUNCAK NIAGA Research Sdn. Bhd.

References

1. Abidin Z. Z., Ismail N., Yunus R., Ahamad I.S. and Idris A., A Preliminary Study on *Jatropha curcas* as Coagulant in Wastewater Treatment, *Environmental Technology*, **32**, 971 **(2011)**

2. Chatterjee T., Chatterjee S. and HanWoo S., Enhanced Coagulation of Bentonite Particles in Water by a Modified Chitosan Biopolymer, *Chemical Engineering Journal*, **148,** 414 **(2009)**

3. Grahama N., Gang F., Fowler G. and Watts M., Characterisation and Coagulation Performance of a Tannin-Based Cationic Polymer: A Preliminary Assessment, *Colloids and Surfaces A: Physicochemical and Engineering Aspects*, **327**, 9 **(2008)**

4. Huang Ch., Chen Sh. and Pan J. R., Optimal Condition for Modification of Chitosan: a Biopolymer for Coagulation of Colloidal Particles, *Wat. Res.*, **34**, 1057 **(2000)**

5. Idris J., Sam A. Md., Musa M., Ku Hamid K. H., Husen R. and Muhd Rodhi M. N., Dragon Fruit Foliage Plant-Based Coagulant for Treatment of Concentrated Latex Effluent: Comparison of Treatment with Ferric Sulfate, *Journal of Chemistry*, **2013**, Article ID 230860, 7 **(2013)**

6. Katayon S., Megat Mohd Noor M. J., Asma M., Abdul Ghani L. A., Thamer A. M., Azni I., Ahmad J., Khor B. C. and Suleyman A. M., Effects of Storage Conditions of *Moringa oleifera* Seeds on its Performance in Coagulation, *Bioresource Technology*, **97**, 1455 **(2006)**

7. Sanghi Rashmi and Singh Ajay, Comparative Decolorisation Study of Malachite Green Dye Solutions using Synthetic and Natural Coagulants, *Res. J. Chem. Environ.*, **5(2)**, 35-37 **(2001)**

8. McLachlan D. R. C., Aluminum and the Risk for Alzheimer's disease, *Environmetrics*, **6**, 233 **(1995)**

9. Miller S. M., Fugate E. J., Craver V. O., Smith J. A. and Zimmerman J. B., Toward Understanding the Efficacy and Mechanism of *Opuntia* spp. as a Natural Coagulant for Potential Application in Water Treatment, *Environ. Sci. Technol.*, **42**, 4274 **(2008)**

10. Ndbigengesere A., Narasiah K.S. and Talbot B.G., Active Agent and Mechanism of Coagulation of Turbid Waters Using *Moringa oleifera*, *Wat. Res.*, **29**, 703 **(1995)**

11. Nkurunziza T., Nduwayezu J. B., Banadda E. N. and Nhapi I., The Effect of Turbidity Levels and *Moringa oleifera* Concentration on the Effectiveness of Coagulation in Water Treatment, *Water Science and Technology*, **59**, 1551 **(2009)**

12. Pritchard M., Mkandawire T., Edmondson A., O'Neill J. G. and Kululanga G., Potential of Using Plant Extracts for Purification of Shallow Well Water in Malawi, *Physics and Chemistry of the Earth*, **34**, 799 **(2009)**

13. Rizzo L., Lofrano G., Grassi M. and Belgiorno V., Pre-Treatment of Olive Mill Wastewater by Chitosan Coagulation and Advanced Oxidation Processes, *Separation and Purification Technology*, **63**, 648 **(2008)**

14. Sanchez-Martin J., Beltran-Heredia J. and Gibello-Pérez P., Adsorbent Biopolymers from Tannin Extracts for Water Treatment, *Chemical Engineering Journal*, **168**, 1241 **(2011)**

15. WHO (World Health Organisation), Guidelines for Drinking-Water Quality, Fourth Edition <http://whqlibdoc.who.int/publications/2011/9789241548151_eng.pdf> **(2011)**

16. Zhang J., Zhang F., Luo Y. and Yang H., A Preliminary Study on Cactus as Coagulant in Water Treatment, *Process Biochemistry*, **41**, 730 **(2006).**

(Received 12th April 2013, accepted 22nd July 2013)

Influences of Interactive Effects in the Flotation of Magnesite with Sodium Oleate as Collector based on Solution Chemistry

Yin Wanzhong and Yao Jin*
College of Resources and Civil Engineering, Northeastern University, Liaoning, Shenyang 110819, CHINA
*yaojin_82@126.com

Abstract

The floatability of magnesite, serpentine and quartz with sodium oleate as collector and the influence of serpentine on the floatability of magnesite and quartz were researched in this study. Crystal chemistry and solution chemistry mechanisms are also discussed. The results showed that serpentines had individual effects on the floatability of magnesite in different fractions and serpentine could suppress the flotation of magnesite while it activates the flotation of quartz. The reasons of this phenomenon are mainly that the ions from the solution of serpentine with relatively high solubility are hydrophilic and easy to reunite with the Mg^{2+} and O^{2-} ions on the surface of magnesite which led to the increment of hydrophilicity of magnesite and decrement of the chance that sodium oleate could adsorb on the surface of magnesite and therefore depress the floatability of magnesite while the complexation of Mg^{2+} ions on the surface of quartz could increase the chance of being collected by sodium oleate.

Keywords: Magnesite, serpentine, solution chemistry, interactive effect and flotation.

Introduction

The discovered storage of magnesite is 13 billion tons in the whole world, 3.12 billion tons of which are located in China accounting for 24%, taking the first place in the world [14]. However, along with the irrational exploration and unscientific utilization, the amount of high quality magnesite is less and less[4]. Therefore, the beneficiation technologies for magnesite are being paid more attention. According to the differences in crystal structure, magnesite can be classed into crystalline and amorphous[11].

The associated minerals of magnesite are mainly dolomite, serpentine, talc and quartz etc[1,2,7,8,12] which can interact in the flotation with magnesite and influence the beneficiation of magnesite. A lot of researches have been done in separating minerals and elements[5,9] and flotation is an efficient and low cost method. Therefore, this study has researched the floatability of magnesite, serpentine and quartz with sodium oleate as collector and the influence of serpentine on the flotation of magnesite and its mixture with quartz in different fractions. Furthermore, the mechanisms are discussed based on crystal chemistry and solution chemistry.

Material and Methods

Materials: The materials were selected from Kuandian and Dashiqiao in Liaoning province, China. High grade raw ores were crushed, ginned and concentrated by gravity method and sieved into four fractions: -0.1mm+0.045mm, -0.1mm+0.067mm, -0.067mm+0.045mm, -0.045mm to be prepared for the experiments. All fractions without notation in this study are of fraction -0.1mm+0.045mm. The purity of pure minerals is all above 95%, tested by X-ray Diffraction (XRD) method and multi-element chemical analysis.

Reagents: In the experiments sodium oleate was chemically pure, hydrochloric acid, sodium hydroxide, sodium hexametaphosphate were of analytical grade and sodium silicate were of industrial grade. All reagents were prepared with deionized water and the pH of deionized water was ca. 6.

Methods: The single mineral and mixed mineral flotation tests were carried out in a mechanical agitation flotation machine at a constant rate of 1100r/min. The mineral suspension was prepared by adding 3.0g minerals to 25mL deionized water and conditioned for 2 minutes. The pH of the mineral suspension was adjusted to desired value by adding NaOH or HCl and conditioned for 2 minutes. Then the regulators and collectors were added into the suspension and conditioned for 2 minutes each and flotation was carried out for a total of 3 minutes. Both floated and unfloated particles were collected, filtered and dried. The flotation recovery of single mineral flotation was calculated based on solid weight distributions between these two products and the recovery of mixed mineral flotation was calculated based on chemical analysis and weight distributions of products.

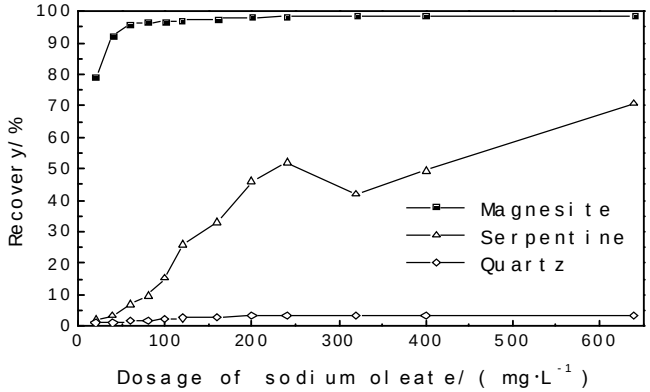

Fig.1: Relationship between recovery of minerals and oleate concentrations

A SSX-550 Scanning Electron Microscope (SEM) and Energy Dispersive Spectrometer (EDS) system produced by Shimadzu Co. Ltd. in Japan were used for observing the morphology and elements distribution of products[6].

Results and Discussion

Single mineral floatability tests: The influence of dosage of sodium oleate on the flotation recovery of magnesite, serpentine and quartz were tested and the results are shown in figure 1. With sodium oleate as collector, magnesite had the best floatability and serpentine had less floatability while quartz hardly had floatability. The differences in floatability of these minerals are related with their crystal structures[10].

The crystal structures of magnesite, serpentine and quartz were plotted with software Materials Studio 5.5 and are shown in figure 2-4.

The bonds easy to break in magnesite were Mg^{2+}-O^{2-} which had strong iconicity and polarity, therefore on the surface of magnesite mostly were Mg^{2+} and O^{2-} exposed which were easy to be collected by fatty acid collectors. Although serpentine had the same broken bonds and ionic on the surface, it was T-O type phyllosilicates with strong hydrophilicity, thus the collectability of fatty acid to it was weakened. The broken bonds in quartz were Si^{4+}-O^{2-}, which were hard to be collected by fatty acid.

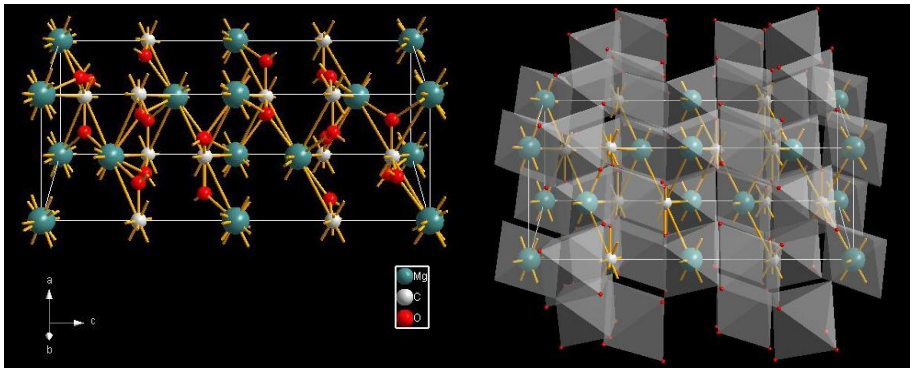

a- Atomic sequence in the crystal lattice, b-The arrangement of polyhedrons in crystal

Fig.2: The crystal structure of magnesite

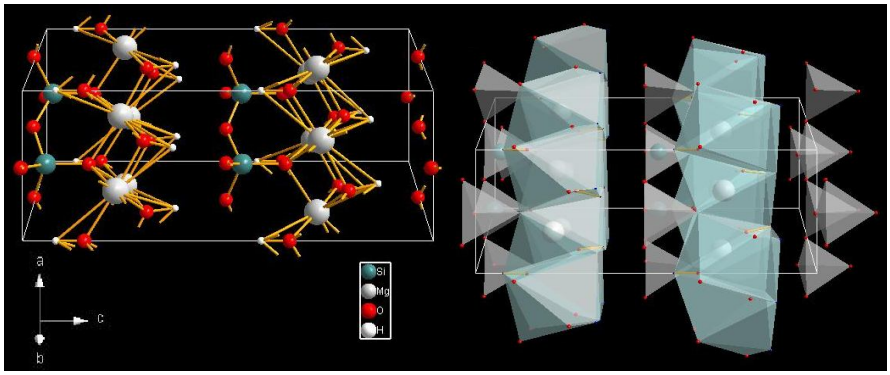

a- Atomic sequence in the crystal lattice b-The arrangement of polyhedrons in crystal

Fig.3: The crystal structure of lizardite

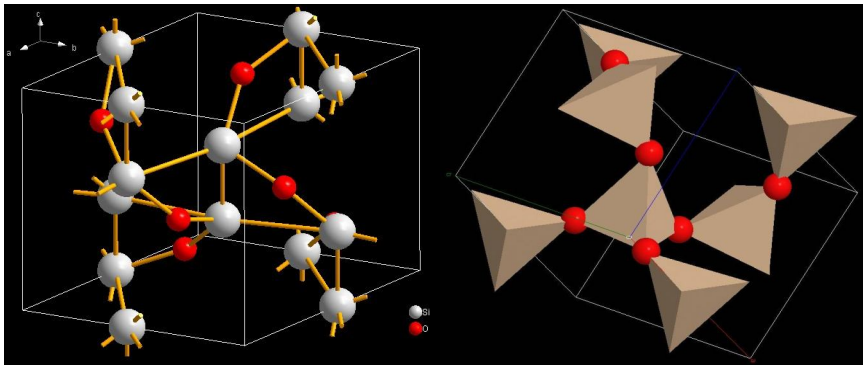

a- Atomic sequence in the crystal lattice b-The arrangement of polyhedrons in crystal

Fig. 4: The crystal structure of quartz

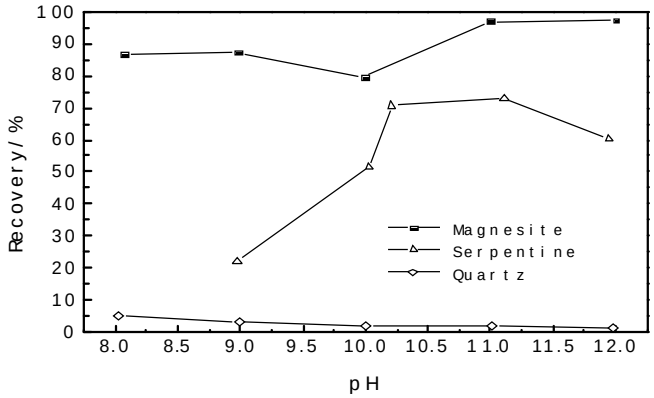

Fig. 5: Relationships between recovery of minerals and pH value in sodium oleate flotation system

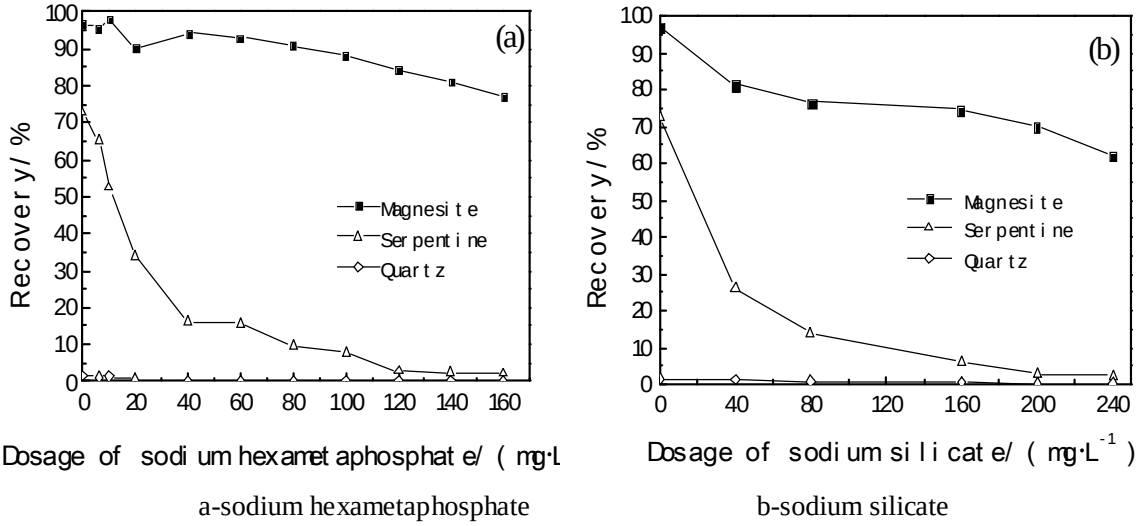

a-sodium hexametaphosphate b-sodium silicate

Fig. 6: Relationship between recovery of minerals and regulator concentrations in sodium oleate flotation system

With different pH conditions and sodium oleate as collector, the flotation recoveries of magnesite, serpentine and quartz are shown in figure 5, from which we can see that the flotation recovery of magnesite was increasing with the pH value and reached peak at pH=11 and the flotation recovery of serpentine was increasing with the pH value but decreased from pH=11 while the recovery of quartz was almost zero in the whole pH scales.

Influences of sodium hexameta phosphate and sodium silicate: The test results of regulators hexameta phosphate and sodium silicate were shown in figure 6. In figure 6 we can see with sodium oleate as collector, hexameta phosphate had suppressing effects on the floating of magnesite and stronger suppressing effects on serpentine. The recovery of serpentine decreased from 70% to under 5% and that of quartz was nearly zero all the time. The suppressing effects of hexameta phosphate were caused by the sparingly soluble precipitation formed by Ca^{2+}, Mg^{2+}, HPO_4^{2-} and $H_2PO_4^-$, which adsorbed on the surface of magnesite and serpentine. Sodium silicate had also suppressing effects on the floating of magnesite and serpentine and decreased the recovery of them by more than 20 percentage. The suppressing effects of sodium silicate were caused by the hydration of $HSiO_3^-$ and silicate colloids[3].

Influences of serpentine on the floatability of magnesite: From the single mineral tests in early stage it could be found that with sodium oleate as collector, hexametaphosphate and sodium silicate played an important role in the flotation of magnesite. Therefore they were chosen as regulators in the dosage tests of serpentine in order to explore the influence of serpentine on the floating of magnesite. The tests conditions were set as the optimal separation condition in the early single mineral tests. Figure 7 showed that serpentine had obvious suppressing effect on magnesite, which decreased the recovery of magnesite from 88% to 10%. Along with the increasing of serpentine, the recovery of magnesite was decreasing. Therefore, the existence of serpentine could significantly harm the floating of magnesite with sodium oleate as collector. Thus proper activators should be used to eliminate serpentine in reverse flotation, or regulators should be used to remove the suppressing effect of serpentine on magnesite in order to improve the recovery of magnesite.

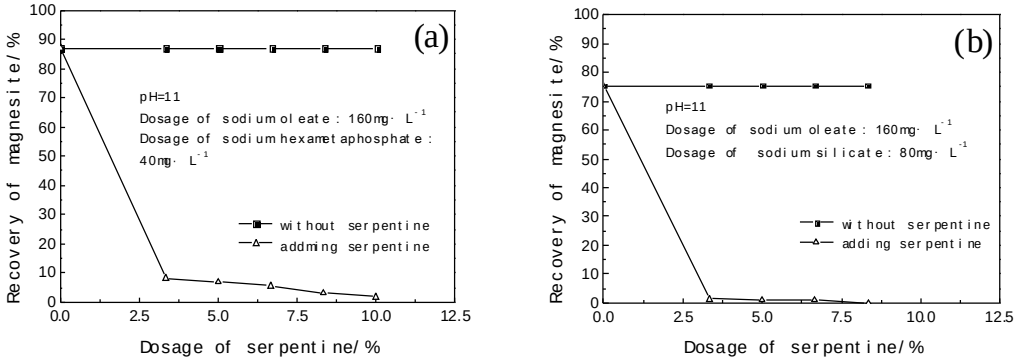

Fig.7: Influence of serpentine on flotation of magnesite in sodium oleate flotation system

Influence of serpentine on the floating of magnesite in different fractions: In order to test the influence of serpentine on the floating of magnesite, the pure mineral samples of magnesite and serpentine were classified into three fractions: -0.1mm+0.067mm, -0.067mm+0.045mm, -0.045mm and the samples contained 10% serpentine and 90% magnesite. The results are shown in figure 8, in which A, B, C stand for the three fractions -0.1mm+0.067mm, -0.067mm+0.045mm and -0.045mm. In each column, two capital letters are used to present the fraction and combination of fractions, where the first letter stands for the fraction of magnesite and the second letter stands for the fraction of serpentine. For example, AA stands for the single mineral tests for magnesite and serpentine in the fraction of -0.1mm+0.067mm and A+A stands for the mixed mineral tests of magnesite and serpentine in the fraction of -0.1mm+0.067mm.

Considering the results showed in figure 8, with sodium oleate as collector and hexametaphosphate as regulator, serpentine had significant suppressing effect on the floating of magnesite, in which serpentines of each fraction suppressed magnesite in the fraction of -0.1mm+0.067mm most and suppressed magnesite in the fraction of -0.045mm least.

With sodium silicate as regulator, the presence of serpentine also suppressed the floating of magnesite in which the suppressing effects of serpentine in all three fractions on magnesite in the fraction of -0.1mm+0.067mm were nearly same and very obvious and the suppressing effects of serpentines in the fractions of -0.1mm+0.067mm and -0.067mm+0.045mm on magnesite in the fraction of -0.067mm+0.045mm were intense while the suppressing effect of serpentine in all three fractions on magnesite in the fraction of -0.045mm were similar.

It can also be found that along with the decreasing of the particle sizes, the recoveries of serpentine slightly increased, while the recoveries of magnesite decreased. Because serpentine has small hardness and in the crushing process it is easy to produce micro particles which can affect the recovery of magnesite. When there are serpentine contained in magnesite ores, the negative influence of serpentine should be removed or reduced first to optimize the flotation separation of magnesite.

Influence of serpentine on the mixture of magnesite and quartz: As the results showed in figure 9, serpentine also had intense suppressing effects on the floating of magnesite in the mixture of magnesite and quartz. Only small amount of serpentine could decrease the recovery of magnesite largely and when it reached 6%, the recovery of magnesite was almost zero.

Analysis and Mechanisms: From the analysis of crystal structure and calculation of chemical bonds[13], it can be known that in the process of crushing, the bonds easy to break in serpentine crystals are the hydrogen bonds between hexagonal cell layer of silica tetrahedron and octahedral cell layer and the Mg-O bonds in magnesium oxide octahedral cell and minor Si-O bonds in silica tetrahedron cell, which generated unsaturated active groups such as Si-O-Si, O-Si-O, hydroxide radical and hydrogen bonds and thus serpentine was easily soluble in slurry. Through thermodynamical data, stoichiometric equations and equilibriums[15], the species distribution diagrams of sodium oleate and serpentine was plotted out and shown in figure 10.

In the diagrams, it shows that the hydrolyzation of sodium oleate was a complex process which included oleic acid molecules, oleic acid ions and molecule-ion polymers etc and the distribution of these species was depended on the pH value of the solution. At pH 11, the species in sodium oleate solution were mainly ions and the species in serpentine solution were mainly $H_3SiO_3^-$, $H_2SiO_4^{2-}$, $H_6Si_2O_4^{2+}$ which were hydrophilic and easy to reunite with the Mg^{2+} and O^{2-} on the surface of magnesite and increased the hydro philicity of magnesite and reduced the chance of these ions to unite with oleic acid ions and therefore suppress the floating of magnesite.

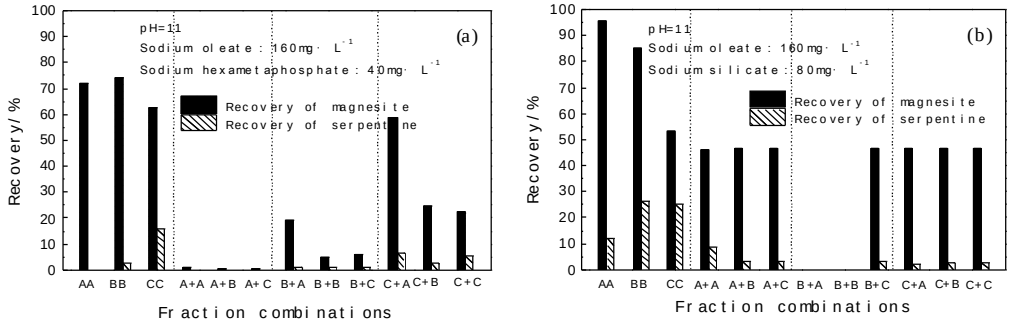

Fig.8: The influence of particle size on recoveries of magnesite and serpentine mixed ore

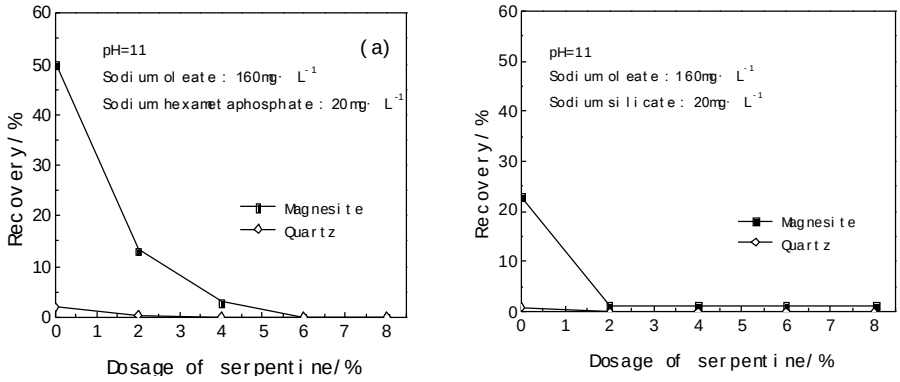

Fig.9: Influence of serpentine on flotation of magnesite and quartz mixed ores

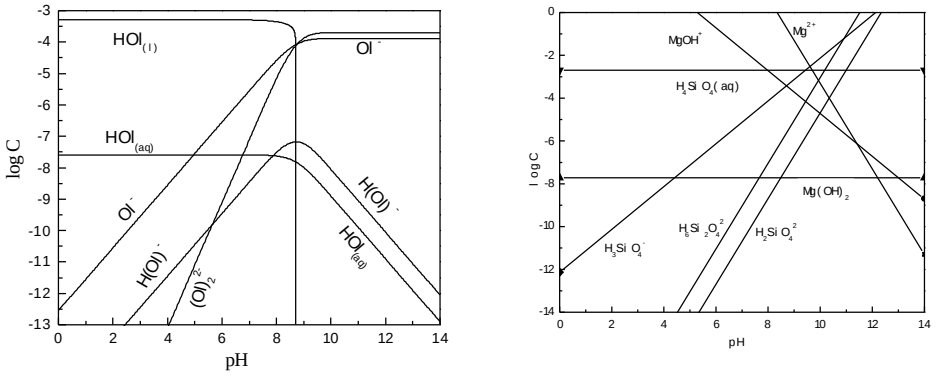

a-sodium oleate b-serpentine

Fig.10: Sodium oleate and serpentine species distribution diagram as a function of pH

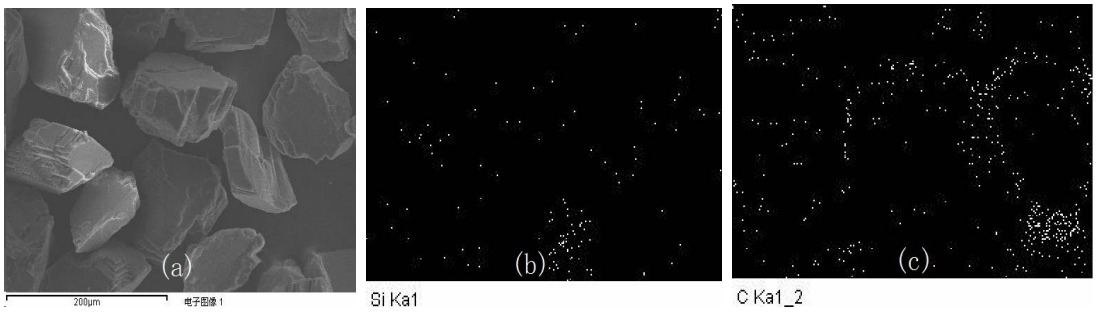

(a) unfloated products (b) Si element distribution (c) C elements distribution

Fig.11: SEM of tailings from core particle of magnesite and core particle of serpentite

Scanning Electron Microscope (SEM) analysis was carried out on the unfloated products of the flotation tests of the mixed samples of magnesite and serpentine in fraction of -0.1 mm+0.067 mm. The results are shown in fig.11 from which we can know that on the surface of those un-floated products, there were Si elements uniformly distributed including the Si from serpentine and the dissolved species of serpentine and sodium silicate. The element C distribution picture could tell that sodium oleate distributed mainly on the edge of magnesite. From those results it can be deduced that the adsorption of the dissloved species of sodium silicate and serpentine on the surface of magnesite prevented sodium oleate from adsorbing on it and kept magnesite away from floating and thus suppressed it which coincides with analysis results above.

Conclusion

1. With sodium oleate as collector, magnesite had the best floatability, second was serpentine and quartz had the worst floatability as determinated by the crystal structures of those minerals.

2. Sodium hexametaphosphate could suppress the floating of magnesite and serpentine which was caused by the sparingly soluble precipitation produced by the combination of Ca^{2+}, Mg^{2+}, HPO_4^{2-} and $H_2PO_4^-$. Sodium silicate could also suppress the floating of magnesite and serpentine.

3. Serpentine in different fractions had various suppressing effects on the floating of magnesite. It can be deduced from the solution species distribution diagram that the ions from the hydrolysis of serpentine having strong hydrophilicity were easy to reunite with the Mg^{2+},O^{2-} on the surface of magnesite, which could increase the hydrophilicity of magnesite and reduce the chance that the ions on the surface of magnesite will unite with oleic acid ions and thus suppress the floating of magnesite.

4. The SEM pictures also proved that the hydrolysis species of serpentine were distributed on the surface of magnesite which prevented oleic acid ions from adsorbing on it and therefore suppressed the floating of magnesite.

References

1. Anastassakis G. N., A study on the separation of magnesite fines by magnetic carrier methods, *Colloids Surf* A, **149(1/2/3)**, 585-593 **(1999)**

2. Botero A.E.C., Torem M.L. and de Mesquita L.M.S., Surface chemistry fundamentals of biosorption of Rhodococcus opacus and its effect in calcite and magnesite flotation, *Miner. Eng.*, **21(1)**, 83-92 **(2008)**

3. Danda S.R. et al, Effectiveness of sodium silicate as gangue depressants in iron ore slimes flotation, *Int. J. Met. Mater.,* **18(5)**, 515-522 **(2011)**

4. Gao Yu-Juan and Yan Ping-ke, Study on the Utilization of Low-grade Magnesite Resources, *China Non-metallic Mining Industry Herald*, **3**, 17-18 (**2011)**

5. Gouet B. et al, Synthesis and X-ray structures of two acidic cobalt (III) complex salts based on oxamide dioxime ligand system, *Res. J. Chem. Environ.*, **16 (2)**, 7-13 **(2012)**

6. Gontijo L.C. et al, Characterization of plasma-nitrided iron by XRD, SEM and XPS, *Sur. Coat. tech*., **183(1)**, 10-17 **(2004)**

7. Hojamberdiev M., Arifov P. and Tadjiev K., Characterization and processing of talc-magnesite from the Zinelbulak deposit, *Min. Sci. Tech.*, **20(3)**, 415-420 **(2010)**

8. Mirabbos H., Pulat A. and Kamil T., Processing of refractory materials using various magnesium sources derived from Zinelbulak talc-magnesite, *Int. J. Met. Mater*, **18(1)**, 105-114 **(2011)**

9. Nikam G.H. and Mohit B.S., Development of analytical method for extraction and separation of copper (II) using cyanex 923, *Res. J. Chem. Environ.*, **16(3)**, 11-17 **(2012)**

10. Plaksin I.N., Shafeyev R.S. and Chanturia V.A., Relation between energy structure of mineral crystal and their flotation properties, 8th International Mineral Processing Conference, Leningrad (**1968)**

11. Santana A.N. and Peres A.E.C., Reverse magnesite flotation, *Miner. Eng*, **14 (1)**, 107-111 **(2001)**

12. Skvarla J. and Kmet S., Non-equilibrium electrokinetic properties of magnesite and dolomite determined by the laser-Doppler electrophoretic light scattering (ELS) technique. A solids concentration effect, *Colloids Surf.*, A, **111(1-2)**, 153-157 **(1996)**

13. Sun Chuan-Yao and Yin Wan-Zhong, Flotation principle of Silicate, Beijing Science press **(2001)**

14. Wang Zhao-Min, Actualities & developing trend of magnesite in China, *China Non-metallic Mining Industry Herald*, **5,** 17-20 **(2006)**

15. Wang Dianzuo and Hu Yuehua, Solution Chemistry of Flotation, Changsha, Hunan science technology press **(1988).**

(Received 13th May 2013, accepted 25th July 2013)

A PVC- based Crown Ether Membrane Sensor for Cu^{2+}

Dwivedi Mithalesh Kumar[1]*, Jain Suresh[2], Jain Neeraj[3] and Bhatnagar Poonam[1]
1. Govt. Holkar Science College, Indore (M.P), INDIA
2. A.S.P.G. College, Mawana, Meerut (U.P), INDIA
3. CSIR-C.B.R.I., Roorkee (Uttaranchal), INDIA
*dwivedimk12@gmail.com

Abstract

A plasticized polyvinyl chloride (PVC) based membrane of 1,4,7,10 tetraoxacyclododecane (12-crown-4) exhibits a good response for Cu^{2+} in a wide concentration range (1.78×10^{-5}-1.00×10^{-1} M) with a super-nernstian slope of 50.0 mv per decade of concentration of Cu^{2+}.The response time of sensor is <30 s and the same can be used in a pH range 3.0 to 6.0. The electrode has been used for a period of 6 months and exhibits good selectivity for Cu^{2+} over alkali, alkaline earth and transition metal ions. It has also been possible to use this assembly as an indicator electrode in potentiometric titrations involving copper ions.

Keywords: Crown ether membrane, Membrane sensor, Ion-selective electrode.

Introduction

Ion Selective Electrodes are being widely used in the fields of environmental, industrial, agricultural and medicinal as they offer several advantages over other methods of analysis. The most attractive features of this technique are the speed with which samples can be analyzed, portability of the device, sample non-destruction, online monitoring, cost effectiveness and large measuring range.

Polymeric membrane ion selective electrodes (ISEs) provide one of the most powerful sensing methods because it is possible to select various sensory elements according to the charge and size of the target ion in clinical and environment assays[1-4]. The ISE dynamic response is generated by selective complexation of the target ion by ionophores dispersed in a polyvinyl chloride (PVC) matrix. Based on the recent advance of host-guest chemistry, polymeric membrane ISEs for copper ion have been extensively developed by the use of crown ether and related macrocyclic hosts as well as acyclic ligands[5-8]. Because of copper absorptions, some genetic defects have been found. The major role of copper in metabolism is oxidation (both in ionic and enzyme form); thus its role in respiration, atherosclerosis (per oxidation) and anemia is important. High uptake of copper results in Wilson's diseases[9].

A variety of potential ion carriers have been employed in the construction of Cu (II) ion selective electrodes. These copper ion carriers include small size thia-crown ethers and acyclic neutral ionophore with dithiocarbamate groups[10-11] and with nitrogen atoms[12], calyx[4] arenas[13-14], macrocyclic diamides[15] and Schiff bases.[16-18] However most of these copper selective sensor suffer from the interfering effect of such cations as Zn^{2+}, Cd^{2+} , Hg^{2+} , Pb^{2+} and Ag^{+} .

The present paper describes the efforts made to develop a Cu^{2+} selective membrane electrode by incorporating 12-crown-4 in PVC matrix. The cavity size of this crown ($0.70A^{o}$) suits well for the uptake of Cu^{2+} ($0.71A^{o}$). The proposed membrane electrode exhibits good selectivity, fast response, longer life time and a fairly wide working concentration range for the estimation of Cu^{2+} ions.

Material and Methods

Reagents: 12-crown-4 was obtained from Fluca and zinc chloride from BDH (Merck). All other chemicals used in these investigations were analytical grade reagents. Double distilled water was used for preparing all solutions.

Electrode Preparation: The method reported by Craggs et al[19] was adopted for the preparation of membranes. A known amount of 12-crown-4, PVC and dibutyl phthalate was dissolved in tetrahydrofuran. After shaking the mixture vigorously for some time and removing all the air bubbles it was poured into a holder and the solvent was made to evaporate at room temperature. The resulting membrane was cut into size, attached to a Pyrex tube with the help of araldite and immersed in Cu^{2+} solution for equilibrium.

The ratios of the membrane ingredients, time and concentration of equilibrating solution were optimized first so that that the membrane developed reproducible potentials and remained stable for a long time. Satisfactory equilibration was achieved with 0.1M Cu^{2+} solution in a contact time of 36 h.

Potential Measurements: Potentials were measured at 25 $\pm0.1^{o}$C with the help of ceramic junction calomel electrodes by setting up the following assembly:

- Internal reference electrode (SCE)
- Internal solution (0.1M Cu^{2+})
- Membrane
- Test solution
- External reference electrode (SCE)

A fixed concentration of Cu^{2+} solution was taken as internal solution (0.1M) and saturated calomel electrodes (SCE) were used as reference electrodes. All pH adjustments were made by appropriate acid or base. pH measurements were made on a digital pH meter (model pH 5652,ECIL, Hyderabad, India; Glass electrodes as pH electrode and calomel as reference electrode).

Results and Discussion

Some important features of various fabrications having ingredients in different ratios are recorded in table 1. The membrane chosen for subsequent work (No.3) is the one which has the optimum slope and the maximum concentration range.

The PVC-based membrane of 12-crown-4 generates very stable potentials when placed in contact with copper nitrate solution. The e.m.f. response of the membrane in presence of a wide concentration range of Cu^{2+} is shown in figure 1. The rectilinear range is 1.78×10^{-5}-1.00×10^{-1} M and can therefore be used for the determination of copper in this concentration range. A super-Nernstian slope of 50 mv per decade of Cu^{2+}concentration is also recorded for this assembly.

Static response time of the membrane sensor is <30 s over the entire working concentration range and potentials stay constant for more than 3 minutes, after which a very slow divergence is recorded. Potentials are reproducible within an error of ±1.0 mV and the membrane can work successfully over a period of six months but the membrane was again equilibrated with 1.0 M copper nitrate solution for 2d.

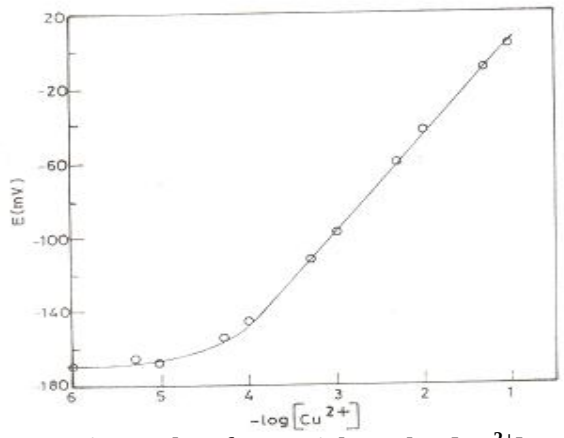

Fig. 1: Plot of potential vs – log [Cu^{2+}]

The working of the membrane electrode in relation to the variation in concentration of reference solutions was also observed. Potentials vs. –log[Cu^{2+}] plots against 1.0×10^{-2} M and 1.0×10^{-3} M concentration of Cu^{2+} as reference solution are depicted in figure 2 and at these concentrations of reference solutions, the working concentration range goes down with simultaneous increase in response time. As such 1.0×10^{-2} M [Cu^{2+}] (Figure 1) was employed as reference solution for all investigations with this membrane electrode.

The working pH range of the proposed assembly has also been ascertained (Figure 3). Potentials stay constant between 3.0 to 6.0 ([Cu^{2+}] =5.0×10^{-3} M) and the same may be taken as the working pH range for this assembly. A sharp change in potentials below pH 3.0 may be due to the protonation of the crown, which loses its capacity to complex with Cu^{2+} under highly acidic conditions.

The selectivity coefficients of the new membranes are very important for determining their quality as ISEs. The selectivity coefficients represent their response to the species to be measured over other ions present in solution. Potentiometric selectivity coefficients $K^{Pot}_{Cu^{2+}M^{n+}}$ were evaluated by the fixed interference method at 1.0×10^{-2} M concentration of interfering ions [Table 2]. As is evident from the table 2, most of the ions show low values of selectivity coefficients, thereby indicating no interference in the performance of the assembly.

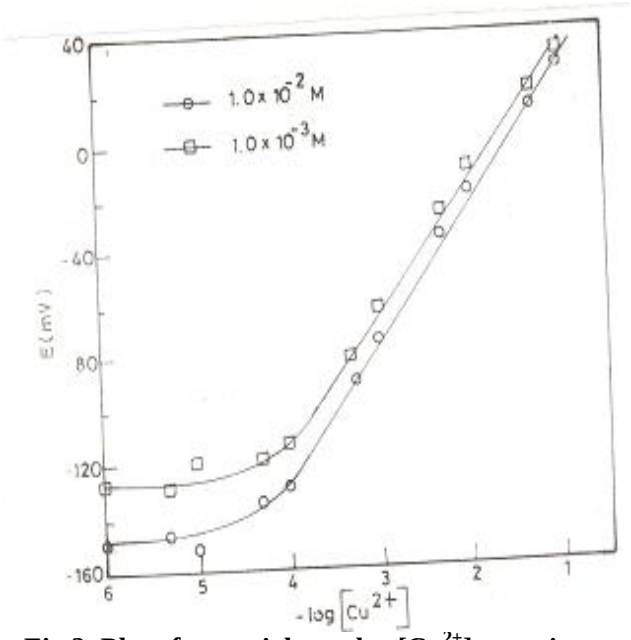

Fig.2: Plot of potential vs - log [Cu^{2+}] at various concentrations of reference solution

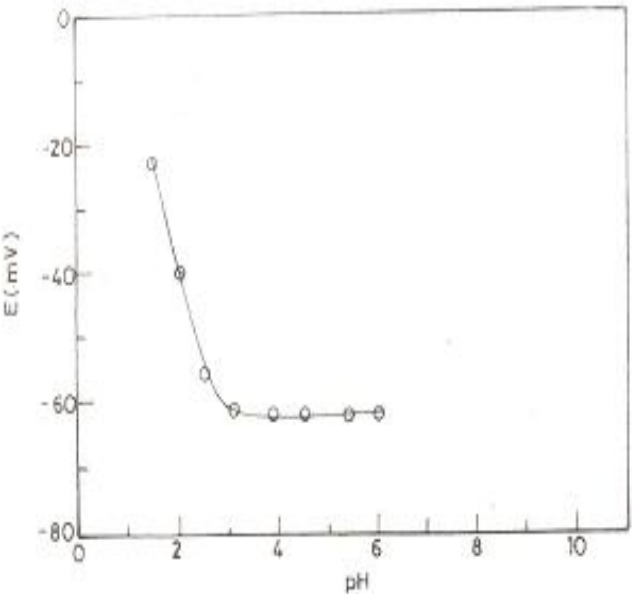

Fig.3: Plot of potential vs pH: [Cu^{2+}] x 5.0 x 10^{-3} M

Table 1
Optimization of membrane ingredients

Membrane No.	Composition in ratio			Detection Limit (M)	Slope (mV decade^{-1})
	Crown ether	PVC	Dibutyl Phthalate		
1	1	15	1.0	1.26×10^{-4}	35.0
2	1	18	1.0	7.00×10^{-5}	41.0
3	1	20	1.0	1.78×10^{-5}	50.0
4	1	20	1.5	5.00×10^{-5}	52.0
5	1	20	2.0	1.00×10^{-4}	31.0
6	2	20	1.0	9.00×10^{-5}	35.0

Table 2
Selective Coefficient ($K^{Pot}_{Cu^{2+}M^{n+}}$) values of other interfering ions for 12-crown-4 membrane as obtained by fixed interference method (interfering ion concentration is 1.0x10^{-2}M)

Ion	NH_4^+	K^+	Na^+	Li^+	Co^{2+}	Mg^{2+}	Pb^{2+}	Ca^{2+}	Cd^{2+}	Sr^{2+}	Cr^{3+}	Fe^{3+}
$(K^{Pot}_{Cu^{2+}M^{n+}})$	1.78×10^{-1}	1.78×10^{-1}	1.90×10^{-1}	2.51×10^{-1}	2.24×10^{-1}	1.99×10^{-1}	2.51×10^{-1}	3.55×10^{-1}	2.51×10^{-1}	3.99×10^{-1}	3.99×10^{-1}	3.99×10^{-1}

Titration: The sensor has also been used as an indicator electrode in the potentiometric titration of Zn^{2+} with EDTA. Figure 4 shows the potential change of 1.0×10^{-3} M Cu^{2+} solution (10.0 mL) with the addition of 1.0×10^{-3} M EDTA. In spite of the small change in potentials, the inflection point is quite sharp and indicates perfect stoichiometry.

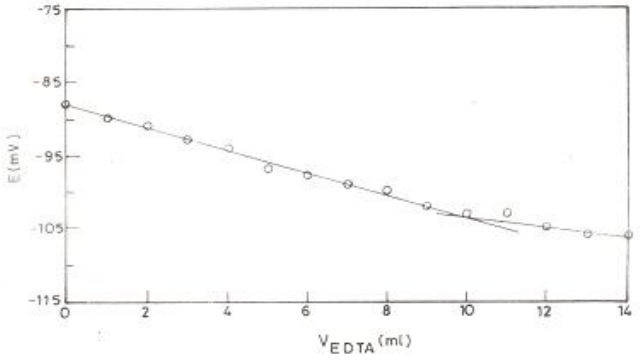

Fig. 4: Titration plot of 10.0ml of 1.0 x 10^{-3}M Cu^{2+} solution with 1.0 x 10^{-3} M EDTA

Solvent effect: The utility of the electrode assembly is also examined in partially non-aqueous medium. The results of the membrane sensor in non-aqueous medium in terms of working concentration range and slope are depicted in table 3. It is evident that the solutions having 25% (v/v) methanol or ethanol do not disturb the functioning of the proposed sensor whereas at higher non-aqueous content (35% or more) a divergence is recorded.

Conclusion

Cu^{2+} in the plasticized PVC-based membrane, incorporating 12-crown-4 as an electroactive phase can be used to determine the concentration range 1.78×10^{-5}-1.00×10^{-1} M with a response slope of 50 mV per decade of Cu^{2+} concentration. The functional pH range of the proposed sensor is 3.0 to 6.0.Basides this, the electrode shows better selectivity, stability and response time (<30s).

Table 3
Performance of the electrode system in 15, 25 and 35% (v/v) non-aqueous medium

Non-aqueous content (%)	Working concentration range (M)	Slope (mV dacade^{-1})
00	1.00×10^{-5} 1.00×10^{-1}	29
Methanol		
15	1.00×10^{-5} 1.00×10^{-1}	29
25	1.00×10^{-5} 1.00×10^{-1}	29
35	1.48×10^{-5} 1.00×10^{-1}	22
Ethanol		
15	7.08×10^{-5} 1.00×10^{-1}	29
25	7.08×10^{-5} 1.00×10^{-1}	29
35	1.00×10^{-5} 1.00×10^{-1}	22

References

1. Shamsipur M., Soleymanpour A., Akhond M., Sharghi H. and Massah A.R., Uranyl selective PVC membrane electrodes based on some recently synthesized benzosubstituted macrocyclic diamides, *Talanta*, **58**, 237-246 **(2002)**

2. Zhang Z.R. and Yu R.Q., The synthesis and membrane transport characteristics of macrocyclic polyether ligands composed of 1,10-phenanthroline as carriers for primary amine species, *Talanta*, **41**, 327-333 **(1994)**

3. Singh A.K., Saxena P., Mehtab S. and Gupta B., Strontium (II)-selective electrode Based on a macrocyclic tetraamide, *Talanta*, **69**, 521-526 **(2006)**

4. Singh A.K., Saxena P. and Panwar A., Manganese (II)-selective PVC membrane electrode based on a

pentaazamacrocyclic manganese complex, *Sens. Actuators* B, **110,** 377-381 **(2005)**

5. Sadeghi S., Eslahi M., Naser M.A., Naeimi I. H., Sharghi H. and Shameli A., Copper Ion Selective Membrane Electrodes Based on Some Schiff Base Derivatives, *Electroanalysis*, **15**, 327 **(2003)**

6. Jain A.K., Gupta V.K., Singh L.P. and Raisoni J.R., Chelating ionophore based membrane sensors for copper(II) ions, *Talanta*, **66**, 1355 **(2005)**

7 Gismera Ma Jesús, Procopio Jesús Rodriguez, Sevilla Ma Teresa and Hernández Lucas, Copper (II) Ion-Selective Electrodes Based on Dithiosalicylic and Thiosalicylic Acids, *Electroanalysis*, **15**, 126 **(2003)**

8. Gismera M. Jesús, Hueso D., Procopio J.R. and Sevilla M.T., Ion-selective carbon paste electrode based on tetraethyl thiuram disulfide for copper(II) and mercury(II), *Anal. Chim. Acta*, **524**, 347 **(2004)**

9. Gaetke L.M. and Chow C.K., Copper toxicity, Oxidative stress and antioxidant nutrients, *Toxicology*, **189**, 147 **(2003)**

10. Kamata S., Bhale A., Fokunaga Y. and Murata H., Copper(II)-selective electrode using thiuram disulfide neutral carriers, *Anal. Chem.*, **60**, 2464 **(1988)**

11. Kumata S., Murata H., Kubo Y. and Bhale A., Copper (II)-selective membrane electrodes based on *o*-xylylene bis(dithiocarbamates) as neutral carriers, *Analyst*, **114**, 1029 **(1989)**

12. Brzozka Z., Transition metal ion-selective membrane electrodes based on complexing compounds with heteroatoms, Part II, Complexing compounds containing sulphur atoms, *Analyst*, **113,** 1803 **(1988)**

13. Arnold M.A. and Meyerhoff M.E., Recent Advances in the Development and Analytical Applications of Biosensing Probes, *Crit. Rev. Anal. Chem.*, **20**, 149 **(1988)**

14. Cobben P.L.H.M., Egberink R.J.M., Bommer J.B., Bergvald P., Verboom W. and Reinhoudt D.N., Transduction of selective recognition of heavy metal ions by chemically modified field effect transistors (CHEMFETs), *J. Am. Chem. Soc*., **114,** 10573 **(1992)**

15. Shamshipur M., Rouhani S., Ganjali M.R., Eshghi H. and Sharghi H., Copper (II)- Selective Membrane Electrode Based on a Recently Synthesized Macrocyclic Diamide, *Microchem. J*, **63**, 202 **(1999)**

16. Ren K., A liquid-state copper (II) ion-selective electrode containing a Complex of Cu(II) with salicylaniline, *Talanta*, **36**, 767 **(1989)**

17. Singh Pratika, Sharma Neelam and Shet M.G., Membrane and Bi-ionic Potential Studies of Li^+, Na^+, K^+ and Rb^+ Cations using Cellulose Ion Selective Membrane Electrodes in Aqueous Media, *Res. J. Chem. Environ.*, **5(2)**, 65-69 **(2001)**

18. Gupta K.C. and Arc M. J. D., Performance evaluation of copper ion selective electrode based on cyanocopolymers, *Sens. Actuators B*, **62**, 171 **(2000)**

19. Cragg A., Moody G.J. and Thomas J.D.R., PVC matrix membrane ion-selective electrodes, Construction and laboratory experiments, *J. Chem. Educ*., **51,** 541 **(1974).**

(Received 05th March 2013, accepted 10th June 2013)

Mercury-induced changes in growth and oxidative metabolism of Field bean (*Dolichos lablab)*

D'Souza Myrene R. [1*] and Devaraj V. R.[2]
1. Dept. of Chemistry, Mount Carmel College, Bangalore – 560 052, INDIA
2. Dept. of Biochemistry, Central College Campus, Bangalore University, Bangalore-560 001, INDIA
*myrene83@gmail.com

Abstract

Effect of mercury on Field bean, Dolichos lablab was evaluated in 10-days old seedlings with 3, 4 and 5 µM $HgCl_2$ over 72 h of exposure. The stress reduced dry and fresh weight, root and shoot length, total chlorophyll and RWC. Antioxidant enzymes such as peroxidase, glutathione reductase and metabolic enzymes like amylase and acid phosphatase were enhanced in leaves. On the other hand, all the enzymes showed a time and concentration-dependent decline in roots, except invertase, amylase, acid phosphatase and peroxidase which were elevated.

Another antioxidant enzyme, catalase declined in both leaves and roots. Antioxidants, ascorbate and glutathione increased in leaves. While in roots, ascorbate was elevated and glutathione was decreased. The levels of malondialdehyde showed a close relation to that of H_2O_2 in both tissues. Levels of proline and total soluble sugars increased in both tissues. The results suggested that primary antioxidative response originates from leaves of Field bean even though roots are involved in the direct uptake of heavy metals. The root tends to accumulate Hg and thus excludes its uptake by leaves.

Keywords: Antioxidants, Catalase, *Dolichos lablab*, MDA, Peroxidase, Proline.

Introduction

Heavy metals have been considered to be major environmental pollutants due to their toxicity to plants. They are present in the environment with wide range of oxidation states and co-ordination numbers and these differences are closely associated with their toxicity[42]. Metals having a density higher than 5 g cm^3 are termed as heavy metals[56]. Environmental contamination has become a worldwide problem leading to severe agricultural losses and hazardous health effects. The metal pollutants, derived from growing number of diverse anthropogenic sources, have had enormous impact on different ecosystems.

The non-biodegradability of metals has led to their persistence in the environment. Their mode of action proceeds in two stages: First, inductive stage, lasting 1-2 days, is confined to the action of heavy metals on the signaling processes and the direct effect on enzymatic processes or the structure of cell wall and cell membranes. At the second stage, lasting over two days, permanent effects involving biochemical diminution of stress and senescence processes leading to degradation of plant tissues occurs[27]. Increased metal content of agricultural soil has lead to selection and colonization of resistant plants to a particular area, thus affecting biodiversity[60].

The toxic effect generated by heavy metals depends on several factors like solubility of the metal, absorbability, transport, its chemical reactivity, pH of the medium and presence of other ions[12]. Heavy metal toxicity may arise from the binding of the metal with the sulfhydryl groups in proteins leading to inhibition of metabolically important enzymes[38]. It could also increase the permeability of the plasma membrane[21] and expression of heat shock proteins (HSPs)[19]. Elevated levels of heavy metals cause water imbalance leading to decrease in relative water content and transpiration, the mechanism of which is distinct from that caused by osmotic stress[23]. Higher levels of heavy metals can disrupt the nutritional status of the plant by preventing the uptake of essential metal ions, inhibition of photosynthesis and chlorophyll biosynthesis.[61]

Hg is a global pollutant with complex and unusual chemical and physical properties. Hg in agricultural soil seems to originate from the degassing of the Earth's crust, volcanic emissions and industrial processes and from various products (e.g. batteries, lamps and thermometers). As Hg can replace metal ions in photosynthetic pigments, it results in decrease of photosynthetic rates[40]. The toxic effects of heavy metals are related to its ability to generate reactive oxygen species (ROS) resulting in unbalanced cellular redox homeostasis[31]. ROS such as superoxide anion (O_2^-), hydrogen peroxide (H_2O_2) and hydroxyl radical (OH^-)[9], may lead to unspecific oxidation of proteins and membrane lipids. A product of lipid peroxidation, malondialdehyde (MDA) has been shown to accumulate during heavy metal stress[34].

The primary constituents of protective mechanisms against ROS-mediated damage include enzymes such as superoxide dismutases, catalase, guaiacol peroxidase and ascorbate peroxidase, glutathione reductase and polyphenol oxidase[44] and free radical scavengers, such as carotenoids, ascorbate, tocopherols, glutathione and total phenols. These are located in various sites throughout the cell. Enzymes of scavenger metabolism such as APX, GR and dehydroascorbate reductase (DHAR) together form the Halliwell-Asada pathway[16].

Legume crops are reported to be tolerant to several heavy

metals. There has been considerable interest in finding legume species that are able to colonize metal-enriched soils for use in land reclamation or for crop production on marginal soils[15]. Because of the importance of legumes in maintaining soil fertility and sustaining plant growth in nitrogen deficient soils, a study was undertaken with Field bean (*Dolichos lablab*) which is extensively cultivated in semi-arid regions. Such crop plants tolerant to heavy metals could be of great value in reclaiming valuable lands.

Material and Methods

Growth conditions: Seeds of *Dolichos lablab* cultivar HA-4 were surface sterilized with 2% sodium hypochlorite for 1 min, rinsed immediately with large volume of sterile distilled water and imbibed overnight in distilled water. The overnight-soaked seeds were sown in trays containing cocopith and acid-washed sand (1:1 w/w) and irrigated daily with distilled water. The germination was carried out under natural greenhouse conditions; day/night temperature and relative humidity were: 30/25 °C and 75/70 % respectively. The average photoperiod was 12 h light/12 h dark.

Heavy metal stress and experimental design: Heavy metal stress was induced by transferring 10-day old seedlings of uniform size to a hydroponic system of half-strength Hoagland media[3] containing $HgCl_2$ (3, 4, 5 µM) for a period of 72 h. Samples of leaves and roots were collected at treatment intervals of 24, 48 and 72 h and frozen until further analysis. Plants grown on half-strength Hoagland media without addition of these $HgCl_2$ served as control. Samples used for determination of RWC, fresh and dry weight were used immediately after collection.

The experimental design used was at random factorial scheme, with 4 media regimes; control and $HgCl_2$ (3, 4 and 5 µM) and 3 evaluation points (24, 48, 72 h). Each experiment was composed of 24 experimental units (leaf + root samples) and done in triplicate.

Determination of seedling length, weight, RWC, Total Chl and metal uptake: Means of shoot and root length were taken by measuring shoot and root length in centimeter of seedlings after 72 h of stress. The dry mass of shoot and root was recorded in 72 h stressed seedlings after keeping them in an oven at 80 °C for 48 h. The relative water content was estimated according to the reported method[53] using the equation:

RWC = (FW-DW) X 100/(TW-DW)

The procedure of chlorophyll determination was based on the absorption of light by aqueous acetone (80%) extracts at 663 and 645 nm[26]. Total leaf and root accumulation of heavy metal in Field bean was determined after 72 h of treatment in order to estimate the accumulation of metal in roots and translocation into leaves. Leaves and roots were harvested, washed in deionised water for 2 min, air dried and then oven dried at 80 °C for 2 days. The tissue was ground into a fine powder using a pestle and mortar. A known amount of this powder (1 g) was dissolved in binary mixture containing 3 parts of 1M HNO_3 and 1 part of 1 M HCl (3:1 ratio) and the metal concentration was analyzed by flame photometer (Systronics India Limited, Model No. 128). Different concentrations of metal salts were used as standards.

Determination of antioxidants and stress markers: Standard procedures were followed for the assay of hydrogen peroxide[54], ascorbic acid (ASC)[46], glutathione (GSH)[8], proline[6], malondialdehyde (MDA)[18] and total soluble sugars (TSS)[45].

Extraction of enzymes: The frozen samples were homogenized with pre-chilled 50 mM sodium phosphate buffer (pH 7.0) containing 5 mM β-mercaptoethanol and 1mM EDTA using pestle and mortar. The homogenate was centrifuged at 12,000g for 15 min at 4 °C. The supernatant was used as a source of enzymes. Soluble protein content was determined using BSA as the standard[25].

Activities of Active Oxygen Quenching Enzymes: Catalase (CAT, EC 1.11.1.6) was assayed by following the decline in optical density at 240 nm ($\varepsilon = 39.4\ M^{-1}\ cm^{-1}$)[1]. Peroxidase (POX, EC 1.11.1.7) was assayed by following an increase in optical density at 470 nm ($\varepsilon = 26.6\ mM^{-1}\ cm^{-1}$)[11]. Glutathione reductase (GR, EC 1.6.4.2) was determined by monitoring the oxidation of NADPH at 340 nm ($\varepsilon = 6220\ M^{-1}\ cm^{-1}$)[10].

Activities of Hydrolytic Enzymes: β-Amylase (AMY, EC 3.2.1.1) was measured using dinitrosalicylic acid reagent[7]. Acid phosphatase (AP, EC 3.1.3.2) activity against p-nitrophenyl phosphate was determined by monitoring the release of p-nitrophenol at 410 nm[20]. Invertase (INV, EC 3.2.1.26) activity was determined according to the reported method[51].

Statistical analysis: The experiments were performed using a randomized design. All data are expressed as means of triplicate experiments unless mentioned otherwise. Comparison of means was done using Prism Graph version 3.02. Data were subjected to a one-way analysis of variance (ANOVA) and the mean differences were compared by lowest standard deviations (LSD) test. Comparisons with $P \leq 0.05$ were considered significantly different. The bar in the diagrams represented ± standard error. Each data point represents mean of three replicates analyzed twice and each value is therefore mean of six estimations (n=6).

Results and Discussion

Growth parameters, RWC, Total Chl and metal uptake: Exposure of Field bean seedlings to Hg caused a marked decrease in the growth parameters such as weight and length (Table 1 and fig. 1). A low shoot/root ratio suggested a pronounced effect of Hg on shoot growth

compared to roots. Other alterations included chlorosis after 48 h of exposure and appearance of dark pigmentation and necrotic lesions on the laminae. Observed chlorosis and reduced biomass is attributed to enhanced production and accumulation of ROS, resulting in reduced photosynthetic activity as apparent from reduction in chloroplastic pigments. The decrease in chloroplast pigments is believed to be due to reduced synthesis or increased oxidative degradation because of the oxidative stress imposed during heavy metal stress.

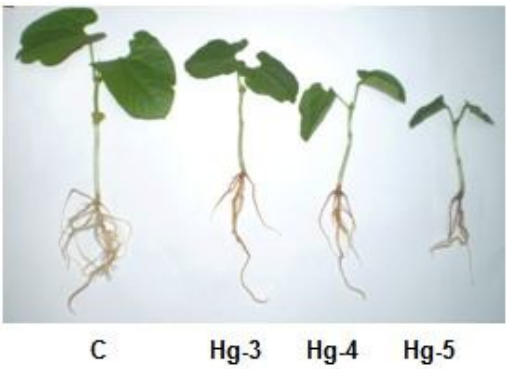

Figure 1: Effect of Hg stress (after 72 h of exposure) in Field bean seedlings treated with different concentrations of the metal

Similar structural alteration in stem, leaf and roots and reduction in dry weight have been reported in Hg treated Indian mustard[47]. Another parameter that gets affected under Hg stress is RWC. The observed reduction in RWC of heavy metal treated Field bean (Table 1) could probably be due to inhibition of absorption and translocation of water as has been observed in other plants[5]. This inhibition could be due to reduction in the size and number of xylem vessels and imbalance in hormone levels imposed by heavy metals[43]. Decrease in chlorophyll contents of leaves in response to abiotic stress is a general phenomenon[39]. Treatment of Field bean with Hg resulted in decreased concentration (~ 42% less) of chloroplastic pigments (Table 1). Decreased concentrations of chloroplastic pigments that lead to chlorosis of leaves may be an outcome of reduced synthesis and/or enhanced oxidative degradation of these pigments by imposed oxidative stress.

Inhibition of ALA dehydratase in Cd-stressed plants as reported[37] could have led to decreased synthesis of chlorophyll. Hg content was relatively higher in roots (3.8-fold in Hg-5) after 72 h of stress than in leaves (Table 1). The rate of uptake of Hg by Field bean was concentration dependent and comparable to the response seen in Zn-treated Hyacinth bean[31], Cd- and Zn-treated *Brassica juncea* plants[50] and Hg-treated Indian mustard[47].

Response of antioxidants and antioxidant enzymes: When the defense system in heavy metal-treated plants is overburdened, the reactive oxygen species (ROS) start to appear in excess and the antioxidative system is strongly activated. The timing of H_2O_2 occurrence observed almost coincides with the action of other stress factors in which signal molecules are involved. Redox metals like Cu^{2+} or Fe^{2+} undergo Fenton reactions producing OH^- from H_2O_2 and O_2^{-}[57]. The OH^- radical is the most reactive and initiates various irreversible modifications in the cells. The hydroperoxyl radical (HO^-_2) generated from O_2^- can induce lipid peroxidation via protonation reaction[30]. Hg^{2+} is non-redox metal and is unable to replace Cu^{2+} or Fe^{2+} in Fenton reactions. Such metals can affect the pro-oxidant status by depleting the antioxidant glutathione (GSH) pool[42].

In the present study, it was found that the H_2O_2 content increased with increasing time and concentration of the heavy metal (Table 2). The increase in H_2O_2 content after 72 h of stress was 3.5 fold in leaves and 3 fold in roots. This is probably due to the declining phase of GSH levels in a concentration-dependent manner after 48 h of stress (Table 2). Cd-induced depletion of GSH has been mainly attributed to phytochelatin synthesis, decreased GR activity[4] and increased utilization for ascorbate synthesis or for direct interaction with heavy metals[41]. These results suggested a close relation between GSH and H_2O_2 contents in leaves of Field bean.

Table 1
Effect of Hg on length, RWC, weight, total Chl and metal uptake after 72 h stress

[Metal] µM	*Length* (cm)			*RWC* (%)			Weight of plant (g)		Total Chl (mg/g)	Metal uptake (µg/g)	
	Leaf	Stem	Root	Leaf	Stem	Root	Fresh	Dry	Leaf	Leaf	Root
0	4.6 ± 0.2	7.2 ± 0.4	2.7 ± 0.9	97.6 ± 0.5	87.7 ± 1.6	94.9 ± 0.0	1.37 ± 0.10	0.21 ± 0.01	8.4 ± 0.7	0.09 ± 0.0	0.29 ± 0.04
3	4.2 ± 0.2	6.9 ± 1.1	2.5 ± 0.6	86.2 ± 3.7	82.4 ± 1.4	89.3 ± 5.3	1.27 ± 0.10	0.11 ± 0.01	5.7 ± 0.6	0.16 ± 0.02	0.78 ± 0.08
4	3.8 ± 0.4	5.5 ± 0.8	2.2 ± 0.8	80.9 ± 6.4	84.8 ± 4.6	81.7 ± 2.4	1.08 ± 0.10	0.09 ± 0.00	4.2 ± 0.1	0.31± 0.08	2.46 ± 0.15
5	3.2 ± 0.9	5.1 ± 0.7	1.8 ± 0.1	71.5 ± 2.9	78.9 ± 4.0	80.3 ± 5.3	0.93 ± 0.07	0.06 ± 0.02	3.5 ± 0.04	0.46 ± 0.11	3.98 ± 0.23

The cell membrane is considered to be the primary site of heavy metal injury. The accumulation of free radicals in stressed plants cause oxidation of polyunsaturated fatty acids in the plasma membrane resulting in the formation of malondialdehyde, MDA[48]. Formation of lipid peroxides serves as an activation signal for plant defense genes through increased activity of the octadecanoid pathways[27]. MDA content of metal-stressed leaves of Field bean exhibited time- and concentration-dependent increase (Table 2). Such increase in MDA levels has been reported in pea[29] and Hyacinth bean[31] stressed with Cd and Zn respectively.

The strength of the oxidative stress relies on the interaction of several factors that determine the antioxidant status of the plant. ASC, the key antioxidant, showed metal specific variations. The increase in ASC levels in leaves exhibited gradation under Hg stress during the entire period of exposure (Table 2). The increases in ASC levels are indicative of an effective free radical scavenging system in plants. As a powerful reducing agent, ASC maintains chloroplastic α-tocopherol and metalloenzyme activities and acts as reductant in enzymatic reactions and free radical scavenging of superoxide and H_2O_2 radicals non-enzymatically[24]. The levels of ASC in Field bean suggested that ASC has a major role in the leaf than in the root system and is mainly synthesized in the leaves.

Table 2
Levels of antioxidants and stress markers in leaves and roots of Field bean (*Doilchos lablab*)

		Stress response component	Control	$HgCl_2$ (µM)		
				3	4	5
LEAF	24h	H_2O_2 *	7.59 ± 1.5	8.7 ± 1.6	9.5 ± 1.8	12.8 ± 1.1
		TSS *	47.5 ± 1.6	48.7 ± 2.7	42.3 ± 2.6	34.8 ± 2.1
		MDA #	4.1 ± 1.2	4.3 ± 1.1	4.7 ± 1.2	4.9 ± 1.4
		GSH *	576.2 ± 5.2	615.9 ± 14.3	635.7 ± 12.0	759.9 ± 10.2
		Ascorbate	1.68 ± 0.0	1.73 ± 0.2	1.89 ± 0.3	2.37 ± 0.5
		Proline	1.09 ± 0.04	1.05 ± 0.06	1.12 ± 0.01	0.949 ± 0.02
	48h	H_2O_2 *	4.4 ± 1.2	11.3 ± 1.3	11.5 ± 1.4	14.1 ± 1.2
		TSS *	31.8 ± 2.2	45.3 ± 2.7	47.8 ± 1.1	48.2 ± 2.3
		MDA #	4.6 ± 0.5	7.8 ± 0.7	7.4 ± 0.9	11.5 ± 1.1
		GSH *	568.1 ± 13.6	845.9 ± 22.3	730.5 ± 25.7	751.1 ± 20.1
		Ascorbate	1.59 ± 0.1	1.97 ± 0.6	2.12 ± 0.4	2.97 ± 0.5
		Proline	0.952 ± 0.04	1.38 ± 0.01	1.34 ± 0.02	1.46 ± 0.04
	72h	H_2O_2 *	5.8 ± 1.2	12.0 ± 1.3	13.5 ± 1.4	16.5 ± 1.2
		TSS *	50.9 ± 1.4	44.3 ± 2.3	67.6 ± 3.0	41.4 ± 1.7
		MDA #	4.8 ± 0.8	5.8 ± 0.4	7.0 ± 0.7	7.9 ± 0.6
		GSH *	529.9 ± 11.6	765.1 ± 13.5	677.6 ± 13.4	670.3 ± 11.9
		Ascorbate	1.81 ± 0.2	2.01 ± 0.2	2.99 ± 0.3	3.16 ± 0.4
		Proline	1.13 ± 0.05	1.64 ± 0.02	1.31 ± 0.01	1.90 ± 0.02
ROOT	24h	H_2O_2 *	1.4 ± 0.2	4.0 ± 0.3	3.4 ± 0.5	6.8 ± 0.7
		TSS *	30.9 ± 0.2	49.3 ± 3.6	52.3 ± 1.7	66.5 ± 3.2
		MDA #	2.2 ± 0.1	4.2 ± 0.5	5.3 ± 0.6	5.6 ± 0.4
		GSH *	32.6 ± 5.2	149.5 ± 7.2	74.1 ± 4.7	64.5 ± 6.3
		Ascorbate	0.49 ± 0.01	0.37 ± 0.04	0.56 ± 0.05	0.66 ± 0.04
		Proline	1.15 ± 0.02	1.53 ± 0.01	1.13 ± 0.02	1.14 ± 0.03
	48h	H_2O_2 *	0.82 ± 0.0	4.7 ± 0.5	4.1 ± 0.02	2.8 ± 0.3
		TSS *	42.0 ± 0.5	54.5 ± 4.9	67.6 ± 6.2	58.1 ± 1.9
		MDA #	3.0 ± 0.4	5.1 ± 0.5	5.9 ± 0.7	6.2 ± 1.1
		GSH *	27.0 ± 0.8	126.2 ± 11.4	47.1 ± 2.3	61.6 ± 4.8
		Ascorbate	0.32 ± 0.02	0.45 ± 0.02	0.51 ± 0.01	0.78 ± 0.03
		Proline	1.06 ± 0.03	1.43 ± 0.02	1.87 ± 0.00	2.70 ± 0.02
	72h	H_2O_2 *	0.0 ± 0.0	1.4 ± 0.31	2.9 ± 0.2	4.0 ± 0.5
		TSS *	35.3 ± 2.4	50.4 ± 2.2	105.4 ± 1.1	60.6 ± 5.3
		MDA #	3.6 ± 1.0	5.2 ± 0.6	5.9 ± 0.6	6.5 ± 0.4
		GSH *	28.6 ± 10.4	11.45 ± 0.1	15.8 ± 0.12	6.32 ± 0.0
		Ascorbate	0.35 ± 0.03	1.27 ± 0.01	1.32 ± 0.02	1.48 ± 0.04
		Proline	1.22 ± 0.01	1.19 ± 0.00	0.997 ± 0.00	1.02 ± 0.01

GSH levels in leaves treated with Hg showed time- and concentration-dependent decline in roots (Table 2). Higher GSH concentrations in foliar tissues of plants exposed to environmental stresses are interpreted as an acclimation, supporting the antioxidative defense systems. Metal concentration dependent decline of GSH in roots could be attributed to sequestration of the heavy metal ions by GSH and metal-catalyzed oxidation to GSSG and also to the synthesis of metal-chelating proteins, phytochelatins[58].

CAT is a heme-containing enzyme that catalyzes the dismutation of H_2O_2 into oxygen and water. The CAT activity decreased significantly in leaves and roots of metal stressed seedlings (Fig 2) causing a parallel increase in H_2O_2, a stress signaling molecule. The decline in CAT could be due to photoinactivation as suggested for rye leaves under Cd stress[52]. An alternative mode of H_2O_2 destruction is via peroxidases (POX) that are found throughout the cell and have a much higher affinity for H_2O_2 than CAT[36]. Like CAT, POX is involved in detoxifying H_2O_2, but at the expense of another substrate being oxidized such as ascorbate. POX is also reported to be enhanced by heavy metal stress and this was positively correlated with heavy metal tolerance[31]. The activity of POX in leaves increased in time- and concentration-dependent manner but decreased steadily in roots (Fig 2). The enhanced POX activity in leaves of Field bean thus indicated an efficient detoxification of ROS in leaves but not in roots. Elevated levels of POX have been implicated in adaptation to stress by lignification[49]. The observed elevation of POX and consequent reduction of growth (Fig 2.1) could be due to limitation of cell expansion via lignification.

Field bean seedlings stressed with Hg showed time- and concentration-dependent increase in leaves (Fig 2). The coincidence of declining GSH and increasing GR activities under suggested that ASC/GSH cycle is operative in this plant, thus regenerating the oxidized ASC to DHA. Such coincidence has been reported under heavy metal stress as well as other oxidative stress.[31-36]

Response of hydrolytic enzymes and soluble sugars: Apart from antioxidant enzymes, which have been indisputably implicated in stress response, there are also reports of induction of metabolite enzymes such as β-AMY, AP and INV under abiotic stress[59]. Plants treated with $HgCl_2$ showed a concentration-dependent increase in activity up to 48 h. However, the levels did not show any alteration relative to control at 72 h of exposure (Fig 3). There are reports of increased activity of β-AMY leading to accumulation of TSS in the stressed plant[31-33]. TSS exhibited a concentration dependent increase after 24 h of stress; however, the increment was marginal in leaves after 48 h and 72 h of treatment. These results corroborate with the findings in *Pisum sativum* where photosynthetic inhibition or stimulation of respiration rate were attributed as a reason for constancy in TSS values[2]. This negative effect of heavy metals on carbon metabolism is a result of their possible interaction with the reactive centre of ribulose bisphosphate carboxylase, RuBisCo[14].

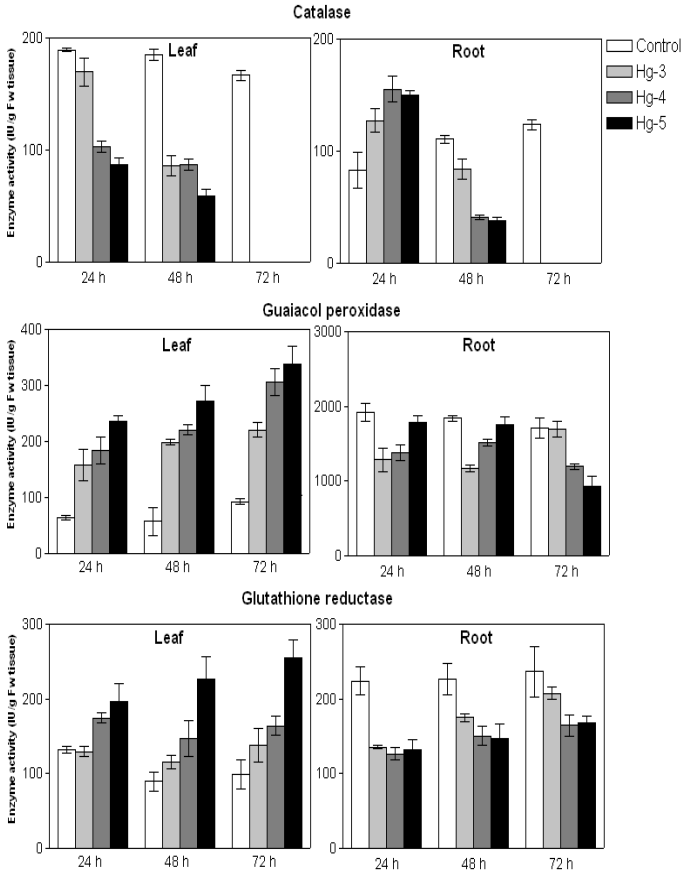

Figure 2: Activity of CAT, POX and GR in leaves and roots of Field bean treated with different concentrations of $HgCl_2$ compared to control. Data plotted are mean ± SE of duplicates of three separate replicates, mean values were compared by one way ANOVA ($P \leq 0.05$).

Acid phosphates widely distributed in plants are involved in hydrolysis of phosphate esters, an important process in energy metabolism, metabolic regulation and a wide variety of cellular signal transduction pathways of plant cells[55]. AP levels increased in both leaf and root tissue in a concentration- and time-dependent manner (Fig 3). Such enhancement in AP could be due to metal induced *denovo* synthesis. This stimulation is believed to increase the orthophosphate (Pi) availability. Free soluble Pi plays a vital role in many biological processes including photosynthesis, respiration, enzyme regulation, energy transfer, metabolic regulation and nucleotide phosphorylation[13] and may help the plant to survive longer under stress conditions.

Invertase activity in leaves showed a clear decrease in response to increasing concentration of Hg (Fig 3). This inhibition of INV in leaves could explain the tendency to accumulate TSS in these stressed tissues. Roots however showed enhanced INV activity followed by inhibition after

48 h of stress. A decrease in INV activity was also reported under other stressful conditions[33].

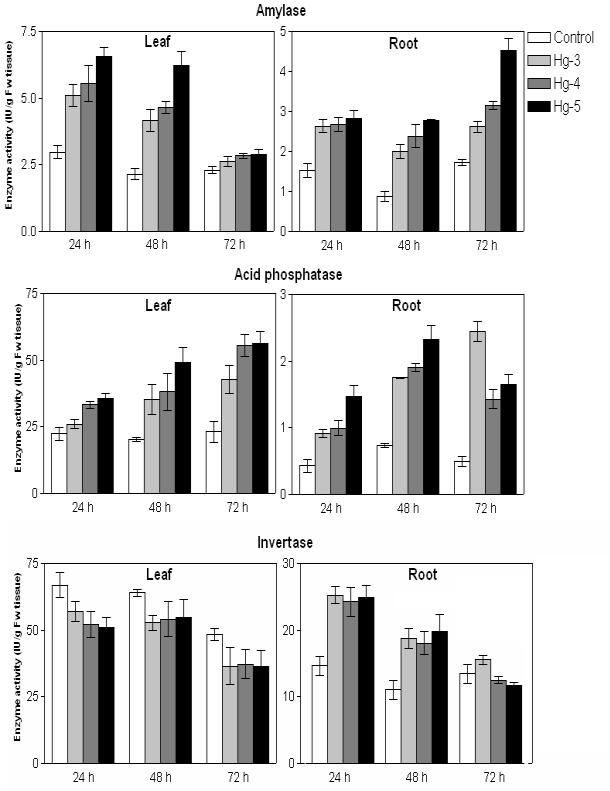

Figure 3: Activity of AMY, AP and INV in leaves and roots of Field bean treated with different concentrations of $HgCl_2$ compared to control. Data plotted are mean ± SE of duplicates of three separate replicates, mean values were compared by one way ANOVA (P≤ 0.05).

Levels of proline: Proline is considered as an important osmoprotectant and its role is valuable under plant abiotic stress response as an antioxidant, regulator of pH, stabilizer of proteins. The increase in proline and TSS (Table 2) in time and concentration dependent manner suggests probability of sugar-mediated proline biosynthesis and acquisition of tolerance. The increased $NADP^+$/NADPH ratio mediated by proline biosynthesis enhances the activity of oxidative pentose phosphate pathway that provides precursors for carbohydrate biosynthesis. Sucrose is known to be a positive effector of proline accumulation[22]. The simultaneous increase and inter-dependence of TSS and proline levels have also been reported in popular plants[17]. In addition to their role in osmoprotection, TSS plays an important role in biosynthetic processes, energy production, stabilization of cellular membranes, maintenance of turgor and signaling[35].

Conclusion

From the results presented in this study, exposure to environmentally realistic Hg concentration seems to disturb the cellular redox status in the leaves and roots of Field bean. Plants cells possess a well-organized antioxidative defense system which operates with the sequential and contemporaneous action of antioxidative enzymes and metabolites. The early-activated antioxidative defense mechanism controls and establishes the redox balance initially, but after a longer metal exposure, biochemical and morphological alterations do occur, even with relatively low, environmentally realistic heavy metal concentration.

Furthermore, the ascorbate-glutathione cycle in leaves appeared to play an important role against Hg induced oxidative stress. As the heavy metal chosen for the study are not redox-active metals, the oxidative stress caused by them is most likely an indirect effect. Therefore, further research on the indirect mechanisms of heavy metal-induced oxidative stress is required to ascertain the underlying molecular and biochemical events.

Acknowledgement

Myrene R. D'souza acknowledges the Council for Scientific and Industrial Research (CSIR), New Delhi, India for SRF (Award No. 09/039(0080)/2007-EMR-I).

References

1. Aebi H., Catalase *in vitro*, *Methods Enzymol*., **105,** 121 **(1984)**

2. Ahmad P., Sharma S. and Srivastava P.S., Differential physio-biochemical responses of high yielding varieties of Mulberry (*Morus alba*) under alkalinity (Na_2CO_3) stress *in vitro*, *Physiol. Mol. Biol. Plants*, **12**, 59 **(2006)**

3. Allen M.M., Simple conditions for growth of unicellular blue green algae on plates, *J. Phycol*., **4**, 1 **(1968)**

4. Aravind P. and Prasad M.N.V., Cadmium-Zinc interactions in a hydroponic system using *Ceratophyllum demersum* L.: adaptive ecophysiology, biochemistry and molecular toxicology, *Braz. J. Plant Physiol*., **17(1)**, 3 **(2005)**

5. Barceló J. and Poschenrieder C., Fast root growth responses, root exudates and internal detoxification as clue to mechanism of aluminium toxicity and resistance, *Env. Exp. Bot.*, **48**, 75 **(2002)**

6. Bates L.S., Waldren R.P. and Teare I.D., Rapid determination of free proline for water stress studies, *Plant Soil*, **39**, 205 **(1973)**

7. Bernfeld P., Amylase α and β, *Methods Enzymol*., **1**, 149 **(1955)**

8. Beutler E., Duron O. and Kelly B.M., Improved method for determination of blood glutathione, *J. Lab. Clin. Med*., **61**, 882 **(1963)**

9. Cakmak I., Role of zinc in protecting plant cells from reactive oxygen species, *New Phytol*., **146**, 185 **(2000)**

10. Carlberg I. and Mannervik B., Glutathione reductase, *Methods Enzymol*., **113**, 488 **(1985)**

11. Chance B. and Maehly A.C., Methods in Enzymology, Vol. II, Academic Press, New York, 764 **(1955)**

12. Das P., Sammantaray S. and Rout G.R., Studies on cadmium toxicity: a review, *Environ. Pollut.*, **98**, 29 **(1997)**

13. Ehsanpour A. A. and Amini F., Effect of salt and drought stresses on acid phosphatase activities in alfalfa (*Medicago sativa* L.) explants under *in vitro* culture, *African J. Biotechnol.*, **2**, 133 **(2003)**

14. Feller U., Anders I. and Demirevska K., Degradation of RuBisCo and other chloroplast proteins under abiotic stress, *Gen. Appl. Plant Physiology*, **34(1)**, 5 **(2008)**

15. Franco A.A. and Munns D.N., Acidity and aluminum restraints on nodulation, nitrogen fixation and growth of *Phaseolus vulgaris* in solution culture, *J. Soil Sci. Soc. Am.*, **46**, 296 **(1982)**

16. Halliwell B. and Gutteridge J.M.C., Free Radicals in Biology and Medicine, 3rd ed., Oxford University Press, Oxford **(1999)**

17. He J., Ma C., Ma Y., Li H., Kang J., Liu T., Polle A., Peng C. and Luo Z.B., Cadmium tolerance in six poplar species, *Environ. Sci. Pollut. Res.*, **20**, 163 **(2003)**

18. Heath R.L. and Packer L., Photoperoxidation in isolated chloroplasts, Kinetics and stoichiometry of fatty acid peroxidation, *Arch. Biochem. Biophys.*, **125**, 189 **(1968)**

19. Heckathorn S.A., Mueller J.K., Laguidice S., Zhu B., Barrett T., Blair B. and Dong Y., Chloroplast small heat-shock proteins protect photosynthesis during heavy metal stress, *Am. J. Bot.*, **91 (9),** 1312 **(2004)**

20. Hoerling N. and Svensmark O., Carboxyl esterase with different substrate specificity in human brain extracts, *J. Neurochem.*, **27**, 523 **(1976)**

21. Janicka-Russak M., Kabała K., Burzyński M. and Kłobus G., Response of plasma membrane H^+-ATPase to heavy metal stress in *Cucumis sativus* roots, *J. Exp. Bot.*, **59(13)**, 3721 **(2008)**

22. Kavi Kishor P.B., Sangam S., Amrutha R.N., Sri Laxmi P., Naidu K.R., Rao K.R.S.S., Sreenath Rao, Reddy K.J., Theriappan P. and Sreenivasulu N., Regulation of proline biosynthesis, degradation, uptake and transport in higher plants: Its implications in plant growth and abiotic stress tolerance, *Current Science*, **88(3)**, 424 **(2005)**

23. Krantev A., Yordanova R. and Popova L., Salicylic acid decreases Cd toxicity in maize plants, *Gen. Appl. Plant Physiology*, Special Issue, 45 **(2006)**

24. Lin K.H., Lo H.F., Lin C.H. and Chan M.T., Cloning and expression analysis of ascorbate peroxidase gene from eggplant under flooding stress, *Bot. Studs.*, **48**, 25 **(2007)**

25. Lowry O.H., Rosebrough N.J., Farr A.R. and Randoll R.J., Protein measurement with Folin–Phenol reagent, *J. Biol. Chem.*, **193**, 265 **(1951)**

26. Mackinney G., Absorption of light by chlorophyll solutions, *J. Biol. Chem.*, **140**, 315 **(1941)**

27. Maksymiec W., Signaling responses in plants to heavy metal stress, *Acta Physiol. Plant*, **29**, 177 **(2007)**

28. Maksymiec W., Signaling responses in plants to heavy metal stress, *Acta Physiol. Plant*, **29**, 177 **(2007)**

29. Metwally A., Safronova V.I., Belimov A.A. and Dietz K.J., Genotypic variation of the response to cadmium toxicity in *Pisum sativum* L., *J. Exp. Bot.*, **56**, 167 **(2005)**

30. Mithofer A., Schulze B. and Boland W., Biotic and heavy metal stress in plants: Evidence for common signals, *FEBS*, **566**, 1 **(2004)**

31. Myrene R. D. and Devaraj V. R., Induction of oxidative stress and antioxidative mechanisms in Hyacinth bean (*Lablab purpureus*) under Zinc stress, *African Crop Science Journal*, **20 (1),** 17 **(2012)**

32. Myrene R.D. and Devaraj V.R., Biochemical responses of Hyacinth bean *(Lablab purpureus)* to salinity stress, *Acta Physiologiae Plantarum*, **32(2)**, 341 **(2010)**

33. Myrene R.D. and Devaraj V.R., Specific and non-specific responses of Hyacinth bean (*Dolichos lablab*) to drought stress, *Indian Journal of Biotechnology*, **10**, 130 **(2011)**

34. Naser A., Anjum N. A., Umar S., Ahmad A., Iqbal M. and Khan N.A., Sulphur protects mustard (*Brassica campestris* L.) from cadmium toxicity by improving leaf ascorbate and glutathione, *Plant Growth Regul.*, **54**, 271 **(2008)**

35. Nayer M. and Reza H., Drought induced accumulation of soluble sugars and proline in two maize varieties, *World Appl. Sci. J.*, **3(3)**, 448 **(2008)**

36. Noctor G. and Foyer C.H., Ascorbate and glutathione: Keeping active oxygen under control, *Annu. Rev. Plant Physiol. Plant Mol. Biol.*, **49**, 249 **(1998)**

37. Noriega G.O., Balestrasse K.B., Batlle A. and Tomaro M.L., Cadmium induced oxidative stress in soybean plants also by the accumulation of d-aminolevulinic acid, *Biometals*, **20**, 841 **(2007)**

38. Panda S.K. and Choudhury S., Changes in nitrate reductase activity and oxidative stress in the moss *Polytrichum commune* subjected to chromium, zinc and copper phytotoxicity, *Braz. J. Plant Physiol.*, **17(2)**, 191 **(2005)**

39. Parida A.K. and Das A.B., Salt tolerance and salinity effects on plants: a review, *Ecotoxicol. Environ. Saf.*, **60**, 324 **(2005)**

40. Patra M., Bhowmik N., Bandopadhyay B. and Sharma A., Comparison of mercury, lead and arsenic with respect to genotoxic effects on plant systems and the development of genetic tolerance, *Environ. Exp. Bot.*, **52**, 199 **(2004)**

41. Pietrini F., Lannelli M.A., Pasqualini S. and Massacci A., Interaction of cadmium with glutathione and photosynthesis in developing leaves and chloroplasts of *Phragmites australis* (Cav.) Trin. ex Steudel, *Plant Physiol.*, **133**, 829 **(2003)**

42. Pinto E., Sigaud-Kutner T.C., Leitao M.A.S., Okamato O.K., Morse D. and Colepicolo P., Heavy metal induced oxidative stress in algae, *J. Phycol.*, **39**, 1008 **(2003)**

43. Ramadevi A. and Srinivasan K., Agricultural Solid Waste for the Removal of Inorganics: Adsorption of Mercury (II) from Aqueous Solution by Tamarind Nt Carbon, *Res. J. Chem. Environ.*, **9(1),** 54-59 **(2005)**

44. Razinger J., Dermastia M., Drinovec L., Drobne D., Zrimec A. and Koce J.D., Antioxidative responses of duckweed (*Lemna*

minor L.) to short-term copper exposure, *Environ Sci Pollut Res*., **14 (3),** 194 **(2007)**

45. Roe J.H., The determination of sugar in blood and spinal fluid with anthrone reagent, *J. Biol. Chem.*, **212**, 335 **(1955)**

46. Sadasivam S. and Manickam A., Biochemical methods, 2nd Edition, New Age International (P) Limited, New Delhi, 185 **(1997)**

47. Shiyab S., Chen J., Han F.X., Monts D.L., Matta F.B., Gu M., Su Y. and Masad M.A., Mercury-induced oxidative stress in Indian mustard (*Brassica juncea* L.), *Environ. Toxicol.*, **24 (5)**, 462 **(2009)**

48. Singh S., Eapen S., D'Souza S.F., Cadmium accumulation and its influence on lipid peroxidation and Antioxidative system in an aquatic plant, *Bacopa monnieri* L., *Chemosphere*, **62**, 233 **(2006)**

49. Smeets K., Cuypers A., Lambrechts A., Semane B., Hoet P., Laere A.V. and Vangronsveld J., Induction of oxidative stress and antioxidative mechanisms in *Phaseolus vulgaris* after Cd application, *Plant Physiol. Biochem.*, **43**, 437 **(2005)**

50. Sridhar B.B.M., Diehl S.V., Han F.X. and Monts D.L., Anatomical changes due to uptake and accumulation of Zn and Cd in Indian mustard (*Brassica juncea*), *Environ. Exp. Bot.*, **54**, 131 **(2005)**

51. Sridhar R. and Ou S.H., Extracellular enzymes produced by *Pyricularia oryzae*, *Philipp. Phytopathol*., **8,** 52 **(1976)**

52. Streb P., Michael-Knauf A. and Feierabend J., Preferential photoinactivation of catalase and photoinhibition of photosystem II are common early symptoms under various osmotic and chemical stress conditions, *Pysiol. Planta*, **88**, 590 **(1993)**

53. Turner N.C. and Kramer P.J., Adaptation of plant to water and high temperature stress, Wiley, New York, 207 **(1980)**

54. Velikova V., Yordanov I. and Edreva A., Oxidative stress and some antioxidant system in acid rain treated bean plants: protective role of exogenous polyamines, *Plant Sci.*, **151**, 59 **(2000)**

55. Vincent J.B., Crowder M.W. and Averil B.A., Hydrolysis of phosphate monoester: A biological problem with multiple chemical solutions, *Trends Biochemistry Science*, **17**, 105 **(1992)**

56. Weast R.C., CRC Handbook of Chemistry and Physics, 64th edition, CRC Press, Boca Raton **(1984)**

57. Winterbourne C.C., Superoxide dependent formation of hydroxyl radicals in the presence of iron salts: a feasible source of hydroxyl radical *in vivo*, *Biochem. J. Lett*., **205**, 461 **(1982)**

58. Yadav S.K., Heavy metals toxicity in plants: an overview on the role of glutathione and phytochelatins in heavy metal stress tolerance of plants, *South African Journal of Botany*, **76 (2)**, 167 **(2010)**

59. Yang S.H., Wang L.J. and Li S.H., Ultraviolet-B irradiation induced freezing tolerance in relation to antioxidant system in winter wheat (*Triticum aestivum* L.) leaves, *Environ. Exp. Bot*., **60,** 300 **(2007)**

60. Ye Y., Tam N.F.Y., Wong Y.S. and Lu C.Y., Growth and physiological responses of two mangrove species (*Bruguiera gymnorrhiza* and *Kandelia candel*) to water logging, *Environ. Exp. Bot*., **49,** 209 **(2003)**

61. Yordanova R., Maslenkova L., Paunova S. and Popova L., Sensitivity of photosynthetic apparatus of pea plants to heavy metal stress, *Biotechnol. & Biotechnol. Eq.*, Special online edition, 347 **(2009).**

(Received 13th June 2013, accepted 02nd August 2013)

Extraction, Characterization and Application as Natural Dyes of extracts from *Terminalia catappa* leaf and seed pericarp

Chitnis K. S.
Department of Life Science, Ramnarain Ruia College, L.N. Road, Matunga, Mumbai, 400019, INDIA
kanchanchitnis@gmail.com

Abstract

Until the middle of last century most of the dyes were derived from plants or animal sources. Later synthetic dyes were developed. But some of the synthetic dyes were found to be carcinogenic and allergenic. Thus natural dyes appeared to be the ideal choice because of their nontoxicity and environmental safety. In the present study dyes were extracted from leaf and seed pericarp of Terminalia catappa and characterized based on parameters like λmax, pH, HPTLC fingerprinting and stability. They were checked for application as natural dyes on cotton. Effect of different mordants on dyeing capacity and color fastness to washing and light was studied.

λmax of Terminalia leaf and seed pericarp extract was characteristic of flavonols like gossypetin. HPTLC fingerprinting showed 4 common bands at R_f 0.08(-0.01), 0.32(0.01), 0.45 and 0.56(-0.01). These can be considered as marker peaks for Terminalia catappa. Leaf dye was color fast to sunlight and washing. Seed pericarp dye was not color fast to sunlight and washing, suggesting requirement of dry cleaning. Yield of dye was economically viable.

Thus water soluble extracts from Terminalia leaf and seed pericarp sources can be used as natural dyes in presence of mordants. They are economically favorable and environmentally friendly.

Keywords: Natural dyes, *Terminalia catappa*, HPTLC Fingerprinting, mordants, environmentally friendly.

Introduction

Until the middle of last century most of the dyes were derived from plants or animal sources. Later synthetic dyes were developed which received faster acceptability due to their ease in dyeing and reproducibility. But some of the synthetic dyes like azo dyes made from aromatic compounds were found to be carcinogenic and allergenic. Thus natural dyes appear to be the ideal choice because of their non-toxicity and environmental safety[7].

Dong et al[3] fabricated natural dye from sappan wood (*Caesalpinia sappan*) for industrial application by using a micro emulsion method. M Chairat et al[2] extracted dye from the dried fruit hulls of mangosteen and used it for dyeing of cotton and silk yarn. They studied the optimum conditions for dyeing and the fastness properties. Mahanta and Tiwari[6] explored the availability of natural dye yielding plants in Arunachal Pradesh and documented the indigenous knowledge and procedures related to preparation of natural dyes. This study suggests *Syzigium cumuni* bark and fruits as source of natural dye. Major color component isolated from pods of *G.sepium* plant is morin, its dyeing behavior was investigated on silk yarn by Konaghatta et al.[5]

Lane 1: *Terminalia* leaf ; Lane 2: *Terminalia* seed pericarp
Figure 1: HPTLC fingerprint of plant samples (366 nm)

Terminalia catappa is a tall deciduous tree reaching 15-25 m, with whorls of nearly horizontal, slightly ascending branches. Leaves are alternate obovate with short petioles spirally clustered at the branch tips, dark green above, paler beneath, leathery and glossy. They turn bright scarlet, dark red, dark purplish-red, or yellow. Fruit is hard, green-red, rounded and flattened, egg-shaped, with two ridges, yellow or reddish when ripe[4].

Material and Methods

Plant Material: *Terminalia catappa* leaf and seed pericarp.

Dye Extraction: 5gm source material was weighed and 100mL DW (distilled water) was added to it. The beaker was kept in water bath at 60ºC for 1 hr. The dye extract was filtered through Whatmann paper no.1.

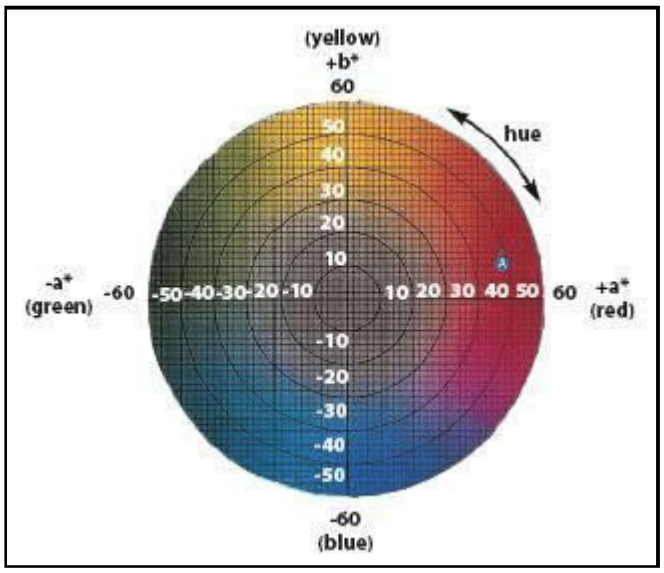

Figure 2: Color Space Diagram

1. Cotton cloth not dyed; 2. Cotton dipped in Control and then dyed(C); 3. Cotton dipped in Mordant 1 and then dyed (M1); 4. Cotton dipped in Mordant 2 and then dyed (M2); 5. Cotton dipped in Mordant 3 and then dyed (M3)

Figure 3: Cloth dyed with *Terminalia* leaf extract

Characterization of dye extract: λmax (UV-1800, Shimadzu UV Spectrophotometer), pH, color, color change at pH 2.0 and 9.0 and stability were checked. Extracts in methanol were separated by HPTLC to get a fingerprint.

Experimental details for HPTLC

Sample Preparation: To *Terminalia* leaf (1g) 10 mL of methanol was added in the stoppered glass test tubes. To *Terminalia* fruit (1g) 5 mL of methanol was added. The tubes were vortexed for 1-2 mins and left to stand overnight at room temperature. Next day, the contents of the tube were filtered through Whatmann filter paper no. 41 and the filtrate obtained was used for further analysis.

Chromatography: The chromatographic conditions were optimized to achieve the best resolution and peak shape[8].

Stationary Phase: Merck Silica gel 60 F254 HPTLC pre-coated plates
Mode of separation: Normal phase
Mobile phase: Toluene: ethyl acetate: methanol: glacial acetic acid (8:1:0.5:0.3, v/v/v/v) (AR Grade)
Development chamber: Camag twin trough chamber
Chamber saturation: 30 mins
Sample applicator: Camag Linomat V
Band width: 7 mm
Space between the bands: 13.2 mm
Rate of sample application: 150 nL/sec
Spotting Volume: 5µl
Development distance: 85 mm
Derivatizing Reagent: 10% methanolic sulphuric acid for 20 seconds, then plate was air dried in oven at 110ºC for 7 min.
Densitometric scanner: Camag Scanner IV winCATS Planar Chromatography manager software.

1. Cotton cloth not dyed; 2. Cotton dipped in Control and then dyed(C); 3. Cotton dipped in Mordant 1 and then dyed (M1); 4. Cotton dipped in Mordant 2 and then dyed (M2); 5. Cotton dipped in Mordant 3 and then dyed (M3)

Figure 4: Cloth dyed with *Terminalia* seed pericarp extract

Application as natural dyes: White cotton fabric was rinsed in water, cut into 3x3 inch pieces and weighed. Dye extract was prepared and divided into 4 beakers. 5 cotton pieces similar in weight were dipped in control (200mL DW), 5 pieces in mordant 1(200mL 4:1 DW: acetic acid), 5pieces in mordant 2 (0.6gm alum+ 0.2gm NaK Bitartarate+ 200mL DW) and 5pieces in mordant 3 (0.6 gm alum+ 0.4gm FeSO4+ 200mL DW). The beakers were kept in water bath at 60ºC for 1 hr.

The cotton pieces were removed, rinsed with water and dipped in the dye for 15 min at 60ºC and 45 min at RT in 4 beakers, corresponding to control, mordant 1, 2 and 3.The cotton pieces were then rinsed with water and dried. Their L*a*b* values were measured [L* = lightness, a* = (+ red, - green), b* = (+ yellow, - blue)] (Spectroscan 5100; Reflectance spectrophotometer; Premier Colorscan). The difference in absorbance of the dye extract before and after dyeing was completed, gave the dye absorbed by the cotton. The average weight of the pieces was calculated to find dye absorbed per gm of the cotton. Color fastness to light (IS:2454:1985 Re 2006) and washing (Test 2; ISO: 105C10:2006) was checked.

Yield of dye: From 1gm of the sample, the dye was extracted initially in 40mL DW, then re-extracted in another 40mL DW and yet again in 20mL DW, in water bath at 60ºC for 1 hr each. All extracts were pooled together and the beaker was kept in water bath till the extract dried. The difference between initial and final weight of the beaker gave the yield of the dye.

Results and Discussion

Characterization: λmax for *Terminalia* leaf extract was 274.5nm (pinkish brown) which changed to 281.5nm (brown color) at pH 9.0 and 264.5nm (cherry red color) at pH 2.0. The λmax for *Terminalia* seed pericarp extract was 273nm (pink) which changed to 279.5nm (green color) at pH 9.0 and 266.5 and 203nm (dark pink color) at pH 2.0. The observed pH for *Terminalia* leaf extract was 5.0 and for *Terminalia* seed pericarp extract it was 4.0 (Table 1, Table 2). The water extracts were not stable beyond one or two days as they became turbid due to microbial growth (Table 3). HPTLC fingerprinting was performed with different mobile phases (Table 4). Among these the best suited mobile phase was found to be Toluene: Ethyl acetate: Methanol: Glacial acetic acid in ratio 8:1:0.5:0.3.(v/v/v/v). HPTLC fingerprinting showed 6 prominent bands for *Terminalia* leaf extract at R_f 0.08, 0.20, 0.32, 0.45, 0.56 and 0.88 with maximum AUC at 0.56 R_f. *Terminalia* seed pericarp extract showed 5 bands at R_f 0.07, 0.26, 0.33, 0.45 and 0.55.with maximum AUC at 0.33 R_f (Figure 1, Table 5, Table 6).

Application as Natural Dyes: The extracts were found to be good dyes on cotton cloth in presence of mordants like acetic acid, alum and $FeSO_4$ and alum and Na K Bi-tartarate. For *Terminalia* leaf extract, the hue was lighter, in yellow green quadrant for control which turned deeper green and more yellow in presence of mordant (Figure 2, Table 7, Figure 3). For *Terminalia* seed, pericarp extract the hue was lighter, in red and blue quadrant (Table 8, Figure 4). For *Terminalia* leaf, mordant 3 allowed maximum dye to be absorbed by the cloth (1.596 absorbance units /gm of cloth) with 31.23% exhaustion as in table 9. For *Terminalia* seed pericarp, mordant 2 allowed maximum dye to be absorbed by the cloth (0.089 absorbance units /gm of cloth) with 13.83% exhaustion (Table 10).

Colour fastness: Colour fastness to light (IS: 2454: 1985 Re 2006) (Atlas CI- 4000, Weather-o-meter, CIRCOT) and washing (Test 2; ISO: 105C10: 2006) (5g/lt non ionic soap at 50°C, 45 min, EEC Launder-o-meter, CIRCOT) was checked and the results obtained were in the form of grades on a scale of 0 to 5. For natural dyes, grade of 3 and above is acceptable. *Terminalia* leaf dye was color fast to sunlight and washing (grade 3-4 in 5 point scale) (Table 11). *Terminalia* seed pericarp dye was not color fast to sunlight and washing (grade 2 in 5 point scale) (Table 12).

Yield of dye: The yield of dye from *Terminalia* leaf and seed pericarp was 7.97% and 11.70% respectively (Table 13, Table 14).

Table 1
Observed λmax of extracts and their λmax at pH 2.0 and 9.0

S.N.	Observed λmax nm	λmax nm after adding 1N NaOH (150µl) pH 9.0	λmax nm after adding 1N HCl (50µl) pH 2.0
1*	274.5	281.5	264.5
2*	273	279.5	266.5, 203

Key: 1*= Terminalia leaf ; 2*= Terminalia seed pericarp

Table 2
Observed pH and color of extract and color change at pH 2.0 and 9.0

S.N.	Observed pH of water extract	Observed colour of water extract	Colour change after adding 1N NaOH(150µl) pH 9.0	Colour change after adding 1N HCl (50µl) pH 2.0
1*	5.0	Pinkish Brown	Brown	Cherry red
2*	4.0	Pink	Green	Dark pink

Table 3
Stability Study of extracts

S.N.	λmax nm	Absorbance on day 1	Absorbance on day 2	Absorbance on day 3
1*	274.5	0.4028	0.3186	Turbidity
2*	273	0.0564	Turbidity	Turbidity

Table 4
Different Mobile Phases studied for fingerprinting of extracts[8]

S.N.	Solvents	Ratio(v/v/v)
1	Ethyl acetate: Formic acid: Glacial acetic acid: water	100: 11:11:26
2	n Butanol: Glacial acetic acid: water	40:10:20
3	Conc HCl: Acetic acid: water (Forestal)	3:30:10
4	Toluene: Ethyl acetate: Methanol: Glacial acetic acid	8:1:0.5:0.3
5	Conc HCl: Formic acid: water	2:5:3
6	n Butanol: Glacial acetic acid: water	40:10:50

Table 5
R_f and AUC values of *Terminalia* leaf HPTLC fingerprint

No. of bands	Max R_f	Height at R_f	Area under curve	% Area under curve
1	0.08	38.7	556.4	6.31
2	0.20	33.8	455.1	5.16
3	0.32	48.2	1048.1	11.88
4	0.45	62.9	1871.8	21.22
5	0.56	134.4	3825.5	43.37
6	0.88	38.3	1064.4	12.07

Table 6
R_f and AUC values of *Terminalia* seed pericarp HPTLC fingerprint

No. of bands	Max R_f	Height at R_f	Area under curve	% Area under curve
1	0.07	17.4	270.6	9.63
2	0.26	12.3	302.8	10.78
3	0.33	36.9	1059.7	37.72
4	0.45	33.4	919.6	32.73
5	0.55	14.2	256.7	9.14

Table 7
L*a*b* readings for cloth dyed with *Terminalia* leaf extract

Sample dipped in	L*	a*	b*
Control	79.95	-0.36	7.61
Mordant1	80.30	-1.28	10.64
Mordant 2	81.60	-3.82	16.03
Mordant 3	70.82	-2.32	10.98

L* = lightness, a* = (+ red, - green), b* = (+ yellow, - blue); Control: 200mL DW; Mordant 1: 200mL 4:1 DW: acetic acid; Mordant 2: 0.6gm alum+ 0.2gm Na K Bi-tartarate+ 200mL DW; Mordant 3: 0.6 gm alum+ 0.4gm $FeSO_4$+ 200mL DW

Table 8
L*a*b* readings for cloth dyed with *Terminalia* seed pericarp extract

Sample dipped in	L*	a*	b*
Control	77.92	6.29	-7.92
Mordant1	79.46	5.25	-5.20
Mordant 2	80.47	4.78	-6.06
Mordant 3	74.99	4.32	-6.04

Table 9
***Terminalia* leaf extract dye absorption (λmax: 277 nm; dilution; 100µl to 3000µl=1:30; factor=30)**

Sample in	Ave weight (gm) of cotton	Abs before dyeing	Abs after dyeing	Difference in absorption	Difference x dilution factor	Divided by 5 (5 pieces dipped together)	Abs per gm of fabric	% E
Control	0.5979	0.4028	0.3374	0.0654	1.962	0.3924	0.656	16.24
Mordant1	0.5415	0.4028	0.3018	0.1010	3.030	0.606	1.119	25.07
Mordant 2	0.5067	0.4028	0.2981	0.1047	3.141	0.6282	1.239	25.99
Mordant 3	0.4730	0.4028	0.2770	0.1258	3.774	0.7548	1.596	31.23

%E = % Exhaustion=$\frac{\text{absorbance before- absorbance after}}{\text{absorbance before}}$ x 100

Table 10
***Terminalia* seed pericarp extract dye absorption (λmax: 276 nm; dilution;100µl to 3000µl=1:30; factor=30)**

Sample in	Ave weight (gm) of cotton	Abs before dyeing	Abs after dyeing	Difference in absorption	Difference x dilution factor	Divided by 5 (5 pieces dipped together)	Abs per gm of fabric	% E
Control	0.4983	0.0564	0.0513	0.0051	0.153	0.0306	0.061	9.04
Mordant1	0.5158	0.0564	0.0537	0.0027	0.081	0.0162	0.031	4.79
Mordant 2	0.5271	0.0564	0.0486	0.0078	0.234	0.0468	0.089	13.83
Mordant 3	0.5556	0.0564	0.0519	0.0045	0.135	0.0270	0.049	7.98

Table 11
Fastness to light and washing for *Terminalia leaf* extract dyed cloth

Sample in	Fastness to light	Fastness to washing: change in colour
Control	5	3 (darker)
Mordant 1	5	3 (darker)
Mordant 2	3-4	3-4 (darker)
Mordant 3	3-4	3-4 (yellower)

Table 12
Fastness to light and washing for *Terminalia seed pericarp* extract dyed cloth

Sample in	Fastness to light	Fastness to washing: change in colour
Control	2	2
Mordant 1	2	2
Mordant 2	2	2
Mordant 3	2	2-3

Table 13
Yield of dye from *Terminalia leaf*

Weight of sample(gm)	Initial Weight of beaker(gm)	Final weight of beaker (gm)	Difference in weight (gm)	Mean (gm)	% Yield
1	106.727	106.812	0.085		
1	88.766	88.853	0.087	0.0797	7.97
1	101.214	101.281	0.067		

Table 14
Yield of dye from *Terminalia seed pericarp*

Weight of sample(gm)	Initial Weight of beaker(gm)	Final weight of beaker (gm)	Difference in weight (gm)	Mean (gm)	% Yield
1	100.166	100.289	0.123		
1	100.937	101.048	0.111	0.117	11.7
1	99.066	99.183	0.117		

Conclusion

λmax of *Terminalia* leaf and seed pericarp extract was characteristic of flavonols like gossypetin.[1,8] HPTLC fingerprinting showed 4 common bands at R_f 0.08(-0.01), 0.32(0.01), 0.45 and 0.56(-0.01). These can be considered as marker peaks for *Terminalia catappa*. Leaf dye was color fast to sunlight and washing. Seed pericarp dye was not color fast to sunlight and washing, suggesting requirement of dry cleaning. The yield was economically viable.

Thus water soluble extracts from *Terminalia* leaf and *Terminalia* seed pericarp sources can be used as natural dyes in presence of mordants. Alum and Sodium Potassium Bi-tartarate and alum and $FeSO_4$ are more effective in dye absorption and retention on cotton cloth. Since only water and no other chemicals is used for extraction of dyes, it is economically favorable and environmentally friendly.

Acknowledgement

Thanks to 1) University of Mumbai for funding this project under Minor Research Grants; 2) Central Institute for Research on Cotton Technology, Indian Council of Agricultural Research,(CIRCOT), Mumbai, for analyzing color and light fastness; 3) Dr. P.S. Ramanathan, Advanced Instrumentation Centre (PSRAIC), Ramnarain Ruia College, Matunga, Mumbai, for analyzing samples on UV-VIS Spectrophotometer.

References

1. Bhat S. V. et al, Natural Products, Chemistry and Applications, Narosa Publishing House **(2009)**

2. Chairat M., Bremmer J.B. and Chantrapromma K., Dyeing of cotton and silk yarn with the extracted dye from the fruit hulls of mangosteen, *Garcinia mangostana* linn, *Fibers and Polymers*, **8(6)**, 613-619 **(2007)**

3. Dong K. L., Dong H.C., Jin H.L. and Hun Y. S., Fabrication of nontoxic natural dye from sappan wood, *Korean J. Chem. Eng*, **25(2),** 354-358 **(2008)**

4. Francis J.K. and Terminalia catappa L., Indian almond, almendra, SO-ITF-SM-23, Rio Piedras, Institute of Tropical Forestry **(1989)**

5. Konaghatta N. V. et al, Extraction, Identification and Adsorption- Kinetic studies of a natural color component from G. sepium, *Natural Science*, **2(5)**, 469-479 **(2010)**

6. Mahanta D. and Tiwari S. C., Natural dye-yielding plants and indigenous knowledge on dye preparation in Arunachal Pradesh, northeast India, *Current Science*, **88**, 9 **(2005)**

7. Vankar P.S., Handbook on Natural Dyes for Industrial Applications, National Institute of Industrial Research, 472 **(2007)**

8. Wagner H. and Bladt S., Plant Drug Analysis- A Thin Layer Chromatography Atlas, 2nd ed., Springer Verlag **(2004)**

9. Tajuddin R., Tumin S.M., Muda K. and Abd Razak N., Superheated Water Extraction (SWE): A potential green extraction technique for natural dyes, *Res. J. Chem. Environ.*, **15(1)**, 62-66 **(2011).**

(Received 13th March 2013, accepted 20th June 2013)